Defining the role of B7-H3 (CD276) in epithelial homeostasis and cancer progression

Alhamad, Salwa

Awarding institution:
King's College London

Defining the role of B7-H3 (CD276) in epithelial homeostasis and cancer progression

Salwa Alhamad

PhD supervisors: Prof. Maddy Parsons and Dr Claire Wells

A thesis submitted to King's College London for the degree of Doctor of Philosophy

2022

Declaration

I, Salwa Alhamad, confirm that the work presented in this thesis is my own. Where information has been derived from other sources, I confirm that this has been indicated in the thesis.

Acknowledgement

الحمد لله الذي بنعمته تتم الصالحات

One year after starting this PhD, a global pandemic had hit the world and in a blink of an eye everything changed. Therefore, this PhD experience has been anything but ordinary. Nonetheless, I have been blessed to call London my second home for the past 4 years, a lively city where I have witnessed historic events and met amazing people!

First, I would like to thank my supervisor, prof. Maddy Parsons. An incredibly supportive and inspiring mentor! From the first ever meeting when I took on this project knowing the challenges that came with B7-H3, all through the uncertainty of the pandemic to the last bit of writing- Maddy, thank you for always being there to support, guide and encourage me. I could not have asked for a better supervisor!

I would like to extend my gratitude for my thesis committee members for their valuable input and suggestions, everyone in the Randall for the interesting conversations and to Imam Abdulrahman bin Faisal University for funding my PhD.

Thanks to everyone in the Parsons lab past and present, for welcoming me to the lab, the nuggets of wisdom and the coffee breaks! Thank you, Claudia for being my desk/analysis/espresso buddy!

My Bay4Bs! Thanks Irina and Aneesa; you two have made this journey a blast! I could never predict the chats and “experiments” in (and outside) our bay, there was always something exciting happening!

To my awesome coffee buddy, Stefania, thank you for the London experiences. I am glad to have found a friend like you!

Last but not least, my family and friends. Words cannot express the gratitude I feel for having you in my life. Special thanks to my parents, for everything they’ve sacrificed to support me. I couldn’t have done this without them! My siblings, thank you for being there for me and for keeping me grounded. My friends, thank you for the endless support.

”ما أعرفه هو أن وجودكم ولو في البعد هو سند هائل لي“

Abstract

B7-H3 (CD276) is a member of the B7 superfamily and shares up to 30% amino acid identity with other B7 family members. It is expressed in a wide range of cell types and tissues and is overexpressed in many cancers. B7-H3 expression has been linked to poor prognosis in several tumour types, including lung cancer, and is suggested to play both co-inhibitory and co-stimulatory roles in tumour-immune modulation. Thus B7-H3 is an appealing target for therapeutic agents to prevent tumourigenesis. However, the physiological functions of B7-H3 in both lung epithelial cells and tumour cells remains poorly understood, and ligands and specific binding partners for this receptor remain unknown. The purpose of this study was to define the effects of overexpression or knockdown of B7-H3 on normal lung epithelial and cancer cell proliferation, migration and invasion as well as to determine the role of B7-H3 in cell-cell adhesion and signalling. Data revealed that B7-H3 localises to cell-cell adhesions in all cell lines and co-localises with E-cadherin and β-catenin. Depletion of B7-H3 lead to reduced levels of the tight junction protein ZO-1 and reduced active GTPases that are known to control F-actin cytoskeleton dynamics. Moreover, B7-H3 depletion led to enhanced proliferation and invasion of lung cancer cells in 3D spheroid assays. Further analysis revealed that B7-H3 in normal lung epithelial cells localises to IMPDH2-positive structures called rods and rings, as well as to a subset of primary cilia. Both structures were absent in lung cancer cells that express high levels of B7-H3, but their appearance increased upon B7-H3 knockdown. Conversely, cilia and rods and rings were reduced upon B7-H3 overexpression in normal lung epithelial cells. Finally, NMR and proteomics analysis revealed that B7-H3 contributes to maintenance of metabolite levels leading to suppression of oxidative stress, potentially through co-regulation of IMPDH2 activity and cilia assembly. The data arising from this study provides novel insight into B7-H3 function in epithelial and lung cancer cells and how this receptor contributes to tumourigenesis.

Table of Contents

List of figures

List of tables

Abbreviations

Abbreviation	Meaning
2D	Two dimensional
3D	Three dimensional
ADC	antibody-drug conjugate
ADP	Adenosine di-phosphate
AJ	Adherens Junction
ARL13B	ADP Ribosylation Factor Like GTPase 13B
ARL2	ADP Ribosylation Factor Like GTPase 2
ARP2/3	Actin-Related Proteins 2/3
ATM	Ataxia-telangiectasia mutated
ATP	Adenosine Triphosphate
ATR	Ataxia telangiectasia and Rad3-related
BCL	B-cell Lymphoma
BSA	Bovine Serum Albumin
CAR T-cell	Chimeric antigen receptor T cell
CDK	Cyclin Dependent Kinase
CDP	Nucleolipid cytidine diphosphate
CKI	Cyclin Dependent Kinase Inhibitor
CRISPR	Clustered regularly interspaced short palindromic repeats
Ctrl	Control
DCs	Dendritic cells
DDR	DNA damage response
DMSO	Dimethyl Sulfoxide
ECM	Extracellular matrix
Ecto	Ectodomain
EEA1	Early endosome antigen 1
EGFR	Epidermal Growth Factor Receptor

EMT	Epithelial to Mesenchymal transition
ER	Endoplasmic reticulum
FA	Focal Adhesion
F-Actin	Filamentous actin
FAK	Focal Adhesion Kinase
FBS	Fetal Bovine Serum
FN	Fibronectin
GAP	GTPase Activating Protein
GDP	Guanine Diphosphate
GEF	Guanine Exchange Factor
GFP	Green fluorescent protein
GSH	Glutathione
GSSH	Oxidized glutathione
GTP	Guanosine triphosphate
IFN-γ	Interferon γ
IgG	Immunoglobulin G
IL-13	Interleukin 13
IL-2	Interleukin 2
IL-4	Interleukin 4
IL-6	Interleukin 6
ILTR4	immunoglobulin-like transcript 4
IMP	Inosine monophosphate
IMPDH	Inosine-5’-monophosphate dehydrogenase
INF	Interferon
JAK3	Janus kinase 3
JAM	Junctional Adhesion Molecule
KD	Knockdown
KIF	Kinesin Family Member
KIF3A	Kinesin Family Member 3A

mAb	Monoclonal antibody
MAP	Microtubule Associated Protein
MAPK	Mitogen Activated Protein Kinase
MET	Mesenchymal to Epithelial Transition
MMPs	Matrix Metalloproteases
MPA	Mycophenolic acid
MT	Microtubule
NAD	Nicotinamide adenine dinucleotide
NADPH	Nicotinamide adenine dinucleotide phosphate
NF	Nuclear transcription Factor
NFκB	Nuclear factor kappa-light-chain-enhancer of activated B cells
NK	Natural killer cells
NMR	Nuclear Magnetic Resonance
NSCLC	Non-Small Cell Lung Cancer
PBD	Pyrrolobenzodiazepine
PBS	Phosphate Buffer Saline
PCN	Pericentrin
PCR	Polymerase Chain Reaction
PD-L1	Programmed death ligand 1
PD-L2	Programmed death ligand 2
PFA	Paraformaldehyde
PI3K	Phosphoinositide 3-Kinase
PPP	Pentose phosphate pathway
pRb	Retinoblastoma protein
PVDF	Polyvynilidine difluoride
RAB10	Ras-related protein 10
RAB11	Ras-related protein 11
Rac1	Ras-related C3 botulinum toxin substrate 1
Rho	Ras homologous

RhoA	Ras homolog family member A
ROCK	Rho-associated Protein Kinase
ROS	Reactive oxygen species
RR	Rods and Rings
RT-PCR	Reverse Transcriptase Polymerase Chain Reaction
sB7-H3	Soluble B7-H3
SCLC	Small Cell Lung Cancer
Shh	Sonic Hedgehog signalling
STAT	Signal Transducer and Activator of Transcription
STAT3	Signal transducer and activator of transcription 3
TAM	Tumour Associated Macrophage
TCA	Glycolysis/tricarboxylic acid cycle
TGFα	Transforming growth factor alpha
TGFβ	Transforming growth factor β
TIL	Tumour infiltrating lymphocytes
TJ	Tight junctions
TNF	Tumour Necrosis Factor
Tregs	T regulatory T cells
VHL	Von Hippel Lindau
ZO	Zonula occludens

Additional abbreviations:

mg – milligram

ml – millilitre

mM – millimolar

µg – microgram

µl – microliter

µM – micromolar

1. Introduction

1.1 Epithelial homeostasis and tumourigenesis

The majority of solid tumours arise from the epithelium and understanding this tissue type aides in determining ways in which cancer cells deviate from homeostasis to become malignant. Epithelia form a protective barrier for all the tissues that they encase (Slattum & Rosenblatt, 2014). The epithelium is polarised and comprises of an apical surface that faces the external environment and a basal surface that faces the basement membrane (Lee & Streuli, 2014). Epithelial integrity and homeostatic cell numbers are maintained by balancing cell death with dividing cells which is essential to survival, and many cellular mechanisms ensure these processes are maintained during growth and in response to damage (Lolo et al., 2012). For instance, when epithelial cells become overcrowded due to proliferation and migration, they induce extrusion of live or apoptotic cells to control epithelial cell numbers (Figure 1) (Eisenhoffer et al., 2012). This requires release of sphingosine-1-phosphate (S1P), which activates basal actomyosin contraction and apical extrusion from the epithelial sheet leading to apoptosis. Localised actomyosin contraction to the basal region of the cell is a result of Rho activation through the p115 RhoGEF, which is transported on microtubules to this region (Fan & Bergmann, 2008; Rosenblatt et al., 2001). Cancer driver mutations can promote basal cell extrusion towards the basement membrane, as well as apically, and invade through the extracellular matrix to metastasise (Figure 1) (Nikolaou & Machesky, 2020).

Cell competition is another mechanism the epithelial cells undergo to ensure removal of suboptimal cells. When a clone of mutant cells is surrounded by wild type cells, the mutant (less-fit) cells at the boundary undergo apoptosis and are replaced by the more-fit cells through compensatory proliferation. The cells sense relative fitness, such that 'super-competitor' neighbours will eliminate a clone of wild-type cells. Expression of an oncogene (driver genes) such as Ras, which would cause hyperproliferation but not invasive outgrowth, can drive invasion in the context of a polarity mutation. The mutant cells would normally be induced to undergo apoptosis by their more-fit neighbours, but the apoptotic signalling is

subverted by the oncogene into a proliferative state that can drive invasive tumourigenesis (Ayukawa et al., 2021; Vincent et al., 2013).

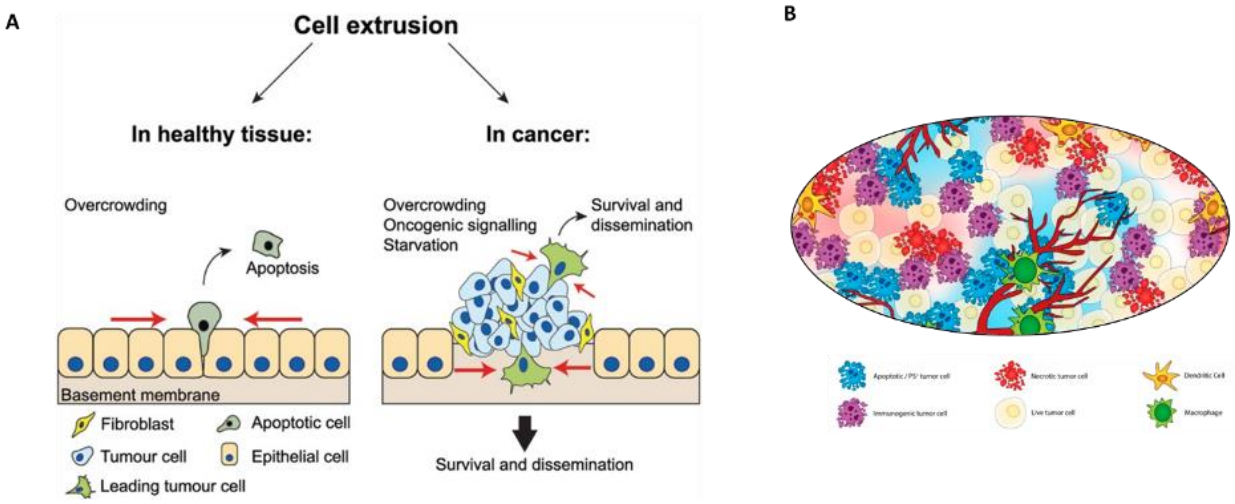

Figure 1: Cell extrusion in health and disease.
A) In healthy tissue, overcrowded cells can extrude apically from the epithelial monolayer and undergo apoptosis promoting efficient removal. In tumours, cancer cells - due to overcrowding, oncogenic signalling, and/or starvation - can be extruded either apically or basally towards the basement membrane and invade through the extracellular matrix to gain access to distant organs. **B)** Heterogeneity of cell death in solid tumours. Immunosuppressive, apoptotic cells (blue) promote immunosuppression and tumour growth and reside within the tumour core. Reproduced from (Nikolaou & Machesky, 2020; Gadiyar et al., 2020).

Tumourigenesis is the acquisition of malignant properties in normal cells: uncontrollable growth, metastasis, evasion of immunosurveillance and apoptosis, dysregulated metabolism and epigenetics, which are regarded as the hallmarks of cancer (Hanahan & Weinberg, 2011). Studies have discovered a large number of somatic gene mutations, that could be associated to these malignant phenotypes in cancer cells (Alexandrov & Stratton, 2014). Acquisition of mutations in tumour suppressor genes and oncogenes can cause these genes to change their expression levels or activities, ultimately leading to neoplastic transformation in normal cells (Domazet-Lošo & Tautz, 2010). Cancer develops in a multistep process known as carcinogenesis which consisting of initiation, promotion, progression, and metastasis (Figure 2). Initiation arises from alteration or mutation of genes, either spontaneously or through induction by exposure to a carcinogenic agent, resulting in dysregulation of biochemical signalling pathways associated with cellular process. The promotion phase is considered to be a reversible stage in which actively proliferating preneoplastic cells accumulate and chemo-preventative agents could be used to affect growth rates. Progression is the final

phase of neoplastic transformation before cells acquire invasive and metastatic potential, thereby enabling invasive cancer to occur. Finally, metastasis describes the spread of cancer cells from the primary site through the bloodstream or the lymph system to other organs/parts of the body (Siddiqui et al., 2015). There are currently no viable treatments to target metastasis, and this remains the key reason for cancer associated deaths.

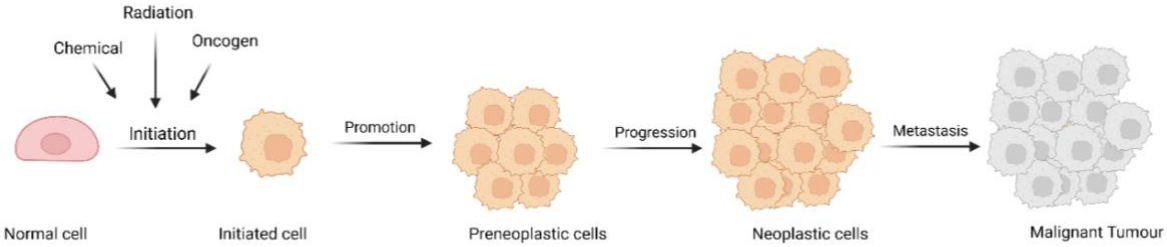

Figure 2: Steps of carcinogenesis.
Carcinogenesis starts with initiation caused by mutations of genes. The mutated initiated cell undergoes clonal expansion in a step called promotion. Acquisition of additional mutations enhances genome instability, leading to abnormal cell proliferation and growth. This results in progression which is the phase between a premalignant lesion and the development of invasive cancer. Metastasis involves the spread of cancer cells from the primary site through the bloodstream or the lymph system. Created with Biorender.com.

1.1.1 Cell proliferation and contributions to cancer progression

Cell proliferation is a fundamental requirement for development and homeostasis. The cell division cycle is a tightly controlled process resulting in precise DNA replication and segregation of duplicated chromosomes to daughter cells from a single parent cell. The cell cycle involves four consecutive stages: the synthesis (S phase), in which the cell replicates its DNA, mitosis (M phase), when the cell divides its replicated DNA into two daughter cells. Two gap phases (G1 and G2) separate DNA synthesis from mitosis; G1 is the cell resting phase which extends from mitosis to the next round of synthesis, while G2 is the gap between S and the next M phase, where cell growth and protein synthesis occurs (Lemmens & Lindqvist, 2019; Matson & Cook, 2017). Cells can also enter G0, which is the non-dividing phase of the cell cycle (Matson & Cook, 2017). A network of proteins known as cyclin-dependent kinases (CDKs) control the correct ordering of cell cycle progression and division. CDKs phosphorylate key substrates allowing DNA synthesis and mitotic progression. Activation of CDKs occurs by binding of cognate cyclin subunits (A,B,C,D,E). Cyclin/CDK activities can be interfered with by intracellular and/or external stimuli that stop progression of the cell cycle through a complex

network of signalling events (Ding et al., 2020). This pause in cell cycle progression is known as a "checkpoint", providing the cell time to repair damaged DNA or obtain necessary levels of growth factors prior to transitioning to the next phase. If the DNA damage is not repaired, the cell may trigger an apoptotic signalling cascade to prevent the transmission of damaged DNA to its new daughter cells. As a result, cell cycle checkpoints ensure ordered cell cycle progression, are vital for sustaining genomic stability, act as barriers to carcinogenesis, and are frequently deregulated in tumours (Figure 3) (Chao et al., 2017). The G1 checkpoint governs cell size, necessary nutrients, and presence of growth factors that are required for appropriate growth conditions, and it responds to DNA damage.

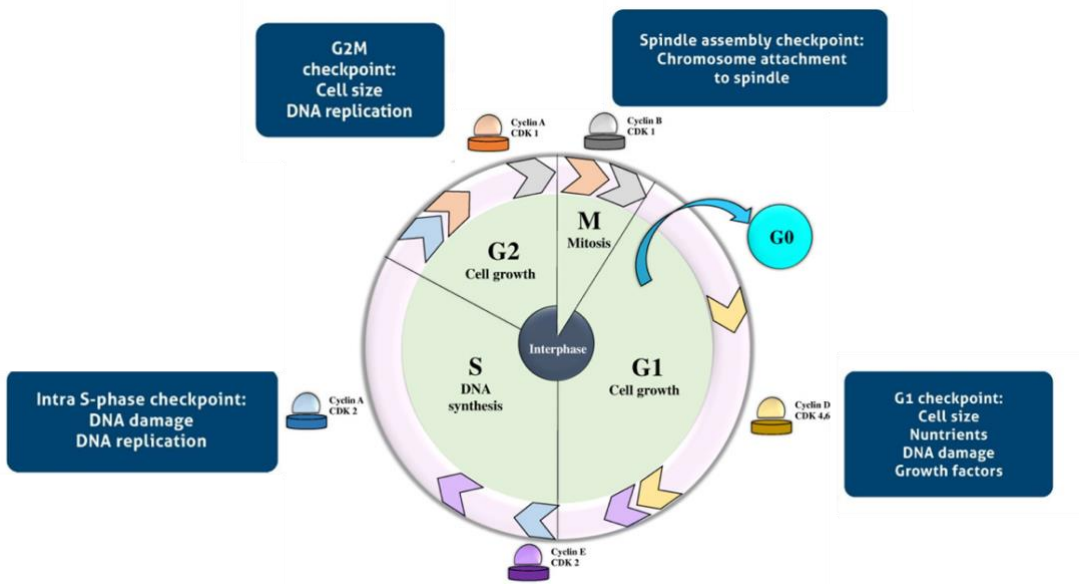

Figure 3: Cell cycle phases and checkpoints.
The cell cycle consists of four stages: Gap1 (G1), Synthesis (S), Gap2 (G2) and mitosis (M). Non-dividing cells exit the cell cycle and go into a quiescent state (G0). Progression through each stage of the cell cycle is controlled by association of specific cyclin dependent kinases (CDKs) with cyclins. Checkpoints enable cell division viability and fidelity. Adapted from (Sadeghi et al., 2020).

One major checkpoint that controls progression from G1 to S phase is the retinoblastoma tumour suppressor protein (pRb), and it inhibits transcription by chromatin remodelling. Phosphorylation of pRb occurs after receiving the right mitogenic cues, thereby becoming inactivated to allow cell cycle progression (Uchida, 2012). Checkpoints that respond to DNA damage occur pre- and post-S phase in G1 and G2 phases and affect the activity of key regulators of DNA damage signalling. These regulators are kinases phosphatidylinositol 3-

kinase (PI3K)-like protein kinases (PI3KKs), ataxia telangiectasia and Rad3-related (ATR) or ataxia telangiectasia mutated (ATM) protein, and the transducer checkpoint kinases CHK1 and CHK2. The DNA damage is detected by ATM/ATR, which then phosphorylates CHK2/CHK1, respectively. Activated CHK2 is involved in p53 activation, leading to p53-dependent early phase G1 arrest. If the DNA is unrepairable, the cells face apoptosis induced by p53 (Foster et al., 2010).

Proliferation in epithelial cells requires cell cycle regulation as well as co-ordination between interacting cells to organise division and reintegration into the epithelial monolayer. In this sense, epithelial cells must maintain adhesion contact with neighbouring cells and the basement membrane in an epithelial monolayer when dividing. Epithelial cells normally divide parallel to the plane of the monolayer, and this allows them to retain adhesion structures and cell polarity (Muthuswamy & Xue, 2012). The orientation of mitotic spindle in epithelial cells is dictated by extracellular matrix (ECM) adhesion formation (Pietro et al., 2016). During the division process, the nucleus migrates apically while forming an actin rich protrusion to maintain contact with the basal lamina (Ragkousi & Gibson, 2014). The dividing cell constricts in the middle and splits orthogonal to the plane of the monolayer (Figure 4) (le Bras & le Borgne, 2014).

However, mutations in genes involved in the regulation of proliferation - such as oncogene activation or tumour suppressor inhibition - can lead to tumour formation (Bower et al., 2017). Proliferation and clonal expansion of the mutated population of cells can occur due to selective pressures. These cells undergo apoptosis more readily due to instability, however additional mutations driving apoptosis inhibition can lead to uncontrolled proliferation and tumour formation (Labi & Erlacher, 2015; Ragkousi & Gibson, 2014).

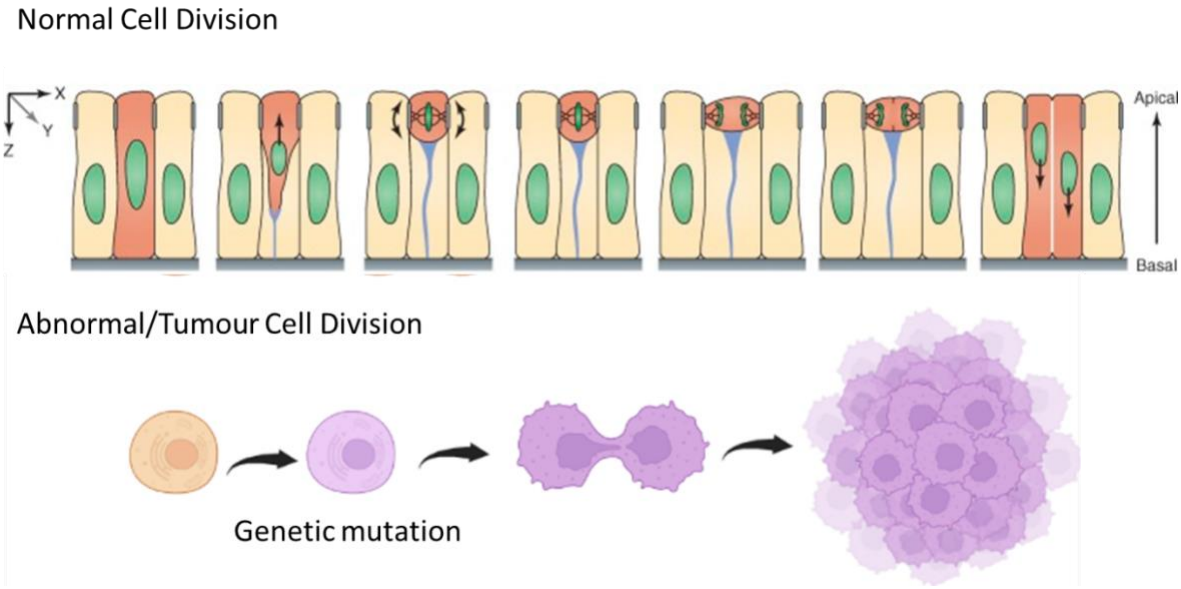

Figure 4: Cell division in an epithelial sheet.
Epithelial cells must sustain adhesion contact with neighbouring cells, as well as the basement membrane in an epithelial monolayer when dividing. Division initiation requires apical translocation of the nucleus and formation of an actin rich protrusion to maintain attachment to the basement membrane. Following division, the cells integrate into the monolayer and the nuclei of the daughter cells move towards the basal pole. In abnormal cells, genetic changes cause cells to divide more quickly than healthy cells, resulting in large numbers of cancer cells that loses cell-cell contact inhibition forming tumour without sustaining apical-basal plane. Normal cells adapted from (Ragkousi and Gibson, 2014) while cancer devision was created with Biorender.

1.1.2 Invasion and metastasis

Cancer metastasis is the spread of cancer cells to tissues and organs to form new tumours beyond its original site. For the tumour cell to successfully metastasise, a number of sequential events occur, termed the metastatic cascade. During the metastatic cascade, alterations in cell-cell and cell-matrix adhesion are important (Martin & Jiang, 2009). This multistep process can be broadly separated into three main events: invasion, intravasation and extravasation. The process of invasion mostly comprises of loss of cell-cell adhesion capacity and changes in cell-matrix interaction, allowing malignant cells to dissociate from the primary tumour mass and invade the surrounding stroma. This involves degradation of the basement membrane and extracellular matrix through the secretion of substances as well as the suppression or expression of proteins that control motility and migration (Hapach et al., 2019). The tumour must also initiate angiogenesis for the intravasation process to

develop. This process occurs through the blood vessels forming around the tumour to provide delivery of nutrients and oxygen to the tumour, and subsequent routes for the detached cells to enter the circulatory system and metastasise to distant sites (Zhong et al., 2020). Finally, the extravasation process starts when tumour cells interact with endothelial cells to penetrate the basement membrane and exit the vasculature, thus reaching the target organ where proliferation occurs and a new tumour is formed (Franssen et al., 2019).

1.1.3 Metabolic contributions to tumourigenesis

Cancer cells undergo complex metabolic rearrangements such as an increase in biosynthetic processes and energy production to support proliferation and cell growth (vander Heiden & DeBerardinis, 2017). Thus, changes in cell metabolism can contribute to tumour progression. Cancer-associated metabolic phenotypes include increased uptake of glucose and fermentation of glucose to lactate by a phenomenon known as Warburg effect (Liberti & Locasale, 2016). The glycolysis/tricarboxylic acid (TCA) cycle, pentose phosphate pathway (PPP) and amino acids uptake increase within the tumour microenvironment (TME) to build and sustain proliferation of cancer cells (Figure 5). Increased nutrient uptake via phagocytosis or micropinocytosis can also occur, alongside increased demand for nitrogen derivatives and their nucleotide conversions (pyrimidines, purines), and non-essential amino acids. Changes in metabolic driven gene regulations can occur by, methylation, acetylation, or metabolic interaction with the TME. This assists tumour growth through exchange of aminoamides, nutrients, secreted growth factors or environmental conditions such as redox stress, hypoxia, and alterations to the extracellular matrix and cell-cell interactions (Figure 6) (Läsche et al., 2020; Pavlova & Thompson, 2016). Tumour-hypoxia leads to advanced but dysfunctional vascularization and acquisition of EMT phenotype resulting in cell mobility and metastasis. Hypoxia alters cells metabolism and contributes to therapy resistance by inducing cell quiescence. Hypoxia stimulates a complex cell signalling network in cancer cells, including the HIF, MAPK, PI3K and NFκB pathways, which interact with each other causing positive and negative feedback loops and enhancing or diminishing hypoxic effects allowing cells to survive (Muz et al., 2015).

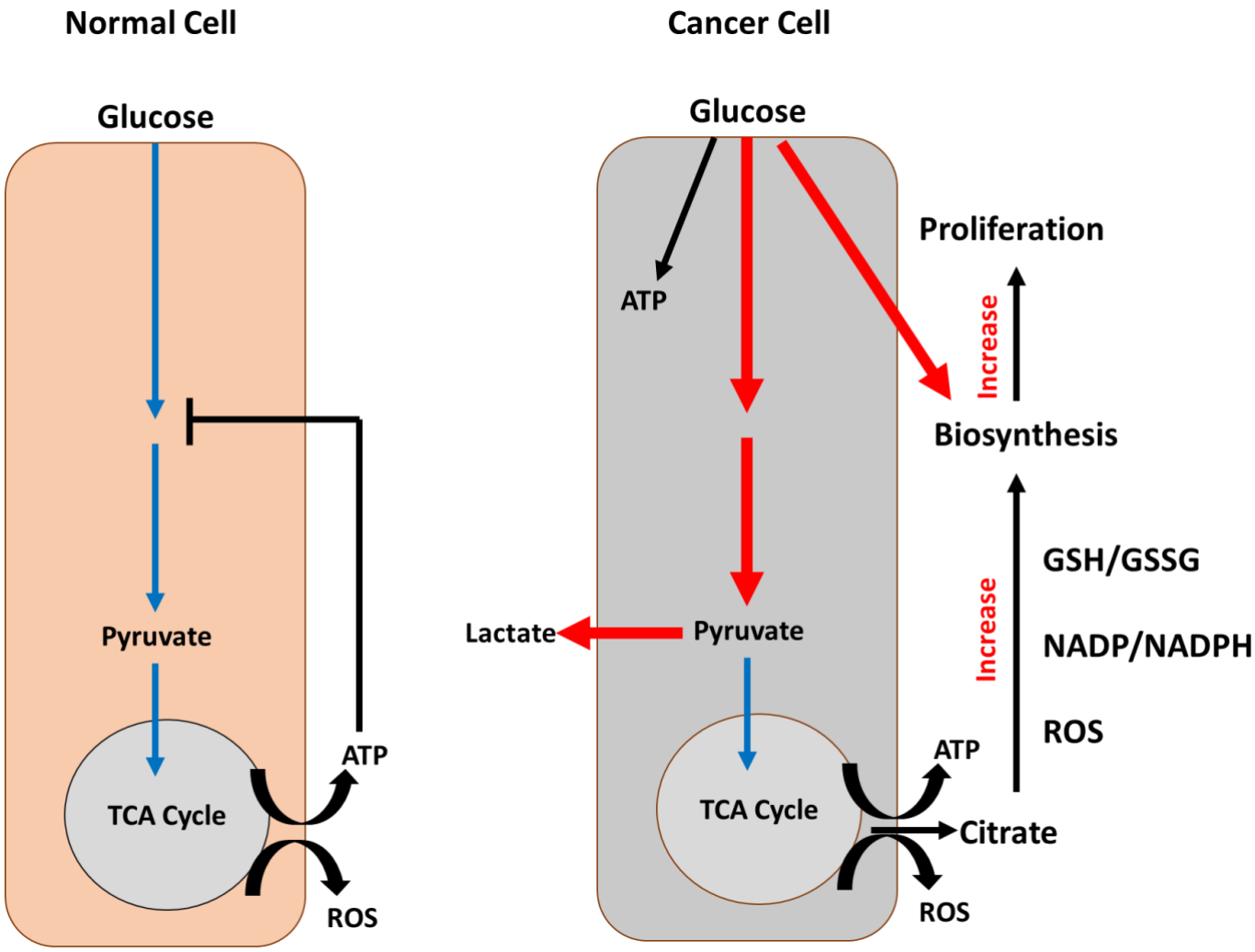

Figure 5: Schematic illustration of the glucose metabolism and changes in metabolites in normal/healthy and cancer cells.
Normal cells convert glucose to pyruvate via glycolysis, and the maximum amount of pyruvate is involved in mitochondrial oxidative process for efficient ATP production. Glucose is mainly used for cellular energy requirements. In normal cells, increased levels of ATP mitigate glycolysis by feedback inhibition. In cancer cells, glucose uptake increases and thereby so does glycolysis. A substantial part of glucose is utilized in biosynthetic pathways to support cell proliferation. Pyruvate is primarily used in lactate production. Oxidative phosphorylation occurs but is separated from augmented glycolysis. The amount of glucose carbon flux is indicated by relative thickness of arrows with red arrows in cancer cell to indicate increased levels. Key metabolism by-products and the metabolic effects on cancer are indicated in bold black arrows.

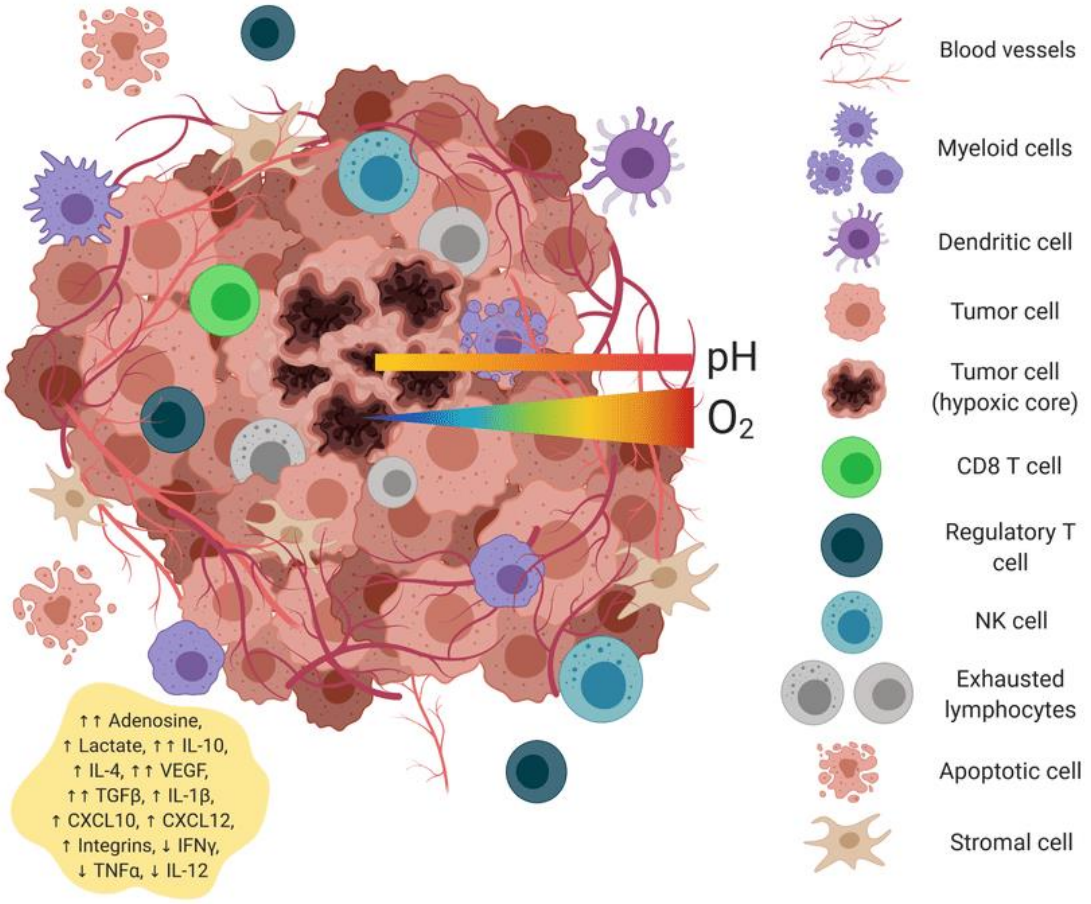

Figure 6: Metabolic interactions with the TME.
The tumour microenvironment is a complex system of heterogeneous tumour cells, stromal cells, and various immune cells residing in a network of poorly controlled vasculature and collagen. Densely packed glycolytic tumour cells and poor perfusion create compartments of reduced oxygen levels, acidic pH, malnutrition loads, chemokines, anti-inflammatory cytokines, and by-products metabolic accumulation, such as lactate. Reproduced from (Piñeiro Fernández et al., 2019).

1.1.3.1 Purine metabolism

Purines are the most abundant metabolic substrates providing building blocks for DNA and RNA. They provide the necessary energy and cofactors to support cell survival and proliferation. Therefore, purines and their derivatives play a key role in most biological processes, including immune responses (Virgilio & Adinolfi, 2017). High levels of purine metabolites have been discovered in tumour cells, which led to the development of the earliest anti-tumour drugs to treat cancers (purine antimetabolites) by blocking both DNA synthesis and cell growth (An et al., 2008). The basic mechanism of action for the purine and pyrimidine antimetabolites including the FDA approved decitabine, nelarabine and vidaza is

similar (Zhang et al., 2007). These compounds, usually with the aid of a membrane transporter, diffuse into cells and are converted to analogues of cellular nucleotides by enzymes of the purine or pyrimidine metabolic pathway. These metabolites then inhibit one or more enzymes that are essential for DNA synthesis, initiating DNA damage and apoptosis (Parker, 2009; Sampath et al., 2003).

Purine metabolism provides cellular pools of adenylate and guanylate through synthesis and degradation of purine nucleotides (Yin et al., 2018). Syntheses of purines occurs by two different pathways: the complementary salvage pathway and *de novo* biosynthetic pathway (Figure 7). The salvage pathway accounts for most of the cellular requirements and recycles the degraded bases (such as guanine, hypoxanthine, adenine) or purine nucleoside (guanosine, inosine, adenosine) producing purine mononucleotide (guanin monophosphate (GMP), inosine 5'-monophosphate (IMP), adenosine 5'-monophosphate (AMP)). There are three ATP biosynthesis salvage pathways: (i) adenine and phosphoribosyl pyrophosphate (PRPP) association to produce AMP by adenine phosphoribosyl transferase; (ii) adenosine kinase directs phosphorylation of adenosine to AMP; and (iii) union of hypoxanthine and PRPP by hypoxanthine phosphoribosyl transferase-1 (HPRT1) to produce IMP, which gets converted to AMP (Li et al., 2015). On the other hand, in the GTP salvage biosynthesis pathway, hypoxanthine or guanine is enzymatically merged with PRPP to produce IMP or GMP, respectively, through HPRT1. The *de novo* GTP and ATP biosynthesis pathways have converting glucose to IMP in common. However, deviation occurs at the IMP substrate where Inosine monophosphate dehydrogenase (IMPDH) and adenylosuccinate synthase (ADSS), form synthesis of GTP and ATP, respectively (Kofuji & Sasaki, 2020) (Figure 7).

Purines and the *de novo* purine biosynthetic pathway enzymes are enhanced in tumour cells (Barfeld et al., 2015). For example, changes in the adenosine to inosine ratio has been found in cancer cells, impacting growth, invasiveness, and metastasis (Shoshan et al., 2015). Purines play a role in modulating immune cell response to cytokine release and are thereby involved in the development of oncogenesis and tumourigenesis (Alvarado *et al*., 2017). In tumour cells, levels of GTP can increase via upregulation of IMPDH compared to that of normal cells

(Naffouje et al., 2019). This activity of IMPDH2 can be supressed by inhibitors such as mycophenolic acid (MPA) (Sobiak et al., 2020) (Figure 7).

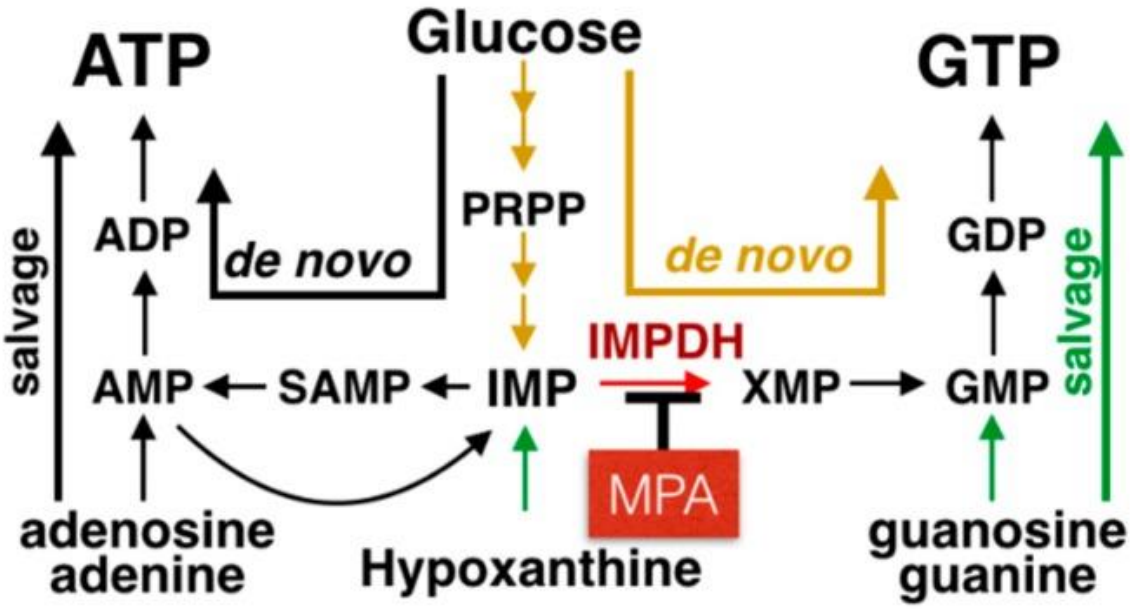

Figure 7: Purine pathways and MPA mechanism of action.
Purine metabolism includes *de novo* and salvage pathways. The *de novo* purine biosynthetic pathway catalyses the transformation of PRPP into IMP via highly conserved steps (yellow). Purine salvage recycles hypoxanthine, guanine, and adenine as substrates to generate purine nucleotides (green). MPA is a potent selective and non-competitive inhibitor of IMPDH, which catalyses the NAD-dependent oxidation of IMP to XMP, an intermediate metabolite in the production of GTP. Adapted from (Naffouje et al., 2019).

1.1.3.2 IMPDH

IMPDH is a rate-limiting enzyme in the *de novo* biosynthesis of purine nucleotides that it is essential for DNA synthesis (Dostalek et al., 2013). IMPDH is involved with cell growth, differentiation and malignant transformation (He et al., 2018). IMPDH has two isoforms, IMPDH1 and IMPDH2, which are encoded by different genes with 84% of their amino acid sequence conserved (Floryk et al., 2004). IMPDH2 is highly expressed in malignant cells, upregulated during proliferation, and can mediate cisplatin chemoresistance and radio-resistance in osteosarcoma cells (Hedstrom, 2009; Jain et al., 2004; Li et al., 2014).

IMPDH2 can assemble into linear or circular micron scale structures referred to as rods and rings (RR) (Carcamo et al., 2011; Gunter et al., 2008). RR assembly correlates with deficiency

in GMP/GTP synthesis and decreased IMPDH2 activity (Carcamo et al., 2011). Therefore, IMPDH2 inhibitors such as MPA or ribavirin can induce rapid formation of RR (Ji et al., 2006; Keppeke et al., 2016). RRs were first discovered following an observation in chronic hepatitis C infection patients treated with a combination of ribavirin and interferon α. These patients developed autoantibodies against structures (later named RR) that react with IMPDH2 (Covini et al., 2012; Seelig et al., 2011). However, RR are not associated with any known organelles (Covini et al., 2012). The function of RR remains controversial, they were initially considered to be a cellular response to increased guanine nucleotide synthesis (Carcamo et al., 2014). However, subsequent studies have shown that IMPDH2 point mutations that promote, or block polymerisation do not affect its activity and that both active and inactive forms of IMPDH2 can aggregate into RR (Anthony et al., 2017). Other work has demonstrated that RR assembly is important for maintaining normal cell proliferation and the GTP pool (Keppeke et al., 2018). Studies on IMPDH2-mutant HeLa cells unable to form RR have also shown IMPDH2 suppression correlates with RR formation and maintenance of normal cell proliferation, suggesting that IMPDH2 polymerization acts as IMPDH2 activity booster (Keppeke et al., 2018). Thus, the role and regulation of IMPDH2 in RR remains unclear, in both normal epithelial and cancer cells (Chang et al., 2015).

1.1.3.3 Oxidative stress

Aberrant cell growth in cancer cells can drive increased metabolism and elevate basal levels of reactive oxygen species (ROS) compared to normal cells. As a result, cancer cells are constantly under oxidative stress (Aboelella et al., 2021). ROS are by-products of cellular respiration, and aerobic metabolism, and are pathologically increased in diseases such as inflammation and cancer. Mitochondria are the main cellular source of ROS production (Zhang & Wong, 2021). ROS can also be produced via endoplasmic reticulum (ER) through the catalytic process of oxidoreductase Ero1 and NADPH oxidase (NOX) (Arfin et al., 2021). Imbalances in redox pairs, such as reduced nicotinamide adenine dinucleotide phosphate hydrogen NADPH/NADP+ or oxidized glutathione GSH/GSSG ratios, lead to elevation of enriched oxygen atoms molecules thereby making them markers of oxidative stress (Figure 8) (Lipinski, 2011) . Peroxisomes can rapidly produce and scavenge H2O2 and O2 (.-) which allows dynamic regulation changes in ROS levels (Sandalio et al., 2013). Moreover, ROS can

be exogenously induced upon exposure to chemotherapy, radiotherapy, or UV (Shah & Rogoff, 2021).

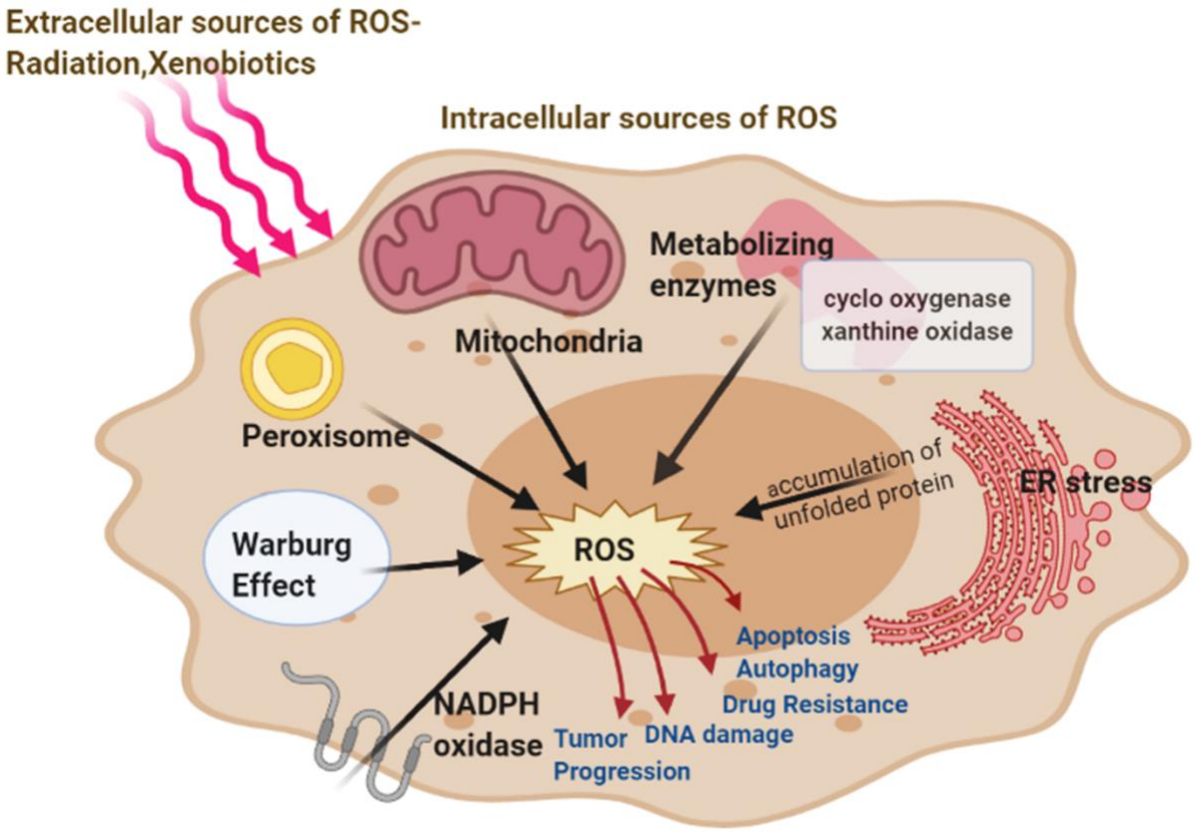

Figure 8: Major Sources of ROS in cells.
Generation of ROS can be produced intercellularly via mitochondria, peroxisomes, ER stress, NADPH oxidase, metabolizing enzymes, and extracellular factors (Radiation, Xenobiotics). ROS are involved in cancer, causing development and progression of the disease. Reproduced from (Arfin et al., 2021).

At low to medium levels, ROS can act as signalling messengers to regulate cellular gene expression, proliferation and differentiation, and immunity against diseases. At high levels however, ROS can cause oxidative DNA damage and can be detrimental to cells (Figure 9). Due to the complex role of ROS in cell survival and function, levels and balance between ROS production and scavenging must be tightly regulated to maintain the redox homeostasis. When this balance is disrupted in cells, oxidative stress occurs (Chio & Tuveson, 2017; Reczek & Chandel, 2017) . In cancer cells, the deregulation in ROS occurs due to abnormal cellular activity such as increased metabolism, oncogene activation, tumour suppressor gene inactivation and adaptation to hypoxia (low oxygen levels) (Chio & Tuveson, 2017; Liou &

Storz, 2010) . This can facilitate chemoresistance, angiogenesis, metastasis and epithelial to mesenchymal transition (EMT), which occurs due to increased activity of matrix metalloproteinases (MMPs) mediating degradation of extracellular matrix (ECM) components (Binker et al., 2009; Ushio-Fukai & Nakamura, 2008; Wu, 2007) . EMT is a highly dynamic process, by which epithelial cells can transform into a mesenchymal phenotype defined by prototypical markers. EMT is not complete in cancer cells as tumour cells are in multiple transitional states and express mixed epithelial and mesenchymal genes. Such hybrid cells in partial EMT can move as clusters collectively and can be more aggressive than cells with a complete EMT phenotype (Marcucci et al., 2016). The process of EMT involves the disruption of cell–cell, cell-matrix adhesion and cellular polarity and remodelling of the cytoskeleton. It is associated with improvement in migratory and invasive properties. In cancers, EMT inducers are hypoxia, cytokines, and growth factors secreted by the tumour microenvironment, stroma crosstalk, metabolic changes, innate and adaptive immune responses, and treatment with antitumor drugs (Roche, 2018).

ROS are important signal mediators in the tumour microenvironment involved in T cell and natural killer cell (NK) activation and subsequent detection/destruction of transformed cells. However, cancer cells can induce tumour-promoting immune cells including regulatory T cells (Tregs), tumour-associated macrophages (TAMs) and myeloid-derived suppressor cells (MDSCs), causing chronic inflammation that can promote cancer progression (Kennel & Greten, 2021). This positive feed-back loop occurs between oxidative stress and inflammatory mediators, shaping the outcome of anti-tumour immune responses (Valacchi et al., 2018). As a result, cancer cells and immunosuppressive cells use ROS in the TME - along with other mechanisms - to create immune tolerance to tumours (Chen et al., 2016; Franchina et al., 2018; Nathan & Cunningham-Bussel, 2013). Cancer cells constantly attempt to enhance their antioxidant defence capacity to counteract excess ROS (Ishimoto et al., 2011). Epithelial cells, primary cells and tissues of mice overexpressing oncogenes at early stages of tumour progression display lower pro-oxidant level and higher antioxidant potential (DeNicola et al., 2011). The subsequent reductive environment promotes proliferation and survival of transformed or cancerous cells and is consequently a promising therapeutic target for cancer treatment and prevention. However, the therapeutic efficacy of anticancer drugs can be

influenced by the cooperation among components that maintain the redox environment of cells. Even though chemotherapeutic agents are expected to kill cancer cells through production of ROS, this can eventually facilitate drug resistance (Masella et al., 2005). Interestingly, a reductive redox environment has been reported to facilitate cancer migration and metastasis (Figure 9). This indicates that tumours adapt to the high threshold of ROS by altering their microenvironment to more reductive conditions (Liu et al., 2016).

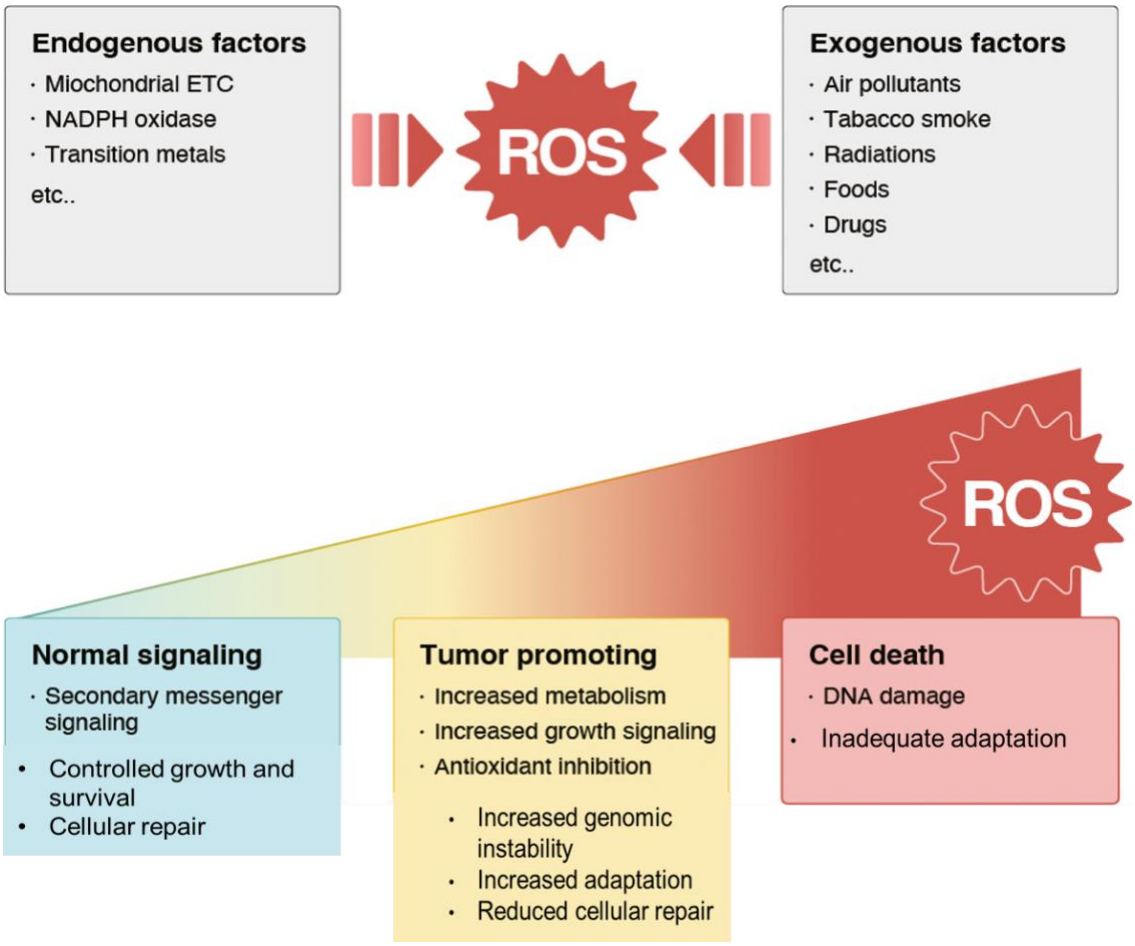

Figure 9: ROS and cancer paradox.
Healthy cells have adequate adaptations to overcome the harmful effects of ROS. Balanced generation of ROS, sufficient cellular repair and antioxidant activity result in controlled cell survival and proliferation. Metabolic activity of tumour cells produces high ROS levels, increasing cell survival and proliferation. This leads to DNA damage, reduced cellular repair by DNA damage repair pathways and genetic instability. Elevated ROS concentrations can cause cellular damage, however, cancer cells readjust with adaptations to conditions including hypoxia and also through initiation of cellular repair pathways. Tumour cells maintain pro-tumourigenic signalling with increased antioxidant activity to remove excessive ROS. If ROS concentrations increase radically to toxic ROS levels, for example by chemotherapy, oxidative stress causes irreparable damage to the cell, reduced adaptations and eventually cancer cell death. Adapted from (Nakamura & Takada, 2021).

1.2 Lung Cancer

In the last century, lung cancer has progressed to the most common type of cancer and most common cause of cancer fatality in the world (Groot et al., 2018). The poor prognosis of lung cancer can be attributed to late diagnosis (Saab et al., 2020). Although cigarette smoking remains the main risk factor of lung cancer (Walser et al., 2008), it can also develop due to environmental factors, workplace exposures to carcinogens, and chronic lung disease (Alberg et al., 2002). Despite recent improvements in survival for many cancers, lung cancer has a relatively poor 5-year survival rate (Li et al., 2022). Treatments include chemotherapy, surgery, radiation, targeted therapy and immunotherapy (Zappa & Mousa, 2016). The field of targeted therapy and immunotherapy have shown promising results of improved survival benefits in lung cancer treatment leading to better development of treatments (Shahid et al., 2019). However, many patients remain refractory to treatment and the reasons for this remain unclear.

1.2.1 Lung cancer subtypes

Lung cancer is classified into 2 types based on biological characteristics: Small Cell Lung Cancer (SCLC) and Non-SCLC (NSCLC) (Lemjabbar-Alaoui et al., 2015). SCLCs represent around 15% of all lung cancers and are neuroendocrine carcinomas characterised by high proliferative rates and early metastasis, with most patients having metastatic cancer at diagnosis and a poorer 5-year survival rate than those affected by NSCLC (Rudin et al., 2021). Current clinical treatment of SCLC can include surgery, radiation and adjuvant platinum-based chemotherapy for the rare occasions where the disease is diagnosed early. Patients with late metastatic stage are treated with systemic chemotherapy with or without immunotherapy (Hiddinga et al., 2021). NSCLC accounts for approximately 85% of lung cancers and is classified into three major subtypes: adenocarcinoma, squamous cell carcinoma and large cell carcinoma (Zappa & Mousa, 2016). Adenocarcinoma is the most common type of lung cancer and comprises around 40% of all diagnoses. It develops in the periphery of the lung from small airway epithelial type II alveolar cells, which secrete mucus and other substances (Herbst et al., 2018). Squamous-cell carcinoma arises from early squamous cells in the bronchial airway in the centre of the lungs and comprises of 25–30% of all lung cancer cases. (Perez-Moreno et

al., 2012). Large cell carcinoma (undifferentiated) is often diagnosed by default through exclusion of other possibilities and accounts for 5–10% of lung cancers (Kenfield et al., 2008).

1.2.2 Common genetic mutations associated with lung cancer

Determining the molecular basis of cancer requires extensive analyses of specific genes and pathways or by genome-wide association studies (GWAS) which have revealed that histologically apparent lung cancers can harbour multiple genetic and epigenetic alterations (Larsen & Minna, 2011). Clinical management of NSCLC has incorporated tumour genotyping with routine testing for KRAS, EGFR, BRAF, ALK, and PD-1. Targeting appropriate molecular biomarkers in tumours has helped improve survival in NSCLC patients (Riely et al., 2009; Villalobos & Wistuba, 2017). The most frequently mutated oncogene in NSCLC is the KRAS G12C (glycine 12 to cysteine) mutation encoding a GTPase that cycles between active (GTP-bound) and inactive (GDP-bound) form, with KRAS mutations inhibiting GTPase activity and favouring the active form (Reita et al., 2022). GTP-bound RAS activates a number of cellular signalling cascades including the RAS-RAF-MEK-ERK pathway, which regulates cell-cycles and proliferation. Another pathway involved is PI3K-AKT-mTOR, which controls cell survival (Addeo et al., 2021). EGFR is a tyrosine kinase cell-surface receptor that can activate cell growth and proliferation associated pathways when activated (Lynch et al., 2004). EGFR gene mutations present in 10–15% of lung cancer adenocarcinomas and drive constant activation of uncontrolled cell division (Pao *et al*., 2004). BRAF is a regulated signal transduction serine/threonine kinase that promotes cell proliferation and survival (Cardarella et al., 2013). BRAF mutations have been found in patients with adenocarcinomas and accounts for 1–4% of all NSCLC (Brose et al., 2002; Pratilas et al., 2008). ALK mutations comprises of 3–7% of all lung tumours arising from rearrangements on chromosome 2p23 due to the fusion between 3’ end of the ALK gene and the 5’ end of the EML-4 gene (Koivunen et al., 2008; Soda et al., 2007). PD-1, programmed death, is an immunotherapy marker in lung cancer expressed mainly on T cells and mediates immune suppression, while its ligand is expressed on tumour cells and tumour inflammatory infiltrating cells including macrophages, dendritic cells, and T cells (Seetharamu et al., 2016). Clinical trials in NSCLC have shown sustained responses in approximately 20% of patients treated with monoclonal antibodies that target the interaction between PD-1 and its ligands PD-L1 and PD-L2 (Brahmer, 2014).

1.3 Epithelial cell adhesion and sensing

Epithelia are sheets of cells organised as mono or multilayers. They form robust tissues that serve as barriers to support the structure and regulate molecular transport in functionally diverse organs, such as lung, kidney, gut, and epidermis (Miller et al., 2013). Epithelial dynamics play an important role in development and wound healing, as well as during carcinogenesis (Lai et al., 2020; Pastar et al., 2014; Thowfeequ et al., 2022). Epithelial cells characteristically exhibit cell-cell adhesions that are vital for maintaining tissue integrity and polarity. These adhesions are mediated by distinctive structures, mainly tight junctions (TJ), adherens junctions (AJ), and desmosomes (Figure 10) (Noronha et al., 2021).

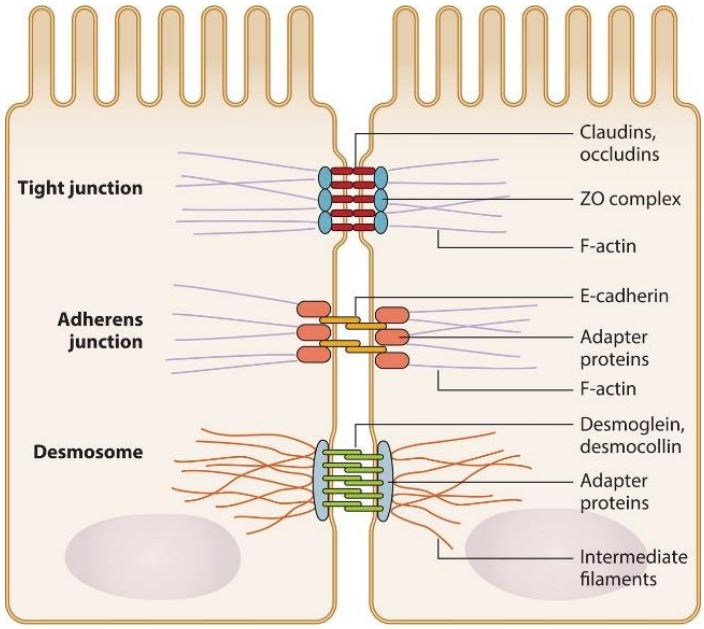

Figure 10: Epithelial adhesion structures at cell-cell junctions.
Adjacent epithelial cells are held together by junctional complexes. Tight junctions at the apical end and are comprised of claudin and occludin proteins that extend over the intercellular space and bind intracellular adapter proteins, such as zonula occludens (ZO). Adherens junctions are formed of E-cadherins and adapter proteins (catenins). Desmosomes are composed of desmoglein and desmocollin proteins that bind internal adapter proteins. Adapter proteins associated with tight junctions, adherens junctions, and desmosomes in turn bind to cytoskeleton components, including F-actin or intermediate filaments. Reproduced from (Hudson et al., 2017).

1.3.1 Tight junctions

TJ serve as barriers for the cell, which restrict entry of molecular transport via active transport in normal cells (Anderson & van Itallie, 2009). TJs are important for maintaining cell polarity

and play a role in signalling cascades with control over differentiation, growth, and development (González-Mariscal et al., 2003). TJs confer polarity of the cell by demarcating the cells apical (upper) and basal (lower) domains. The main proteins involved in formation and maturation of TJs are occludins, claudins and junctional adhesion molecules (JAM) (Balda & Matter, 2009). Other TJ proteins including Zona occludens (ZO-1, ZO-2, ZO-3) are scaffolding proteins connecting the actin cytoskeleton to transmembrane proteins, as well as forming a link between the AJ and TJ (Guillemot et al., 2008; Hartsock & Nelson, 2008). ZO proteins form the central protein interactions, with three different ZO proteins that share structural features; Src homology 3 (SH3) domain, N-terminal region with 3 PDZ domains, and guanylate kinase (GUK) domain (Doi et al., 2012). Downregulation of ZO-1 has been reported to increase motility in several types of cancer (Doi et al., 2012). However, upregulation of ZO-1 has also been reported in melanoma cells (Smalley et al., 2005). Disruption of TJs due to mutations, inflammation or aberrant signalling mechanisms disturbs proper cell functions and subsequently results in diseases including cancer (Resnick et al., 2005).

1.3.2 Adherens junctions

Adherens junctions (AJ) facilitatesmultiple functions including initiation and stabilisation of cell-cell adhesion, intracellular signalling, transcriptional regulation and modulation of the actin cytoskeleton. Interactions among transmembrane glycoproteins such as the cadherin superfamily (including E-cadherin) and catenin family members (including p120-catenin, β-catenin, and α-catenin) control the formation, maintenance, and function of AJ (Hartsock & Nelson, 2008). E-cadherin is Ca^{2+}-dependent transmembrane receptor and a member of the cadherin family that also includes N-, P, and R-cadherin (Halbleib & Nelson, 2006). Cadherins have extracellular cadherin (EC) domains that form *in trans* interactions between neighbouring cells and initiate weak cell-cell adhesion (Gooding et al., 2004). EC domain binding to Ca2+ is required for the right conformational organisation of the cadherin extracellular domain and adhesion (Patel et al., 2006; Pokutta et al., 1994). The cytoplasmic domain of E-cadherin regulates its endocytosis, recycling and degradation, intracellular signalling, and local control of the actin cytoskeleton through binding to specific proteins. Within the cytoplasmic domain of E-cadherin, there are two catenin binding domains. They encompass a 94 amino acid juxtamembrane domain that binds p120-catenin, and a C-

terminal extended region that binds β-catenin in a phospho-regulated manner (Aberle et al., 1994; Yap et al., 1998). These proteins recruit and organize actin filaments. cadherin-β-catenin complex binds to *α*-catenin that bridges these components to actin. Many actin binding proteins have been reported to bind *α*-catenin, including vinculin and *α*-actinin, suggesting that they could also link the cadherin-catenin complex to the actin cytoskeleton (Drees et al., 2005). Reduction in E-cadherin expression leads to defects in localisation of α- and β-catenin, and the tight junction protein ZO-1, leading to loss of barrier integrity (Capaldo & Macara, 2007). Catenins provide a link between cadherin and the actin cytoskeleton (Harris, 2012). In addition to playing a structural role in stabilising cell-cell junctions and forming polarised epithelial tissues, cadherin-catenin complexes play a key role in activating multiple signal transduction pathways. β -catenin is a critical regulator in the Wnt signalling cascade, where cytoplasmic β-catenin moves to the nucleus and functions as a transcription factor that results in subsequent cellular effects including cellular adhesion, tissue morphogenesis and tumour development (Valenta et al., 2012). Loss of cadherin-mediated cell adhesion can promote β-catenin release and thus its signalling activity (Heuberger & Birchmeier, 2010).

1.3.3 Focal Adhesions

Focal adhesions (FA) are plaques formed at the plasma membrane, where integrin transmembrane receptors interact indirectly with the actin cytoskeleton inside the cell and with the extracellular matrix (ECM) on the outside of the cell (Belvitch *et al*., 2018). FA-mediated adhesion regulates several cellular processes including proliferation, differentiation, anchorage-dependent survival, and migration (Burridge, 2017). Connections between FA and the ECM require recognition by integrins of specific peptide motifs, such as Arg-Gly-Asp (RGD) in proteins such as fibronectin, vitronectin, and fibrinogen (Ludwig et al., 2021; Schwartz, 2010; Wheaton et al., 2016). Integrins are transmembrane heterodimers formed from one beta and one alpha subunit, and their corresponding ligands categorise these receptors into four groups: RGD receptors, laminin receptors, collagen receptors and leukocyte-specific receptors (Gardel et al., 2010). The cytoplasmic intracellular domains of integrins can bind to the cytoskeleton via adapter proteins such as vinculin, talin, α-actinin, filamin, and tensin. Non-receptor tyrosine kinases, such as focal adhesion kinase (FAK) and Src, bind to and mediate integrin-adapter protein–cytoskeleton complex formation,

which is important during adhesion formation and maturation as these forms the basis of a focal adhesion (Tucker & Adams, 2014). The assembly and disassembly of FA play a key role in cell migration. The composition and the morphology of the FA changes in a migrating cell. Initially, at the leading edge of the cell (lamellipodia), small FA called focal complexes (FXs) are formed which consist of integrins and adapter proteins (Geiger & Yamada, 2011). Many FXs are transient in nature and fail to mature so are disassembled as the lamellipodia retracts. However, some FXs mature into stable and larger FAs, and recruit more proteins to the FA in a sequential manner to support formation of a more stable structure connected to f-actin stress fibres. Once in place, cells use mature FA as an anchor to support migration (Stutchbury et al., 2017). Aberrant expression and altered functions of FA proteins contribute to tumourigenesis and metastasis (Yam et al., 2009).

1.3.4 Changes to adhesion types in cancer

Maintenance of epithelial cell-cell adhesion is crucial for tissue homeostasis and the dysregulation of cellular adhesion promotes malignant transformation and metastasis (Morris et al., 2008). It is generally thought that for cancer cells to metastasise, interactions between cell-cell need to be disturbed via regulation of adhesion molecules (Okegawa et al., 2004; Martin & Jiang, 2009). Epithelial–mesenchymal transition (EMT) is a cellular mechanism vital for embryogenesis, wound healing and cancer progression (Knights et al., 2012). Reduced cell-cell adhesion has been implicated in pathological EMT, leading to oncogenic transformation and metastasis. Upon EMT activation, the expression of E-cadherin (AJ) and certain cytokeratins is suppressed, which leads to the loss of the typical polygonal morphology of epithelial cells (Lamouille et al., 2014). The cells acquire a more mesenchymal morphology and express markers that are associated with the mesenchymal cell state, notably neural cadherin (N-cadherin), fibronectin, vimentin and β3 integrins (Loh et al., 2019). Subsequent degradation of the basement membrane enables cell invasion into the neighbouring stroma (Chang & Chaudhuri, 2019). Binding of E-cadherin between cells is important in mediating contact inhibition of proliferation when cells reach confluence. Loss of E-cadherin expression leads to loss of contact inhibition and is associated with increased cell motility and advanced stages of cancer (Mendonsa et al., 2018). Although most previous studies have suggested that reduced E-cadherin is the hallmark of EMT, more recent analysis

has shown that the loss of E-cadherin is not essential for EMT and that rescuing E-cadherin expression in E-cadherin negative malignant cells did not reverse EMT (Hollestelle *et al*., 2013). Other recent studies have argued that cells can undergo partial EMT where E-cadherin can enhance cell survival during metastasis and promote resistance to anti-cancer drugs (Saitoh, 2018). One of the key pathways involved in EMT is the Wnt/β-catenin pathway (Mylavarapu et al., 2019). β-catenin (AJ) can act as a transcription factor upon induction to translocate to the nucleus and activate β-catenin-mediated transcription via the Wnt signalling pathway, promoting malignancy phenotypes (Bian et al., 2020). β-catenin can also activate zinc finger E-box binding homeobox 1 (ZEB1) leading to reduction in expression of TJ and AJ proteins such as Claudin 7 and E- cadherin (Kim et al., 2019). TJ proteins are also involved in EMT, with ZO-1 originally considered as a tumour suppressor with reported loss of expression in breast or colorectal cancers (Kaihara et al., 2003; Martin & Jiang, 2009; Neyrinck-Leglantier et al., 2021). However, overexpression of ZO-1 has also been found in different types of cancers including gastric, pancreatic or melanoma (Kleeff et al., 2001; Resnick et al., 2005; Smalley et al., 2005). Thus, the balance of TJ and AJ protein expression can play key roles in regulating development of a range of cancer types.

1.3.5 Primary cilia in normal epithelia and cancer

1.3.5.1 Structure and role

The primary cilium is a microtubule-based organelle that protrudes from the surface of many cell types (Bisgrove & Yost, 2006). The primary cilium is an immotile structure comprised of 9 outer microtubules with no inner microtubules, differing from motile cilia that have 9 outer and 2 inner microtubules arrangements (Figure 11) (Gluenz et al., 2010). Primary cilia consist of an axoneme that extends from a basal body anchored in the cell, which is derived from the mother centriole. The mother centriole is crucial for the formation of the centrosome, as it serves as component of the centrosome and microtubule organizing centre prior to ciliation (Kim & Dynlacht, 2013). Cilia assembly is dynamically regulated during cell cycle progression; they are present during G0 and G1, and usually in S/G2, but are resorbed preceding entry into mitosis (Izawa et al., 2015). Therefore, there is a negative correlation between the presence of the primary cilia and cell proliferation. If the cell is dividing, the centrosome acts as the mitotic pole as the cilium retracts into the cell (Goto et al., 2013). Resorption involves the

regulation of intraflagellar transport (IFT), the mechanism that controls the growth and maintenance of the cilium and the de-acetylation of axonemal microtubules via the transport of proteins up the axoneme (Pugacheva et al., 2007). IFT trafficking to the cilium from the base of the cilium to the tip is a highly coordinated process that is heavily dependent on kinesin superfamily proteins (KIFs). One of the most highly expressed KIFs in cells is KIF3 which is crucial for ciliogenesis and cilia maintenance (Lancaster & Gleeson, 2009).

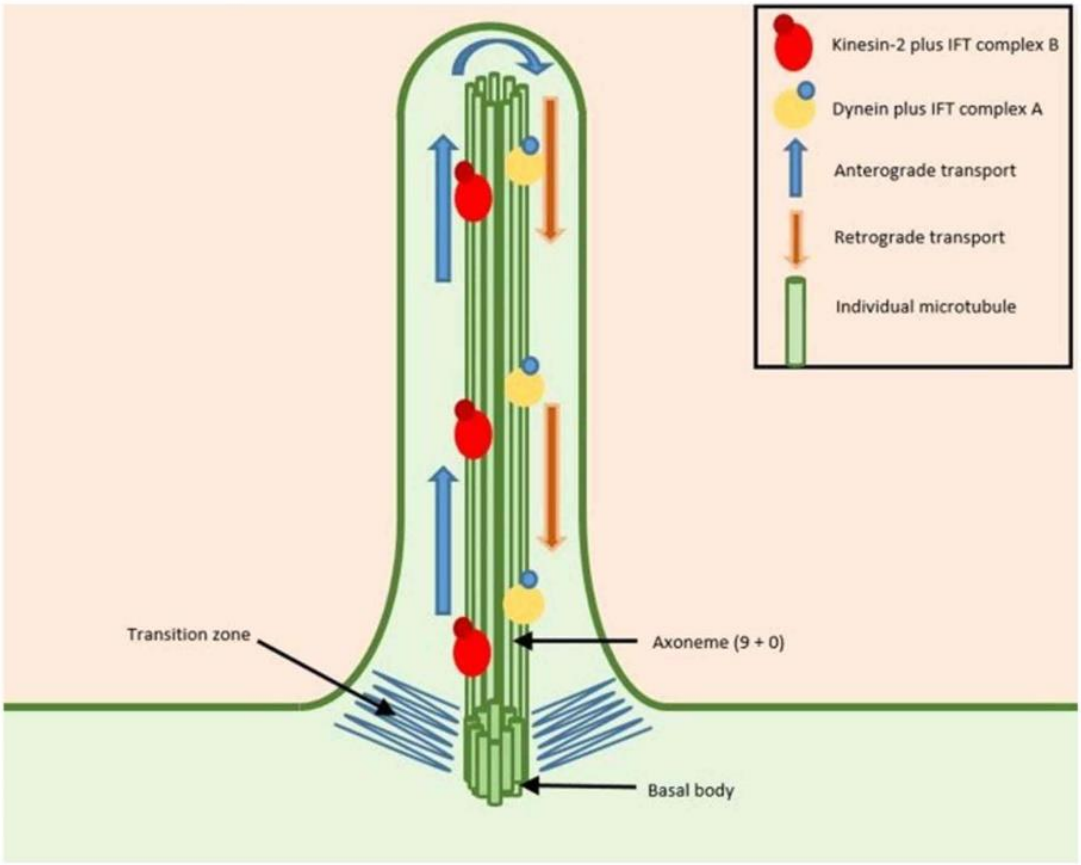

Figure 11: Structure of the primary cilium.
The primary cilium is formed in a process termed IFT. The primary cilium consists of an axoneme formed around 9 outer microtubule doublets and no inner microtubules (9+0). Trafficking of transport channels and ciliary proteins are directed from the bottom of the cilium to its tip (Anterograde); the reverse can also occur in retrograde transport, causing disassembly of the cilium. Kinesin-2 forms a complex with IFT complex B to allow anterograde motor protein transports ciliary proteins, while the IFT complex A does the reverse by binding to dynein 1b and channelling ciliary proteins from the cilium to the basal body. Reproduced from (Higgins et al., 2019).

The primary cilium is a sensory structure that has a diverse range of functions. It has been shown to be a crucial sensing and signal transduction hub, including signalling pathways involved in development and diseases, such as polycystic kidney disease and cancer (Lancaster & Gleeson, 2009). The primary cilium has a number of signalling receptors localised to it, including receptors for sonic hedgehog (Shh), Notch canonical and non-canonical Wnt signalling. Several components of the Wnt signalling pathway have been determined to localise to the cilium, including Frizzled3, β-catenin, Dishevelled2 (Dsh), and glycogen synthase kinase-3β (Grisanti et al., 2016; May-Simera & Kelley, 2012; Rohatgi et al., 2007). Knockout of KIF3A (that controls cilia formation) in mouse embryos leads to abnormal β-catenin and dysfunctional canonical Wnt responses (Corbit et al., 2008). Shh signalling is essential for embryo development and cell proliferation. Another study has also demonstrated that IFT88 and KIF3A ciliary proteins are required for hedgehog signalling (Chang & Serra, 2013). Notch receptors have been shown to co-localise to the primary cilium and play a role in cell fate and cell-cell communication (Ezratty et al., 2011).

1.3.5.2 Primary cilia in cancer

Given the association between cell cycle regulation and the primary cilium as well as oncogenic protein localisation or regulation by cilia, there is an increased focus on the role of primary cilia in cancer. Signalling pathways that are involved in normal cellular growth and tissue development are disregulated in all stages of oncogenesis. In cancer, altered signalling pathways mediate resistance to cancer therapy, cell death, and evasion to immunosurveillance. The primary cilium, by displaying both the protein receptors required for signal interception, as well as the downstream molecular effectors, is a key mediator of the impaired signalling that induces malignancy by sensing signals from the extracellular environment (Fabbri et al., 2019).

Studies have previously shown loss of cilia in several cancer types, including pancreatic and renal cancers (Basten et al., 2013; Seeley et al., 2009). Several ciliary-associated genes are dysregulated in cancer. Mutation in the von Hippel Lindau (VHL), a tumour suppressor gene that is involved in ciliogenesis, have been found in clear renal cell carcinomas and primary

cilia have been shown to be lost in patients with VHL disease (Arjumand & Sultana, 2012). Notably a restoration of cilia expression was gained upon re-expression of VHL protein in clear cell renal carcinoma (Esteban et al., 2006). Loss of primary cilia have also been demonstrated in primary human melanoma cells, compared with primary melanocytes (Snedecor et al., 2015). Reports have also demonstrated that inhibition of aurora A kinase (AURA), a gene involved in cilia assembly, induces cell cycle arrest in ovarian cancer cells (Chefetz et al., 2011). Moreover, overexpression and the centrosomal localisation of AURA on the ovarian surface epithelium reduced Shh signalling, causing disturbance to the normal epithelial function which led to the eventual onset of tumour formation (Egeberg et al., 2012).

Another study however investigated the potential association between the presence/absence of primary cilia and the prognosis of pancreatic ductal adenocarcinoma (PDAC), which showed that patients who were primary cilia-positive had a higher rate of lymph node metastasis and thereby a poorer prognosis (Emoto et al., 2014). These data are contrary to reports of absent primary cilia in numerous cancer cell lines indicating a different role of primary cilia in different types of cancers. As cellular proliferation affects the presence of cilia, it is notable that renal and pancreatic cancer cells do not contain primary cilia, independent of any increases or decreases in Ki67 staining (a cell proliferation marker) (Yuan et al., 2010). This would support the notion that the loss of cilia in these cancer types is not associated with the rate of cell proliferation, supporting the correlation between primary cilium and carcinogenesis.

1.4 The cell cytoskeleton and motility

The cytoskeleton is a dynamic network made up of filamentous proteins that extend across the cytoplasm, and it is required for cell structure, cell division and cell migration. The cytoskeleton is made up by three types of networks: Actin, microtubules (α - and β - tubulin) and intermediate filaments (Hohmann & Dehghani, 2019). These networks differ in their protein composition as well as the type of filaments and structures they form, ranging from fast assembling actin networks of the lamellipodium, able to generate forces necessary for cell movement, to single microtubule filaments as transport structures, and intermediate

filaments able to promote or inhibit cell movement and stabilising the cell in response to stress (Dominguez & Holmes, 2011).

1.4.1 Actin cytoskeleton

Actin is considered the most dynamic of the three cytoskeletal proteins, capable of strong structural changes in short time periods. It exists in two states within the cell, monomeric G-actin and filamentous F-actin. Actin cytoskeleton modulation is orchestrated by the balance between G- and F-actin and by actin associated proteins. The polarized filaments of the actin cytoskeleton mediate force generation necessary for movement, focal adhesion, and shape changes (Rotty & Bear, 2015). Actin filaments have a helical structure, with the less actively polymerising end termed as the (−)- end and the more active (+)- end having a ten times higher polymerisation rate than the (−)- end. The (+)- and (−)- ends can be distinguished by their ATP/ADP status. If the growth is inhibited at the (−)- end, the (+)- end contains higher amounts of ATP bound actin while the (−)- end has ADP bound actin (Pollard, 2016). Actin assembly is regulated by different binding proteins which contribute to the organisation and dynamics of the actin network (Pollard, 2016).

During cell migration, the actin cytoskeleton at the leading edge of the cell provides the driving force. It is organised in parallel bundles that form filopodia, finger-like protrusion that are involved in probing the extracellular environment and orientating the Lamellipodium. Lamellipodia are formed by a dense meshwork of ruffling that promotes forward movement. Some classes of filopodia have receptors at their tips such as integrins, allowing sensing of ECM (Fischer et al., 2019). Behind the leading edge, F-actin forms stress fibres responsible for the contraction of the cell body and retraction of the trailing edge (Figure 12) (Etienne-Manneville, 2004). Cellular morphogenesis, migration and cell–cell interactions are regulated by the ability of the cell to extend, retract or stabilise membrane protrusions in a defined direction (Trepat et al., 2012).

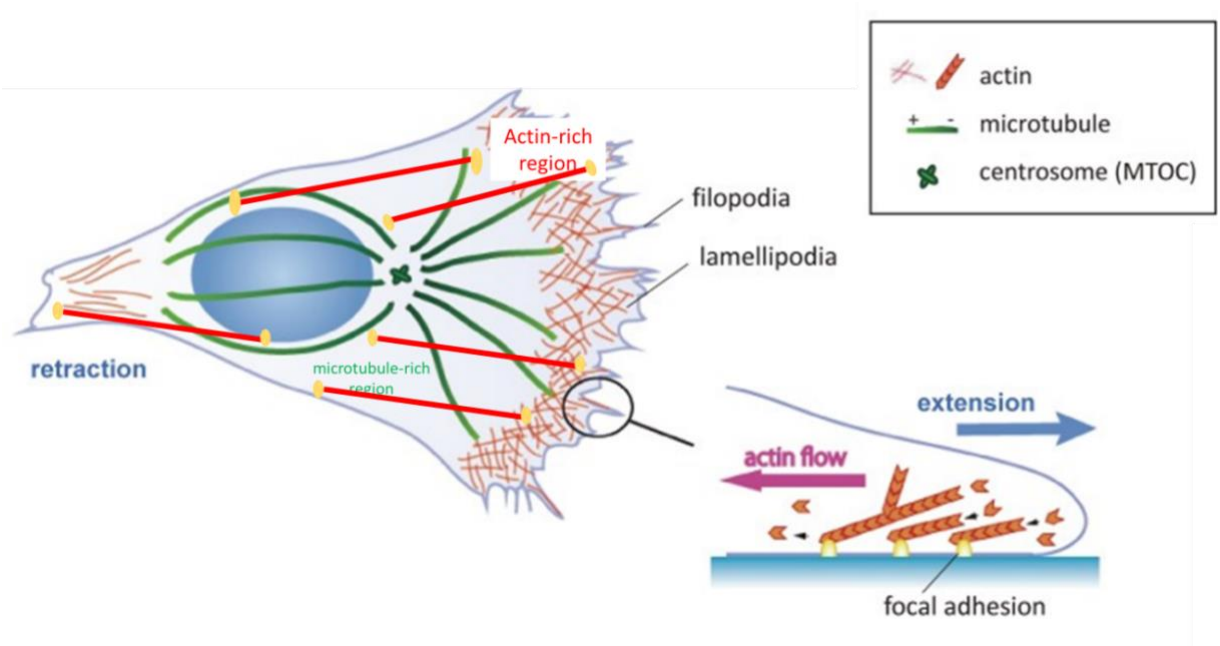

Figure 12: Actin and microtubule cytoskeleton organisation in cellular protrusions.
Two regions can be defined in a cellular protrusion: an actin-rich region (red) containing actin bundles arranged into filopodia, a dense meshwork of actin forming a ruffling lamellipodia and a few pioneer microtubules; and a microtubule-rich region (green), where microtubules extend from the centrosome (dark green star) with their (+)-ends directed towards the plasma membrane and where actin structures are limited to stress fibres (thick red lines), anchored via focal adhesions (yellow dots) to the substrate. Adapted from (Kengaku, 2018).

1.4.2 Rho GTPases

The actin cytoskeleton mediates a variety of essential biological functions in addition to defining cell shape and polarity. One of the key group of regulators of the actin cytoskeleton are the Rho family of small guanosine triphosphatases (GTPases) including Rho, Rac, and Cdc42 (Nobes & Hall, 1995). The Rho family are highly conserved, and most members cycle between active GTP-bound and inactive GDP-bound (Tcherkezian & Lamarche-Vane, 2007).

Rho activation acts as a molecular switch to control signal transduction pathways that link membrane receptors to the cytoskeleton (Sah et al., 2000). The first step of actin polymerization, known as nucleation, is initiated by Rho GTPases, which involves the formation of a stable multimer of actin monomers that will allow elongation of the new filament (Hanna et al., 2017). This is governed by activated Rac1 GTPases binding to actin-nucleating proteins including the actin-related protein 2/3 (Arp2/3) complex and formins

(Hurst et al., 2003). Moreover, Rho GTPases are important in activation of Rac which is necessary for lamellipodium formation and migration (Ridley, 2015). Rho can induce the formation of stress fibres and is required for stability of focal adhesions, while Rac activation also leads to an accumulation of actin at intercellular junctions in epithelial cells (Hall, 1998) (Wozniak et al., 2004). Moreover, cadherin-based adherens junctions, which are also closely associated with the actin cytoskeleton, require RhoA and Rac for their assembly (Braga et al., 1999). Rho GTPases are also involved in regulation of kinase cascades, cell growth, transformation, and gene expression (Haga & Ridley, 2016). Rho GTPases not only contribute organisation of the actin cytoskeleton, but they also regulate gene expression, vesicle trafficking, cell cycle progression, cell morphogenesis, cell polarity and migration (Etienne-Manneville & Hall, 2002). Therefore, Rho GTPases play an important role in pathological processes including cancer progression.

1.5 B7-H3

B7-H3, also known as CD276, is an immune checkpoint protein and a member of the B7 superfamily of proteins. B7-H3 has gained a lot of interest as a promising target for cancer treatment due to its overexpression in several kinds of tumour tissues including non-small-cell lung cancer (NSCLC), ovarian and prostate cancer. Its expression is highly associated with poor treatment outcomes and survival.

1.5.1 B7 family members

The B7 family members have either positive or negative roles in modulating immune cell responses (Li et al., 2020; Picarda et al., 2016). The B7/CD28 superfamily of immune checkpoints that regulate the T-cell response consist of; B7-1 (CD80), B7-2 (CD86), B7-H1 (PD-L1), B7-DC (PD-L2), B7-H2 (CD275), B7-H3 (CD276), B7-H4 (VTCN1), B7-H5 (VISTA), B7-H6 (NCR3LG1), and B7-H7 (HHLA2) (Figure 13) (Wang et al., 2020). Studies suggested that the up-regulation of B7 inhibitory molecules in the TME correlates with immune evasion by the tumour (Zou & Chen, 2008). During an immune response, T cell receptors (TCR) on naive T cells interact with a complex of major-histocompatibility complex (MHC) and peptide expressed by antigen presenting cells (APC). This first signal is not sufficient to fully activate T

cells. Full T cell activation is a result of a second signal provided by the interaction of co-stimulatory molecules including B7-1/2 and CD28. Following activation, co-inhibitory molecules such as cytotoxic T-lymphocyte associated protein 4 (CTLA-4) restrains T cell responses, leading to T cell exhaustion and tolerance. T cell co-stimulation, co-inhibition, activation, tolerance, exhaustion, effector function, memory generation and differentiation are all regulated by interactions between members of the B7 ligand family and the CD28 receptor family (Picarda et al., 2016).

Immune checkpoints, such as PD-1, PD-L1, PD-L2, and CTLA4, participate in many receptor-ligand interactions to evade the immune system and promote tumourigenesis. Several monoclonal antibodies (mAbs) that block these proteins have been developed to suppress the inhibitory immune response and facilitate the cytotoxicity of T cells to eradicate tumour cells (Goodman et al., 2017). Inhibitors targeting PD-1 or CTLA4 have been successfully used for treating patients with metastatic melanoma, with improved responses and prolonged survival (Wu et al., 2012). This success led to the development of such agents for treating a wide range of cancers, including NSCLC (Borghaei et al., 2015; Garon et al., 2015), renal cell carcinoma (RCC) (Motzer et al., 2015), and acute myeloid leukemia (AML) (Liao et al., 2019), which further enhanced the response and survival rate compared to conventional treatments.

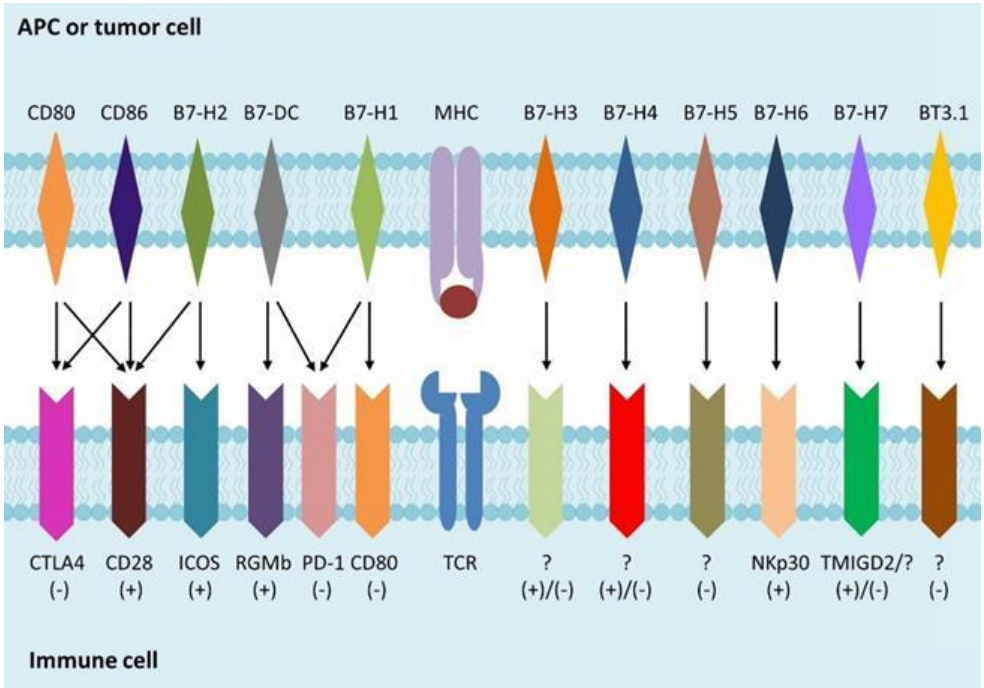

Figure 13: B7 family of immune checkpoints.
The B7 molecules are membrane proteins found on APC. Immune cell response is signalled via interaction between a specific antigen presented by MHC molecules on APC or tumour cells to TCR on T cells and co-signalling receptors that drive positive (+) or negative (-) signals. The ligands/receptors for B7-H3, B7-H4, B7-H5 and BT3.1 are yet to be discovered. Reproduced from (Yang et al., 2020).

1.5.2 B7-H3 structure and isoforms

B7-H3, like the other members of the B7 family, is important in the modulation of immune responses. B7-H3 mRNA levels are widely expressed in most tissues, while the protein has been detected at low levels in normal lung, liver, bladder, testes, prostate, breast, placenta, and lymphoid organs (Sun et al., 2006). Additionally, B7-H3 is expressed in myeloid cells, including T- and B-cells, macrophages, monocytes, and dendritic cells (DCs). Recent studies have found that B7-H3 is upregulated in both T-cells and APCs. It has also been reported to be both a co-stimulatory and co-inhibitory immune checkpoint molecule.

B7-H3 is functional in both membrane-associated and soluble forms (Figure 14) (Zhou & Jin, 2021). Residing on chromosome 15, B7-H3 is a type 1 transmembrane protein characterised by extracellular IgV and IgC domains linked to the variable and constant regions of immunoglobulins, a transmembrane region, and short cytoplasmic domain (Steinberger et al., 2004). Mouse B7-H3 is a 2-Ig molecule, whereas in human cells, even though the 2-Ig form can be present, the 4-Ig molecule appears to be dominant, which means it has a duplicated extracellular domain with two extracellular tandem IgV-IgC domains (Figure 14) (Sun et al., 2002). However, the function of these repeats is still unknown. In addition, B7-H3 can be cleaved from the cell surface via membrane metalloproteases (MMPs) and endopeptidases, resulting in a soluble circulating form of the protein (sB7-H3) that has been detected in serum and culture media (Chen et al., 2013). sB7-H3 can promote $CD4^+$ and $CD8^+$ T-cell proliferation, activate T-effector cells and stimulate IFN-γ and IL-10 production (Figure 16) (Chapoval et al., 2001). Along with its immunomodulatory functions, it plays a role in cell signalling in exosome biogenesis (Figure 16) (Wang et al., 2018).

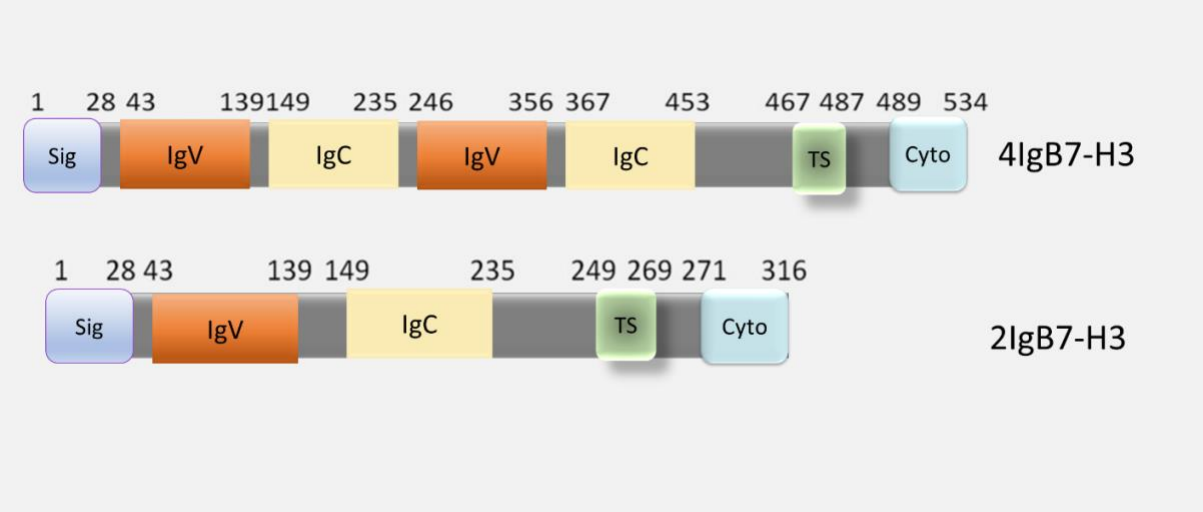

Figure 14: B7-H3 isoforms.
B7-H3 in humans has two isoforms. Belonging to the immunoglobulin family. The structure of the two isoforms is very similar with the exception that 4IgB7-H3 has an extra IgC-IgV immunoglobulin domain in the extracellular domain. Numbers indicate amino acid (aa), Sig= signal peptides (first 28 aa, encoded by exon 1), IgV= Immunoglobulin variable domain, IgC= Immunoglobulin constant domain, Ts= transmembrane domain, cyto=cytoplasmic tail.

The structure of the mouse 2-Ig B7-H3 protein suggested that the molecule was able to form a stable dimer in solution upon extended incubation at high protein concentration (Figure 15). The physicochemical features responsible for B7-H3 dimer formation was identified by subjecting the monomeric murine B7-H3 to a range of conditions including ionic strength, pH, redox condition, and temperatures, none of which altered dimer formation. Nonetheless, comparison between the monomer model of mB7-H3 and the dimer structure has revealed that the sequence connecting the strands G and F of the IgV domain can have at least two conformations, thus promoting the ability of B7-H3 to dimerise. This was tested by observing the dimerization of FG loop mutants and FG-PD-L1 chimera. Dimer formation was significantly slower for mutants and the FG loop chimera. The FG loop of the IgV domain of mB7-H3 was able to inhibit naive T cell proliferation *in vitro* and the dimeric mB7-H3 did not differ from the monomeric form in its ability to reduce T cell proliferation. Taken together, the FG loop in mB7-H3 suggests that the WT sequence may serve a role in destabilising the monomeric form of mB7-H3 and the dimerization of mB7-H3 alone does not change the molecule's inhibitory property (Vigdorovich et al., 2013).

B7-H3 protein has been found to be highly glycosylated in oral cancer compared with normal cells, and the *N*-glycan structures were aberrant between normal vs. cancer cells (Chen et al., 2015). Abnormal glycosylation has been observed in several kinds of cancer cells. Changes in glycosylation state are common features of cancer cells as the increased expression of branched-*N*-glycan structures prevents epithelial cadherin-mediated cell-cell adhesion, resulting in cancer cell dissociation and invasion (Thomas et al., 2021).

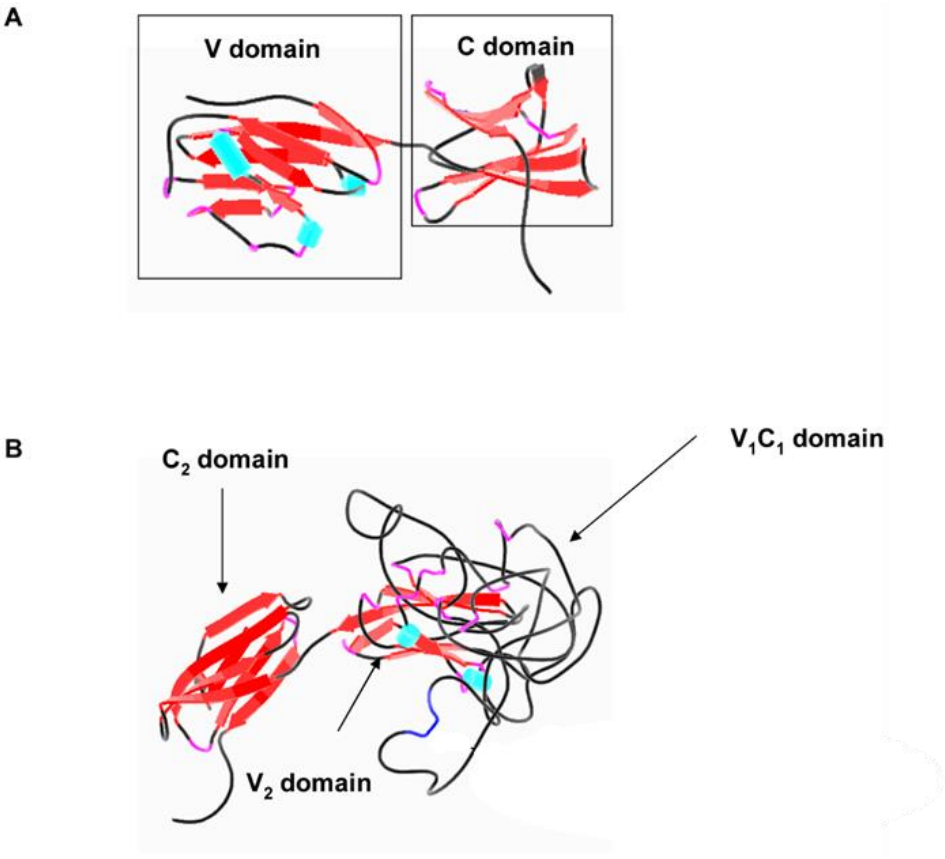

Figure 15: Structure of B7-H3.
(A) 3D structure model of 2IgB7-H3 corresponds well to the PD-L1 structure in human. **(B)** 3D structure of 4Ig isoform. Reproduced from (Sun et al., 2011).

1.5.3 B7-H3 and immune cell interactions in cancer

Co-stimulatory and co-inhibitory cell surface signalling molecules (CSSMs) provide immune cells with information essential for responses to a primary signal. In a tumour environment, CSSMs are susceptible to manipulation by tumour cells, thus mediating inaccurate signal information to T-cell activation, deactivation, differentiation, effector functions and survival (Kanchan et al., 2022). Many studies have shown increased B7-H3 expression in a range of

malignancies, including NSCLC (Sun et al., 2006), prostate cancer (Zang et al., 2007), pancreatic cancer (Yamato et al., 2009), melanoma (Wang et al., 2013), glioma (Zhou et al., 2013), breast cancer (Flies et al., 2014), renal cell carcinoma (Wang et al., 2016), ovarian carcinoma (Fauci et al., 2012), and colorectal cancer (Ingebrigtsen et al., 2012). Interestingly, B7-H3 has been reported to have dual co-stimulatory and co-inhibitory abilities in different tumour microenvironments. B7-H3 was first identified as a positive regulator of T-cell function, increasing $CD4^+$ and $CD8^+$ T-cell proliferation, triggering cytotoxic T-cell function, and inducing IFN-γ production (Chapoval et al., 2001). B7-H3 is not constitutively expressed on T cells, NK cells, and APCs but can be induced upon activation (Figure 16) (Steinberger et al., 2004), B7-H3 demonstrated anti-tumour activity when its expression was induced in murine lymphomas via $CD8^+$ T and NK cells activation (Sun et al., 2003). In a murine mastocytoma model, B7-H3 caused tumour regression through cytotoxic T cell induction (Figure 16) (Luo et al., 2004). Similar results were observed in murine models of colorectal carcinomas, suggesting that enrichment of B7-H3 led to a strong anti-tumour immune response (Lupu et al., 2006).

Although early studies found B7-H3 to have a stimulatory role in cancer, most of the recent research has revealed that B7-H3 induces a strong immune evasive effect. High levels of tumour-infiltrating immune cells (TIL) coupled with an immune-suppressive effects help tumour growth and progression, leading to poorer outcomes. B7-H3 expression on APCs, tumour cells, and TILs supports its immune regulatory role in the TME. Expression of B7-H3 was negatively correlated with circulating CD8+ tumour-infiltrating lymphocytes, suggesting a role in tumour evasion in both hypopharyngeal squamous cell carcinoma and osteosarcoma (Katayama, 2011; Wang et al., 2013). The density of CD8+ T cells was critical to patient survival and responsiveness to immunotherapy. Similarly, in clear cell RCC (Inamura et al., 2019) and NSCLC (Jin et al., 2015), expression of B7-H3 was highly correlated with circulating T regulatory T cells (Tregs) that suppress inflammation to promote secretion of cytokines and growth factors, leading to tumour progression. B7-H3 inhibited the proliferation of both CD4+ and CD8+ T-cells and decreased the production of IL-2 and IFN-γ, likely through suppression of nuclear factor κ B (NF-κB) mediated signalling pathways (Figure 16) (Prasad et al., 2004). In breast cancer, B7-H3 expression is strongly correlated with IL-10 cytokine production by

tumour cells and metastases (Liu et al., 2013). B7-H3 expression can be driven by immunoglobulin-like transcript 4 (ILTR4), an inhibitory factor implicated in tumour evasion in NSCLC, via PI3K/AKT/mTOR signalling, resulting in a reduction in TILs and overall survival (Figure 16) (Zhang et al., 2015). The effects of depleting B7-H3 on lymphoma and melanoma tumour growth has been studied in mice to further support its immune evasive role. Subcutaneously generated tumours were suppressed in both B7-H3 knockdown and wild-type mice treated with B7-H3 blocking antibodies. However, depletion of CD8+ T lymphocytes or NK cells in these tumours decreased the anti-tumour effect of B7-H3 inhibition. Notably, B7-H3 knockdown tumours with depleted NK cells and CD8+ T lymphocytes had the largest tumours, indicating anti-tumour effects of B7-H3 depletion are dependent on NK and CD8+ T cells (Lee et al., 2017).

Downregulation of B7-H3 by siRNA showed reduced cell adhesion to fibronectin, migration and invasion in melanoma, breast cancer cells and prostate cancer cells (Chen et al., 2008). Decreased expression of B7-H3 in MDA-MB-435 cell xenografts in nude mice reduced metastatic capacity and increased mouse survival (Yuan et al., 2011). The Jak2/STAT3/Slug signalling pathway has been implicated in B7-H3 contributions to EMT (Figure 16) (Kang et al., 2015). Downregulation of B7-H3 expression sensitises breast cancer cells to AKT/mTOR inhibitors and reduced the glycolytic capacity (Nunes-Xavier et al., 2016). These studies suggest B7-H3 has non-immunological roles in cancer and could contribute to cellular metabolism and sensitivity to chemotherapeutic compounds. Indeed, knockdown of B7-H3 counteracted cellular resistance to paclitaxel, and abrogated Stat3 phosphorylation on Tyr705 via inactivation of Janus kinase 2 (Jak2), leading to downregulation of the downstream target genes (Figure 16) (Liu et al., 2011). Another recent study found B7-H3 depletion in melanoma cells increased *in vivo* and *in vitro* sensitivity to cisplatin and dacarbazine in parallel with a reduction in p38 MAPK phosphorylation (Figure 16) (Flem-Karlsen et al., 2019). B7-H3 have been also found to stabilize hypoxia inducible factor-1 (HIF-1α) through the transcription factor Nrf2 and its target genes SOD1, SOD2 and PRX3 and activated downstream glycolytic enzymes to exert a hyperglycolytic role (Zuo et al., 2018). Moreover, B7-H3 silencing decreased the production of ATP, lactate, c-Myc and LDHA, indicating that B7-H3 alters metabolism by affecting the activity of ENO1 and the c-Myc-LDHA axis. These studies support

the involvement of B7-H3 in the dysregulation of cancer cell metabolism and its contribution to tumorigenesis (Deng et al., 2021).

The precise role of B7-H3 in tumour-infiltrating immune cells and its' activity in cancer cells remains elusive. This is due in large part to discrepancy of studies that have demonstrated B7-H3 to be either co-stimulatory or co-inhibitory in various disease models. Additionally, the B7-H3 receptor/s has yet to be identified, magnifying the scrutiny. However, the aberrant expression of B7-H3 consists of a promising immune checkpoint target for multiple cancer immunotherapy approaches.

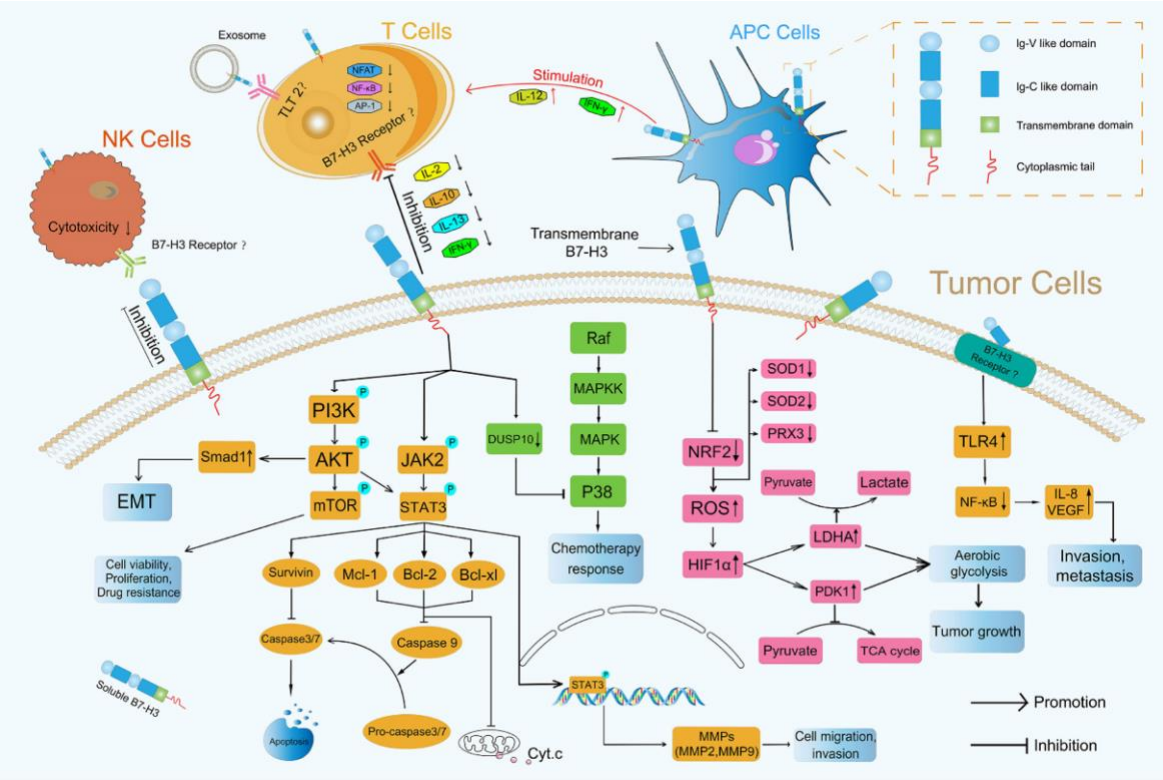

Figure 16: Roles of B7-H3 in TME.
Schematic representation of published studies on B7-H3 possible functions and pathways to promote tumour progression. Reproduced from (Zhou & Jin, 2021).

1.6 Hypothesis

Based on previous evidence and unpublished data in our lab, we hypothesize that B7-H3 acts at cell-cell adhesion sites to control proliferation and migration of lung cancer cells, contributing to tumourigenesis independent of immune cell interactions.

1.7 Aims

The experiments in this thesis are designed to address the following aims:

- To determine the effects of overexpression and knockout of B7-H3 on cell morphology, adhesion and migration in normal lung epithelial cells and NSCLC tumour cells in 2D and 3D experimental conditions.
- To define the domains of B7-H3 controlling receptor function and the role of B7-H3 in adhesion and signalling; and whether B7-H3 can act as a ligand for itself in order to inform development of better more effective therapeutics in cold tumours.

These aims will be investigated by achieving the following outcomes:

1. Define the expression levels and localisation of B7-H3 in normal lung epithelial and cancer cells.
2. Explore the effects of overexpression, knockdown and B7-H3 manipulation on morphology, adhesion and migration.
3. Identify B7-H3 associated proteins and define the mechanisms of which it is contributing to metabolism and chemoresistance in 2D.
4. Determine the role of B7-H3 and associated protein on proliferation and invasion in 3D model.

2. Materials & Methods

2.1 Materials

2.1.1 Reagents

Table 1: Cell culture reagents

Reagent	Source
6 well plate	Greiner
8 well chamber	Ibidi
24 well plate	Greiner
DMSO (Dimethyl sulphoxide)	Sigma-Aldrich
Dharmafect	Horizon
Fetal Bovine Serum (FBS)	Gibco
Fibronectin	Millipore
HEPES	Sigma-Aldrich
High Glucose Dulbecco's Modified Eagle's Media (DMEM)	Sigma-Aldrich
L-Glutamine	Sigma-Aldrich
Lipofectamine 3000	Thermofisher
Methylcellulose	Sigma
Minimum Essential Medium Eagle (MEM)	Sigma
Opti-MEM	Gibco
PBS (Phosphate Buffered Saline)	Sigma-Aldrich
Penicillin/Streptomycin	Sigma-Aldrich
Polybrene	GE Healthcare
Rat Tail Collagen, Type I	Corning
Roswell Park Memorial Institute 1640 (RPM I)	Gibco
Trypsin/ EDTA	Sigma-Aldrich

Table 2: Molecular biology reagents

Reagent	Source
5x reaction buffer	New England Biolabs
Agarose	Sigma-Aldrich
Ampicillin	Sigma-Aldrich
Deoxynucleosides (dNTPs)	Bioline
High Fidelity Buffer	New England Biolabs
Hyperladder I	Biolabs
Kanamycin	Sigma-Aldrich
LunaScript™ RT SuperMix Kit	New England Biolabs
Luria-Bertani Agar and Broth	Sigma-Aldrich
Midiprep Kit	Qiagen
OneShot TOP10 Chemically Competent E. coli	Thermofisher
Phusion DNA polymerase	New England Biolabs
PNGase F	New England Biolabs
RNeasy Mini Kit	Qiagen
Safeview	NBS Biologicals

Table 3: Biochemical and immunocytochemistry assay reagents

Reagent	Source
1 ml Cuvettes	Fisherbrand
1 mm Cassettes	ThermoFisher
1.5 mm Cassettes	ThermoFisher
11mm snap Ring Glass Vial	Fisherbrand
β-mercaptoethanol	Sigma-Aldrich
30% Acrylamide/Bis solution	Bio-Rad
Acetic acid	Sigma-Aldrich
Agarose resin	ThermoFisher
Ammonium acetate	Sigma-Aldrich
Ammonium persulphate (APS)	Sigma-Aldrich

Bromophenol Blue	Sigma-Aldrich
BSA (Bovine Serum Albumin)	Sigma-Aldrich
Chloroform	Sigma-Aldrich
Clarity Western ECL Substrate	Bio-Rad
Dithiothreitol (DTT)	Sigma-Aldrich
EDTA	Sigma-Aldrich
Fluorsafe Mounting Media	Calbiochem
Formalin	Sigma
GFP-trap®_A beads	Chromotek
G-LISA Kit	Cytoskeleton
Glycerol	VWR International
Glycine	Sigma-Aldrich
Immersion 5101 Immersion oil	Zeiss
Immobilon-P PVDF Membrane	Merch
InstantBlue™ Protein Stain	Expedeon
Magnesium chloride	Sigma-Aldrich
Methanol	Sigma-Aldrich
NP-40	Sigma-Aldrich
PBS Tablets	Thermo Scientific
PeqGOLD Protein Marker V	Thermo Scientific
PFA (Paraformaldehyde)	Sigma-Aldrich
Phosphatase Inhibitor Cocktail Set II (Stock 100x) containing: 200 mM Imidazole, 100 mM Sodium Fluoride, 115 mM Sodium Molybdate, 100 mM Sodium Orthovanadate, 400 mM Sodium Tartrate, dyhydrate	Millipore
Protease Inhibitor Cocktail set I (Stock 100x) containing: AEBSF, Hydrochloride - 500 µM Aprotinin, Bovine lung, crystalline – 150 nM E-64 Protease Inhibitor - 1 µM EDTA Disodium – 0.5 mM Leupeptin, Hemisulphate – 1 µM	Millipore
Protein A/G Beads 25% Slurry	Sigma-Aldrich
Re-blot strong solution	Chemicon
Sodium Chloride	Sigma-Aldrich

Sodium Dodecyl Sulphate	Sigma-Aldrich
Sodium Fluoride	Acros organics
Sodium Orthovanadate (Vanadate)	New England Biolabs
Tetramethylethylenediamine (TEMED)	Sigma-Aldrich
Tris-Base	Sigma-Aldrich
Tris-HCl	Sigma-Aldrich
Triton X-100	Sigma-Aldrich
Tween-20	Calbiochem
Water, for HPLC gradient grade	ThermoFisher

Table 4: Materials and solutions for biochemical assays

Buffer/ Solution	Composition
10% SDS-PAGE resolving gel	10% 30%-acrylamide mix, 400 mM Tris pH 8.8, 0.1% SDS, 0.1% ammonium persulphate (APS), 0.05% TEMED
8% Resolving Acrylamide Gel	8% 30%-acrylamide mix, 400 mM Tris (pH8.8), 0.1% SDS, 0.1% APS, 0.05% TEMED
GFP Lysis and wash buffer	50 mM Tris-HCl pH7.4, 200 mM NaCl, 1% NP40, 10% glycerol, 2 mM $MgCl_2$, Protease inhibitor cocktail, NaF, Phosphatase inhibitor cocktail
IP lysis and wash buffer	50mM Tris Base, 150mM NaCl, 1mM EDTA, 50mM Sodium fluoride, 1% NP-40, 1% Triton X-100, adjust pH to 7.4 and volume to 1L with dH2O, Protease inhibitor cocktail set 1
PBS-T (1x)	10 tablets of Phosphate buffered saline, 0.5% Tween 20
RIPA buffer	10 mM Tris Base, 150 mM NaCl, 1mM EDTA, 1% Triton X-100, adjusted to pH 7.4 and volume to 1L
Running Buffer (10x)	0.25 M Tris base, 1.92 M glycine, 1% SDS
SDS Sample Buffer 2x	60mM Tris-HCl (pH 6.8), 25% Glycerol, 2.5% SDS, 0.02% Bromophenol blue, 2% β-mercaptoethanol
Stacking Acrylamide gel	16% 30%-acrylamide mix, 400 mM Tris (pH 8.8), 0.1% SDS, 0.1% APS, 0.05% TEMED
TBS-Tween (10x)	20 mM Tris-base (pH 7.5), 150mM NaCl, 0.1% Tween- 20
Transfer Buffer (10x)	0.25 M Tris base, 1.86 M glycine, 20% methanol

Table 5: Treatments (Inhibitors/Proteins/Detection reagents)

Compound	Source	Concentration	Duration	Dosage optimisation	Control
CD276 (B7-H3) Monoclonal Antibody (MIH35), Functional Grade	ThermoFisher	10 µg/ml	3-24 hours	Used concentration to match Recombinant Ectodomain	IgG Control
CellEvent™ Caspase-3/7 Green Detection Reagent	ThermoFisher	4 µm	30 minutes	Optimised from a series of concentrations: 2um, 4um and 6um	-
CellROX™ Deep Red Reagent, for oxidative stress detection	ThermoFisher	5 µM	30 minutes	Recommended dosage by ThermoFisher	-
Cisplatin	Cambridge Bioscience	5 µM	48 hours	Dosage optimised from a series of concentrations	DMSO
Cycloheximide Blocks protein synthesis	Sigma-Aldrich	50 mM	0-6-24 hours	Optimised previously in the Parsons Lab	DMSO
DMSO	Sigma-Aldrich	—	—		
Leupeptin (blocks degradation via lysosomes)	Sigma-Aldrich	100 µM	16 hours	Dosage optimised from a series of concentrations and time points	DMSO with Cycloheximide
Anti-B7-H3 (MAB1027)	Santa Cruz	10 µg/ml	3-24 hours	Optimised previously in the Parsons Lab	IgG Control
MG132 (blocks degradation via proteasome)	Sigma-Aldrich	20 µM	16 hours	Dosage optimised from a series of concentrations and time points	DMSO with Cycloheximide
Mycophenolic acid (MPA; IMPDH inhibitor)	Sigma-Adrich	1 µM	24-48 hours	series of concentrations and time points starting from 4 hours	Methanol
Recombinant Human B7-H3 His-tag Protein	R&D Systems	10 µg/ml	3-24 hours	Optimised previously in the Parsons Lab	IgG Control

Table 6: Antibodies

Primary antibodies	Species	Dilution	Source
Anti- AnnexinA2	Mouse	1:500 (WB)	R&D Systems

Anti β-Actin	Mouse	1:500 (WB)	Abcam
Anti-A/B Tubulin	Rabbit	1:500 (WB)	Cell Signaling
Anti-Arl13b	Mouse	1:400 (IF) 1:500 (WB)	Abcam
Anti-Arl13b	Rabbit	1:800 (IF)	Proteintech
Anti-B7-H3	Rabbit	3 µg (IP)	Thermofisher
Anti-B7H3 (AF1027)	Mouse	1:1000 (WB)	BD Bioscience
Anti-B7-H3 (MAB1027)	Goat	1:200 (IF)	Santa Cruz
Anti-E-Cadherin (24E10)	Mouse	1:200 (IF)	Cell Signaling
Anti-E-Cadherin (SC-67A4)	Mouse	1:1000 (WB)	Abcam
Anti-EEA1	Rabbit	1:200 (IF)	Cell Signaling
Anti-GFP	Mouse	1:1000 (WB)	MBL
Anti-HSC70	Mouse	1:5000 (WB)	Santa Cruz
Anti-IMPDH2	Rabbit	1:1000 (WB) 1:200 (IF)	Proteintech
Anti-KIF3A	Rabbit	1:1000 (Wb)	Abcam
Anti-Pericentrin1	Rabbit	1:500 (IF)	Abcam
Anti-Rac1	Rabbit	1:500 (WB)	Cytoskeleton ARC01
Anti-Rap10	Rabbit	1:500 (IF)	Abcam
Anti-Rap11	Rabbit	1:400 (IF)	Cell Signaling
Anti-RhoA	Rabbit	1:500 (WB)	Cell signaling
Anti-Vinculin	Mouse	1:200 (IF)	Sigma-Aldrich
Anti-ZO-1	Rabbit	1:200 (If) 1:500 (WB)	Santa Cruz
Anti-β-Catenin (aa.571-781)	Rabbit	1:1000 (WB)	Sigma-Aldrich
Anti-β-Catenin	Rabbit	1:200 (IF)	Santa Cruz
IgG Negative Control	Rabbit	3 µg (IP)	Dako
Myosin Heavy Chain II-A	Rabbit	1:500 (WB)	Covance

Myosin Heavy Chain II-B	Rabbit	1:500 (WB)	Covance
Secondary antibody/dye	Species	Dilution	Source
Anti-Goat-HRP	Rabbit	1:5000 (WB)	Dako
Anti-Mouse Alexafluor 488	Goat	1:500 (IF)	Molecular probe
Anti-Mouse Alexafluor 568	Goat	1:500 (IF)	Molecular probe
Anti-Mouse-HRP	Goat	1:5000 (WB)	Dako
Anti-Rabbit Alexafluor 488	Goat	1:500 (IF)	Molecular probe
Anti-Rabbit Alexafluor 568	Goat	1:500 (IF)	Molecular probe
Anti-Rabbit-HRP	Goat	1:5000 (WB)	Dako
DAPI (861045)	N/A	1:1000 (IF)	Sigma-Aldrich
LysoTracker™ Deep Red	N/A	50 nM	ThermoFisher
Phalloidin Alexafluor 488	N/A	1:500 (IF)	Invitrogen
Phalloidin Alexafluor 647	N/A	1:500 (IF)	Invitrogen

Abbreviations: Western blotting (WB), immunofluorescence (IF)

2.1.2 Expression plasmids

Table 7: Plasmids

Plasmid	Type	Insert and tag	Original reference/ Source
B7-H3, CD276 CRISPR Guide RNA 1	Transient	Guide RNA: TGCACAGTTTCACCGAAGGC, GFP tag	GenScript
B7-H3, CD276 CRISPR Guide RNA 2	Transient	Guide RNA: TTGATGTGCACAGCGTCCTG, GFP tag	GenScript
B7-H3, CD276 CRISPR Guide RNA 3	Transient	Guide RNA: CACGGCTCTGTCACCATCAC, GFP tag	GenScript
B7-H3-GFP	Transient	B7-H3, GFP tag	Generated by Brooke Lumicisi (Parsons lab) from a human B7-H3 expression vector gifted by MedImmune
CD63-GFP	Transient	Full length Human CD63, GFP tag	Fedor Beditchevski (University of Birmingham)

GFP	Transient	eGFP tag	Clontech
LifeAct-GFP	Lentiviral	LifeAct – an actin filament reporter, eGFP tag	Scales *et al*. 2013

2.2 Methods

2.2.1 Molecular Biology

2.2.1.1 Bacteria transformation

DNA constructs were amplified by transforming into chemically-competent Top10 E.Coli cells which were thawed on ice prior to addition of 50-100 ng of DNA. DNA was incubated with the 50 µl E.Coli solution for 30 minutes on ice. The bacteria were heat-shocked at 42°C for 45 seconds and then incubated on ice for a further 2 minutes. This was followed by the addition of 500 µl of LB broth to the heat-shocked bacteria-DNA mixture and incubated for 1 hour at 37°C with agitation. Following incubation, the transformed bacterium was spread onto agar plates with the appropriate selection antibiotic (Ampicillin 100µg/ml or Kanamycin 50 µg/ml). and allowed to grow overnight at 37°C. Single colonies were picked and amplified in 100ml LB broth overnight at 37°C. Cells were pelleted by centrifugation at 4000 RPM for 15 minutes at 4^{o}C, the supernatant was discarded and the pellets were stored at -20°C for purification.

2.2.1.2 Midiprep of DNA plasmids

To Purify plasmid DNA from E.Coli bacterial culture, QIAgen miniprep kit was used as per manufacturer's instructions. The pelleted bacteria were resuspended in 4 ml Buffer P1 from the kit followed by 4 ml of buffer P2, mixed by inverting several times and incubated at room temperature for 3 minutes. 4 ml of buffer S3 was added to the lysate and mixed by inverting several times. The sample was transferred to a QIAfilter Cartridge and incubated at room temperature for 10 minutes. The sample was passed through the column by plunging, and 2ml of buffer BB was added to the flow-through. The sample was mixed by inversion and transferred to a plasmid plus midi spin column mounted on a vacuum manifold. The column was then washed with 0.7 ml of buffer ETR and buffer PE sequentially and the column was dried by centrifuging for 1 minute at 10,000 RPM to remove any residual wash buffer. The column was then placed in a clean 1.5 ml Eppendorf tube and the DNA eluted with 50-200 ul buffer EB by centrifugation at 10000xg for 1 minute. The concentration of the DNA was measured using a nanodrop Spectrophotometer (Labtech International).

2.2.1.3 RNA isolation and reverse-transcription polymerase chain reaction (RT-PCR)

Total RNA was isolated using the RNeasy Qiagen kit according to the manufacturer's instructions. Cells were trypsinised, pelleted then resuspended with buffer RLT. Then, lysate was placed in a RNeasy spin column and centrifuged for 15 seconds. Flow-through was discarded, and 700 µL of Buffer RW1 was added to the column. Buffer RPE was added twice to wash the column, then the column was centrifuged to remove any excess liquid. The column was then transferred into a new Eppendorf before 50 µL of RNase-free water was used to elute the RNA. The resulting RNA was used for cDNA synthesis using the LunaScript™ RT SuperMix Kit. cDNA synthesis reaction, consisting of 4 µL of 5X LunaScript RT SuperMix, 1 µg of RNA and Nuclease-free water, was prepared. Using a thermal cycler, the reaction was initialised by a primer annealing step of 25^{o}C for two minutes, followed by a cDNA synthesis step at 55^{o}C for ten minutes, and a heat inactivation step of 95^{o}C for one minute.

Quantitative real-time PCR (qPCR) was performed using the following primers:

B7-H3 primer forward 5' CCTA-GGTACC-AA-TACGACGCCTCTTCTCCG 3'

B7-H3 primer reverse 5'CGGCCAGGAAATCGCC-CCATGG-ATGC 3'

18S primer forward 5'-CCCATCACCATCTTCCAGGAGC -3'

18S primer reverse 5'-CCAGTGAGCTTCCCGTTCAGC -3'

qPCR was performed in triplicates by mixing 5 µL of 2x Luna Universal Probe One-Step Master Mix, 1 µL of forward primer (10 µM), 1 µL of reverse primer (10 µM), 1 µL of template cDNA or water as negative control and PCR grade water up to 10 µL. Using a QuantStudio 5 (Applied Biosystems/ThermoFisher) thermal cycler, the reaction was heated to 95^{o}C for 1 minute, followed by 40 cycles of 95^{o}C for 10 seconds. This was followed by 30 seconds of an extension time of at 60^{o}C.

2.2.2 Cell Culture

Three different epithelially derived lung cancer cell lines were used in this study: Normal human bronchial epithelial cell line 16HBE, (a gift from Dr. Dieter Gruenert, UCSF), adenocarcinomic human alveolar basal epithelial cells A549 (originally from ATCC, obtained as a gift from Santis lab, KCL), and bronchioalveolar carcinoma cell line NCI-

H358 (purchased from ATCC, a gift from Medimmune). HEK293T cells were used for lentiviral transfection, originally sourced from ATCC. Human normal cell-based systems are needed for drug discovery, investigating function, mechanisms and toxicity evaluation and thus 16HBE have been added as a model for normal cells in this study in an attempt to understand the effect of B7-H3 expression on cell growth, epithelial phenotype and function. Both A549 and NCI-H358 were originally extracted from explant culture of lung carcinoma and has been shown to have malignant mobility in xenograft mouse models (Basu et al., 2011; Giard et al., 1973). Cultured tumour derived cell lines have been shown to retain their differentiation properties, and thus can provide an easily manipulated experimental model for cancer (Mirabelli et al., 2019). This allows measurement of specific factors on the signalling and functional outputs of the cell lines and is often validated by using multiple different cell lines. However, studies have shown that although many of the phenotypic properties of the tumour cells in these immortalised cell lines are retained, there are many differences in gene and protein expression and function, phenotype, morphology, and functional outputs between these cells and non-immortalised primary cells (Geppert et al., 1980; Scherzer et al., 2015). These vary between cell types and experimental conditions. Continuing these experiments in the future with primary cells may aid in further confirming the results discussed in this thesis. Difficulties also arise when taking into account the effect of the TME. Stromal and immune cells specifically play a crucial role in the tumourigenicity, metastatic potential and survival of cancer cells. Including more complex systems by creating co-cultures would be the next step in these experiments, and is discussed in the future directions section of this thesis.

Cells were either grown in Minimum Essentia Media (MEM) for 16HBE cells, Dulbecco modified eagle medium (DMEM) for both A549 and HEK293T, and RPM I-1640 for the NCI-H358 cells, media was supplemented with 10% v/v fetal calf serum, 2mM L-Glutamine, 100 units/ml penicillin, 0.1 mg/ml streptomycin. Cells were maintained at 37°C, 5% CO2 in a humidified incubator.

All cells were passaged when 80% confluent by washing once with Phosphate Buffer Saline (PBS), without calcium or magnesium, followed by trypsinisation using trypsin in EDTA (0.05% concentration). Once cells were detached, normal growth media was used to wash and collect the cells. cells were centrifuged for 3 minutes at 1200 RPM, the supernatant was removed

and the pellet was resuspended in complete media and plated into a sterilised tissue culture flasks.

To freeze cells for future use; the cells pellet was resuspended in 3 ml of freezing media which consists of 50% complete media, 40% FBS and 10% DMSO. Cells were frozen in 1 ml aliquots in cryovials. Cryovials were frozen overnight at -80°C and then transferred to liquid nitrogen for long term storage. To thaw frozen cell stocks, a cryovial was removed from liquid nitrogen storage and thawed until 10% of volume remained frozen at 37°C. Thawed cell solution was resuspended in 5ml pre-warmed complete media and centrifuged at 1200 RPM for 3 minutes. Cell pellet was resuspended in 5ml complete media and added to a sterilised tissue culture flask. Media was changed to fresh complete media after 24 hours.

2.2.2.1 Generation of Lifeact-GFP lentivirus from HEK-293T cells

HEK-293T cells were plated at 40-50% confluency in T-25 cm^2 sterilised tissue culture flasks a day prior to transfection. A transfection mixture containing a total of 7.5 µg DNA (2.8125 µg of pCMVΔ8.91 plasmid, 0.9375µg of pMD.G plasmid and 3.75ug of Lifeact-GFP expression plasmid) was mixed in 500 µL of OptiMEM. Subsequently, 22.5 µg of PEI transfection reagent was added to the transfection mixture (3:1 ratio to total DNA). The DNA/PEI mix was incubated for 15 minutes at room temperature before being added to HEK-293T cells with OptiMEM. After the cells were incubated with the transfection mixture for 5 hours at 37 °C, OptiMEM was replaced by complete media. Lentivirus was harvested 48 hours post-infection by removing the media, and centrifugation at 1200 RPM for 3 minutes to remove HEK-293T cells. Viruses were filtered through 0.4 µm and kept in 1 mL aliquots at -80°C.

2.2.2.2 Lentiviral infection of cell lines

16HBE, A549 and H358 cells were plated in T-25 cm^2 flasks to 40% confluency 24 hours prior to viral infection. Polybrene (8 µg/ml final concentration) was added to complete media to increase the efficiency of viral infection. 1mL of lentiviral containing media was added to the cells and left to incubate at 37°C for 24-72 hours. Media was replaced 24 hours post-infection to remove the virus and cells were grown and passaged.

2.2.2.3 Transient transfection of cell lines

16HBE, A549 and H358 cells were plated in a 6 well plate 24 hours prior to transfection at 75-80% confluency. Lipofectamine 3000 was used according to the manufacturer's instructions; 2.5 µg of DNA was diluted in a 125 µl of OptiMEM and 10 µl of p3000 reagent. In a separate tube, 5 µl of Lipofectamine 3000 were diluted in 125 µl of OptiMEM and both tubes were left to incubate at room temperature for 5 minutes. The DNA and lipofectamine solutions were then mixed and incubated at room temperature for a further 20 minutes. The DNA/lipofectamine complexes were then added to cells in OptiMEM and incubated at 37°C with 5% CO2 for 5 hours. Subsequently, the DNA/lipofectamine containing media was removed and the cells were washed gently with complete media and left to incubate for 48 hours in complete media at 37°C with 5% CO2.

2.2.2.4 Generation of cell lines with stable B7-H3 knockdown

B7-H3-CRISPR cell lines were established via transient transfection of parental cells with three CD276 Guide RNA vectors carrying a GFP tag and targeting three different sequences (1: TGCACAGTTTCACCGAAGGC, 2: TTGATGTGCACAGCGTCCTG, 3: CACGGCTCTGTCACCATCAC). 16HBE, A549 and H358 parental cells were plated in triplicates in 12 well plates and cells in each well were transfected with one of the three CD276 CRISPR Guide RNA vectors. After 24 hours, the GFP-tagged cells were sorted using flow cytometry to obtain a homogenous but non-clonal cell population. B7-H3 protein expression was analysed by Western blot upon transfection of cells with each CD276 CRISPR Guide RNA vector. 16HBE cells did not respond to any of the B7-H3 CRISPR knockdowns while A549 and H358 cells presenting the lowest B7-H3 expression level were chosen for further experiments. B7-H3-depletion in CRISPR cells was further validated by qPCR and immunofluorescence.

2.2.2.5 siRNA transfection of cell lines

For acute knockdown of endogenous B7-H3, KIF3A and IMPDH2 RNA interference was used. All siRNA SMARTpool oligos and non-targeting control siRNA pools were purchased from Horizon Discovery LTD.

16HBE, A549 and H358 cells were plated in 6 well plate 24 hours prior to transfection at 60-70 confluency. siRNA (Stock solution 20 µM) was diluted in 190 µL of OptiMEM. In a separate tube, 5 µL of DharmaFECT was also diluted in 190 µl of OPTIMEM and both tubes were incubated for 5 minutes at room temperature. The DNA and DharmaFECT solutions were mixed gently and incubated at room temperature for another 15 minutes. The DNA/ DharmaFECT solution was added dropwise to the cells containing 2 ml of OptiMEM. Cells were incubated for 6 hours at 37°C, after which the media was aspirated and replaced with complete growth media. Cells were grown for 48-72 hours post-transfection and the efficiency of transfection was assessed by immunocytochemistry and Western blot.

2.2.2.6 Drug treatments

Cells were plated in the relevant tissue culture plates and once at the correct confluence, treated with reagents as described in Table 5. DMSO or Methanol only treated cells were used as a control.

2.2.3 Biochemical analysis

2.2.3.1 GFP-trap immunoprecipitation

16HBE, A549 and H358 cells were transiently transfected with GFP control or GFP-tagged B7-H3 and cultured on 10 cm dishes. The following day, they were either treated with Methanol as vehicle control or MPA as in Table 5. When cells reached 100% confluency, they were washed twice with ice-cold PBS before 500 µl of cold IP buffer, containing protease and phosphatase inhibitor cocktails (1:100), was added to the cells. Subsequently, cells were scraped and centrifuged at 13,000 RPM for 10 minutes at 4°C. 5 µl of GFP-trap® beads and 15 µl of agarose resin suspension mix were washed three times in GFP IP lysis buffer. Supernatants obtained from cell lysates were then added to the beads mix and incubated for 3 hours at 4^0C on a rotator. 50 µl of each supernatant was also set aside to be used as input. Afterwards, the beads were washed three times with GFP IP lysis buffer. 2x sample buffer containing β-mercaptoethanol (1:200) was added to the beads, boiled for 10 minutes at 95 °C and centrifuged to clear cell debris and beads. 40 µl of samples were loaded onto 10% polyacrylamide gels and immunoblotted.

2.2.3.2 Endogenous immunoprecipitation pulldown

16HBE, A549 and H358 cells were treated with or without MPA as in Table 5 and grown to 100% confluency in a 10 cm^2 sterile tissue culture dish. Cells were then lysed in 500 µl of IP Lysis buffer containing protease and phosphatase inhibitors (1:100). Lysates were then collected into a 1.5 ml microcentrifuge tube and rotated for 15 min at 4°C on a rotator. Samples were then briefly centrifuged to pellet insoluble material, and 50 µl lysate was kept (1:1 IP buffer: sample buffer) at -20°C for an input sample. The remaining supernatant containing cell lysate was moved to a tube containing 30 µl of the A/G agarose affinity matrix suspension that has been already washed twice in IP wash buffer. In order to pre-clear the lysates, the latter were incubated with the A/G bead for 30 minutes at 4°C on a rotator then centrifuged at 2000 x g for 3 min at 4°C. The supernatant was split into a 2 new Eppendorf tubes and 3 ug of antibody of interest (B7-H3, IMPDH2) or control IgG antibody to control for non-specific binding was added to the lysates and left tumbling overnight at 4°C. Afterwards, a 100 ul of washed protein A/G bead slurry was added to the antibody/lysates mixture and tumbled for 2 hours to allow to bind at 4°C. the samples were then spun down at 2000 x g for 3 min at 4°C, the supernatant was discarded and beads were washed three times with IP wash buffer. After the final wash, the beads were pelleted and the supernatant was discarded. Beads were boiled with 50 µl of 2x sample buffer containing (1:200) β-mercaptoethanol for 10 mins at 95°C and 30 µl of each sample was loaded in each well of 10% gel and subjected to SDS-PAGE followed by immunoblotting.

2.2.3.3 SDS-PAGE analysis

To separate protein expression based on their molecular weights, sodium dodecyl sulphate-polyacrylamide gel electrophoresis (SDS-PAGE) was performed using gels with 8-10% (v/v) polyacrylamide resolving layer and a 4% (v/v) stacking layers. Cells were lysed in RIPA buffer containing protease inhibitors and phosphatase inhibitors (1:100) followed by adding (1:1) 2x Laemmli sample buffer supplemented with β-mercaptoethanol (1:100) to denatures the protein and induce a negative charge resulting in migration toward the positive cathode pole when electrical charge is applied. Proteins were separated under an SDS-PAGE system and PeqGold Protein Marker V was run alongside samples for protein size reference. A constant voltage of 80 V was applied until the lysates moved through the stacking gel and then the

voltage was increased to 180 V until the gel band-front had moved through the separating gel.

2.2.3.4 Western blotting

Western blotting was used to detect proteins of interest following separation of proteins in a sample from SDS-PAGE. Proteins were transferred from polyacrylamide gels onto PVDF membrane for 1 hour and 30 minutes at 20V using a transfer kit (Invitrogen) in transfer buffer (with 20% Methanol). The membranes were blocked using blocking buffer (5% Bovine Serum Albumin in TBST (0.1% Tween in PBS) for 1 hour at room temperature. This was followed by incubation with primary antibodies, as listed in Table 6, in blocking buffer overnight at 4°C. Membranes were then washed three times for 10 minutes in TBST before incubation with horseradish peroxidase (HRP)-conjugated secondary antibodies for 1 hour at room temperature. After washing membranes three times with TBST, proteins were detected by ECL chemiluminescence kit (BioRad) and directly imaged using the BioRad imager digital imaging system. Blots were analysed and processed using Biorad Image Lab. For re-probing, membranes were stripped with Re-blot strong (10x) (Chemicon) diluted to 1x in distilled water for 10 min at room temperature, then treated as before. BioRad Image Lab software (v5.2.1) was used to analyse Western blots.

2.2.3.5 PNGase F treatment

PNGase F was used to cleave all N-linked oligosaccharides from B7-H3. After cell lysates were collected, 20 µg of glycoprotein, 1x Glycoprotein Denaturing Buffer and water was combined and denatured at 95°C for 10 minutes. This was followed by the addition of 1x GlycoBuffer 2, 1% NP-40 and PNGase F and water. The reaction mix was incubated for 1 hour at 37°C before Western blot analysis.

2.2.3.6 Identifying protein in complex with B7-H3 via Liquid Chromatography-Tandem Mass Spectrometry (LC-MS/MS)

All samples were analysed by the King's College London Proteomics Facility. Samples

obtained from GFP-trap immunoprecipitation were run into a 1D gel (single 10%, not a gradient) and resolved for 20 mins at 80 V to effectively stack the protein complement into a small gel section. The gel was subsequently stained with InstantBlue-Coomassie protein stain for 15 minutes followed by washing the gel with HPLC/LCMS water thrice. The bands of interest were then excised using a scalpel, transferred to a clean Eppendorf tube and left to de-stain in HPLC/LCMS water overnight before sending the gel slices for protein identification by Liquid Chromatography - Tandem Mass Spectrometry (LC-MS/MS). Trypsin digestion of gel sections was carried out at room temperature overnight after initial incubation of 2 hours at 37^{o}C. This was followed by peptide extraction and samples were individually resuspended in 18 µl of resuspension buffer (2% ACN in 0.05% FA), 6 µl of which was injected to be analysed by LC-MS/MS. Chromatographic separation was performed using a U3000 UHPLC NanoLC system (ThermoFisherScientific, UK). Peptides were resolved by reversed phase chromatography on a 75 µm C18 Pepmap column using a three-step linear gradient of 80% acetonitrile in 0.1% formic acid. The gradient was delivered to elute the peptides at a flow rate of 250nl/min over 60 min starting at 5% B (0-5 minutes) and increasing solvent to 40% B (5-40 minutes) before a wash step at 99% B (40-45 minutes) followed by an equilibration step at 5% B (45-60 minutes). Ionization of the eluate was performed by electrospray ionisation using an Orbitrap Fusion Lumos (ThermoFisherScientific, UK) operating under Xcalibur v4.3. The instrument was programmed to acquire using an Orbitrap-Ion Trap method by defining a 3s cycle time between a full MS scan and MS/MS fragmentation by collision induced dissociation. Orbitrap spectra (FTMS1) were collected at a resolution of 120,000 over a scan range of m/z 375-1800 with an automatic gain control (AGC) setting of 4.0e5 (100%) with a maximum injection time of 35 ms. Monoisotopic precursor ions were filtered using charge state (+2 to +7) with an intensity threshold set between 5.0e3 to 1.0e20 and a dynamic exclusion window of 35s ± 10 ppm. MS2 precursor ions were isolated in the quadrupole set to a mass width filter of 1.6 m/z. Ion trap fragmentation spectra (ITMS2) were collected with an AGC target setting of 1.0e4 (100%) with a maximum injection time of 35 ms with CID collision energy set at 35%. Raw mass spectrometry data were processed into peak list files using Proteome Discoverer (ThermoScientific; v2.5). The raw data file was processed and searched using the Mascot (www.matrixscience.com) & Sequest (Eng *et al*; PMID 24226387) search algorithms against the Uniprot Human Taxonomy (50,351 entries) database. The database output file was uploaded in to Scaffold software (v 4.11.0; www.proteomesoftware.com) for visualisation and manual verification to create a .sfd file

for further analysis.

2.2.3.7 Dual Phase Metabolite Extraction using CHCl3, MeOH and H2O for Nuclear magnetic resonance (NMR) analysis

16HBE cells were transfected with B7-H3 siRNA to knockdown B7-H3 or non-targetted siRNA as a control. The following day, to ensure the cells are metabolically active at the time of extraction as well as having enough material for detection, 5 million cells of each 16HBE parental and siRNA transfect cells, A549 and H358 parental and CRISPR lines were plated in a 15cm^2 sterile tissue culture dish and left to adhere overnight. Afterwards, the media was aspirated from the cells and the culture plates were washed twice with 20 ml of ice-cold PBS ensuring it was completely removed from the plates after each wash. The dry plates were then incubated on dry ice for 2 minutes in order to quench the metabolome. The cells were scraped after adding 2.2 ml of ice-cold methanol and transferred to pre-cooled 15 ml tube followed by the addition of 2.2 ml chloroform on top then left to rotate for 10 minutes at 4°C. Subsequently, 2.2 ml of MilliQ H2O was added to the tube and mixed by inverting, the mixture was left to incubate on ice for 10 minutes to allow the formation of a stable bilayer then tubes were centrifuged at 1550 RPM for 45 mins at 4°C. After the centrifugation step, 3 layers were formed. The top (aqueous) layer contained metabolites soluble in the polar fraction, a middle white layer contained proteins, and a bottom layer contained metabolites that are soluble in the apolar fraction. The top (polar) fraction was collected into pre-cooled 2 ml micro-centrifuge tubes which was then completely dried in an Eppendorf concentrator for around 8 hours at 30°C; mode – V-Aat, and samples were stored at -80°C until analysis. The interphase layer was discarded, and bottom (apolar) fraction was transferred into a glass vial that was left uncapped into the fume hood overnight then store at -80°C. Five different repeats of each cell line (top and bottom fractions) were sent to the Nuclear magnetic resonance (NMR) facility at King's College London to analyse the effect of B7-H3 on different metabolites in cells. Once the samples were dried, the samples were resuspended with 600 µl of $CDCl_3$ with 0.1% v/v of TetraMethylSilane (TMS) and transferred to a 5 mm tube for lipid extracts, and 600 µl of a D2O solution with 100 mM Na_2HPO_4, 4 mM NaN_3 and 5 mM TrimethylSilylPropionate TSP and transferred to a 5 mm tube for aqueous extracts. The samples were analysed on a Bruker Avance NEO 600 MHz equipped with a TCI Cryoprobe

Prodigy (Bruker). Spectra were acquired at 298 K and consisted for each lipid sample of a pulse-acquire (named zg in Topspin) with 64 scans, an acquisition time of 2.75s and an inter-scan delay of 3s, and for each aqueous sample of a ^{1}H PresatURation using GradiEnts (PURGE) spectrum, with 128 scans, an acquisition time of 2.62s and an inter-scan delay of 4s. After acquisition, all spectra were then phase corrected, baseline corrected and the chemical shifts were referenced to the TMS peak or the TSP peak at 0.0 ppm, respectively for lipid samples and aqueous samples. For identification, 2D spectra were acquired on one aqueous extract and one lipid extract, consisting of a Total Correlation SpectroscopY (TOCSY), using the Bruker pulse sequence "dipsi2gpphzs", slightly modified to include presaturation, which 8 scans, 256 t_1 increments, a spectral width of 13.7 ppm in both dimensions and an inter-scan delay of 2s, along with a Heteronuclear Single-Quantum Correlation (HSQC) spectrum, using the Bruker pulse sequence "hsqcetgpsisp2.2", with 16 scans, 256 t_1 increments, a spectral width of 170 ppm in the ^{13}C dimension and 12 ppm in the ^{1}H dimension and an inter-scan delay of 2 s. Data was uploaded to MetaboAnalyst platform for metabolomics data processing and analysis.

2.2.3.8 LC-MS/MS Metabolite Extraction using H_2O and methanol

2 million cells of each 16HBE parental and siRNA (control and B7-H3) transfected cells, A549 and H358 parental and CRISPR lines were plated in a 15cm^2 sterile tissue culture dish and left to adhere overnight. The following day, parental lines were either vehicle or MPA-treated as in table 5. 48 hours post-treatment, media was aspirated from the cells and the culture plates were washed twice with 20 ml of ice-cold 150 mM Ammonium Acetate ensuring it was completely removed from the plates after each wash. The dry plates were then incubated on dry ice for 2 minutes to quench the metabolome. Next, 2.2 ml of ice-cold methanol was added, the cells were scraped and transferred to pre-cooled 15 ml tube and left to rotate for 10 minutes at 4°C. Then, 2.2 ml of HPLC/LCMS H2O was added to the tube and mixed thoroughly by vortexing, the mixture was centrifuged at 1550 RPM for 45 mins at 4°C. The supernatant was then transferred to a clean Eppendorf tube and dried in an Eppendorf concentrator until completely dry. 1 ml of MeOH:H2O 1:1 was added to the dry tube, vortexed thoroughly to make sure everything goes in suspension. Finally, the tube was dried once more to make it easier to resuspend in minimal volume of method-specific diluent before running the LC-MS. All samples were sent to be analysed by MS facilities for quantitative analysis at

the National Phenomics Centre in Imperial College London where all dried cell samples extracts were reconstituted in 100 uL of method-specific diluent. Aliquots of 10 uL from each sample were pooled together to generate a study reference (SR) sample that was analysed along with study samples. Then all study samples and SR sample were injected in triplicate in randomised order to enable quality control of the data and LC-MS instrument-specific software (TargetLynx) was used to extract and integrate the peaks of the defined panel of metabolites and isotopically labelled standards that were added to each sample. The stable isotope labelled standards were added to the samples for LC-MS analysis to account for any matrix effects in the samples and MS detector possible variations during the analysis.

The results were presented in triplicate for each metabolite-sample as a ratio of area of each peak of metabolite to the peak area of internal standard with the closest retention time and/or structure. The average value for each metabolite and sample was calculated and used as final result. RSD% (relative standard deviation) was calculated for each triplicate set of results (sample- metabolite) as a measure of precision. Thresholds were implemented of RSD% which are, less than 20 is excellent, 20-30 is good and greater than 30 were flagged. Some metabolites had to be removed due to low intensity and consequently high imprecision of peak integrals. For the rest of metabolites that are presented in this study, each peak was checked individually, especially in the cases where the RSD% values were 20-30% and higher than 30%. The metabolites of primary interest were measured with high confidence (low RSD%) across all samples and replicate measurements.

2.2.3.9 RhoA and Rac1 GTPase activation assay

Cells as in LC-MS/MS Metabolite Extraction were culture in 10 cm dishes for 48 hours then washed with ice cold PBS and lysed on ice in 500 µl of ice-cold lysis buffer following the Cytoskeleton G-LISA kit protocol. The lysates were transferred to clean tubes and centrifuged at 10,000 x g, 4°C for 1 minutes to remove insoluble material. Supernatants were aliquoted in different volumes of 50 µl for Western blotting, 20 µl for protein quantification and 100 µl for RhoA/Rac1 activity assay and were immediately snap-frozen in liquid-nitrogen to store at -80^{0}C. To measure lysate's protein concentration, aliquots of 20 µl were mixed with 1 ml of

Precision Red Advanced Protein Assay Reagent provided and incubated for 1 minute at room temperature in spectrophotometer cuvettes. The spectrophotometer (WPA Biochrom) was first blanked with the lysis buffer at 600 nm and the absorbance of lysates samples in each cuvette was read and calculated to reach the identical protein concentration of 1.5 mg/ml in each sample. Subsequently, frozen samples were tested with G-LISA kit according to the manufacturer's instructions. Briefly, frozen samples were equalised according to the protein quantifications, mixed with the binding buffer provided. 50 µl of each sample/binding buffer mix, positive control, or blank buffer were added into wells of the RhoA-GTP/Rac1-GTP binding plate. Immediately, the plate was placed on a cold orbital microplate shaker at 400 RPM for 30 minutes at 4^0C. The plate's wells were then washed twice with the provided washing buffer and incubated with the antigen-presenting buffer for 2 minutes at room temperature. Afterwards, wells were immediately washed three times again and anti-RhoA or anti-Rac1 primary antibody was added into the wells. The plate was left on an orbital microplate shaker at 400 RPM at room temperature for 45 minutes. The wells were subsequently washed three times and incubated with the secondary antibody on the shaker for 45 minutes. Wells were incubated with HRP detection reagents for 10-15 minutes at 37^{o}C after they have been washed again thrice. When sufficient colour development was reached, HRP stop buffer was added to each well and the absorbance signal of each well was measured (optical density at 490nm) with a microplate spectrophotometer (POLARstar Omega).

2.2.4 Microscopy

2.2.4.1 Immunofluorescence

Cells were plated on 13 mm glass coverslips placed into a 24 well sterile tissue culture plate and allowed to adhere overnight in normal growth media. When cells were ready to be fixed post plating (or treatment if any as in table 5), they were washed with 1x with PBS then fixed using 4% paraformaldehyde (PFA) for 15 minutes at room temperature followed by three washes with PBS. Cells were then permeabilized with 0.2% TX-100 in PBS for 10 minutes, then washed in PBS and blocked by incubating the coverslips in 5% w/v BSA in PBST at room temperature for 1 hour. Incubation of cells with various primary antibodies as listed in table 6 diluted in 5% BSA/PBST was then carried out in a dark humidified chamber placed at 4°C overnight. Coverslips were subsequently washed by submerging in PBST then incubated with

secondary antibodies and DAPI diluted in 5% BSA/PBST for 1 hour at room temperature. Coverslips were washed three times in PBST and once in MilliQ water, then finally mounted to glass slide using Fluorsave™ mounting solution. Images of fixed cells were acquired using a confocal microscope with a 60x oil immersion objective in ND2 Nikon NIS-elements (v 4.51.01) image format, exported as TIFFs, and analysed in ImageJ.

2.2.4.2 Confocal microscopy

Images of fixed and live cells were acquired on a Nikon A1R inverted confocal microscope (Nikon Instruments UK) with an environmental chamber maintained at 37°C/5% CO2. Images were captured using a 20x or 60x Plan Fluor oil immersion objective (numerical aperture of 0.45 and 1.4, respectively). Excitation wavelengths of 488 nm (diode laser), 561 nm (diode laser) or 640 nm (diode laser) were used. Images were acquired using NIS-Elements imaging software (v4) and were saved in Nikon Elements in the.ND2 format exported as TIFFs, and processed in ImageJ software.

2.2.4.3 Live cell imaging

16HBE, A549 and H358 cells transfected with LifeAct-GFP were plated in a chambered 8 wells tissue culture slide (ibidi) and allowed to adhere overnight at 37°C. After 24 hours, HEPES was added to the media at a final concentration of 25 µM together with either control IgG, B7-H3 (MAB1027) or recombinant human B7-H3 ectodomain (NS0-derived) at a 10 µg/ml as in table 5 and left to incubate for 3 hours at 37°C. Cells were then imaged every minute for one hour. The same reagents were also added to coverslips and fixed after 8 and 24 hours of incubation.

2.2.4.4 Total internal reflection fluorescence (TIRF) microscopy

Images of live cells were acquired on an Eclipse Ti-E inverted microscope (Nikon) with an environmental chamber maintained at 37°C and a DU-897 X-3430 camera (Andor). TIRF utilises the evanescent wave resulted from the total reflection of a laser beam at the interface between a glass surface and an aqueous medium. The evanescent wave is capable of exciting fluorophores within a limited distance from the interface as its energy decays exponentially. Images were taken using a 60x oil immersion objective with a numerical aperture of 1.4.

Excitation wavelengths of 488 nm was used. Images were acquired using NIS-Elements imaging software (v4) and were saved in the .nd2 format. Image processing and analysis was performed using ImageJ.

2.2.4.5 Time-lapse fluorescence microscopy

Cells expressing fluorescent proteins were imaged using phase time-lapse microscopy EVOS FL Auto 2 (Thermofisher) with an environmental chamber maintained at 37°C. Images were taken using 10x or 20X objectives 3.2 MP CMOS camera. Excitation using DAPI, GFP or RFP LED light cubes were used. Images were acquired using EVOS (v2) software and processed with ImageJ and saved as TIFF files.

2.2.4.6 Cell migration assay

Parental/siRNA control and B7-H3 siRNA/CRISPR knockdown cells were seeded in same number of each well of a 24 well plate and incubated for 24 hours at 37°C. Complete growth media was replaced and supplemented with 25 µM Hepes. Time-lapse experiments were set up using EVOS microscope. Images were acquired using a 20x objective at intervals of 10 minutes over a 16 hours time period. Velocity and distance were analysed using a manual tracking and ADAPT plugins in ImageJ.

2.2.4.7 Proliferation and colony size assays

10000 cells were plated for each cell line on a 24 well plate and incubated for 24 or 48 hours at 37^{o}C 5% CO_2. Cells that were supplemented with control IgG, B7-H3 mAb or B7-H3 ectodomain were treated 24 hours post-plating. The control 0-hour time point was assumed when cells adhere. Then cells were fixed with 4% PFA/PBS for 15 minutes and stained with DAPI to enable cell quantification and phalloidin to measure colonies size using automated analysis on ImageJ software. Images were acquired using an EVOS FL Auto 2 fluorescent microscope (Thermofisher) with 10x objective, cells in all wells were tile scanned and saved as TIFFs using ImageJ software and total cell count was obtained by thresholding for nuclear stain followed by automated counting.

2.2.4.8 Oxidative stress detection

16HBE parental, siRNA control and B7-H3 siRNA knockdowns, A549 and H358 Parental or B7-H3 CRISPR cells were plated onto a 96 wells plate and left to adhere overnight. Cells were then washed with PBS and media was changed to either complete media (control), complete media supplemented with MPA for parental lines only or media without FBS (serum staved) and left to incubate for 48 hours. A fluorogenic probe for measuring cellular oxidative stress CellRox Deep Red reagent was added to the cells at 5 µM concentration together with DAPI to normalize the cells' oxidative stress fluorescence to cell number. Cells were washed three times with PBS and imaged on the EVOS microscope as described previously in *Time-lapse fluorescence microscopy* Section. The fluorescent levels were measured using Image J software.

2.2.4.9 Chemoresistance and survival assay

A549 and H358 parental and B7-H3 knockdown cells were used in this experiment in different conditions, cells were either untreated, MPA-treated or starved for 48 hours, and each condition was supplemented with 5 µM of either DMSO as vehicle control or Cisplatin to trigger cells apoptosis. After 48 hours, growth media was removed, CellEvent^{TM} Caspase-3/7 Green Detection Reagent was added to wells at 0.4 µM together with DAPI for 30 minutes as per manufacturer's protocol. Cells were then imaged using the GFP and DAPI channels on an EVOS microscope. Green cells fluorescence was measured and number of cells was counted, both using ImageJ software.

2.2.4.10 Hanging drop spheroid invasion assay

To generate hanging drops for spheroids; methylcellulose stock solution was made by pre-heating 250 mL DMEM to 60˚C and using pre-heated DMEM to dissolve 6 g of autoclaved methylcellulose powder then stirring the solution for 20 minutes at room temperature. An additional 250 mL DMEM was added, and the solution was stirred at 4˚C overnight. Methylcellulose solution was then cleared by centrifugation in 50 mL Falcon tubes at 5000 xg at room temperature for 2 hours. Cleared methylcellulose solution was transferred to fresh 50 mL Falcon tubes and stored at 4˚C for use within a year.

$75x10^3$ H358 parental and B7-H3 CRISPR knockdown cells and $50x10^3$ A549 parental and B7-H3 CRISPR knockdown cells were resuspended in 2.25 ml of DMEM or RPMI media respectively containing 0.5% FBS. 750 µl of methylcellulose was then added to the cell suspension. 20 µl aliquots of the cell suspension was dropped on to the lid of a square petri dish using a multichannel pipette and 10 ml of PBS was added to the bottom of the dish. The lid containing the drops was carefully inverted and placed over the PBS. The hanging drops were incubated at 37°C, 5% CO2 in a water saturated incubator for 48 hours to allow spheroids to form.

In order to perform the invasion assay, a collagen mix containing 2 mg/ml collagen (Rat Tail Type I collagen), 20 mM Hepes, 10 mM fibronectin, 17.5 mM NaOH and OptiMEM was made to embed the spheroids. 100 µl of the collagen mix was added into each well of a 96 well plate. Each spheroid was removed from the hanging drop using a 20 µl pipette set to 5 µl and dropped into each well before the collagen had set. The gels were then left to set at 37°C for 1 hour. Once the collagen was set, 100 µl of media was added into each well. Phase- contrast images of the spheroids post-embedding were acquired using the Evos FL Auto 2 fluorescent microscope (Thermofisher) and the 3.2 MP CMOS camera with a 10x objective at 0 and 48 hours. Cell invasion was quantified using ImageJ software. The acquired images (.TIFF format) were imported in ImageJ, a region of interest was manually drawn around each spheroid and the area was quantified by the software. 0 hours post-embedding spheroids were only comprised of a spheroid core, whereas 24 hours post-embedding cells started leaving the core and spheroids were comprised of invading cells in addition to a spheroid core. Regions of interest were drawn around the entire spheroid (including invading cells). Spheroid cell invasion was quantified by dividing the spheroid area at 24 hours by the spheroid area measured at 0 hours post-embedding. For experiments in which the spheroids were treated with MPA, the inhibitor was diluted in media and added on top of the embedded spheroids formed as previously.

To further analyse the spheroids, they were fixed in 10% formalin solution for 2 hours at 37˚C. Next, samples were washed thrice for 10 mins in PBS followed by permeabilization using 0.25% Triton X-100 in PBS (PBST, v/v) for 30 mins on a rocker at room temperature. Samples were washed again thrice for 10 mins before blocking with 5% BSA in PBST for 1 hour at room temperature on a rocker. Following blocking, DAPI and Phalloidin 488 diluted in blocking buffer were added to each embedded spheroid and left to stain on the rocker overnight. Finally, samples were washed for 10 mins three times before final addition of 100 µL PBS and stored at 4˚C covered in foil until imaging. Images were acquired as described previously using the confocal microscope and then analysed using QuPath software

2.2.5 Image analysis

Table 8: Software used for image analysis

Software	Source	Version	Use
JACoP	JACoP (Just Another Co-localisation Plugin) (nih.gov)	V 1.53p on ImageJ	Co-localisation analysis
ImageJ	National Institute of Health	V 1.53p	Western blot and Image analysis
Prism 9	GraphPad	V 9.2.0	Statistical analysis
QuPath	QuPath: Open source software for quantitative pathology & Bioimage analysis	0.3.0	Spheroids proliferation, area, and packing

2.2.5.1 Western Blot analysis

Images taken on the BioRad digital imaging system were imported into ImageJ for analysis. Lanes were selected by drawing a rectangle around areas of interest that were then plotted as peaks, labelled and measured. Areas of peaks measurements were normalised for total protein by HSC70 or B7-H3-GFP peaks measurements depending on the experiment, unless otherwise stated. Data was exported into excel and then into GraphPad Prism for statistical analysis.

2.2.5.2 Intensity of B7-H3 at the membrane and cytoplasm

The membrane intensity of cells stained with B7-H3 were analysed on ImageJ. Only cells in groups/colonies were analysed across all images to be able to determine B7-H3 levels at junctions. A region of interest was drawn around a single cell including the visible membrane boundary, 8 ROIs were selected for each field of view and the grey values were measured. In order to measure the B7-H3 intensity at the cytoplasm, the ROI of each selection was reduced on all sides of the cell by clicking the enlarge option by -7 pixels. This was enough to capture the membrane contribution (Figure 17). The grey value of the smaller ROI was then measured. Values were exported to excel and the percentage of the total signal at the membrane was

calculated by dividing the smaller value (cytoplasm) by the larger one (membrane+cytoplasm). GraphPad Prism was used for statistical analysis.

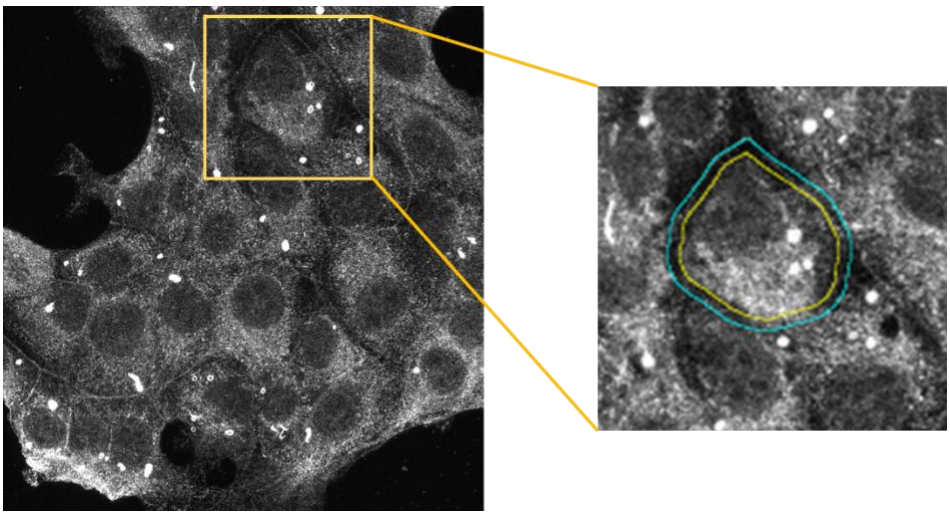

Figure 17: B7-H3 intensity at the membrane and cytoplasm analysis.
An example image of 16HBE cells population stained for B7-H3. The selected areas depict the intensity at the cytoplasm (smaller yellow area), the whole cell (large cyan area) and the membrane between the yellow and blue selected areas.

2.2.5.3 Co-localisation analysis

Images were acquired using methods as previously described in Confocal microscopy and using the same laser settings and objectives across all samples. Images were then opened in ImageJ and channels were split. Using the JACoP plug-in (https://imagej.nih.gov/ij/plugins/track/jacop.html), the Mander's correlation coefficient between two channels of interest were generated (Figure 18). Mander's correlation coefficient values below 0.4 were considered coincidental overlap. Data was exported into excel and then into GraphPad Prism for statistical analysis.

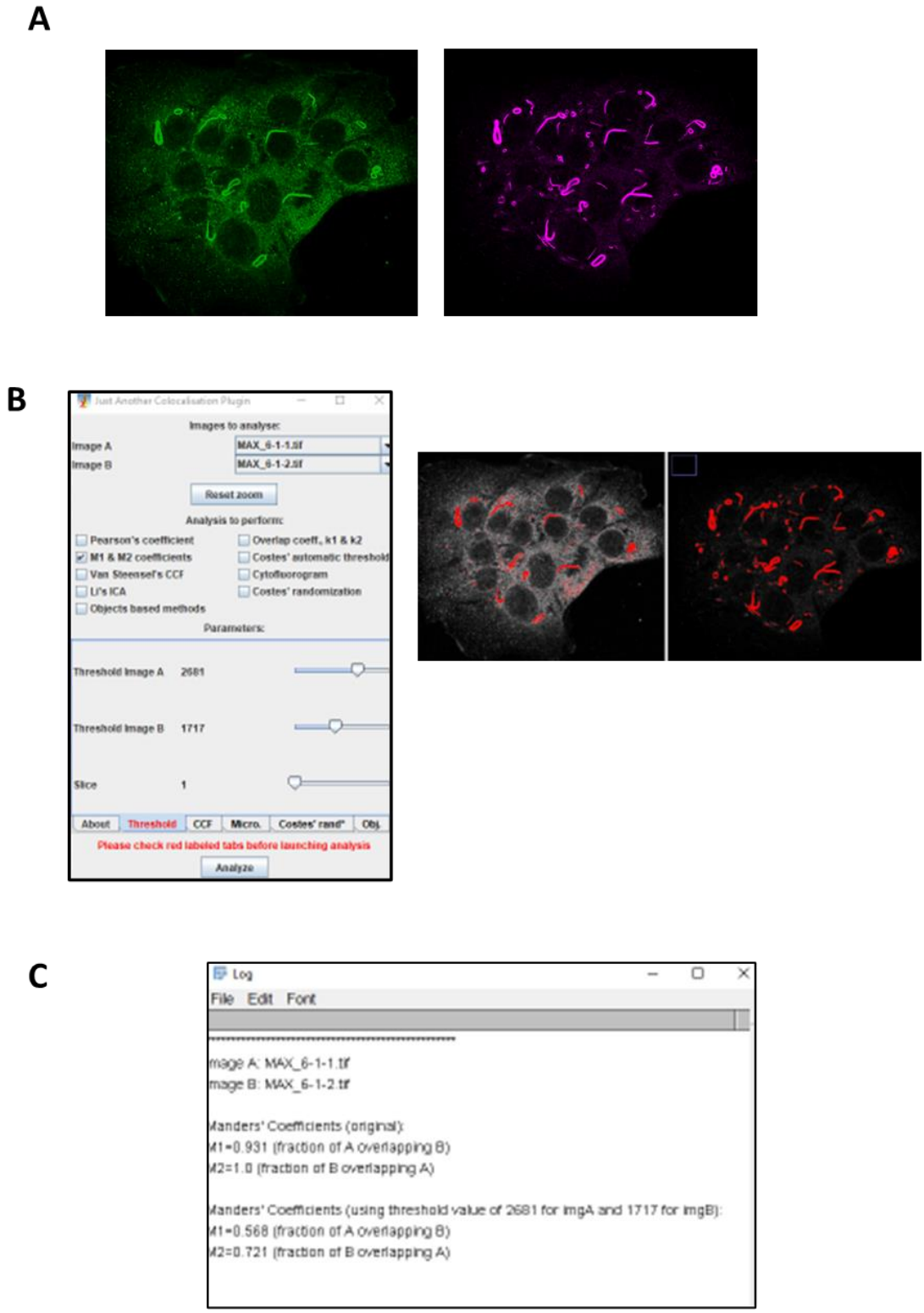

Figure 18: Co-localisation analysis workflow.
A) Confocal image of a 16HBE cells treated with MPA and stained with B7-H3 (green) and with IMPDH2 (magenta). Channels were separated and the JACoP plug-in was used to calculate M1 and M2 coefficients. **(B)** Images were then thresholded and co-localisation was measured **(C)** giving values for Mander's M1 and M2 coefficients.

2.2.5.4 Line scan analysis

To analyse protein distribution at cell-cell junctions, cells were fixed and stained with β-catenin antibody as a marker for cell junction. In each experiment images were acquired as described in *2.2.4.2 Confocal microscopy* section, using identical acquisition settings to ensure comparable intensities at cell-cell junctions. In ImageJ, lines of 20 µm in length and 1 µm in width were drawn perpendicular to junctions identified via β-catenin localisation (Figure 19A). Lines were aligned so that the 10 µm point was at the centre of junctions. The intensity of each channel was measured using a script developed in lab (Figure 19B) and exported. The individual scans were normalized to the highest intensity cell of each scan.

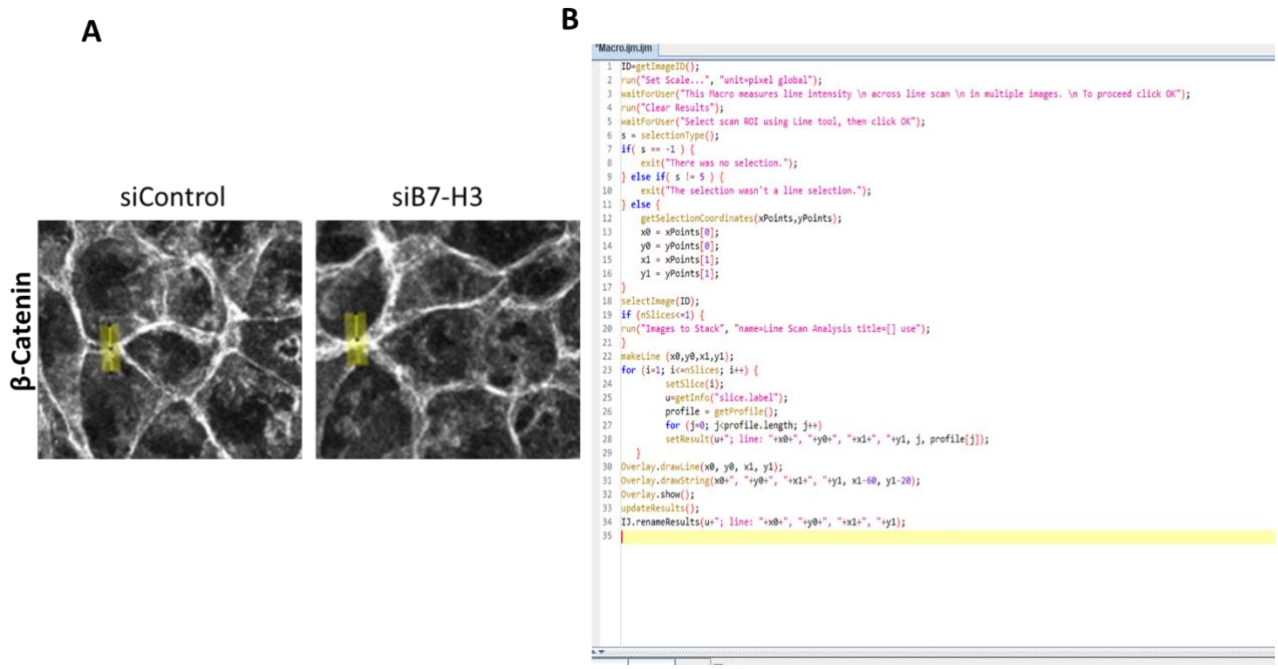

Figure 19: Line scan analysis.
A) Example images of 16HBE cells showing lines drawn across cell-cell junctions (yellow lines). (B) Script of line scan analysis.

2.2.5.5 Velocity and Distance analysis

Time lapse movies from 16HBE, A549 and H358 siRNA Control/parental or B7-H3 knockdown cells were imported into ImageJ. A total of 30 cells were selected at random from 3 different experiments. Cells were tracked over time using the ImageJ plugin manual tracking, velocity was calculated as µM/hour. Data was exported into excel and then into Graphpad Prism for statistical analysis.

2.2.5.6 Focal adhesion analysis

To analyse the area of focal adhesions, cells were fixed and stained with antibody against vinculin to label focal adhesions. The analysis was carried out using methods described in (Horzum, Ozdil and Pesen-Okvur, 2014). Brierly, images were opened on imageJ and subtract background selection was applied. The rolling ball radius set to 50 pixels and sliding paraboloid option was ticked. CLAHE (Contrast Limited Adaptive Histogram Equalization) plugin was run to enhance the local contrast of the image using the following values: block size = 19, histogram bins = 256, maximum slope = 6, no mask and fast. Mathematical exponential (EXP) was applied to further minimize the background and the brightness & contrast were adjusted automatically. Images were then thresholded and finally analyse particles command was applied. Values were exported into excel and then into GraphPad Prism for statistical analysis.

2.2.5.7 Primary cilia quantification

Cells were fixed under basal conditions and primary cilia were identified by staining cells with ARL13B as a marker of primary cilia. Z-stack was taken of images on the confocal and primary cilia was detected at the top focal planes. ARL13B positive cells were counted manually, and the percentage was calculated against the total number of cells in the field of view.

2.2.5.8 Fluorescence intensity analysis

Measurement of fluorescence intensity for CellEvent™ Caspase-3/7 Green Detection Reagent and CellROX™ Deep Red Reagent was carried out on live cells imaged on the EVOS. Images of cells were imported into ImageJ where Raw Integrated Density levels were measured and normalised to total cell number by counting nuclei stained with DAPI. Statistics was carried out using GraphPad Prism.

2.2.5.9 Phenotype analysis

Cells incubated with the B7-H3 antibody or B7-H3 ectodomain were identified and characterized based on the present of ruffles or stress fibre formation. Phenotypes were then

scored and counted with at least 10 cells from 7 different fields of view per cell line per experiment (figure 20).

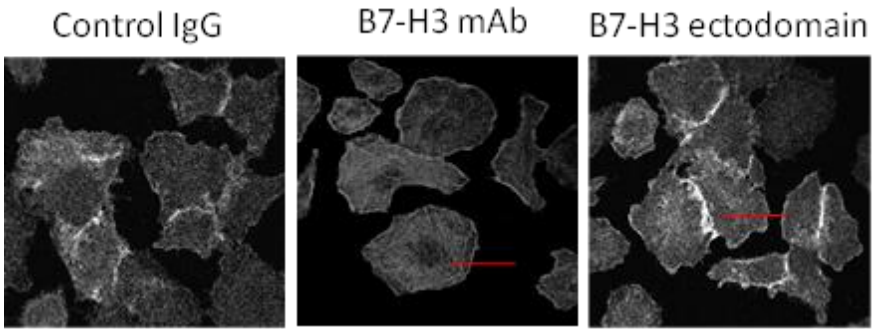

Figure 20: Representation of actin phenotypic changes of different cell lines treated with control IgG, B7-H3 Antibody or B7-H3 ectodomain.
A549 example images of how cells were classified based on the changes represented and scored upon identification of normal, stress fiber or ruffle formation denoted by the red line in Control, B7-H3 mAb, and B7-H3 ectodomain respectively. Cells were stained for F-actin.

2.2.5.10 Spheroid 3D invasion and QuPath analysis

For the invasion assay, Images were acquired and analysed on ImageJ as described in *2.2.4.10 Hanging drop and spheroids invasion assay* of the methods section (Figure 21).

To further analyse the spheroids, the area and number of cells in a spheroid was quantified using QuPath software. Images were captured as described in the "Hanging drop and spheroids invasion assay" section. The images were imported to QuPath software where they were designated as 'Fluorescence' images and DAPI channel was selected to show nuclei in spheroids embedded in collagen gels for 24 hours. From each spheroid, the middle slice of a Z-stack imaged spheroid was chosen for analysis. This was repeated for each of at least six spheroids per treatment/condition of 3 independent experiments. The total nuclei were annotated using the polygon tool (Figure 22A, yellow). Following annotation, cell detection was applied to identify individual nuclei (Figure 22.B, red) and these individual detections were fed into the 2D Delaunay Clustering analysis option to allow output of mean neighbour distance, nuclei number and area. These outputs were entered into Prism and compared between cell lines/treatments to identify differences in proliferation and cell packing.

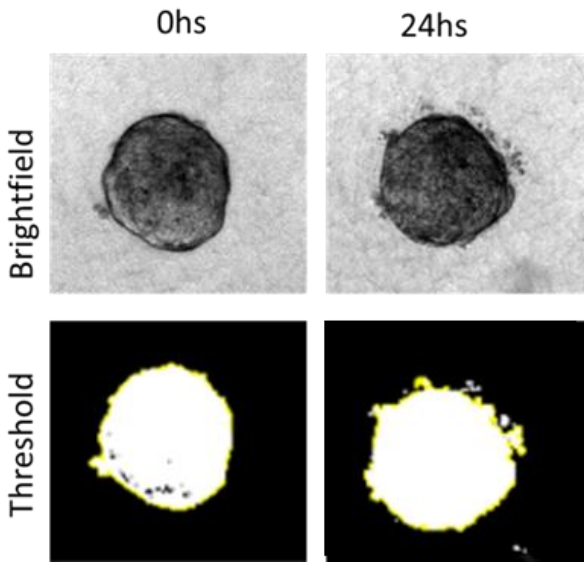

Figure 21: Image Analysis Pipeline for Quantification of Total Spheroid Invasive Area.
Top panel shows example images of H358 spheroids taken immediately or 24 hours post embedding. Bottom panel shows Thresholded images of same spheroids region selected for quantification.

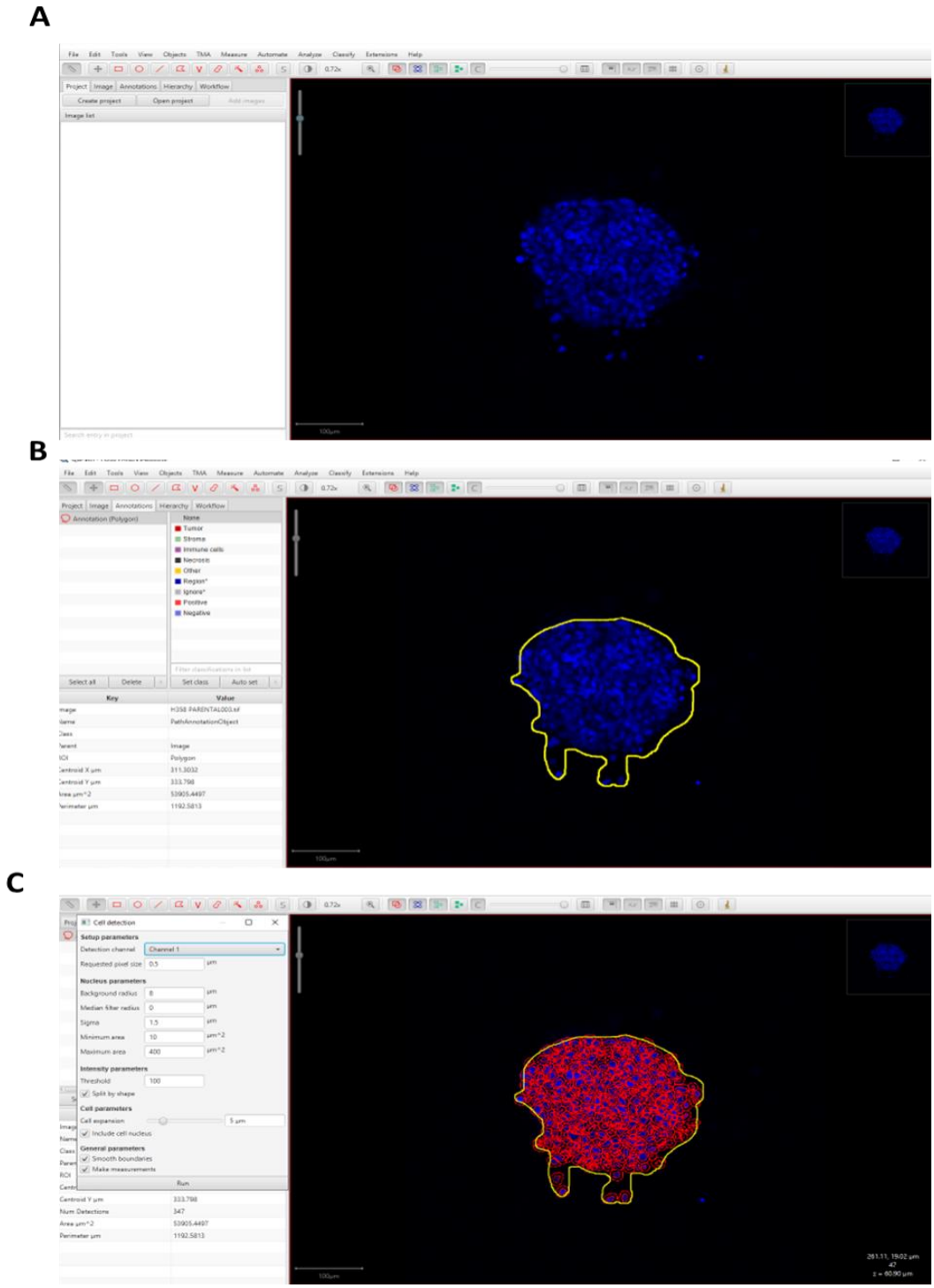

Figure 22: Image Analysis Pipeline for Quantification of Nuclei and cell packing using QuPath A) Representative of the middle slice of an H358 spheroid stained for DAPI as displayed in QuPath **(B)** Displayed annotation area after application of polygon tool, shown in yellow. **(C)** Displayed detection of individual nuclei after application of the cell detection tool, shown in red. All proliferation analyses were run in QuPath (version 0.3.0) with statistical analyses in Prism 9.

2.2.6 Statistical analysis

Data values are expressed as mean ± standard error of mean (SEM) of at least three experiments unless stated. All statistical tests were carried out using GraphPad Prism, version 9. Student's t-test was used for comparing two groups for statistical analysis. One or two-way analysis of variance (ANOVA) with Tukey's post hoc was used for multiple comparisons. Statistically significant values were taken as * = $p < 0.05$, ** = $p < 0.01$, *** = $p < 0.001$, **** = $p < 0.0001$ and were assigned in specific figures and experiments as shown.

3. Characterisation of B7-H3 expression and localisation in normal lung epithelial and cancer cells

3.1 Introduction

B7-H3 is highly expressed in cancer and one of the B7/CD28 superfamily of immune checkpoints that regulate the T-cell response. B7-H3 mRNA levels are widely expressed in most tissues. The protein expression of B7-H3 has been detected in immune cells, and identified at low levels in normal lung, liver, bladder, testes, prostate, breast, placenta and lymphoid organs (Dong *et al*., 2018). Studies have found that B7-H3 protein is upregulated in T-cells, antigen presenting cells (APC) and natural killer cells (NK), and is highly expressed in many types of tumours, including NSCLC, prostate, kidney, ovary, colorectal and breast cancer, where its presence is associated with poor prognosis (Brunner *et al*., 2012). However, the specific function and ligand for B7-H3 remains unclear as conflicting reports suggest it can both stimulate and inhibit the immune response. One study demonstrated a co-stimulatory role where B7-H3 binding enhanced IFN-γ-producing CD8 T-cells and increased IL-12 levels (Chapoval *et al*., 2001). Conversely, another study suggested a co-inhibitory role where B7-H3 inhibited the proliferation of both CD4 and CD8 T-cells and decreased the production of IL-2 and IFN-γ, likely through suppression of nuclear factor κB (NF-κB) mediated signalling pathways (Prasad *et al*., 2004). Moreover, most previous studies have focused on the interaction between B7-H3 and immune cells. However, previous unpublished work in the Parsons lab has demonstrated that B7-H3 is localised between adjacent cells, raising the possibility that B7-H3 is a cell-cell adhesion protein. Nevertheless, the role of localisation of B7-H3 in normal epithelial vs. cancer cells and how this contributes to tumourigenesis remain unclear.

Cell-cell adhesions are vital for maintaining epithelial cell and tissue integrity, polarity and regulating biological processes (Garcia *et al*., 2018). Generally, epithelial cells have three intercellular junction systems: gap junctions, which serve as intercellular channels that allow small molecules, ions and electrical impulses to directly pass through; tight junctions, that form a barrier that is impermeable to most soluble molecules between the two sides of the epithelium; and anchoring junctions, such as adherens junctions (AJs) that connect with the cortical cytoskeleton to provide structural support and cell-cell sensing and integrate intercellular signalling, including regulation of transcription pathways (Jamora & Fuchs, 2002). E-cadherin/β-catenin complexes are among constituent structural molecules that assemble

to form AJ. They can activate multiple key signal transduction pathways and are actively involved in epithelial to mesenchymal transition (EMT), an important mechanism in cancer progression and initial step of metastasis, thus playing a critical role in tumourigenesis (Bedi *et al*., 2008).

Primary cilia also serve key signalling roles in maintaining epithelial cell state (Higgins *et al*., 2019). The primary cilium is a microtubule-based nonmotile structure that protrudes from the surface of almost all mammalian cells (Gluenz *et al*., 2010b). Primary cilia consist of axoneme which is anchored to the cell by the basal body that is nucleated by the mother centriole (Lattao *et al*., 2017). One of the highly enriched proteins in cilia is ARL13B, which plays a role in regulating GTPases and cilia length from within cilia (Gigante *et al*., 2020). A recent study demonstrated that ARL13B interacts with purine biosynthetic enzyme Inosine-5'-monophosphate dehydrogenase 2 (IMPDH2) and by depleting ARL13B it enhanced salvage purine biosynthesis of damaged environmental purines (Shireman *et al*., 2019). The presence of cilia is dynamically regulated during cell cycle progression; if the cell is dividing the cilium retracts into the cell and the centrosome acts as the mitotic pole (Goto *et al*., 2013). It has been reported that cilia are lost in multiple cancer types and that it is due to several ciliary-associated genes being heavily dysregulated in cancer (Basten *et al*., 2013; Seeley *et al*., 2009).

Given the uncertainty around localisation and function of B7-H3, experiments in this first chapter aimed to study and characterise this in both normal human lung epithelial and cancer cells with a view to understanding whether the widely observed upregulation in B7-H3 levels in cancer alters localisation and function.

3.2 Results

3.2.1 B7-H3 expression in 16HBE, A549 and H358 Cell lines

In order to begin to understand B7-H3 function, it was first necessary to characterise the expression levels of the mRNA and protein in the different three cell lines.

Cell lines used in this study were 16HBE, which is a normal lung epithelial cell line, and A549 and H358, which are both human lung adenocarcinoma cell lines. To compare the mRNA expression levels between the three cell lines, qPCR was carried out using primers against B7-H3. Data demonstrated that H358 cells had the highest mRNA expression of B7-H3 compared to A549 and 16HBE (Figure 23A). To investigate the expression levels of B7-H3 protein, whole cell lysates were extracted from cells and run on a Western blot then probed with an antibody against B7-H3. Consistent with mRNA levels, quantification of bands from Western blots demonstrated that 16HBE cells expressed significantly lower levels of endogenous B7-H3 compared to both adenocarcinoma cell lines, while H358 express the highest levels compared to A549 and 16HBE cells (Figure 23B-C).

A range of molecular weight banding patterns was seen in the three cell lines tested, inferring that B7-H3 undergoes post-translational modification, possibly through glycosylation, as has been previously suggested (Chen *et al*., 2015). Protein glycosylation helps in proper folding of proteins, stability and in function of membrane receptors. Different glycosylation patterns in these three cell lines could point to different functional outcomes (Parekh' *et al*., 1992). Even though it has been shown previously that B7-H3 is glycosylated, functional implications for this glycosylation are still unknown (Chen *et al*., 2015). To determine whether the different banding pattern was due to glycosylation, whole cell lysates were subjected to treatment with PNGase F, which is an enzyme that cleaves N-linked glycosides from proteins. Cell lysates were treated with PNGase F for 1 hour at 37°C followed by Western blotting probed for B7-H3 and HSC70 as a loading control. Following PNGase F treatment, the molecular weight of the resulting bands was visibly reduced from 100kDa to 70kDa indicating a loss of glycol groups from the protein (Figure 23D). This confirms that B7-H3 is heavily glycosylated in all three cell lines, which may play a role in the function of this receptor.

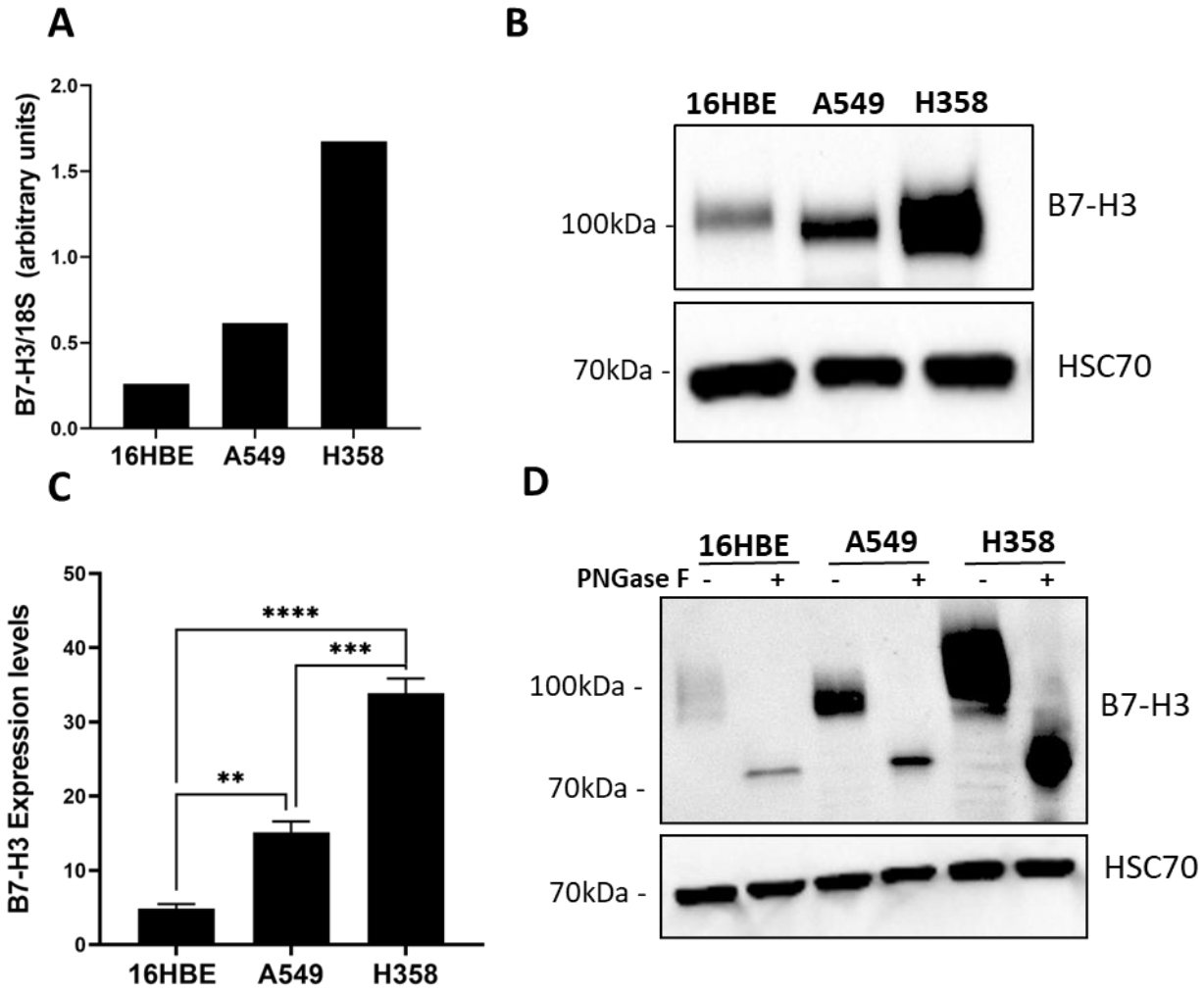

Figure 23: B7-H3 expression is increased in lung cancer cell lines compared to normal lung epithelial cells.

(A) mRNA levels of B7-H3 as measured by qPCR in 16HBE, A549 and H358 cells. **(B)** Western blot of lysates from 16HBE, A549 and H348 cells probed for B7-H3 and HSC70 **(C)** Quantification of Western blots as in (B) from 3 independent experiments. Graph shows mean +/- SEM. Significance assessed by one-way ANOVA; **p<0.01, *** p<0.005, ****p<0.001 **(D)** Western blot of lysates from specified control cells (-) or those cells treated with PNGaseF glycosylation inhibitor (+) probed for B7-H3 and HSC70. Representative of 4 experiments.

3.2.2 B7-H3 subcellular localisation differs between lung epithelial and cancer cells

To determine B7-H3 localisation in 16HBE, A549 and H358 cell lines, cells were grown on coverslips, fixed, and stained with an anti B7-H3 antibody, DAPI and Phalloidin. Representative confocal images in Figure 24.A demonstrated that B7-H3 is localised predominantly to the cell periphery in adenocarcinoma cell lines and enriched at sites of cell-cell adhesion. 16HBE cells displayed lower plasma membrane staining and more punctate cytoplasmic staining compared to the two tumour cell lines (Figure 24A). Quantification of the signal intensity of the protein at the plasma membrane compared to the cytoplasm demonstrated that H358 showed significantly higher membrane B7-H3 compared to both A549 and 16HBE cells, with ~80% of B7-H3 fluorescence intensity in 16HBE and A549 was in the cytoplasm (Figure 24.B). The B7-H3 staining intensity correlated to the expression levels observed by Western blotting.

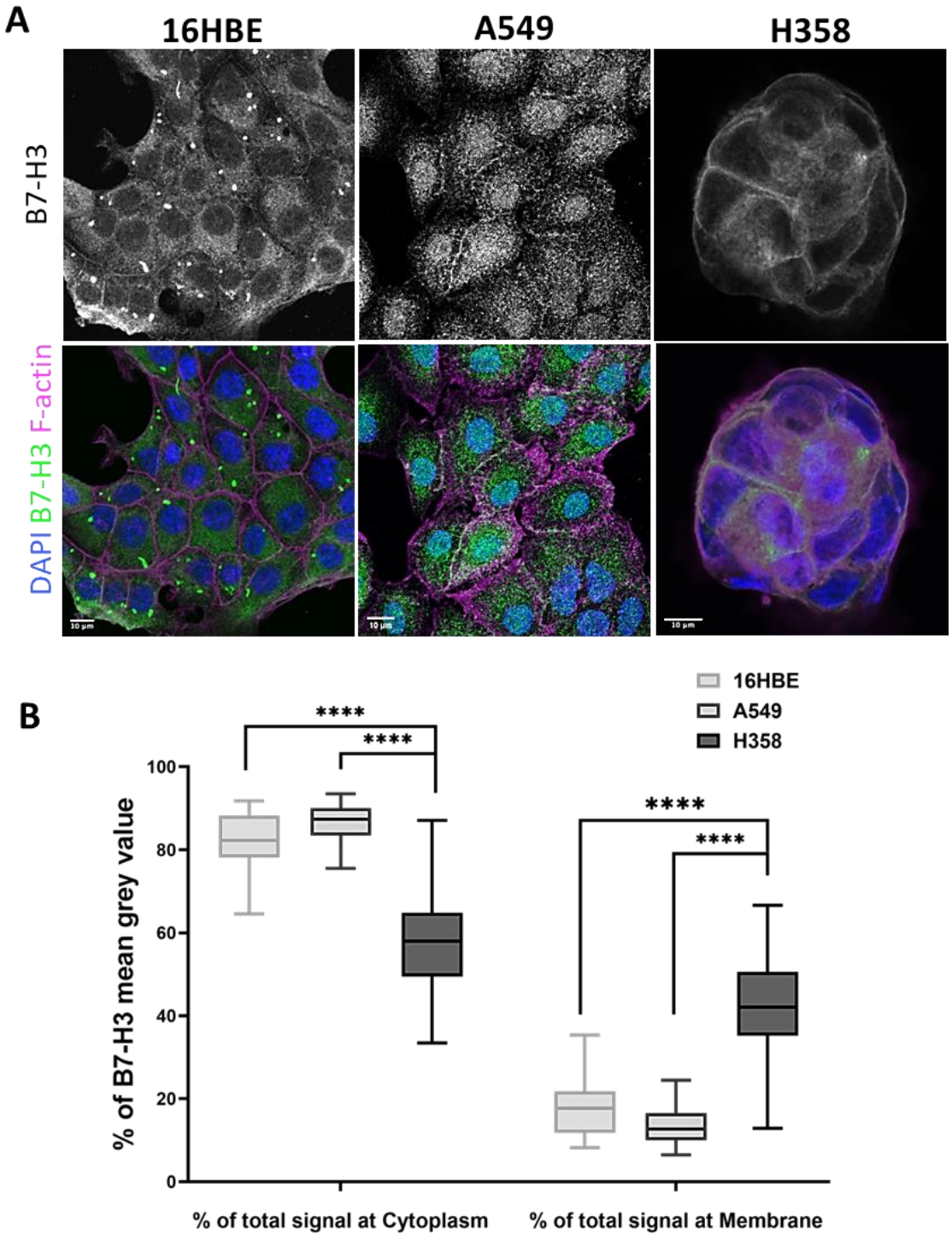

Figure 24: B7-H3 localisation differs between lung epithelial and cancer cells.
(A) Representative confocal images of 16HBE, A549 and H358 cells stained for B7-H3 endogenous levels (top panel). Bottom panel shows merged B7-H3 (green), F-actin (magenta) and DAPI (blue). Scale bars 10 µm. **(B)** Quantification of fluorescence intensity of B7-H3 in the cytoplasm and at plasma membrane in all cells. Graph shows pooled data from 3 independent experiments, at least 50 cells per experiment per condition. Data is shown as mean +/- SEM, significance assessed by one-way ANOVA; ****p<0.001.

3.2.3 B7-H3 levels are regulated by degradation

Glycosylation of membrane receptor proteins plays a crucial role in protein conformation and stability (Lee *et al*., 2015). In order to assess whether the stability of B7-H3 was altered between normal and cancer cells, cultures were treated with the protein synthesis inhibitor cycloheximide and levels of B7-H3 protein were analysed by Western blotting after 6 or 24 hours of treatment. Western blots (Figure 25A) and subsequent quantification (Figure 25B) revealed that levels of B7-H3 were significantly reduced after 24 hours of treatment compared to DMSO controls, suggesting that the protein is being degraded at a similar rate in all cell lines.

To further investigate the mode of degradation of B7-H3, cells were treated with cycloheximide in the presence or absence of MG132 or Leupeptin (proteasomal and lysosomal-dependent protein degradation inhibitors, respectively). Treating cells with MG132 did not have an effect on B7-H3 levels (Figure 25C, D). However, B7-H3 levels accumulated after leupeptin treatment in all three cell lines after 16 hours of treatment (Figure 25E, F). Collectively, these results indicate that B7-H3 is being degraded through the lysosomal pathway in agreement with a recent report (Zhang *et al*., 2021), and that this turnover occurs to a similar degree in normal and cancer cell lines.

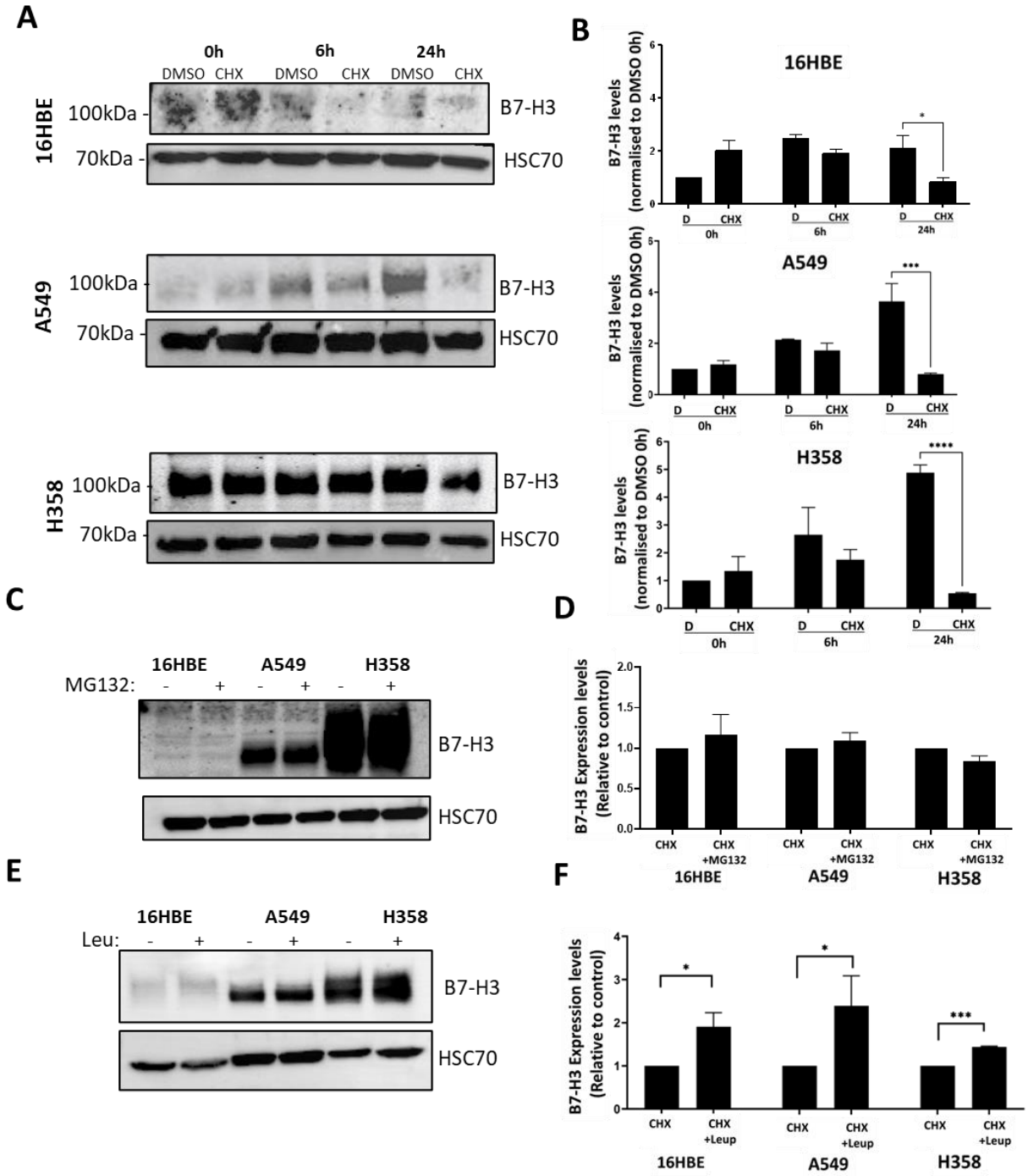

Figure 25: B7-H3 protein expression is regulated by lysosomal degradation.
(A) Representative blots of lysate from specified cells treated with either control (DMSO) or 50 mM of Cycloheximide (CHX) and lysed immediately, and after 6- or 24-hours post-treatment. **(B)** Quantification of 3 independent experiments per cell line as in (A). **(C)** Western blot of lysates from specified cells treated with CHX +/-20 µM MG132 (proteosome inhibitor) for 16 hours, probed for B7-H3. **(D)** Quantification of blots from 3 independent experiments as in (C). **(E)** Western blot of lysates from specified cells treated with CHX +/-100µM Leupeptin (lysosome inhibitor) for 16 hours, probed for B7-H3. **(F)** Quantification of blots from 3 independent experiments as in (C). All graphs show means +/- SEM. Statistical analysis performed by 2-way ANOVA. Significance values are * =p<0.05, **=p<0.01, ***= p<0.005.

3.2.4 B7-H3 localises to adherens and tight junctions in all cells

As B7-H3 is located at the plasma membrane and appears to be enriched at cell-cell junctions, the next goal was to determine whether B7-H3 co-localised with adherens or tight junction proteins. 16HBE, A549 and H358 cells were seeded onto coverslips, fixed, and stained for B7-H3 (green) and E-cadherin (magenta) antibody as a marker for adherens junctions. Representative confocal images demonstrated co-localisation of E-cadherin and B7-H3 to cell-cell adhesion sites (Figure 26A). Quantification of confocal images using Mander's correlation coefficient analysis revealed that B7-H3 showed high co-localisation with E-cadherin in H358 cells and this was reduced in A549 and 16HBE (Figure 26B), consistent with levels of B7-H3 at the plasma membrane in the respective cell lines (Figure 24B).

Staining of parallel coverslips with antibodies to ZO-1, a marker for tight junctions (magenta) and B7-H3 (green) revealed a similar degree of high co-localisation in H358 cells, which was reduced in A549 and 16HBE cells (Figure 26C). These data collectively indicate that B7-H3 can co-localise with cell-cell adhesion markers and that this is enhanced in cancer cells compared to normal lung epithelial cells.

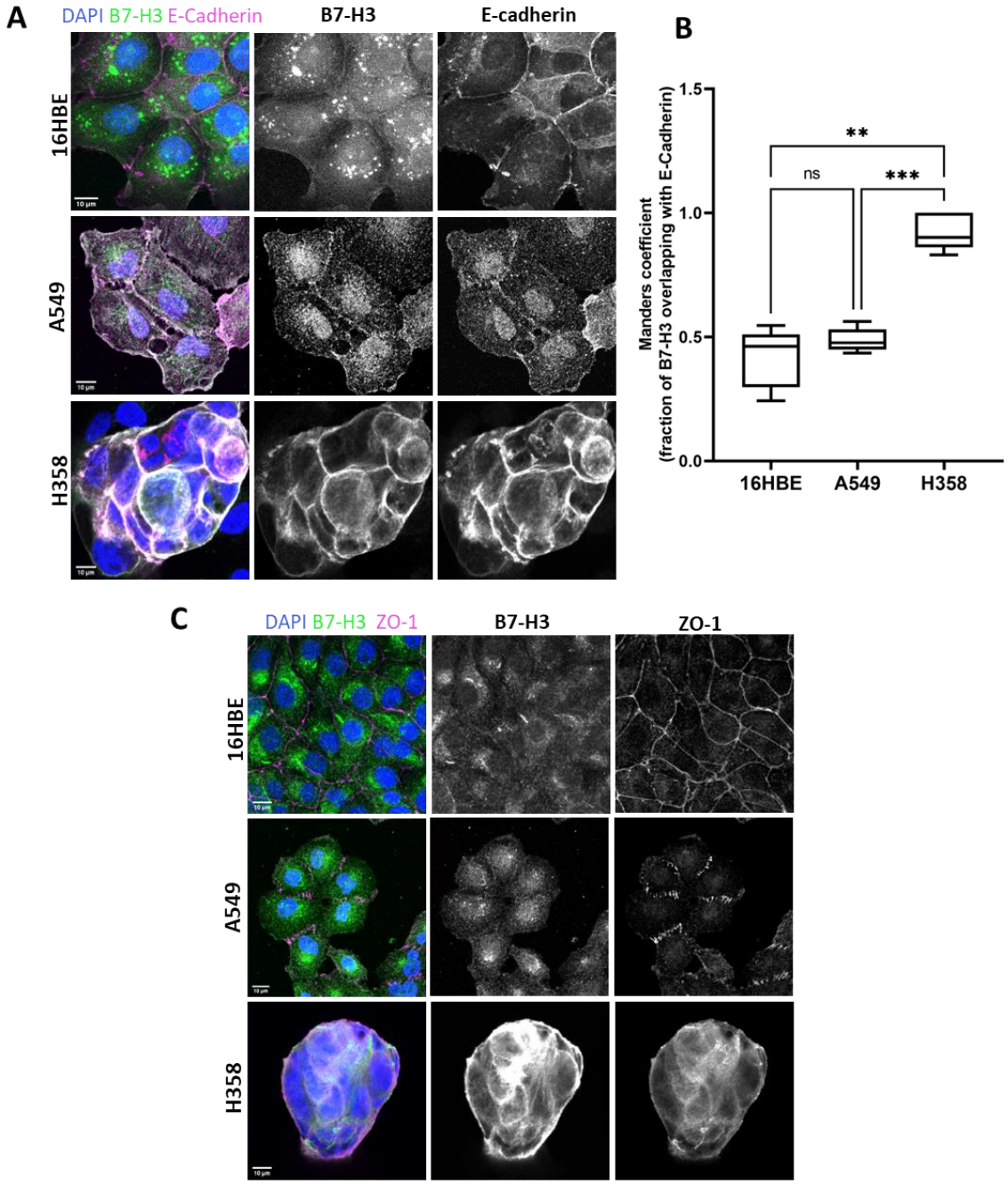

Figure 26: B7-H3 localises to cell-cell adhesion sites and tight junctions.
(A) Representative confocal images of 16HBE, A549 and H358 cells stained for nuclei (blue), B7-H3 (green and middle panel) and E-cadherin as a marker of AJ (magenta and right panel). **(B)** Quantification of Mander's co-localisation coefficient from images as in (A)**.** B7-H3 overlapping with E-cadherin intensity is shown from at least 50 cells and 6 fields of view. **(C)** Representative confocal images of cells as in A stained for nuclei (blue), B7-H3 (green and middle panel) and ZO-1 as a marker of TJ (magenta). Data is shown as mean +/- SEM, significance assessed by one-way ANOVA; **=p<0.01, ***= p<0.001. Scale bars 10 µm.

3.2.5 B7-H3 does not localise to endosomes or lysosomal compartments

Previous images of B7-H3 in 16HBE normal lung epithelial cells showed that B7-H3 localises to some specific cytoplasmic compartments (Figure 24A).

To investigate the nature of these structures, 16HEB cells were plated onto coverslips, fixed and stained for B7-H3 (green) and selected endosomal markers (magenta); Rab10 and Rab11 that are regulators of intracellular transport of proteins (Lucken-Ardjomande Häsler *et al*., 2020), and EEA1 an early endosomal marker and effector protein involved in the docking of incoming endocytic vesicles prior to fusion with early endosomes (Wilson *et al*., 2000). None of these endosomal proteins showed co-localisation with B7-H3 (Figure 27A)

To test whether B7-H3 was located to the lysosomal compartments in 16HBE, cells were labelled with lysosomal probe LysoTracker™ (magenta) prior to fixing the cells and staining for B7-H3 (green). CD63, a lysosomal integral membrane protein described as a main factor in endosomal cargo sorting and extracellular vesicle production (Hurwitz *et al*., 2018), was used as an additional marker for lysosomes. As no antibodies were available that were compatible with B7-H3 staining, CD63-GFP was transiently transfected (magenta) into 16HBE cells followed by fixing and staining for B7-H3 (green). Confocal images revealed that B7-H3 was not co-localised with either lysosomal markers (Figure 27B).

This data suggests that B7-H3 does not localise to endosomal or lysosomal compartments in 16HBE cells.

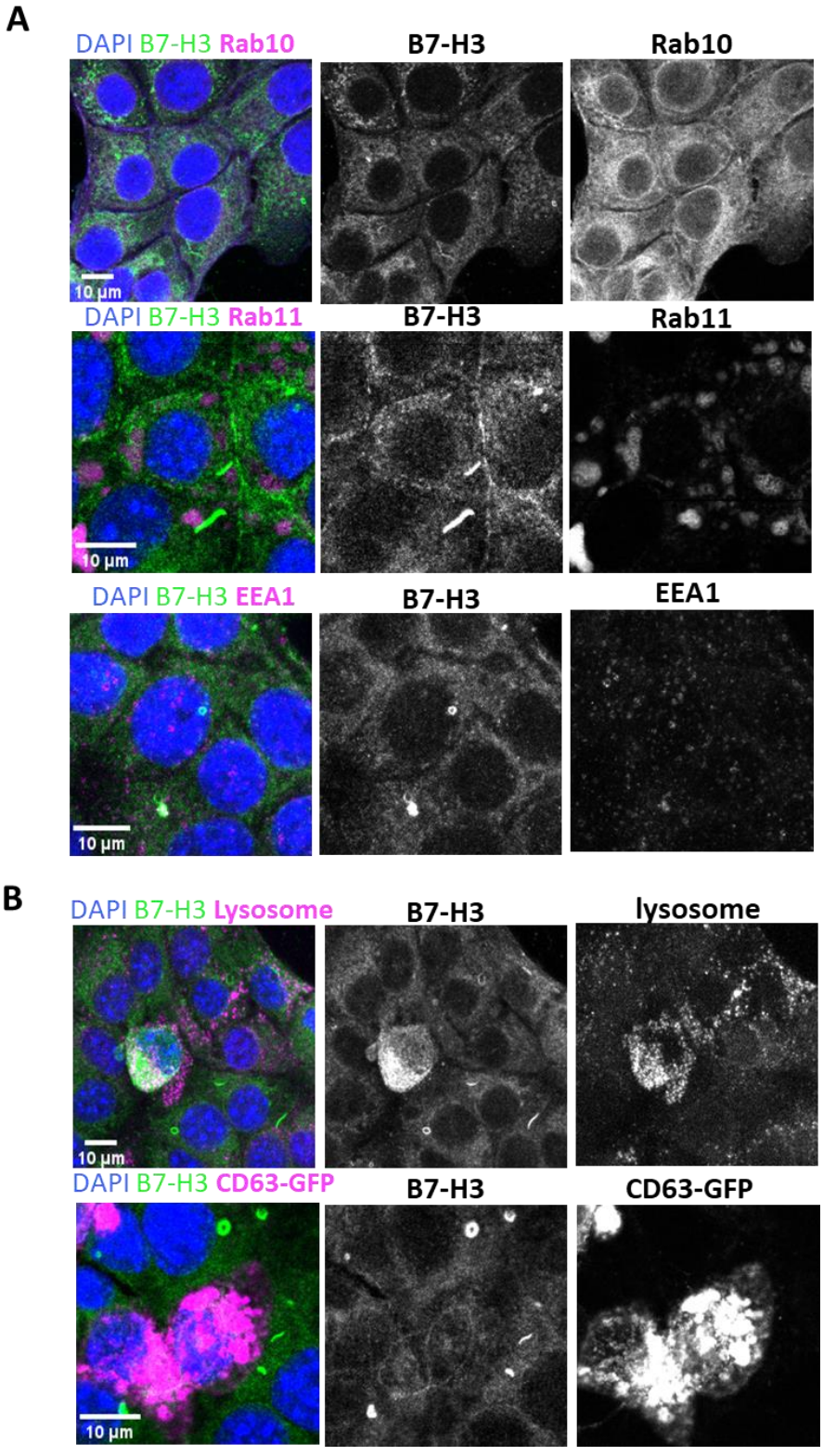

Figure 27: B7-H3 does not localise to endosomes or lysosomal compartments in 16HBE cells. **(A-B)** Representative confocal images of 16HBE cells stained for nuclei (blue), B7-H3 (green middle panel) and either Rab10, Rab11 or EEA1 (magenta and far right panel). **(B)** B7-H3 staining (green) with Lysotracker or overexpressed CD63-GFP (magenta and far right panel). Scale bars 10 µm.

3.2.6 B7-H3 localises to primary cilia in 16HBE cells

Upon closer inspection of confocal Z-stacks of B7-H3 stained 16HBE cells, both punctate localisation in the cytoplasm and at the apical surface of cells were visible. We postulated that the latter localisation within discrete apical regions may be primary cilia.

To investigate B7-H3 localisation to primary cilia, 16HBE cells were fixed, and stained for B7-H3 (green) and 2 different primary cilia antibodies; ARL13B and Pericentrin (magenta) (Figure 28A). ARL13B which is enriched in the primary cilia membrane/axoneme (Gigante *et al*., 2020), co-localised with B7-H3 in apical sections of the Z-stack confocal images (Figure 28A left panel). To further confirm B7-H3 localisation to primary cilia, pericentrin (PCN), which localises to the base of primary cilia (Jurczyk *et al*., 2004), was used. More basal view images of Z-stack confocal sections showed that B7-H3 also co-localised with PCN (Figure 28A right panel).

Analysis of the percentage of cells with both primary cilia markers demonstrated that ~40% of the cells were ARL13B/PCN positive, and ~20% of these cells showed B7-H3 co-localising with these two markers (Figure 28B). Taken together, this data demonstrates that B7-H3 localises with primary cilia markers in normal lung epithelial cells.

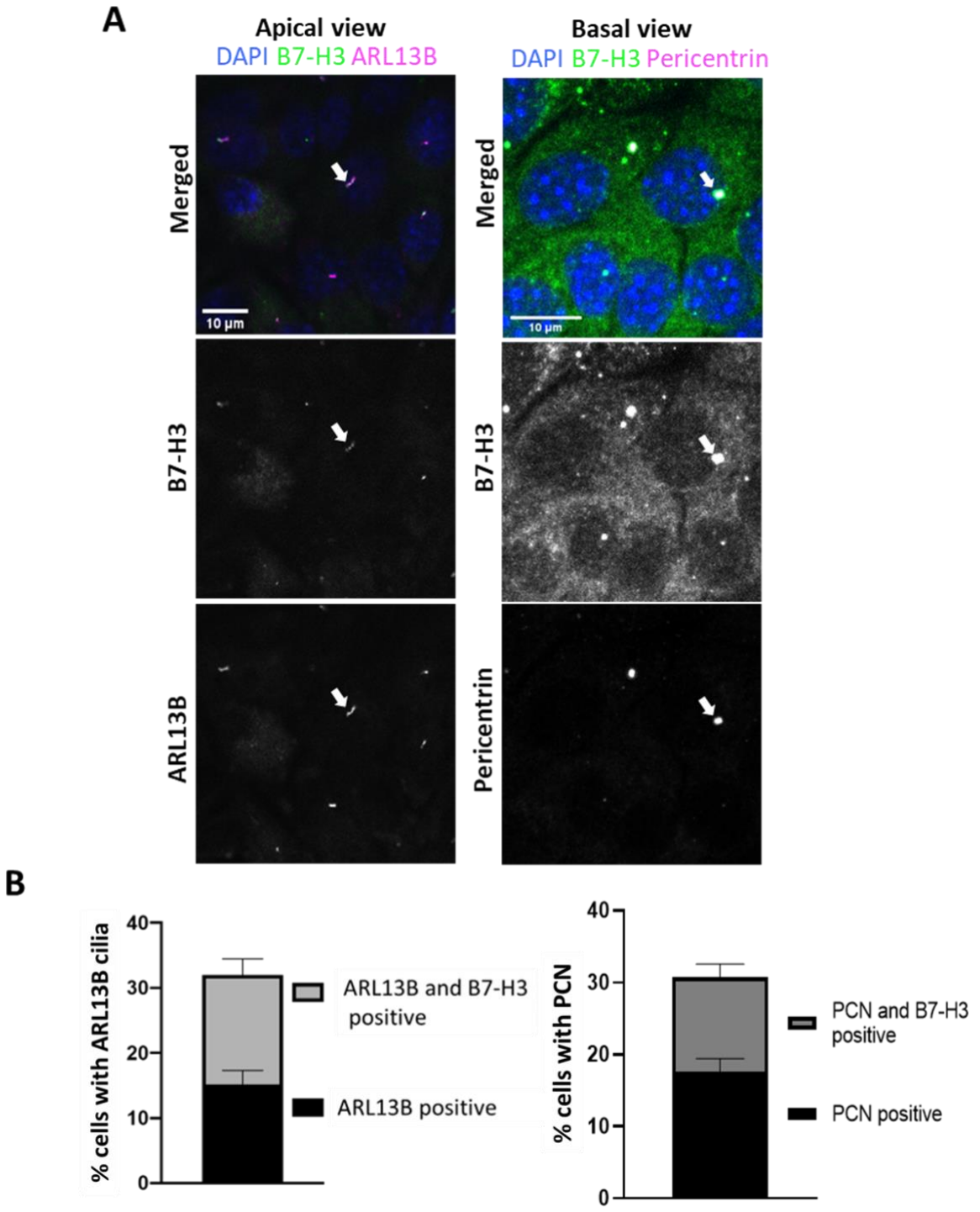

Figure 28: B7-H3 localises to primary cilia in 16HBE cells.
(A) Representative apical and basal confocal images of 16HBE cells stained for nuclei (blue), B7-H3 (green middle panel) and cilia markers (Arrow); ARL13B or Pericentrin (magenta bottom panel). **(B)** Quantification of the percentage of cells in (A) that has cilia. B7-H3 overlapping with either ARL13B as a marker of ciliary membrane or Pericentrin (PCN) marker of the basal body intensity were plotted. Cells quantified shown from at least 40 cells and 7 fields of view. Values were obtained from three independent experiments. Scale bars 10 µm.

3.2.7 B7-H3 localises to Rods & Rings in 16HBE cells

Whilst the cilia markers revealed co-localisation with B7-H3 at apical surfaces, these markers did not overlap with the highly defined cytoplasmic accumulations of B7-H3 in circular or linear structures. Upon consulting the literature, these structures were reminiscent of polymers of IMPDH (inosine monophosphate dehydrogenase) known as rods and rings (RR) (Schiavon *et al*., 2018).

In order to determine whether B7-H3 localised to RR in 16HBE cells, cells were stained for IMPDH2 and B7-H3. Representative confocal images (Figure 29A) showed B7-H3 (green) overlapping with IMPDH2 (magenta) at RR in the cytoplasm of 16HBE cells. Moreover, Mander's coefficient analysis showed ~60% co-localisation between B7-H3 and IMPDH2 in these structures (Figure 29B). Quantification of the mean number of RR per cell showed the range of RR/cell varied between 1 to 3 (Figure 29C). This data combined with the previous figure demonstrate that B7-H3 localises to primary cilia and RR in normal human lung epithelial cells.

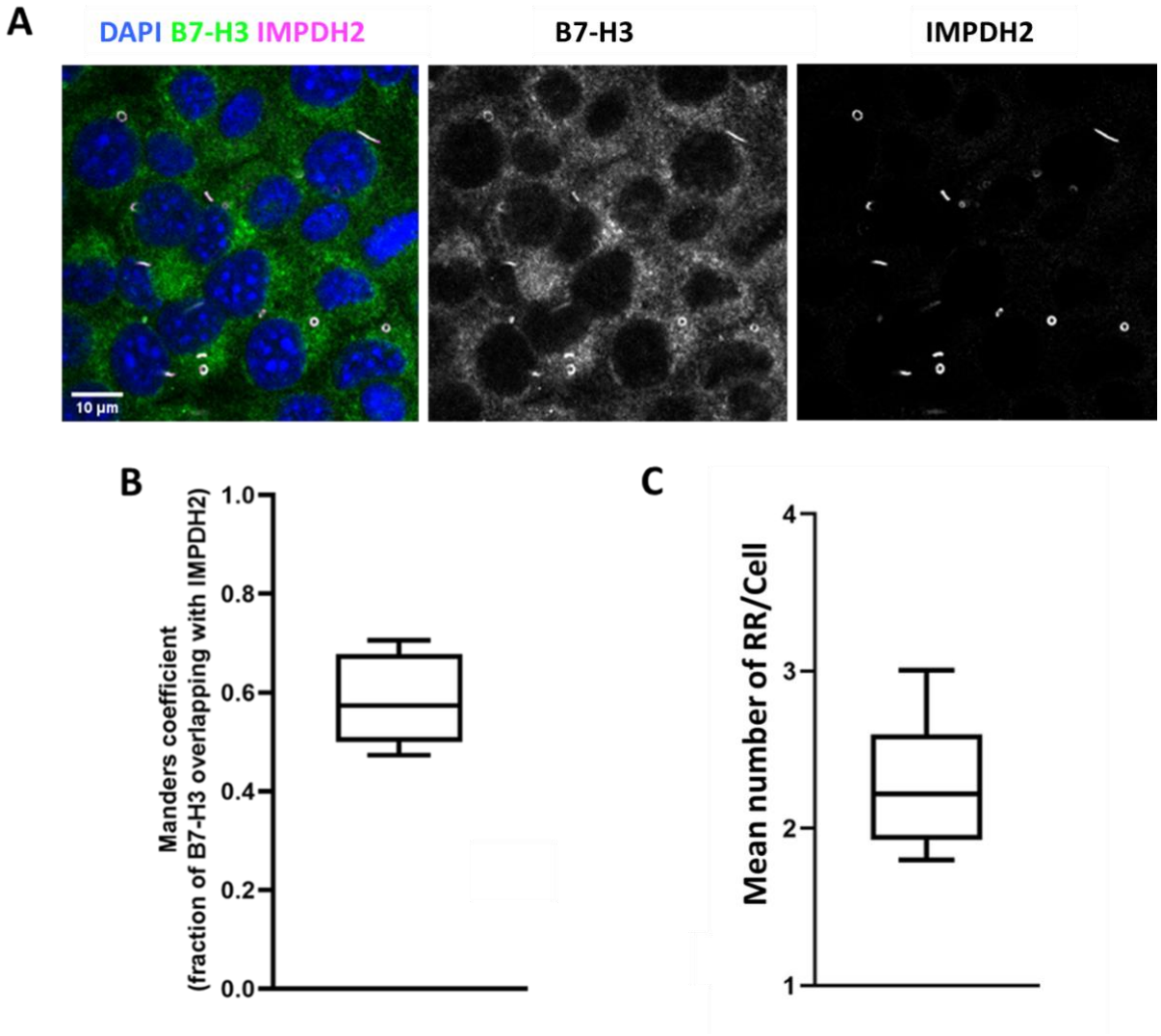

Figure 29: B7-H3 localises to Rods and Rings in 16HBE cells.
(A) Representative confocal images of 16HBE cells stained for nuclei (blue), B7-H3 (green middle panel) and IMPDH2 (magenta and far right panel). Scale bars 10 µm. **(B-C)** Quantification of co-localisation and mean number of Rods and Rings (RR) per cell from images of B7-H3 and IMPDH2 stained cells. Quantification of IMPDH2 and B7-H3 co-localisation was carried out using Mander's coefficient and represents mean +/- SEM from 5 fields of view with at least 10 cells/field of view and from 7 independent experiments.

3.2.8 Higher B7-H3 expression in cancer cell lines correlates with lower cilia numbers

Data thus far indicates that B7-H3 localises to primary cilia in 16HBE cells which exhibited the lowest levels of B7-H3 compared to the lung adenocarcinoma cell lines. In order to explore whether B7-H3 expression correlated with formation of primary cilia, A549 and H358 cells were fixed and stained for ARL13B (magenta) to analyse the presence of primary cilia (Figure 30A). Quantification of ARL13B positive cells was then carried out from confocal images and revealed significantly higher percentage of 16HBE cells displaying primary cilia compared to both A549 and H358 (Figure 30B). This data suggests that A549 and H358 cells assemble a significantly decreased number of primary cilia compared to normal lung epithelial cells, and the levels of B7-H3 expression inversely correlates with the assembly of primary cilia.

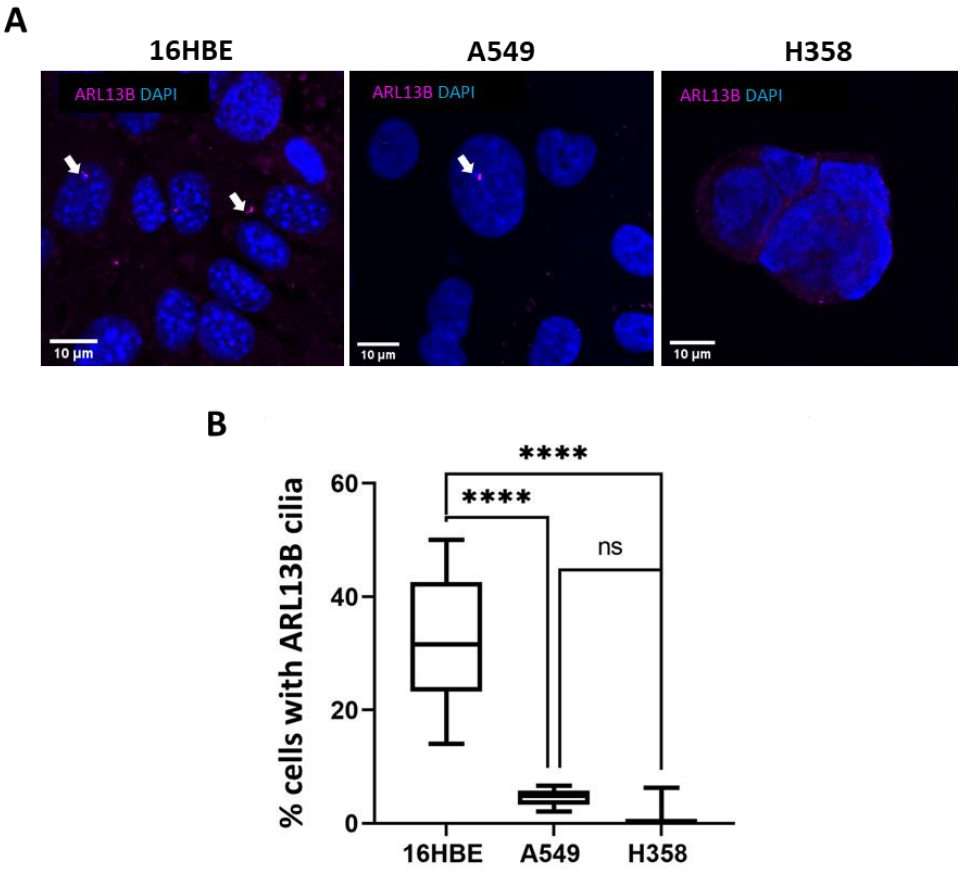

Figure 30: Higher B7-H3 expression in cancer cell lines correlates with lower cilia numbers. **(A)** Representative confocal images of 16HBE, A549 and H358 cells stained for nuclei (blue), ARL13B (magenta). **(B)** Quantification of the percentage of cells forming cilia. Data is shown as mean +/- SEM, significance assessed by one-way ANOVA; ****p<0.0001. Quantification from at least 40 cells and 10 fields of view. Values are obtained from three independent experiments. Scale bars 10 µm.

3.2.9 Overexpressing B7-H3 in 16HBE increases B7-H3 membrane localisation and reduces cilia formation

To investigate the theory that B7-H3 expression levels negatively correlate with primary cilia formation, 16HBE cells were transiently transfected with either non-targeted GFP plasmid as a control, or B7-H3-GFP to overexpress the protein in a subset of cells. Cells were then fixed and stained for B7-H3 (magenta) and ARL13B (cyan) (Figure 31A). Confocal images showed B7-H3-GFP localising more at cell-cell junctions compared to endogenous B7-H3 in these cells. To analyse this in more detail, the intensity of B7-H3 at the membrane was measured and compared to intensity at the cytoplasm in control 16HBE and B7-H3-GFP overexpressing cells. Levels of plasma membrane associated B7-H3-GFP were significantly higher compared to endogenous B7-H3 (Figure 31B). Moreover, overexpressing B7-H3-GFP significantly reduced the number of primary cilia compared to control cells, reaching levels seen previously in A549 and H358 cancer cells (Figure 31C). This data suggests that overexpressing B7-H3 results in higher translocation to the plasma membrane, and that B7-H3 might negatively regulate primary cilia assembly.

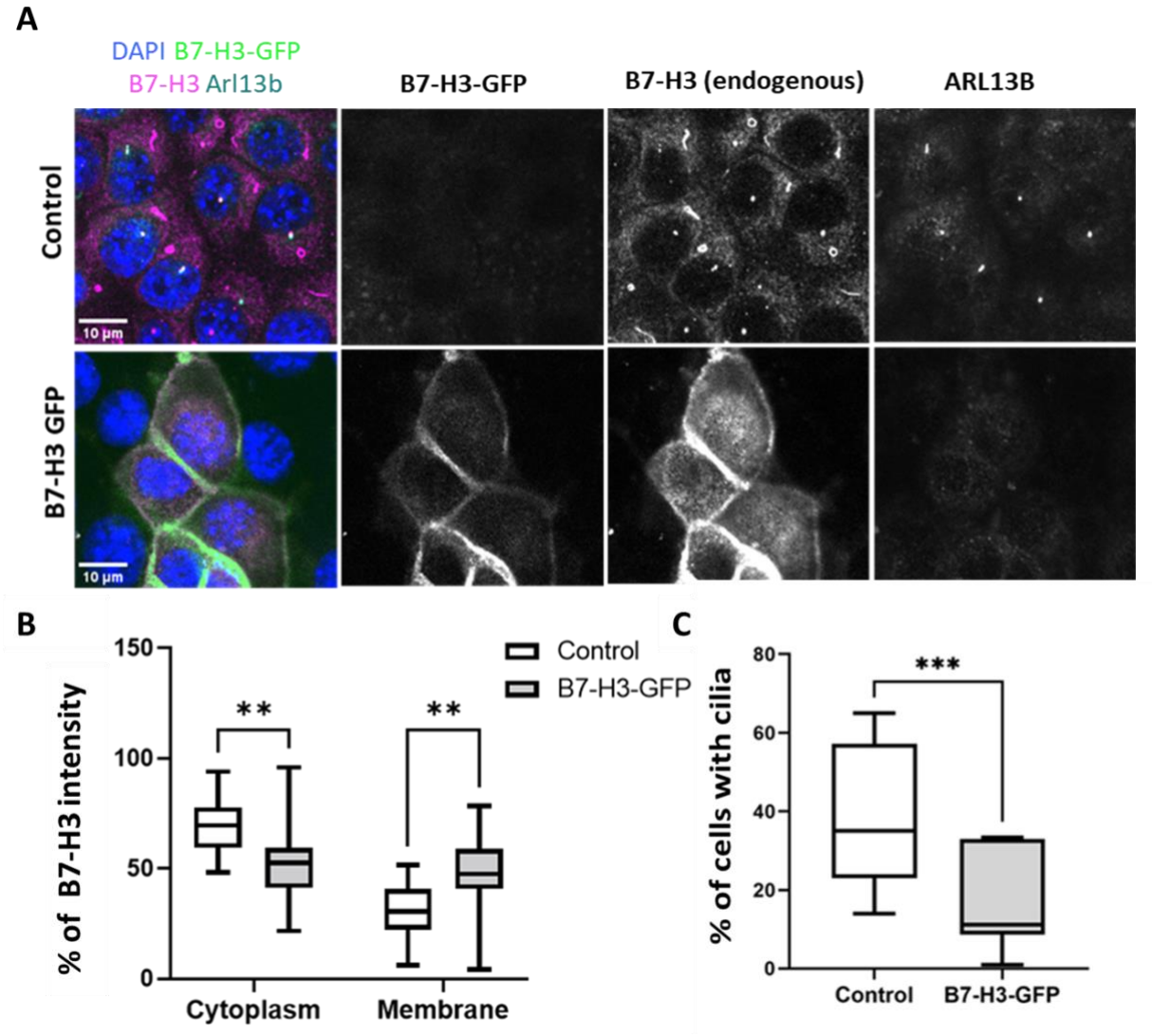

Figure 31: Overexpressing B7-H3 increases B7-H3 membrane localization and reduces cilia formation in 16HBE cells.

(A) Representative confocal images of control GFP transfected 16HBE cells or B7-H3-GFP overexpressing cells stained for nuclei (blue), GFP (green), B7-H3 (magenta) and ARL13B (cyan). **(B)** Quantification of the percentage of B7-H3 intensity at the membrane and the cytoplasm in B7-H3 transfected cells and control. **(C)** Quantification of the percentage of cells forming cilia. Data is shown as mean +/- SEM, significance assessed by one-way ANOVA; significance values are **=p<0.01, ***= p<0.005. Cells quantified shown from at least 40 cells and 10 fields of view. Values were obtained from three independent experiments. Scale bars 10 µm.

3.2.10 Reducing cilia in 16HBE cells does not change B7-H3 localisation

Previous data presented in this chapter demonstrated that B7-H3 localised to primary cilia, expression correlated with cilia formation and that overexpression reduced cilia assembly. We next aimed to investigate whether assembly of cilia could influence B7-H3 subcellular localisation in normal lung epithelial cells. To explore this, siRNA targeting KIF3A was transfected into 16HBE cells; KIF3A is a ciliary protein that is crucial for primary cilia development (Ma *et al*., 2020). 72 hours post-transfection, cells were lysed, run on a Western blot, and probed for KIF3A to confirm efficacy of the knockdown (KD) (Figure 32A). ARL13B and B7-H3 were also probed for and showed no change in expression upon KIF3A depletion (Figure 32A). KIF3A control or KD cells were also plated onto coverslips and co-stained for ARL13B (magenta) and B7-H3 (green) (Figure 32B). No changes were seen in B7-H3 localisation, to RR or cell-cell junctions, between KIF3AKD and control cells, although cilia were significantly reduced upon KIF3AKD (Figures 32C, D).

In order to further explore whether cilia assembly was linked to formation of RR (to which B7-H3 localise), KIF3AKD cells were fixed and co-stained for B7-H3 (green) and IMPDH2 (magenta) (Figure 32E). Quantification of the mean number of RR/cell from representative confocal images showed no significant change in RR numbers compared to siRNA control cells (Figure 32E, F). Taken together, this data suggest that reducing cilia in normal lung epithelia cells does not change B7-H3 levels or localisation, or influence RR formation.

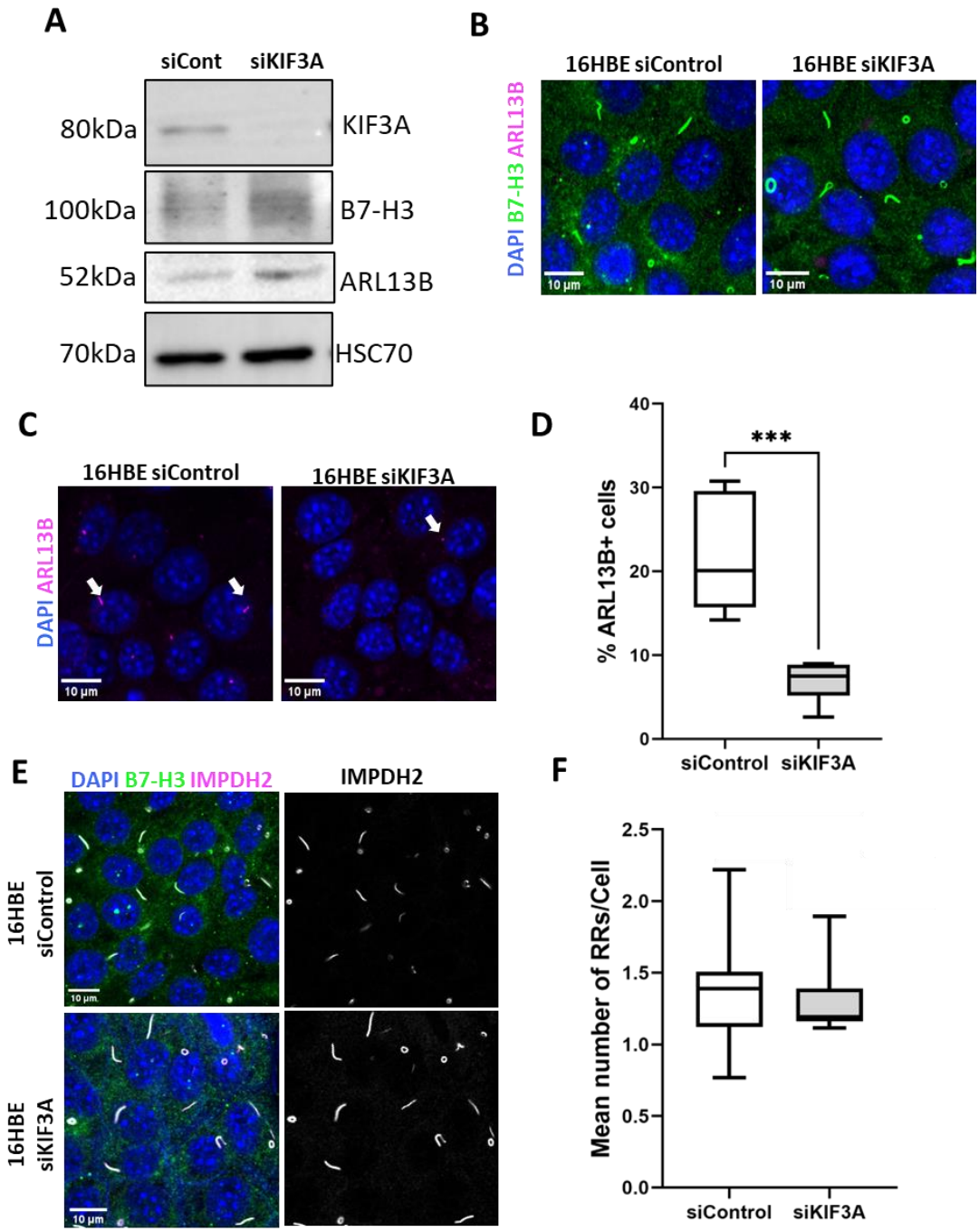

Figure 32: Reducing cilia (siKIF3A) in 16HBE cells does not change B7-H3 localisation.
(A) Western blot of lysates probed for KIF3A, B7-H3, ARL13B and HSC70 from 16HBE cells transfected with siRNA recognising KIF3A **(B)** representative confocal images of B7-H3 (green) unchanged localisation in KIF3A knockdown cells**. (C-D)** Confocal images of ARL13B (Magenta) stained cells and quantification of the percentage of cells forming primary cilia in control and KIF3A siRNA **(E-F)** confocal images of IMPDH2 (green) unchanged localisation in KIF3A knockdown cells and quantification of the mean number of RR in KIF3AKD cells compared to the control. White arrows indicate primary cilia. Data shown as mean +/- SEM from 3 independent experiments. Significance assessed by two-way ANOVA;, *** p<0.001. Scale bars 10 µm.

3.2.11 IMPDH2 knockdown does not change B7-H3 localisation

Having shown that cilia assembly do not contribute to B7-H3 localisation or RR formation**,** we postulated that RR may instead play a role in cilia or B7-H3 localisation. To investigate this, siRNA targeting IMPDH2 was transfected into 16HBE, A549 and H358 cells and knockdown confirmed as ~50% by Western blotting (Figure 33A). The localisation of B7-H3 in IMPDH2KD cells was analysed by staining cells for B7-H3 and comparing them to control siRNA transfected cells. Confocal images showed no clear change in B7-H3 localisation upon IMPDH2 knockdown (Figure 33B).

To determine whether RR could influence cilia assembly, IMPDH2KD cells were stained for ARL13B and the percentage of cells forming primary cilia was quantified. Analysis revealed that the number of cilia was significantly increased in IMPDH2KD cells compared to control (Figure 33C). However, the localisation of B7-H3 to IMPDH2-containing RR in 16HBE cells was unchanged upon IMPDH2 knockdown (Figure 33D).

Collectively, this data demonstrates that reducing IMPDH2 levels can enhance cilia formation, but this is not coupled to reduced B7-H3 localisation to RR.

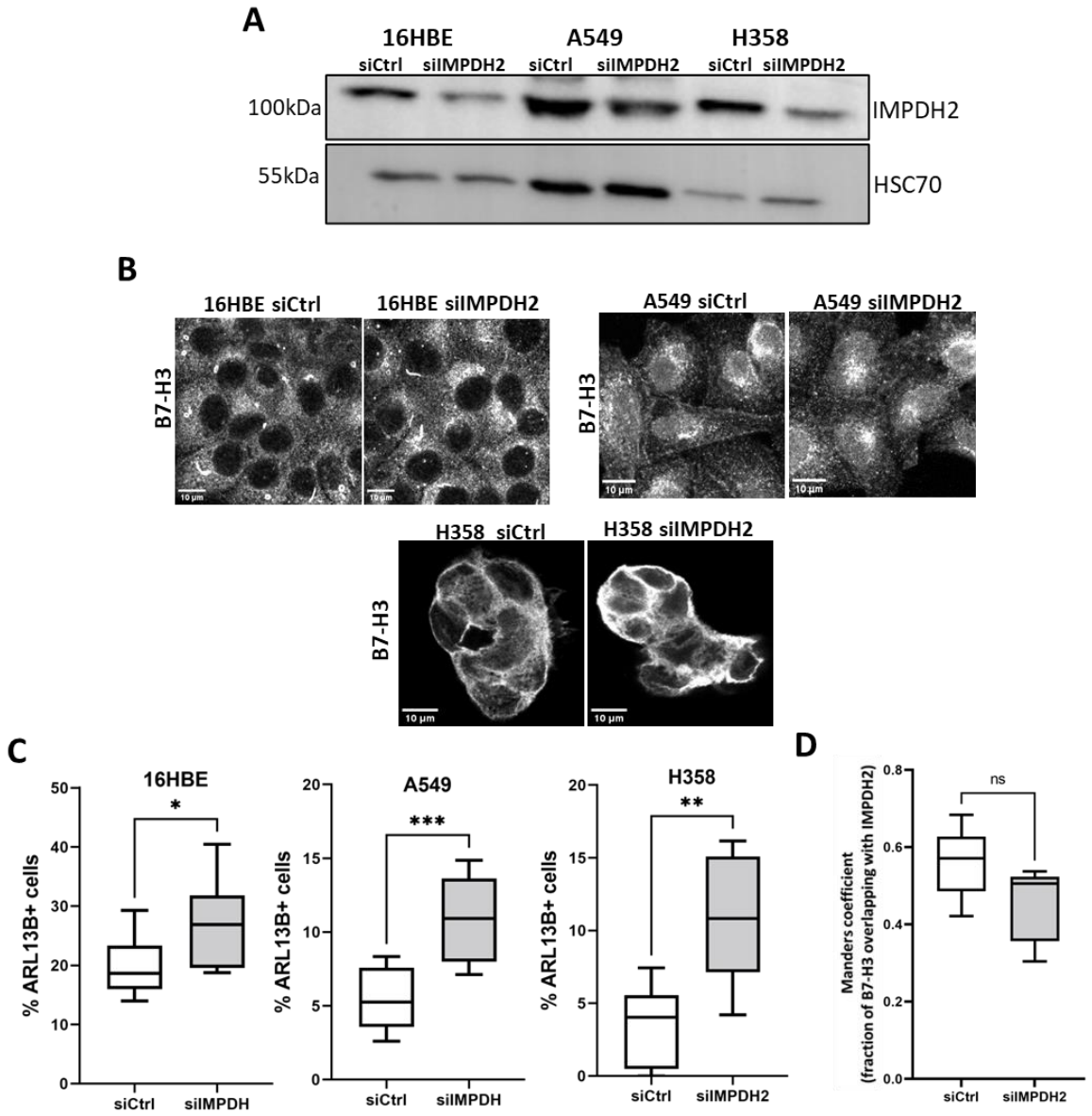

Figure 33: IMPDH2 siRNA does not change B7-H3 localisation.
(A) Western blot of lysates probed for IMPDH2 and HSC70 from 16HBE, A549 and H358 cells transfected with siRNA recognising IMPDH2. **(B)** example confocal images of B7-H3 unchanged localisation in all cells. **(C)** quantification of the percentage of cells forming primary cilia in control (Ctrl) and IMPDH2 siRNA. **(D)** Quantification of IMPDH2 and B7-H3 co-localisation in RR using Mander's coefficient and represents mean +/- SEM from at least 10 cells from 5 fields of view from 3 independent experiments. Significance assessed by t-test, significance values are * =p<0.05, **=p<0.01, ***= p<0.001. Scale bars 10 µm.

3.2.12 Inhibiting IMPDH2 activity leads to enhanced B7-H3 localisation to rods and rings in 16HBE cells

Mycophenolic acid (MPA) is a potent IMPDH non-competitive inhibitor that leads to an increase in IMPDH2 aggregation in RR (Ji *et al*., 2006). Given that B7-H3 localisation was not altered following reduction of IMPDH2 levels, MPA was employed to study the effect of blocking IMPDH2 activity on B7-H3 levels as well as location.

To assess any changes to B7-H3 levels, cells were treated with 1 μM of MPA and lysed 48 hours post-treatment followed by probing for B7-H3 (Figure 34A). Quantification of Western blots showed a trend towards a reduction in B7-H3 protein levels in MPA-treated cells, but this was not significantly different when compared to control cells (Figure 34B). To explore effects on B7-H3 localisation, MPA-treated cells were plated onto coverslips and stained for B7-H3 (green) and IMPDH2 (magenta) (Figure 34C). Images demonstrated an increase of RR number and size.

Quantification of the co-localisation between B7-H3 and IMPDH2 at RR was carried out using Mander's coefficient analysis which revealed a significant increase in co-localisation upon MPA treatment (Figure 34D). Moreover, as shown by previous studies, the number of RR in 16HBE cells was enhanced, MPA treatment also significantly increased RR formation in A549 and H358 cells at low levels compared to 16HBE cells (Figure 34E).

Taken together, data suggests that blocking IMPDH2 activity leads to enhanced recruitment of B7-H3 to RRs, suggesting IMPDH2 activity negatively regulates this localisation of B7-H3.

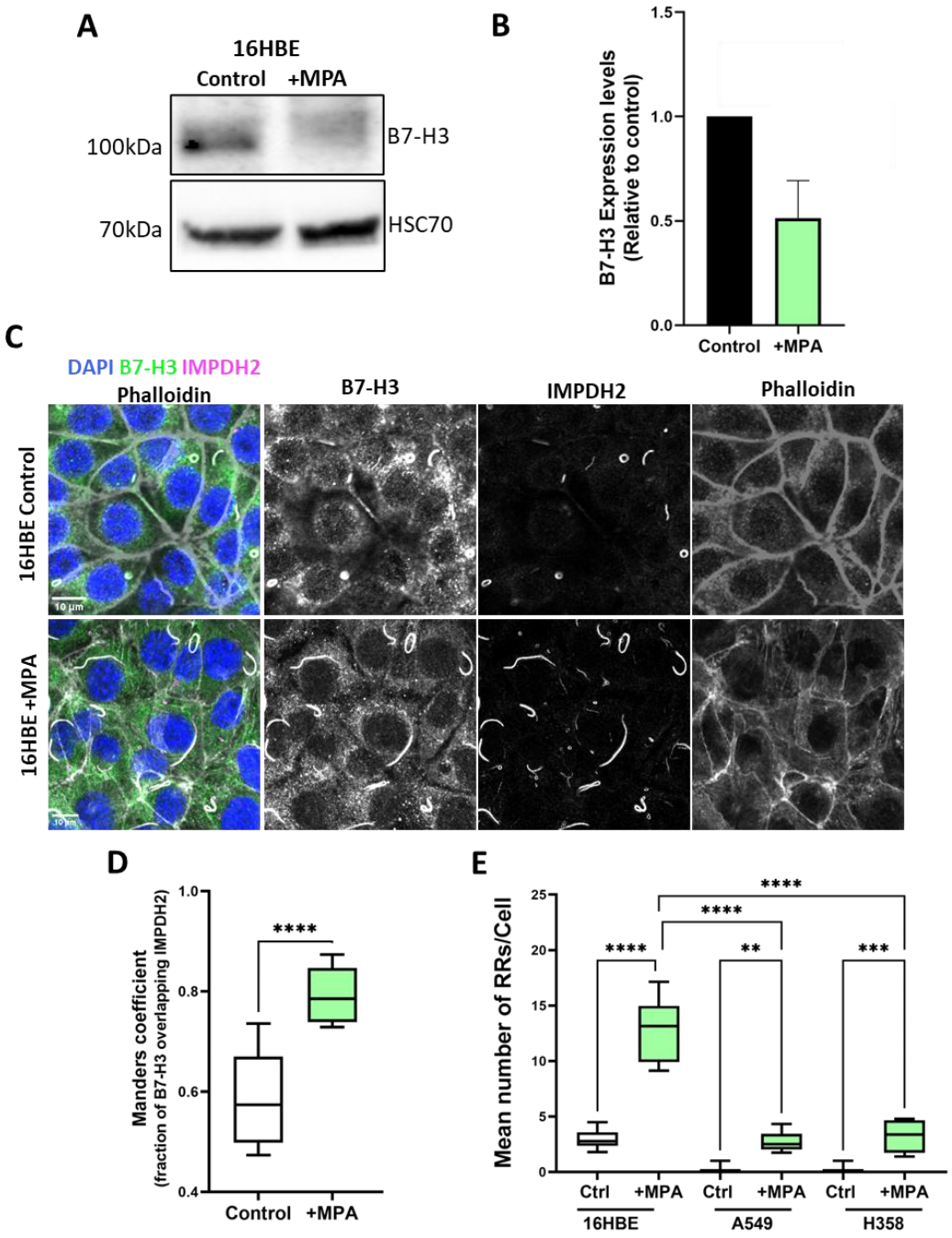

Figure 34: Blocking IMPDH2 activity increases B7-H3 localisation to RR.
(A) Western blot of lysates probed for B7-H3 from 16HBE cells treated with MPA for 48 hours. **(B)** quantification of MPA-treated and control cells showing B7-H3 expression levels from Western blots. **(C)** representative confocal images of 16HBE cells stained for B7-H3 and IMPDH2 post 48 hours of MPA treatment. **(D)** Quantification of co-localisation of B7-H3 and IMPDH2 in RR from cells stained for both proteins and treated with MPA for 48 hours. **(E)** Quantification of the mean number of RR per cell from images of 16HBE, A549 and H358, treated with MPA and stained for IMPDH2, from 7 or more cells from 8 fields of view pooled from 3 independent experiments. Graphs shown as mean +/- SEM. Significance assessed by t-test or one-way ANOVA; **p<0.01, *** p<0.005, ****p<0.0001. Scale bars 10 µm.

3.3 Discussion

3.3.1 B7-H3 expression and membrane localisation increase in cancer cells compared to normal epithelia

In this chapter we aimed to identify the localisation and expression levels of B7-H3 in normal lung epithelial cells compared to cancer cells. Data in this chapter demonstrated that B7-H3 localises to cell-cell junctions in 16HBE cells but this was at a lower level when compared to the two lung adenocarcinoma cell lines. B7-H3 was also identified to localise to other compartments within the cytoplasm in 16HBE cells.

Firstly, we discovered that B7-H3 localises to the primary cilia. There is a precedent for cell-cell adhesion proteins localising to cilia (Luyten *et al*., 2010). The Wnt signalling and adherens junction protein β-Catenin has been shown to be present in cilia. KIF3A knockout mice showed abnormal β-Catenin level and dysfunctional Wnt responses, suggesting that cilia have diverse roles in intercellular communication and may either restrict or stimulate activity depending on the pathway (Corbit *et al*., 2008). Secondly, we found strong and specific staining for B7-H3 in the cytoplasm of structures known as Rods and Rings (RRs). These structures have been found in a wide variety of cell types under normal growth conditions and can be induced in some cell lines (Carcamo *et al*., 2011; Gunter *et al*., 2008; Noree *et al*., 2010; Ramer *et al*., 2010; Willingham *et al*., 1987). However, the composition and function of RR remains poorly understood. B7-H3 has not been previously reported in these structures and is not reported with the 21 identified proteins present in RR in the human protein atlas (Rods and rings - The Human Protein Atlas, 2022) . Interestingly however, SCRIB is present in RR and is also involved in cell-cell adhesions. SCRIB is required to maintain epithelial integrity and its loss drives epithelial cells to be susceptible to EMT (Yamben *et al*., 2013). However, the link between SCRIB and RR formation has not been explored. Moreover, β2 integrins have also been shown to be present in RR, raising the possibility that other transmembrane receptors reside in these structures (Rods and rings - The Human Protein Atlas, 2022). The potential role for B7-H3 in controlling RR formation will be explored in the next chapter.

Data shown in this chapter indicates that overexpression of B7-H3 can suppress cilia assembly. The primary cilium plays a key role in controlling β-catenin independent (non-canonical) Wnt signalling, and perturbation of ciliary genes activates β-catenin dependent Wnt signalling and disrupts β-catenin independent Wnt signalling (Oh and Katsanis, 2013). Moreover, overactivation of β-catenin dependent Wnt signalling leads to a loss of primary cilia (Saito *et al*., 2015). Increased β-catenin expression levels in basal-like breast cancer correlate with poor prognosis (Khramtsov *et al*., 2010). This suggests that higher expression of B7-H3 leads to movement of the protein from primary cilia to junctions as observed in B7-H3-overexpressed 16HBE cells. Further analysis of whether loss of B7-H3 can regulate cilia assembly will be addressed in the next chapter.

Epithelial-mesenchymal transition (EMT) has been reported to be accompanied by the loss of epithelial markers and the gain of mesenchymal markers. Clinical microarray results demonstrated that increased levels of vimentin mRNA (a marker for mesenchymal cells) after chemotherapy correlated to a poor prognosis of breast cancer patients. Vimentin depletion induced reorganisation of cytoskeletons and reduced focal adhesions, which resulted in impaired mechanical strength because of reduced cell stiffness and contractile force. In addition, overexpressing vimentin increased cell stiffness, elevated cell motility and directional migration, reoriented microtubule polarity, and increased EMT phenotypes due to the increased β1-integrin and the loss of junction protein E-cadherin (Liu *et al*., 2015). B7-H3 is localised at the junctions between tumour cells, however that does not necessarily correlate with more intact cell-cell adhesions, as A549 show less well organized/looser junctions compared to 16HBE or H358 cells. Recently, the link between EMT and cancer cell invasion has been challenged. A landmark study demonstrated that distal metastases often maintain E-cadherin at adhesions, and this can promote survival in metastatic breast cancer through reduced apoptosis induced by oxidative stress (Padmanaban *et al*., 2019). E-cadherin junctional contacts were also found to be retained in various epithelial tumours undergoing collective cell migration (Janiszewska *et al*., 2020). Indeed, a more recent concept of 'partial EMT' suggests E-cadherin and cell-cell adhesion integrity may play a more nuanced role in promoting cancer cell dissemination, survival, and metastasis (Saxena *et al*., 2020). Thus, the enhanced localisation of B7-H3 to cell-cell adhesion sites observed in lung cancer compared

to normal epithelial cells may indicate a role for B7-H3 in controlling these structures and downstream functional consequences. Potential contributions of B7-H3 to cell-cell/cell-matrix adhesion formation, proliferation and invasion will be explored in the next chapter.

The movement of B7-H3 to distinct subcellular compartments suggests this molecule is likely to undergo either trafficking through the endosomal system, or lateral movement on the plasma membrane. Data shown in this chapter indicated that B7-H3 does not co-localise with some key endosomal markers. Nonetheless, B7-H3 is degraded via lysosomes, and it has been shown that B7-H3 partially co-localises with early endosomes and lysosomes in breast cancer cells upon cellular uptake of fluorescently labelled B7-H3-indocyanine green antibody (Wilson *et al*., 2017). However, previous data from the Parsons lab demonstrated no internalisation of B7-H3 in adenocarcinoma cell lines in time frame of up to 4 hours using different approaches. Therefore, movement of B7-H3 could occur via slower, non-specific routes such as macropinocytosis, which is a form of endocytosis that mediates uptake of soluble molecules, nutrients and antigens and shown to be upregulated in cancer cells (Recouvreux & Commisso, 2017). Moreover, this process is actin-dependent, initiated from surface membrane ruffles that brings about large endocytic vacuoles called macropinosomes (Lim & Gleeson, 2011). Given this relationship with actin and subsequently cell motility, the role of B7-H3 in organisation of cytoskeletal assembly will be investigated in the next chapter.

To determine if B7-H3 is internalised via macropinosomes, further studies through the use fluorescently tagged fluid-phase markers known to be predominantly internalised by macropinocytosis, such as dextran, Lucifer Yellow and horseradish peroxidase would need to be performed, and subsequent B7-H3 localisation need to be analysed in more detail. Alternatively, internalisation of the B7-H3 could be carried out by receptor crosslinking on the cell surface. Moody *et al* reported that increasing crosslinking of the HER2 directed monoclonal antibody Trastuzumab drives HER2 internalisation and subsequently redirect endocytic trafficking to lysosomes in breast cancer cell lines (Moody *et al*., 2015). Therefore, incubation of B7-H3 with biotinylated cargo followed by addition of streptavidin to crosslink

receptor:cargo–biotin complexes and subsequent observation of B7-H3 localisation would give confirmation if this is the case for B7-H3 internalisation.

Conversely, it has been reported that B7-1, a member of the B7 family, cytoplasmic domain did not contain a linear ER export motif (Peotter et al., 2019). This cytoplasmic tail enhanced intracellular transport of both a reporter protein (human alpha fetal protein) and a single-chain antibody. This could happen through interaction with the cellular transport machinery, such as (Sec23/Sec24) in the Coat Protein complex II (COPII), that accelerate trafficking to Golgi apparatus and cell surface (Lin et al., 2013). The cytoplasmic tail of type I transmembrane proteins rarely has ER export motifs. This could be tested for B7-H3 by mutating Sar1 protein, which is required for COPII assembly and fusion, and treating cells with single-chain antibodies then measuring the accumulation of single-chain antibody on the cells surface as a readout of B7-H3 intracellular transport rate (Lin et al., 2013). Exploring these pathways would be valuable to further understand how B7-H3 moves between compartments within the cell.

3.3.2 Potential importance of B7-H3 in primary cilia and roles in cancer

Primary cilia are microtubule-based protruding organelles that are found in nearly all human cells and contain sets of nine microtubule doublets surrounded by a phospholipid membrane (Wheway *et al*., 2018). This membrane is continuous with the plasma membrane topologically surrounding the rest of the cell, which might indicate B7-H3 localisation in the cilia. B7-H3 also co-localises with pericentrin a centriole marker (Figure 28). It has been found that p-S47 β-catenin epitope, which is involved in canonical Wnt signalling and subsequently cilium assembly, localises to the mother centriole subdistal appendages during ciliogenesis (Kyun *et al*., 2020). Ciliogenesis, occurs in several stages. First, to free centrioles for axoneme nucleation, cells must exit the mitotic cycle. Then, centrioles are termed basal bodies when addition of distal appendages and docking to a ciliary vesicle that fuses with the plasma membrane occurs. Finally, extension of the ciliary axoneme and membrane is facilitated by a process termed intraflagellar transport (IFT). This process requires the bidirectional transport of microtubule motors and protein complexes, known as IFT, proteins (Pedersen &

Rosenbaum, 2008). The main role of primary cilia is to sense a variety of external cues and functions as a signal transduction hub, involving signalling pathways with relevance to development and diseases including cancer (Lancaster & Gleeson, 2009). The primary cilium has several signalling receptors localised to it, including receptors for sonic hedgehog canonical and non-canonical Wnt signalling (Grisanti *et al*., 2016; May-Simera & Kelley, 2012). There is increasing evidence suggesting cilia antagonise cell cycle progression, and this has increased the focus on the role of primary cilia in cancer. A dysregulated cilium can lead to signalling impairments, causing an initiation of tumourigenesis (May-Simera & Kelley, 2012). Primary cilia have been shown to be frequently lost in different cancer types (Kim & Tsiokas, 2011). Data in this chapter demonstrated that knocking down KIF3A in 16HBE cells resulted in a significant decrease in the number of primary cilia, and therefore reduced B7-H3 in cilia. However, this did not lead to altered B7-H3 localisation to the junction or to RRs, suggesting that loss of primary cilia alone is not sufficient to initiate changes in B7-H3 levels or localisation seen in cancer cells. Thus, it could be hypothesised that the loss of cilia in cancer occurs independently (or after) increased B7-H3. Further testing of B7-H3 involvement in primary cilia formation will be addressed in the next chapter.

There have been various reports of a connection between the cilium and polarity of cells, a study conducted by Sabur*i et al* demonstrated that KIF3A-mutant mice induced cilia loss while also causing aberrant polarity and abnormalities in cell division (Saburi *et al*., 2008). The ciliary membrane contains receptors for Wnt, Hedgehog Notch and other growth factors as well as harbouring integrin and cadherin family members, which allows receipt of a robust variety of signals (Seeger-Nukpezah & Golemis, 2012). Furthermore, disruptions in the extracellular environment alter signals received by cilia affecting cell growth properties. Specialised ciliary membrane displays receptors that form proteins which influence the ECM interactions, EMT and cell polarity (Donnelly *et al*., 2009). One example of transmembrane protein flux in the ciliary membrane is provided by Smo, a seven-transmembrane protein essential for Sonic Hedgehog pathway (Byrne *et al*., 2016; Corbit *et al*., 2005). Smo trafficking to the ciliary membrane could potentially be through lateral diffusion from the plasma membrane (Milenkovic *et al*., 2009). Reports have shown that cholesterol binding to Smo at its extracellular domain could be the agonist-induced event that results in activation of Smo in

the Sonic Hedgehog signalling (Shh) (Byrne *et al*., 2016). Upon activation of Shh, accumulation of endogenous Smo occurs in cilia gradually over hours (Huang *et al*., 2016). Polycystin-1 (PC1) and Polycystin-2 (PC2) are one of the G proteins–coupled receptors found to be localised to cilia as well as exosomes (Pazour *et al*., 2002). PC2 is mostly found in the endoplasmic reticulum (ER), and PC1 promotes its trafficking to cilia from the ER (Cai *et al*., 2014). PC1/2 ligand is yet to be discovered, however, they might be functioning in cilia as "regulated" cation channels (Ha *et al*., 2020). Future studies on B7-H3's cytoplasmic tail by introducing mutations and observing key ciliary pathways would help in understanding how B7-H3 is recruited to primary cilia and whether it is involved in accelerating ciliary machinery.

3.3.3 B7-H3 is a novel component of RR

Previous studies on B7-H3 have mainly focused on its contribution to cancer with very few investigations of the role of this receptor in normal cells. One study showed B7-H3 staining in both normal breast epithelial and endothelial cells using immunohistochemical (IHC) analysis (K. E. Wilson *et al*., 2017). Another study showed staining in normal mammary tissues where B7-H3 was located at very low levels in endothelial and epithelial cells of murine tissue (Bachawal *et al*., 2020). No previous reports have shown B7-H3 localisation to RR in normal lung epithelial cells, as we demonstrate here. Further staining of B7-H3 together with IMPDH2 in normal epithelial cells from other tissues would be beneficial to further confirm its localisation to RR and whether cell type tested normally form these structures. RR are thought to contribute to the regulation of *de novo* guanine nucleotide synthesis, however, the function and regulation of RR remains unclear. A recent study has found ARL2, a highly conserved GTPase within the ARF superfamily, is localised to RRs. In the earliest stages of RR formation, only IMPDH2 was present, this was followed by ARL2 recruitment and finally calnexin was recruited to fully formed RR (Schiavon *et al*., 2018). Recruitment of ARL2 to RR may serve to sequester it from other sites thus, reducing its activity. These recruitment events have been referred to as "higher order signalling", which may potentially also be the case for B7-H3 (Francis *et al*., 2016).

RR induction has been commonly observed upon treatment of cells with drugs that inhibit IMPDH such as MPA, which traps a covalent intermediate of IMPDH with covalently bound nucleotide and inhibits this rate limiting step in guanine nucleotide biosynthesis (Schiavon *et al*., 2018). MPA interrupts purine biosynthesis and induces macroaggregates of IMPDH protein (Ji *et al*., 2006). As shown in this chapter, treating cells with MPA significantly increased RR formation and B7-H3 localisation at these structures. On the other hand, knocking down IMPDH2 did not show any effect on RR formation in 16HBE cells, this could be because MPA is a potent inhibitor of IMPDH2 and thus aggregates it in RR which then recruits B7-H3 to RR as seen in cells that do not typically form RR in normal growth conditions, such as A549 and H358 adenocarcinoma lines. Another reason for the low effect of IMPDH2KD using siRNA compared to inhibiting via MPA is that KD levels in the cells here was only achieved to ~50%, which may not be sufficient to initiate changes in RR aggregation and subsequent increased B7-H3 recruitment. A study conducted by Carcamo *et al* showed knocking down 95% of IMPDH2 in cells increased RR formation while overexpression of the protein inhibited RR formation (Carcamo *et al*., 2011). Therefore, improved reduction as well as overexpression of IMPDH2 levels would be valuable to investigate its effects on B7-H3 localisation and RR formation. The effect of overexpressing B7-H3 on RR formation will be explored in the next chapter.

3.3.4 Relationships between cilia and RR – potential function in epithelium and cancer

A recent study has reported that ALR13B, a ciliary protein and a member of the ARF superfamily, interacts with IMPDH2 (Shireman *et al*., 2021). This raises the possibility of some form of previously unexplored interplay between cilia and RR.

One study on ARL2 and IMPDH2 co-localisation, reported that ARL2 binding partner engulfment and motility domain-containing protein 2 (ELMOD2) also localised to RR. Moreover, the study found cofactor D, which is involved in αβ-tubulin biogenesis and forms a complex with ARL2 and β-tubulin, co-localised with ARL2 at RR (Schiavon *et al*., 2018). α- and β-tubulin are the building blocks to forming microtubules, of which ARL2 is a key regulator

(Khalifa *et al*., 2020; Zhou *et al*., 2006). ARL2 has also been linked to centrosome stability demonstrating function of ARL2 in transport of myristoylated cargo proteins (Jaiswal *et al*., 2016). Moreover, ARL2 works together with ELMOD2 in the mitochondrial intermembrane space to affect fusion (Schiavon *et al*., 2019). Furthermore, despite previous reports on RR not associating with a membrane when visualized using Electron microscope (EM) (Ji *et al*., 2006; Juda *et al*., 2014; Thomas *et al*., 2012), membrane proteins such as calnexin was found to co-localise along the entire RR length seen by immunofluorescence (Schiavon *et al*., 2018). However, Schiavon *et al* examination and visualization of organelle markers using transmission EM led to the discovery that several ER proteins localised to RR, half seemed to be in proximity to ER membrane and a quarter close to mitochondrial membranes yet, the membranes did not run along the entire length RR (Schiavon *et al*., 2018). It is still not clear what impact or function these proteins have on RR or why they are recruited there. However, further studies on B7-H3 co-localisation with different ER and mitochondrial markers, α-β-tubulin and ARL2 and whether the latter works as a cargo to transport B7-H3 in between primary cilia and RR would be vital in identifying how B7-H3 gets recruited into RR and if it follows the higher order signalling.

Another study conducted by Ji *et al* revealed that knockdown of IMPDH2 significantly hindered proliferation and EMT of NSCLC cells, whereas the opposite results were achieved by IMPDH2 overexpression (Ji *et al*., 2006). They further demonstrated that the downregulation of IMPDH2 inhibited the Wnt/β-catenin signalling pathway by reducing the expression levels of Wnt3a and β-catenin, while increasing the expression levels of phosphorylated glycogen synthase kinase-3β in NSCLC cells which could explain the increased number of primary cilia in IMPDH2 inhibited cells. Primary cilia can form independently of the Wnt/β-catenin pathway (Gigante *et al*., 2020) and GSK3β can co-regulate ciliogenesis by promoting ciliary membrane assembly (Zhang *et al*., 2015). Data shown in this chapter indicates that IMPDH2 inhibition increases primary cilia assembly. It would be interesting to determine whether this occurs downstream of GSK3β and whether B7-H3 might be required for this. This could be tested by blocking the phosphorylation cite of GSK3β or treating cells with GSK3β inhibitors followed by analysing IMPDH2, B7-H3 and ARL13B localisation and expression levels.

Conversely, data shown here demonstrates that knockdown of KIF3A reduced cilia formation but did not alter RR assembly or B7-H3 localisation to these structures. The ARL13B-IMPDH2 interaction functions as a negative regulator for purine salvaging, as knockdown of ARL13B enhanced DNA damage by forcing glioblastoma cells to rely on the purine salvage pathway (Shireman *et al*., 2021). Recently, the role of various small GTPases, including the members in ARF/ARL subfamilies, in cilia formation and function have been highlighted. ARL3, a small GTPase, is important in concentrating lipid-modified proteins in the primary cilia (Strom *et al*., 2016). It possesses an amphipathic helix to associate with membranes in a GTP-dependent manner. ARL13B has a palmitoylation motif localises it to the cilia (Roy *et al*., 2017). It has been shown that ARL13B functions as a Guanine nucleotide exchange factors for ARL3, which would produce an active node of ARL3-GTP within cilia (Gotthardt *et al*., 2015). ARL3-GDP is mostly concentrated in the cytoplasm whereas ARL3-GTP is in the cilium, this would be achieved by the localisation of ARL13B in the cilia. ARL13B activates GDP-bound ARL3 into ARL3-GTP. Cargo and its carrier trafficking into the cilium allow interaction with ARL3-GTP that causes release of the cargo from the carrier, which would then pass back into the cell to bind other cargo. ARL3-GTP also exits the cilium down its concentration gradient into the cell where it is converted into ARL3-GDP (Powell *et al*., 2021). It would be interesting to study the co-localisation of modified ciliary lipid cargo with B7-H3. Moreover, IMPDH2 is known to catalyse the rate-limiting step in *de novo* GTP biosynthesis and has been reported to form RR to produce necessary amounts of guanine nucleotides to maintain normal cell functions (Huang *et al*., 2008). When nucleotide consumption is reduced, cell cycle arrest may occur thereby increase the intracellular level of GTP, which may induce IMPDH RR disassembly. Indicating that RR are highly dynamic and associated with GTP intracellular levels (Keppeke *et al*., 2018). Since B7-H3 co-localises to both IMPDH2 and ARL13B positive compartments, it could possibly regulate small GTPases as well as GTP levels within the cell. Investigating the role of B7-H3 in GTPases activation as well as analysing cilia/RR interplay with B7-H3 levels, will be further explored in the next chapter.

In summary: data in this chapter revealed different expression levels and subsequent localisation of B7-H3 in normal lung epithelial versus adenocarcinoma lines. Experiments in the next chapter will explore the role of B7-H3 in cell behaviour, junction formation as well as its contribution to ciliogenesis and RR formation.

4. Exploring roles for B7-H3 in cell behaviour and ciliogenesis

4.1 Introduction

B7-H3, similar to other members of the B7 family, is characterised by extracellular IgV and IgC domains linked to the variable and constant regions of immunoglobulins and short cytoplasmic domain (Collins *et al*., 2005). Even though the 2-Ig form can be present, the 4-Ig molecule appears to be dominant in humans. However, the functional consequences of these isoforms remain unknown (Sun *et al*., 2002). In addition, B7-H3 can be cleaved from the cell surface via MMPs and endopeptidases, resulting in a soluble circulating form of the protein that has been detected in serum and culture media (sB7-H3) (Lemke *et al*., 2012; Zhang *et al*., 2008).

B7-H3 increased expression in cancer cells has been linked to poor prognosis and is therefore an attractive target for therapy. Little is known about any potential functional effect of B7-H3 expression on cancer cells compared to its immune regulatory effects. Chimeric antigen receptor (CAR) T cells targeting B7-H3 have been shown to control growth of ovarian cancer, neuroblastoma and pancreatic ductal adenocarcinoma (Du *et al*., 2019; Majzner *et al*., 2019). Recent studies have also shown that modulating B7-H3 expression in pancreatic, colorectal and melanoma cells can alter migration, invasion and metastasis (Liu *et al*., 2015; Xie *et al*., 2016). Reducing B7-H3 expression levels can suppress migration and invasion in melanoma and breast cancer cells (Tekle *et al*., 2012). Conversely, B7-H3 overexpression and treatment with B7-H3 soluble molecule promotes migration and invasion in pancreatic and colorectal cancer derived cell lines (Liu *et al*., 2015; Xie *et al*., 2016). *In vivo* studies have also demonstrated that B7-H3 monoclonal antibody treatment may suppress head and neck squamous cell carcinoma growth (Wang *et al*., 2021). Therefore, understanding the functional roles of B7-H3 expression in normal vs cancer cells and the mechanism by which it promotes these effects could inform better therapeutics for cancer treatment in the future. The goal of experiments in this chapter was to manipulate B7-H3 levels and ectodomain function in normal lung epithelial and lung adenocarcinoma cells to further explore functional consequences, in proliferation, migration and invasion, and potential mechanisms.

4.2 Results

4.2.1 Generation of B7-H3 depleted cell lines

B7-H3 is a promising target for anti-cancer treatment as it is highly expressed in many cancer types and has been linked to poor prognosis (Yang *et al*., 2020). Despite the interest in B7-H3 as a therapeutic target, its biological role in cancer cells is still poorly understood, as most of previous research has been focused on its interactions with immune cells.

To determine whether B7-H3 contributes to the hallmarks seen in cancer cells of increased proliferation, migration, and invasion, B7-H3 expression was knocked down in A549 and H358 cells using a transient CRISPR-CAS9 expression plasmid containing GFP reporter. This was followed by FACS sorting to enrich for GFP+ cells and obtain a population sufficient for analysis of efficiency of knockdown. CRISPR-CAS9 knockdown method was unsuccessful in 16HBE cells, so B7-H3KD was established by targeted siRNA treatment where cells were treated with siRNA to B7-H3 or a control siRNA for 48 hours.

B7-H3KD was validated via qPCR, Western blot, and immunofluorescence. To compare B7-H3 mRNA expression levels between parental and B7-H3KD cells, qPCR was carried out using primers against B7-H3 (Figure 35A). The graph in Figure 35A shows that B7-H3 mRNA expression was reduced by ~60% in 16HBE and A549 cells, while H358 expression was reduced to ~95%. To analyse B7-H3 protein levels, whole cell lysates were extracted from all parental/siRNA control and B7-H3-CRISPR/siRNA cells and run on a Western blot then probed using an anti-B7-H3 antibody (Figure 35B). Data demonstrated that B7-H3KD was highly efficient in A549 and H358 cells and significantly reduced in 16HBE cells (Figure 35B). Loss of B7-H3 in the same cell lines was further confirmed by confocal microscopy using an antibody against B7-H3 (Figure 35C).

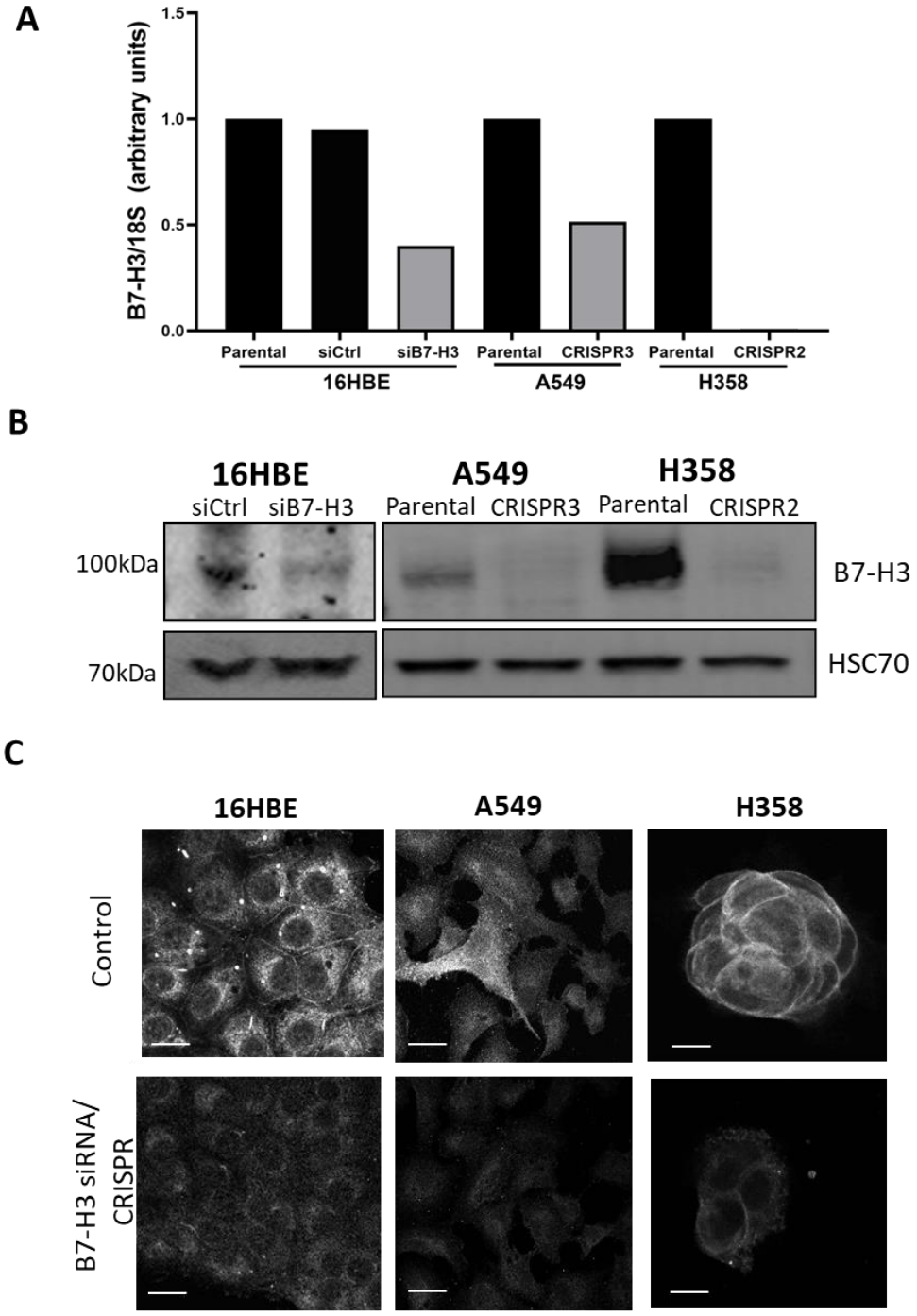

Figure 35: Generation of B7-H3 knockdown cells.
(A) B7-H3 mRNA expression was measured by qPCR in 16HBE, A549, and H358 parental and B7-H3-CRISPR/siRNA transfected cells as indicated on the graph. **(B)** Lysates from 16HBE cells transfected with siRNA targeting B7-H3, and A549 and H358 cells transfected with CRISPR/CAS9 constructs targeting B7-H3 probed for B7-H3 and HSC70 as a loading control. **(C)** Representative confocal images of parental or B7-H3 siRNA/CRISPR cells fixed and stained for B7-H3. Scale bars 10 µm.

4.2.2 B7-H3 knockdown does not alter levels or localisation of β-Catenin

As data shown in the previous chapter indicated that B7-H3 was located at cell-cell adhesions, the next goal was to test whether B7-H3KD might alter localisation of the main cell junctional proteins such as E-cadherin and β-catenin. The relative levels of E-cadherin and β-catenin expressed in 16HBE, A549, and H358 cell lines were firstly analysed by Western blotting of whole cell lysates (Figure 36A). Quantification showed that H358 had the highest expression levels of both E-cadherin and β-catenin, followed by A549 and 16HBE with equal expression levels, corresponding to B7-H3 protein levels in the respective cell lines (Figure 36B).

Even though loss of cell-cell adhesion has been identified as a pro-tumourigenic characteristic, various tumours maintain cell-cell adhesions, allowing the adoption of collective cell migration (Janiszewska *et al*., 2020). Therefore, 16HBE, A549, and H358 Parental/siRNA control and B7-H3KD cells were fixed and stained using an antibody against cell-cell adhesion molecule β-catenin (Figure 36C). Figure 36C shows confocal images of the central plane of cells where cell lines displayed a clear localisation of β-catenin at cell-cell contacts. To quantify the effects of B7-H3KD on β-catenin localisation at cell-cell junctions, line scan analysis was performed, and the signal intensity of the adhesion marker was compared across the junction of the different cell lines (Figure 36D). No significant changes were observed in β-catenin intensity levels across junctions between control and B7-H3KD cell lines in 16HBE, A549, and H358. Taken together, this data suggests that knocking B7-H3 down did not influence β-catenin localisation and that B7-H3KD cells were still able to form monolayers with intact adherens junctions.

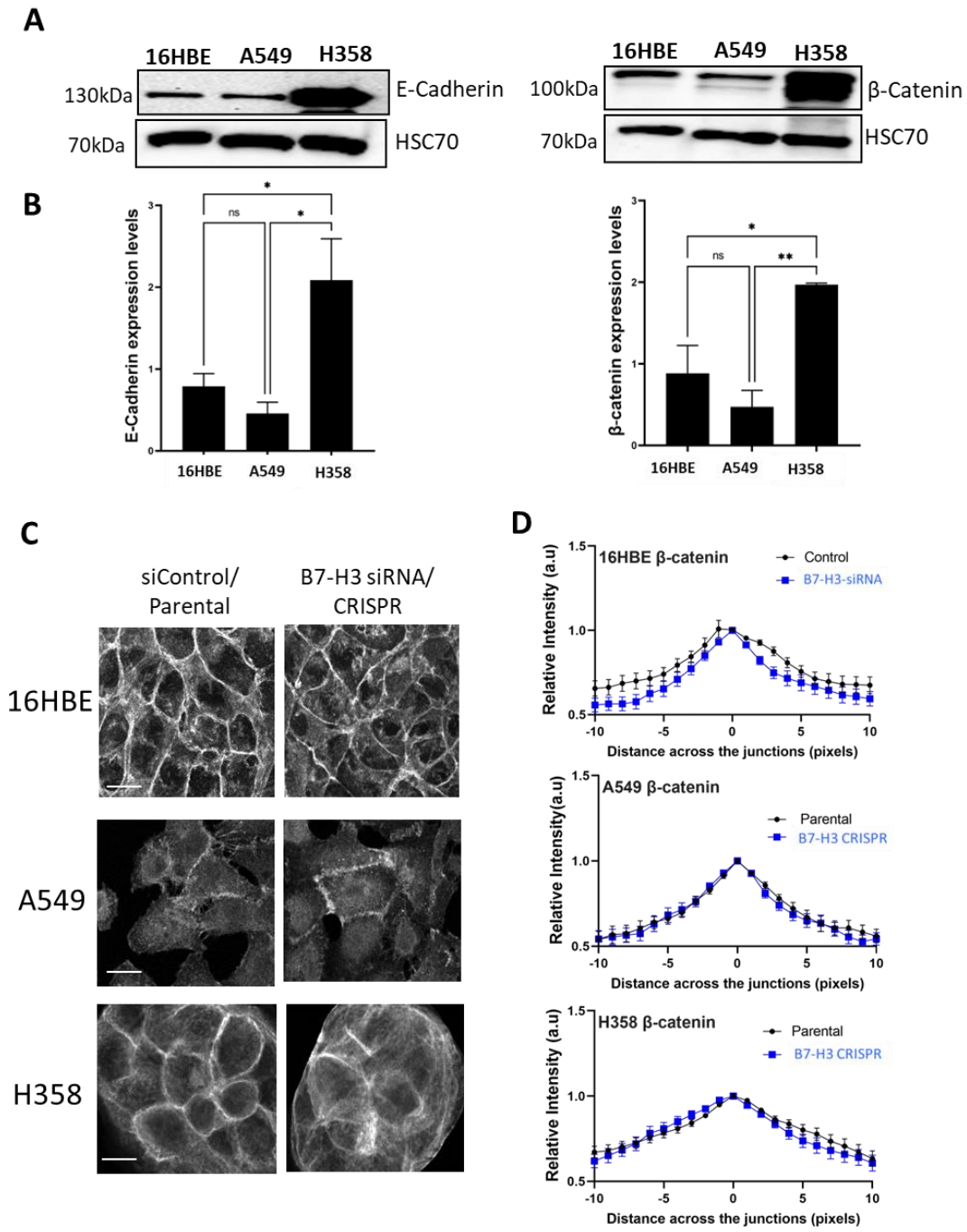

Figure 36: B7-H3 knockdown does not alter levels or localisation of β-Catenin at the adherens junction.

(A) Western blot analysis of lysates from 16HBE, A549, and H358 cells, probed for β-Catenin or E-cadherin and HSC70 (loading control). **(B)** β-Catenin and E-cadherin expression levels were measured in 16HBE, A549, and H358 cells. **(C)** Representative confocal images of siRNA control or Parental lines compared to B7-H3 siRNA/CRISPR cells fixed and stained for β-Catenin. **(D)** Quantitative line scan analysis of β-catenin signal intensity at the junction. Data from 20 junctions per cell line from 5 different fields of view of 3 independent experiments. The data shown is representative of one independent experiment showing mean +/- SEM. One-way ANOVA was used to compare statistical significance. Scale bars 10 µm.

4.2.3 B7-H3 knockdown reduces levels and localisation of ZO-1

Since previous data in chapter 3 showed B7-H3 co-localised with ZO-1 at tight junctions, we sought to explore any changes on ZO-1 levels and formation upon B7-H3KD. To assess ZO-1 protein levels, whole cell lysates of both siRNA Control/parental and B7-H3 siRNA/CRISPR KD cells were subjected to Western blot and probed for ZO-1 and B7-H3 (Figure 37A). Quantification of data revealed that 16HBE B7-H3 siRNA cells showed a trend towards a decrease in ZO-1 levels, while A549 and H359 CRISPR KD displayed a significant decrease in ZO-1 levels compared to parental lines (Figure 37B).

To further confirm the reduction of ZO-1 levels at tight junctions in B7-H3KD cells, cells were fixed, stained for ZO-1 (magenta) and B7-H3 (green). Confocal images were taken from the apical sections of the Z-stack and showed a noticeable reduction in ZO-1 intensity at the junction when B7-H3 was reduced compared to control cells (Figure 37C). This was quantified by measuring the overall raw integrated intensity of ZO-1 (Figure 37D).

Taken together, data so far suggest that even though B7-H3 localises to both tight and adherens junctions, knocking it down reduces tight junction formation but not adherens junction formation.

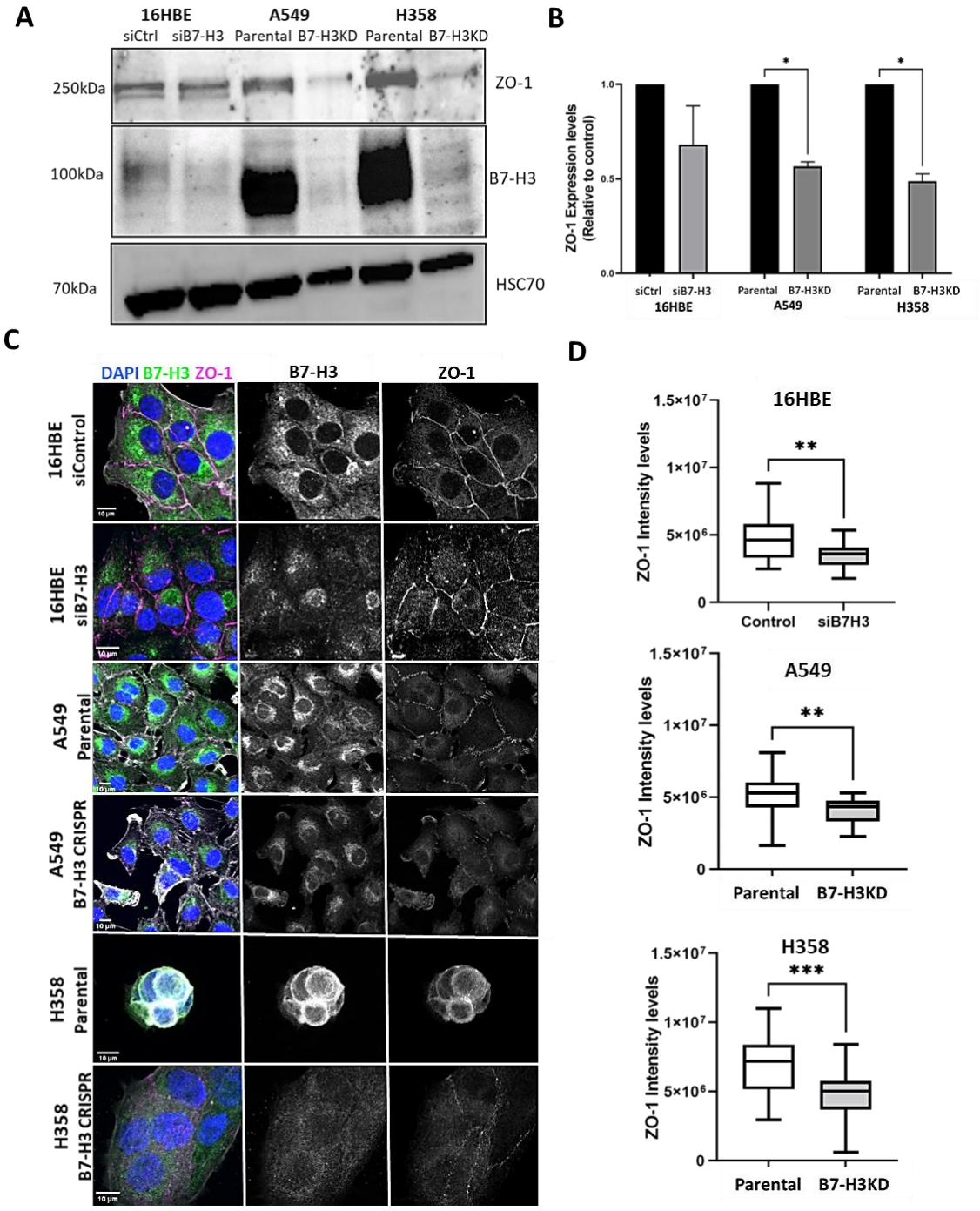

Figure 37: B7-H3 knockdown reduces ZO-1 levels and localisation to tight junctions.
(A) Western blot of ZO-1 expression levels in lysates from 16HBE, A549, and H358 control and B7-H3KD cells, probed for ZO-1, B7-H3, and HSC70 (loading control). **(B)** Quantification of data as in (A) from n=4 experiments. **(C)** Representative confocal images of siRNA control/Parental or B7-H3 siRNA/CRISPR cells fixed and stained for DAPI (blue), ZO-1 (magenta), and B7-H3 (green). **(D)** Quantification of fluorescence intensity of ZO-1 from images as in (C). intensity is shown from at least 50 cells per cell line and 10 fields of view from 3 independent experiments. Data is shown as mean +/- SEM, significance assessed by t-test or one-way ANOVA; *p<0.05, **=p<0.01, ***=p<0.001. Scale bars 10 µm.

4.2.4 B7-H3 knockdown leads to reduced focal adhesion size

There is known to be considerable crosstalk between cell-cell and cell-matrix adhesions in both normal epithelial and cancer cells (Borghi *et al*., 2010; Janiszewska *et al*., 2020). Reduced integrity of adherens or tight junctions can lead to changes in focal adhesions to facilitate increased migration such as is seen in partial or complete EMT (Smith *et al*., 2016). Integrin-based focal adhesions form the main link between the cell and the ECM and as such, are critical in supporting cancer cell proliferation and invasion (Maziveyi & Alahari, 2017). To explore whether the reduced ZO-1 localisation at cell-cell adhesions in B7-H3KD cells resulted in altered cell-matrix adhesions, cells were plated onto coverslips then fixed and stained for vinculin (magenta) as a marker for focal adhesions. Figure 38A shows confocal images taken at the basal plane in single cells displaying punctate vinculin-positive focal adhesions visible at the cell periphery. Quantification of the focal adhesion size demonstrated a significant reduction in focal adhesion area when B7-H3 is knocked down in all cell lines (Figure 38B).

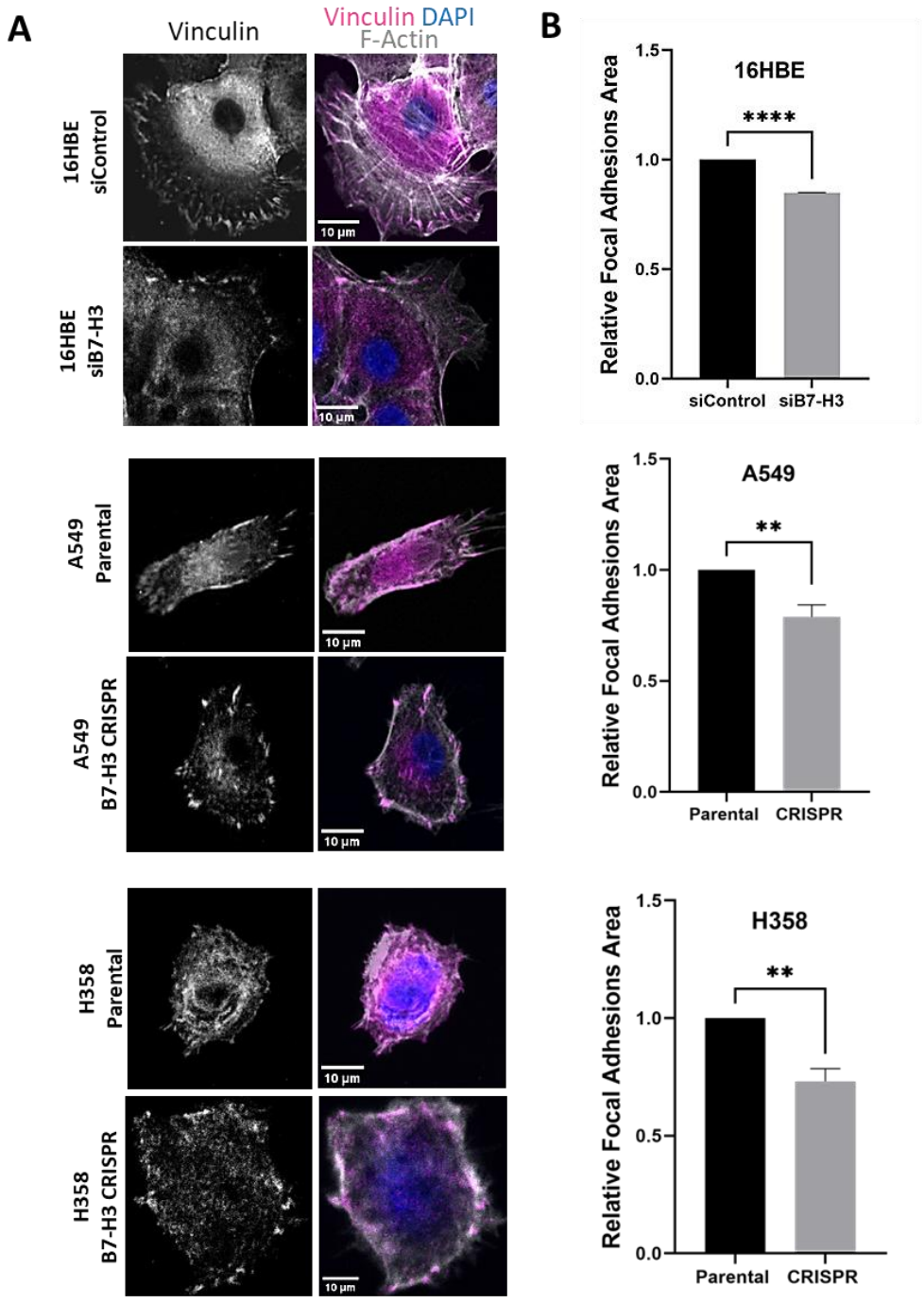

Figure 38: B7-H3 knockdown leads to reduced focal adhesion size.
(A) Representative confocal images of siRNA control/Parental or B7-H3 siRNA/CRISPR cells fixed and stained for DAPI (Blue), Vinculin (Magenta), and F-actin (grey). **(B)** Quantification of focal adhesion area using an automated analysis in ImageJ. Data is pooled from 3 independent experiments where at least 10 cells were analysed per cell line. Data is shown as mean +/- SEM, statistical analysis performed by t-Test. **=p<0.01, ****=p<0.0001. Scale bars 10 µm.

4.2.5 B7-H3 knockdown leads to increased F-actin ruffle formation

The F-actin cytoskeleton plays a critical role in controlling cell proliferation and invasion in response to changes in cell-cell and cell-matrix adhesion (Papakonstanti & Stournaras, 2008). Given the changes in adhesion observed in B7-H3KD cells, we next aimed to determine whether these changes were coupled with alterations in organisation of F-actin structures. 16HBE, A549, and H358 Parental/siRNA control and B7-H3KD cells were plated onto coverslips and stained for F-actin (Figure 39A). Images appeared to show a reduction in F-actin bundles and increase in F-actin peripheral ruffles upon depletion of B7-H3. The percentage of cells exhibiting ruffles were classified and quantified for each cell line. Data showed a significant increase in the proportion of cells showing F-actin peripheral ruffles in the B7-H3KD cells in comparison to the parental/siControl cells (Figure 39B).

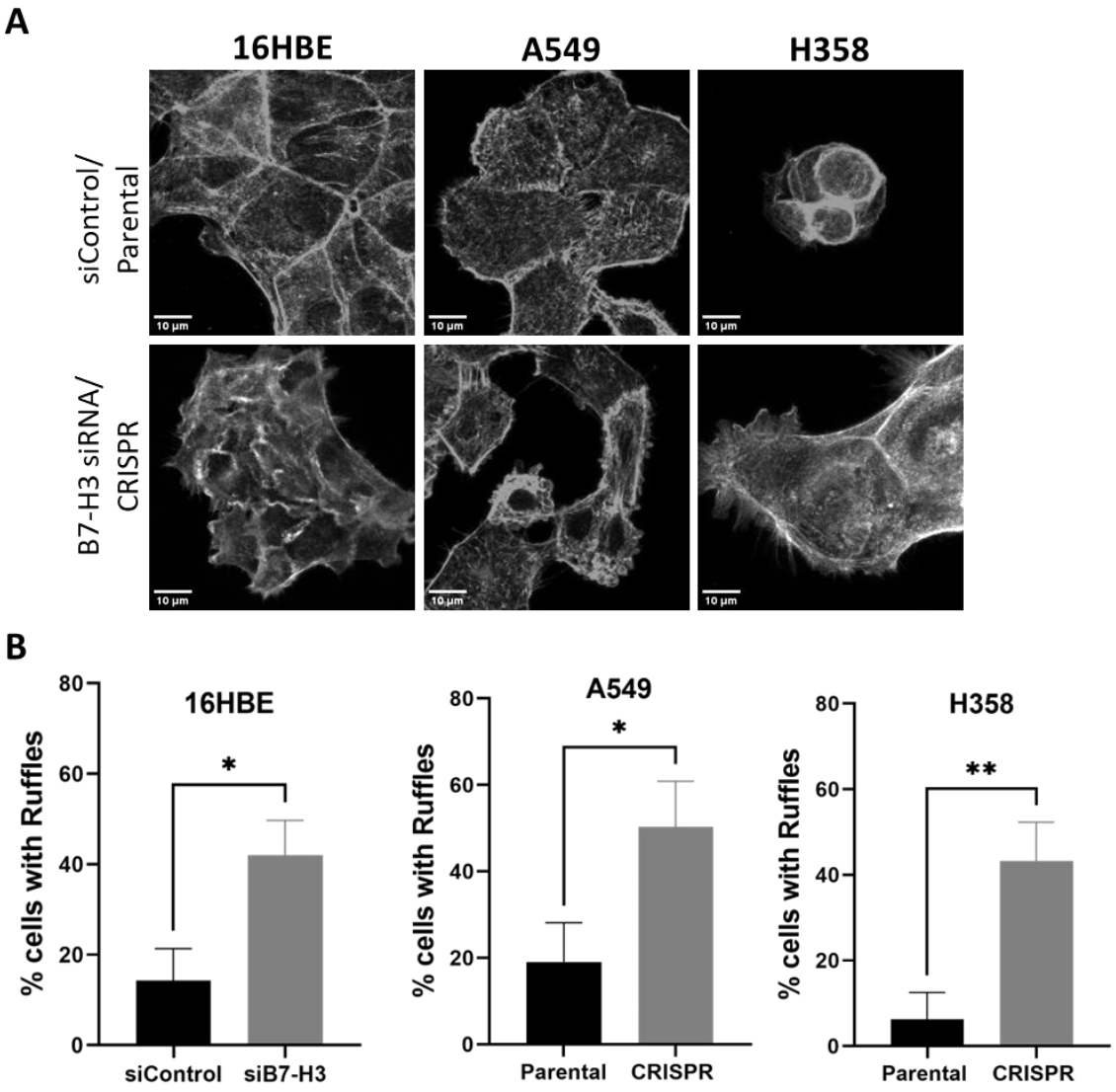

Figure 39: B7-H3 knockdown leads to F-actin ruffle formation.
(A) Representative confocal images of siRNA control/Parental or B7-H3 siRNA/CRISPR cells fixed and stained for F-actin (grey). **(B)** Quantification of the total percentage of cells forming actin ruffling in siRNA control/parental compared to B7-H3KD cells. At least 3 cells were analysed from 7 different fields of view per cell line from 3 independent experiments. Data is representative of one experiment shown as mean +/- SEM, statistical analysis performed by t-test. *=p<0. 05, **=p<0.01. Scale bars 10 µm.

4.2.6 B7-H3 restricts primary cilia formation

Data in chapter 3 showed that B7-H3 localises to primary cilia in 16HBE cells while A549 and H358 cells assemble far fewer cilia than 16HBE cells and this negatively correlates with B7-H3 expression levels. To explore whether B7-H3 plays a role in primary cilia assembly, control and B7-H3KD cell lines were fixed and stained for ARL13B (magenta) as the marker for primary cilia (Figure 40A). Images were then quantified for the percentage of ARL13B positive cells in each cell line. B7-H3KD cells showed significantly higher numbers of primary cilia across all cell lines with ~20% of cells assembling cilia in A549 and H358 B7-H3KD (Figure 40B). This data demonstrates that reduction in B7-H3 levels increases the ability of lung adenocarcinoma cells to form primary cilia, similar to that seen in 16HBE cell line.

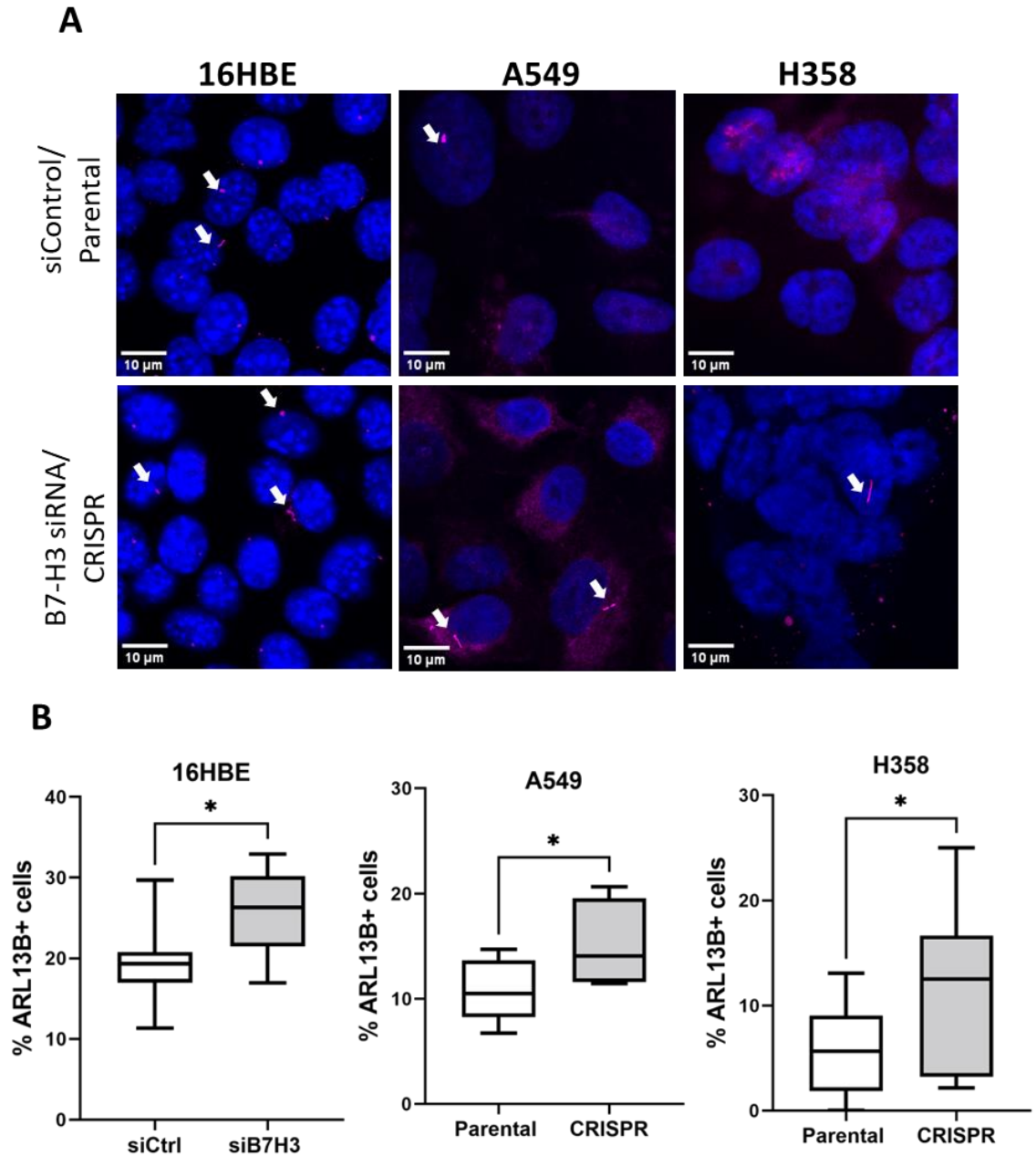

Figure 40: B7-H3 suppresses cilia formation.
(A) Representative confocal images of siRNA control/Parental or B7-H3 siRNA/CRISPR cells fixed and stained for DAPI (blue) and ARL13B (magenta). **(B)** Quantification of the percentage of ARL13B positive cells in all cell lines. 9 fields of view and at least 5 cells/field of view were analysed from 3 independent experiments. White arrows indicate primary cilia. Data is representative of 3 experiments and shown as mean +/- SEM, statistical analysis performed by t-test. *=$p<0.05$, Scale bars 10 µm.

4.2.7 B7-H3 suppresses RR formation in 16HBE cells

Previous data illustrated that B7-H3 co-localises with IMPDH2 at the RR in 16HBE cells. To determine whether B7-H3 levels influence RR formation, 16HBE cells were transfected with control or B7-H3 siRNA followed by treatment with vehicle or MPA for 48 hours prior to fixation and staining for IMPDH2 (magenta) (Figure 41A). Analysis of the mean number of RR/cell showed a significant increase in RR formation in B7-H3KD cells compared to control lines. Treatment with MPA led to a significant increase in the number of RR in siRNA control cells compared to the vehicle-treated line, confirming previous result in Figure 34-chapter 3. However, B7-H3KD cells showed a significant reduction in RRs formation compared to both B7-H3KD vehicle and MPA-treated siRNA control cells (Figure 41B).

Data so far suggests that B7-H3KD alters the number of primary cilia and RR formation. Whereas knocking down primary cilia did not appear to change B7-H3 RR localisation or number. On the other hand, knocking down IMPDH2 increased the number of primary cilia formation but not RR, while blocking IMPDH2 increased the number of RR in control but not B7-H3KD cells. To test the role of blocking IMPDH2 on primary cilia formation, staining of parallel coverslips with antibodies for ARL13B was carried out, thus, to quantify the percentage of cells forming primary cilia. MPA treatment did not change the percentage of cells with ARL13B-positive cilia (Figure 41C), indicating that blocking IMPDH2 activity does not influence primary cilia assembly/disassembly in 16HBE cells.

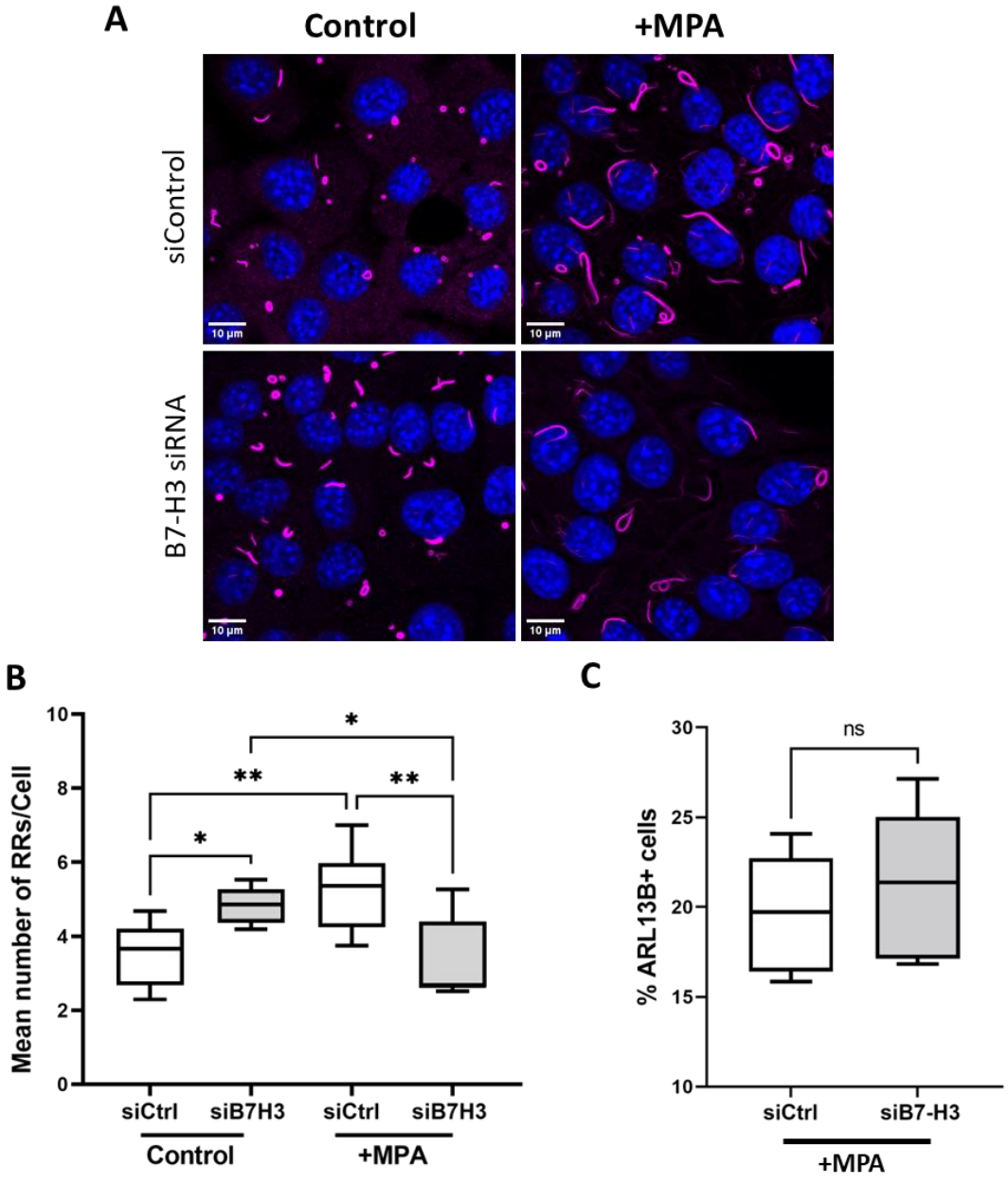

Figure 41: B7-H3 suppresses rods and rings formation in 16HBE cells.
(A) Representative confocal images of siRNA control or B7-H3 siRNA transfected 16HBE cells fixed and stained for DAPI (blue) and IMPDH2 (magenta). **(B)** Quantification of the mean number of RR per cell from images of control or MPA-treated cells in both siRNA control and siB7-H3 in 16HBE cells. Data is representative of three independent experiments. 3-9 fields of view of 7 or more cells were analysed. **(C)** Quantification of the percentage of ARL13B positive cells in MPA-treated 16HBE siContol or siB7-H3 cell lines. 5 fields of view of at least 5 cells were analysed from 2 independent experiments. Graphs are shown as mean +/- SEM. Significance assessed by t-test or one-way ANOVA; *p<0.05, ** p<0.001. Scale bars 10 µm**.**

4.2.8 B7-H3 overexpression in 16HBE cells reduces RR formation

To further explore the effects of B7-H3 levels on RR number, 16HBE cells were transiently transfected with B7-H3 tagged to GFP to over express the protein. Cells were fixed 48 hours post-transfection and stained for B7-H3 (magenta) and IMPDH2 (cyan) (Figure 42A). Confocal images showed an enriched localisation of B7-H3 at the cell-cell junctions as seen previously in Chapter 3 Figure 31, with an apparent reduction in RRs number and size. Subsequent quantification demonstrated a significant decrease in the mean number of RRs in B7-H3-GFP-expressing cells compared to untransfected cells in the same field of view (Figure 42B). This data further confirms that B7-H3 levels, whether overexpressed or reduced, alters the number of RRs as well as primary cilia formation.

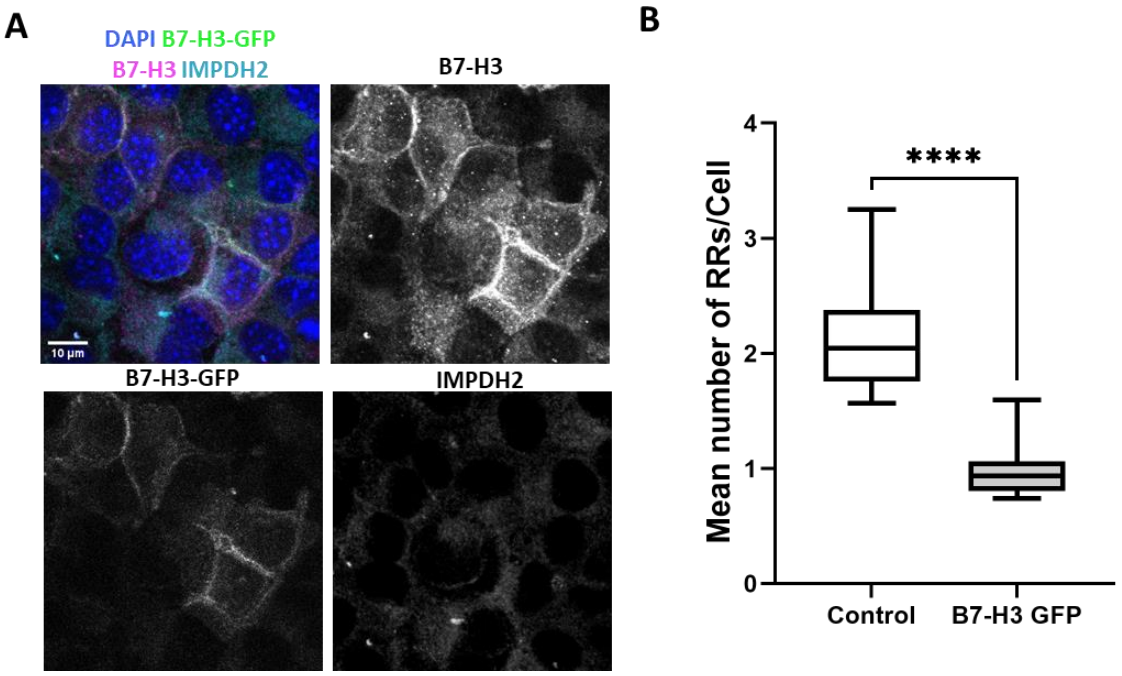

Figure 42: B7-H3 overexpression in 16HBE cells reduces the formation of rods and rings. **(A)** Representative confocal images of B7-H3-GFP overexpression (green) in 16HBE cells fixed and stained for DAPI (blue), endogenous B7-H3 (magenta), and IMPDH2 (cyan). **(B)** Quantification of the mean number of RRs per cell from images of control and B7-H3-GFP cells. Data is pooled from three independent experiments. 7 fields of view of at least 7 or more cells were analysed. Graphs shown as mean +/- SEM. Significance assessed by t-test; **** $p<0.0001$. Scale bars 10 µm.

4.2.9 B7-H3 promotes Rho GTPase activity in 16HBE cells

Data so far has shown that B7-H3 can co-localise with IMPDH2 and ARL13B and that B7-H3 levels regulate RR assembly, cilia, and F-actin organisation. One common signalling nexus that relates to all these structures are the Rho family of small GTPases. We therefore aimed to next explore whether B7-H3 regulates levels of GTP that is essential for Rho GTPase activity and subsequently, reorganisation of actin and cell invasion. To investigate this, 16HBE, A549 and H358 control or B7-H3KD or cells treated with MPA were lysed and analysed by Western blot and G-LISA assays to determine RhoA and Rac1 levels and activity, respectively. G-LISA data demonstrated a significant decrease in both RhoA and Rac1 activity in B7-H3KD 16HBE cells compared to controls, but levels in A549 or H358 cells were unchanged. (Figure 43A). However, activity of both RhoA and Rac1 was reduced in normal epithelial and cancer cell lines following treatment with MPA (Figures 43A), confirming a critical role for IMPDH2 as a rate-limiting step in *de novo* GTP synthesis.

To determine whether changes in RhoA and Rac1 GTPase activity were due to changes in total Rac1 and RhoA protein levels, Western blot analysis was performed on the same samples used for the G-LISA assay (Figure 43B). Data revealed no significant changes in total protein levels for both Rac1 (Figure 43C left panel) and RhoA (Figure 43C right panel) following B7-H3KD or treatment with MPA for both normal and cancer cells. However, interestingly both cancer cell lines showed lower levels of total Rac1 compared to 16HBE (Figure 43C left panel).

Taken together, these data demonstrate that IMPDH2 plays an important role in regulating GTPase activity in human normal and lung cancer epithelial cells, and further demonstrate that B7-H3 may contribute to this pathway in normal lung epithelial cells.

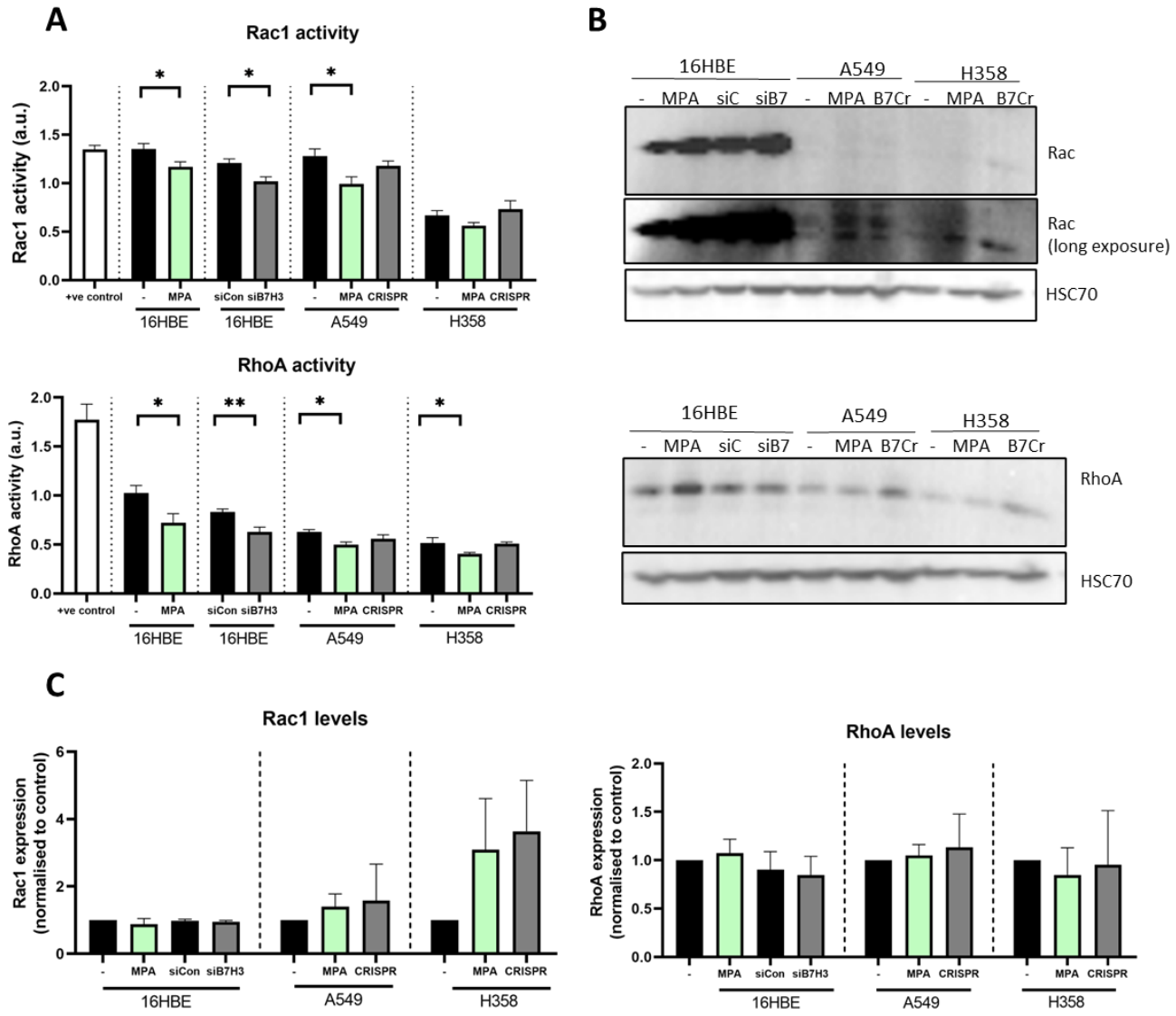

Figure 43: B7-H3 promotes Rho GTPase activity in 16HBE cells.
(A) 16HBE, A549 and H358 control or B7-H3KD cells or treated with MPA. Cells were lysed 48 hours post-treatment followed by measuring the activation of Rac 1 (top panel) and RhoA (bottom panel), activation was assessed by G-LISA. The levels of activated RhoA and Rac1 were measured by absorbance at 490 nm. Data pooled from 3 independent experiments. **(B)** Same lysates as those for G-LISA were used to measure the expression levels via Western blot that was probed for either Rac1 (top panel) or RhoA (bottom panel) and HSC70 was included as a loading control. **(C)** Quantification of Western blot data pooled from 3 independent experiments normalised to respective controls for each cell line. Data is shown as mean +/- SEM. Statistical analysis performed by one-way ANOVA. *=p<0.05, **P<0.01. Plus (+) indicates positive control, minus (-) indicates untreated, siC is siRNA control, siB7 is siRNA B7-H3, B7Cr is B7-H3 CRISPR KD cells.

4.2.10 B7-H3 mAb and ectodomain treatment does not affect localisation of β-Catenin

The ligand for B7-H3 is unknown, but we hypothesise that B7-H3 may act as a homo-dimer to enable self-binding and trigger intracellular responses, as occurs for other transmembrane receptors at cell-cell adhesions (Troyanovsky *et al*., 2007). To investigate whether external manipulation of B7-H3 could change adherens junction formation, 16HBE, A549 and H358 parental cells were incubated for 24 hours with 10 μg/ml of either control IgG, B7-H3 monoclonal antibody (B7-H3 mAb) or B7-H3 ectodomain (B7-H3 Ecto) in a serum free media before fixing and staining the cells with antibodies against β-Catenin. The B7-H3 mAb was raised against the Leu29-Pro245 region (the exact epitope is unknown) and the B7-H3 ectodomain protein encompasses Leu29-Pro245 region. Both are expected to bind to/recognise the same region of the Ig domains in the 4IgB7-H3 variant expressed in human cells. IgG alone was included as a control to determine whether addition of any protein/antibody agent would alter junction formation. B7-H3 localisation post-treatment was not imaged as antibodies recognise ectodomain which would expected to be masked in the presence of these reagents. Confocal images did not show a visible relocation of β-Catenin at cell-cell junctions following the different treatments (Figure 44A). To analyse this in more detail, junctional line scans were performed to compare the signal intensity of β-Catenin at adherens junction, which revealed no change in any cell lines upon treatment with either reagent compared to control IgG (Figure 44B). This data demonstrates that normal and cancer cells are still able to form intact adherens junctions despite any external manipulation of B7-H3, in agreement with the previous data from this chapter seen when B7-H3 is knocked down (Figure 36).

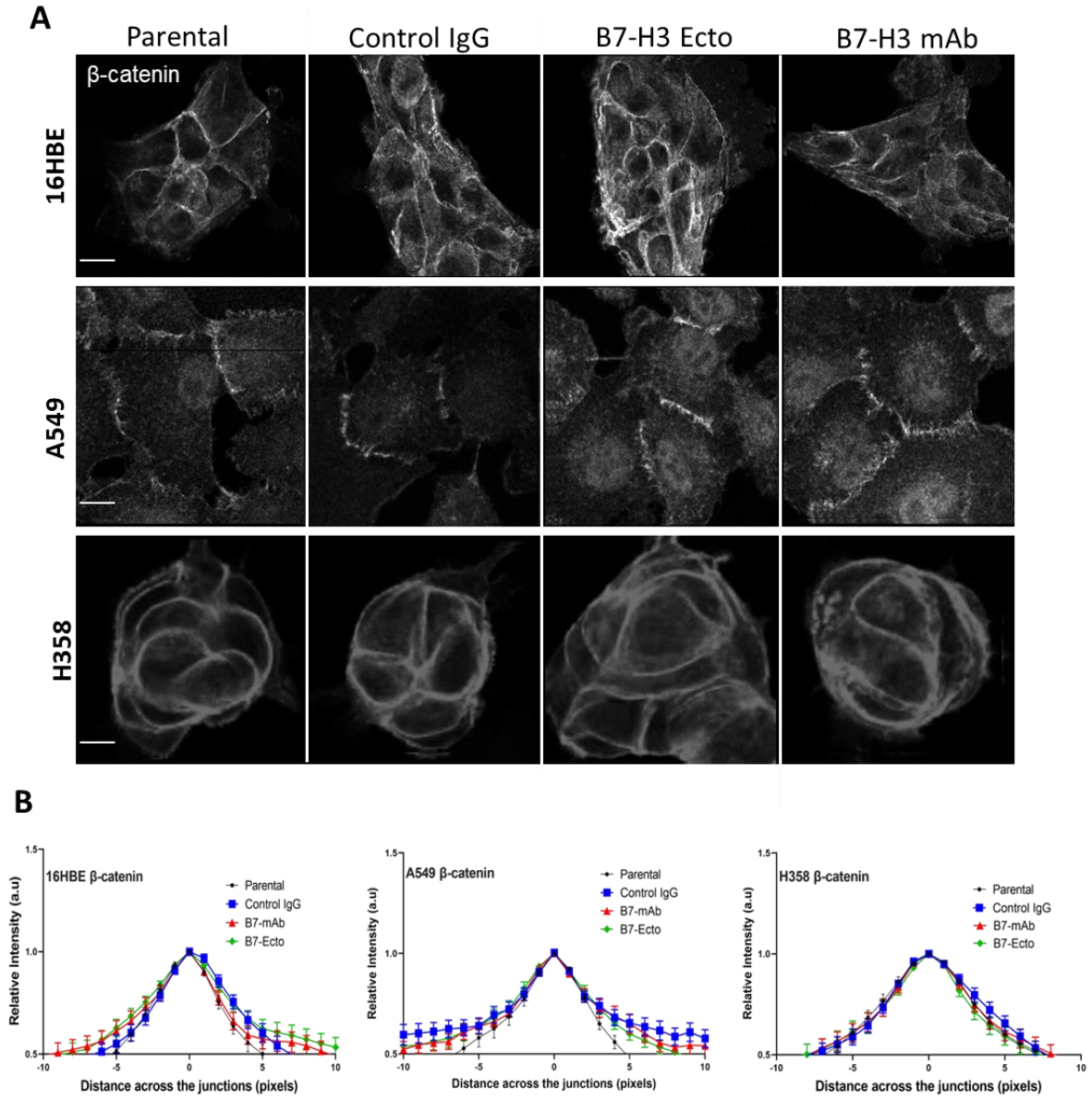

Figure 44: B7-H3 mAb/ectodomain treatment does not affect localisation of β-Catenin at the adherens junction.

(A) Representative confocal images of 16HBE, A549 and H358 parental cells treated with either; IgG control, B7-H3 ectodomain or B7-H3 mAb for 24 hours, fixed and stained for β-catenin. **(B)** Quantitative line scan analysis of β-catenin signal intensity at junctions. Data pooled from 20 junctions per cell line from 5 different fields of view. Data shown is representative of 3 independent experiments and shows mean +/- SEM. One-way ANOVA was used to compare statistical significance. Scale bars 10 µm.

4.2.11 B7-H3 mAb treatment leads to increased stress fibre formation

To investigate the potential role of treating cells with the B7-H3 mAb and ectodomain on the actin cytoskeleton organisation, 16HBE, A549 and H358 stable cell lines expressing Lifeact-GFP were generated and incubated for 3 hours with either control IgG, B7-H3 mAb or B7-H3 ectodomain in a serum free media before monitoring changes of the cells dynamics over the period of 1 hour by confocal time-lapse microscopy. Upon incubation with the ectodomain, all cells displayed increased membrane ruffling and actin-rich protrusions compared to control IgG treated-cells (Figure 45A, 1st vs 2nd columns). In contrast, treatment with the antibody led to assembly of larger actin stress fibres in all cells and more prominently in A549 which are atypical for these cells (Figure 45A, 3rd column). Whilst the fibres were harder to observe in H358 cells, due to their tight stratified colony nature, these cells showed a more flattened phenotype indicative of assembly of more architectural stress fibres. To further investigate whether these phenotypes were due to blocking of B7-H3, cells were incubated with another characterised B7-H3 monoclonal antibody (B7-H3 Blocking mAb) that has been reported to be function-blocking in the context of B7-H3 role as a checkpoint molecule (Wang *et al*., 2021). Increased levels of stress fibres were observed upon B7-H3 Blocking mAb treatment (Figure 45A, 4th column). The experiment was then repeated for the three cell lines, but cells were fixed and stained with phalloidin after 24 hours of incubation with reagents, and cells exhibiting ruffle or stress fibre formation were identified and quantified. Treatment with B7-H3 ectodomain resulted in a significant increase in cells with ruffles compared to other conditions (Figure 45B blue bars). Conversely, treatment with the B7-H3 mAb led to significantly higher F-actin stress fibre formation than was seen in both control and B7-H3 Ecto-treated cells. This was further increased by treatment with the B7-H3 blocking mAb (Figure 45B red bars).

This data demonstrates that B7-H3 mAb and ectodomain treatments lead to opposite phenotypes in terms of F-actin organisation, and indicate that blocking B7-H3 function promotes stress fibre assembly.

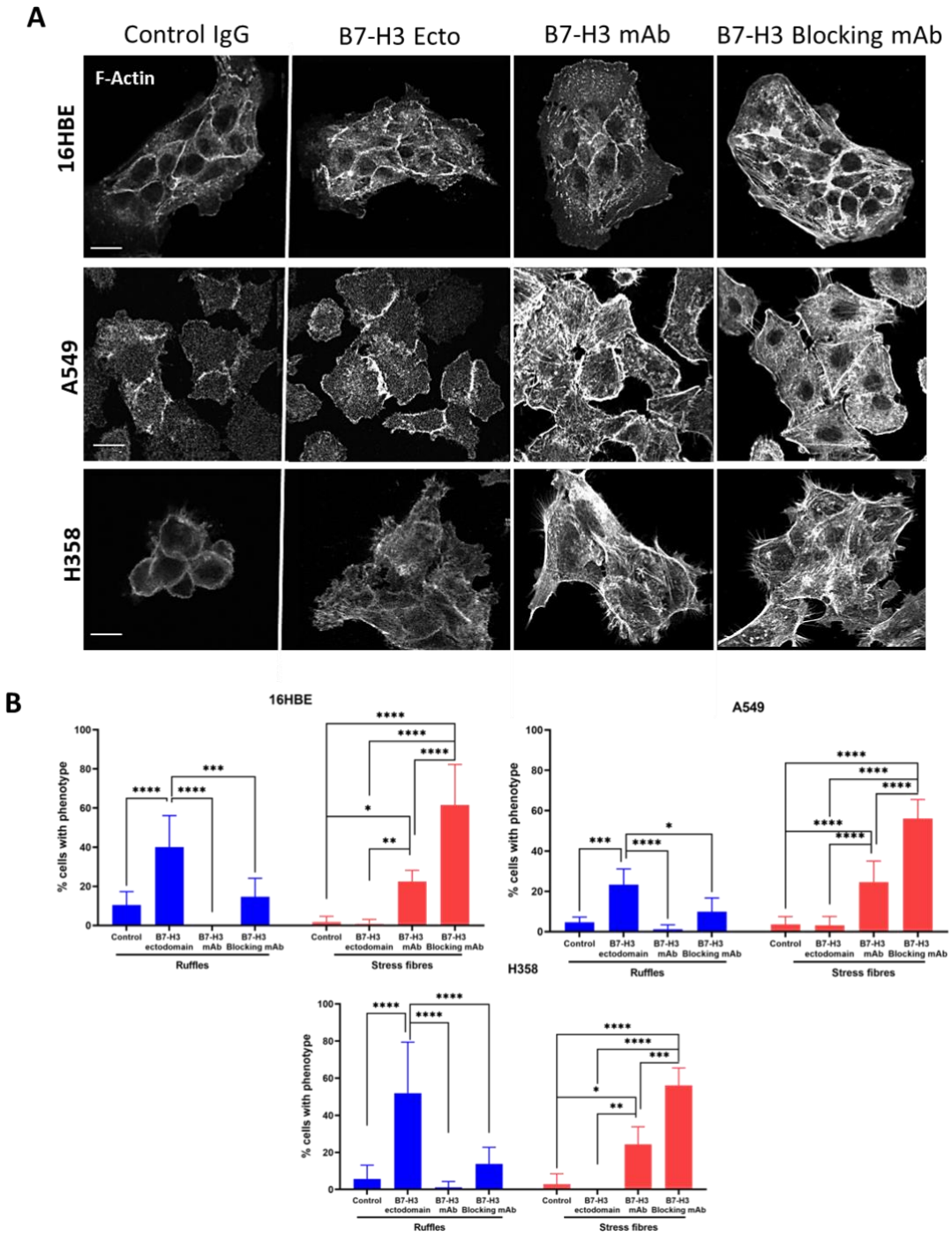

Figure 45: B7-H3 mAb treatment leads to increased stress fibre formation.
(A) Representative confocal images of 16HBE, A549 and H358 parental cells treated with either; IgG control, B7-H3 Ecto, B7-H3 mAb or B7-H3 function blocking mAb for 24 hours, fixed and stained for phalloidin. **(B)** Quantification of the total percentage of cells forming actin ruffles or stress fibres in cells as in (A). At least 10 cells were analysed from 7 different fields of view per cell line per experiment. Data shown is representative of 3 independent experiments and shows mean +/- SEM, statistical analysis performed by 2-way ANOVA. *=p<0.05, **=p<0.01, ****=p<0.0001. Scale bars 10 µm.

4.2.12 B7-H3 knockdown does not affect cell proliferation or circularity in 2D

Previous studies have shown that B7-H3 plays both positive and negative roles in cell proliferation depending on cell type studied (Chen *et al*., 2020; Y. Li, Zhang, *et al*., 2017). To determine whether B7-H3 contributes to proliferation in normal and lung adenocarcinoma cell lines, the same number of 16HBE, A549 and H358 parental/siControl or B7-H3 siRNA/CRISPR cells were plated, allowed to grow, and fixed at 24, 48 hours post-plating followed by staining with DAPI to visualise the nuclei. Cells were then analysed by tile scanned using the EVOS microscope and the number of DAPI positive nuclei per well were counted. Data demonstrated a significant increase in the number of cells at 48 hours post-plating compared to 24 hours confirming cells were proliferating. However, no difference in cell numbers between parental/siControl and B7-H3KD cells was seen in any cell line (Figure 46A).

Previous data in this chapter suggested B7-H3 plays a role in actin organisation. To further explore whether this translated into changes in cell shape, parallel cultures were stained for phalloidin to enable analysis of cell area and circularity. No significant differences in cell surface area (Figure 46B) or circularity (Figure 46C) were observed between control and B7-H3KDs across all cell lines. This data demonstrates that B7-H3KD does not alter normal lung epithelial or lung cancer cell proliferation or cell shape in 2D models.

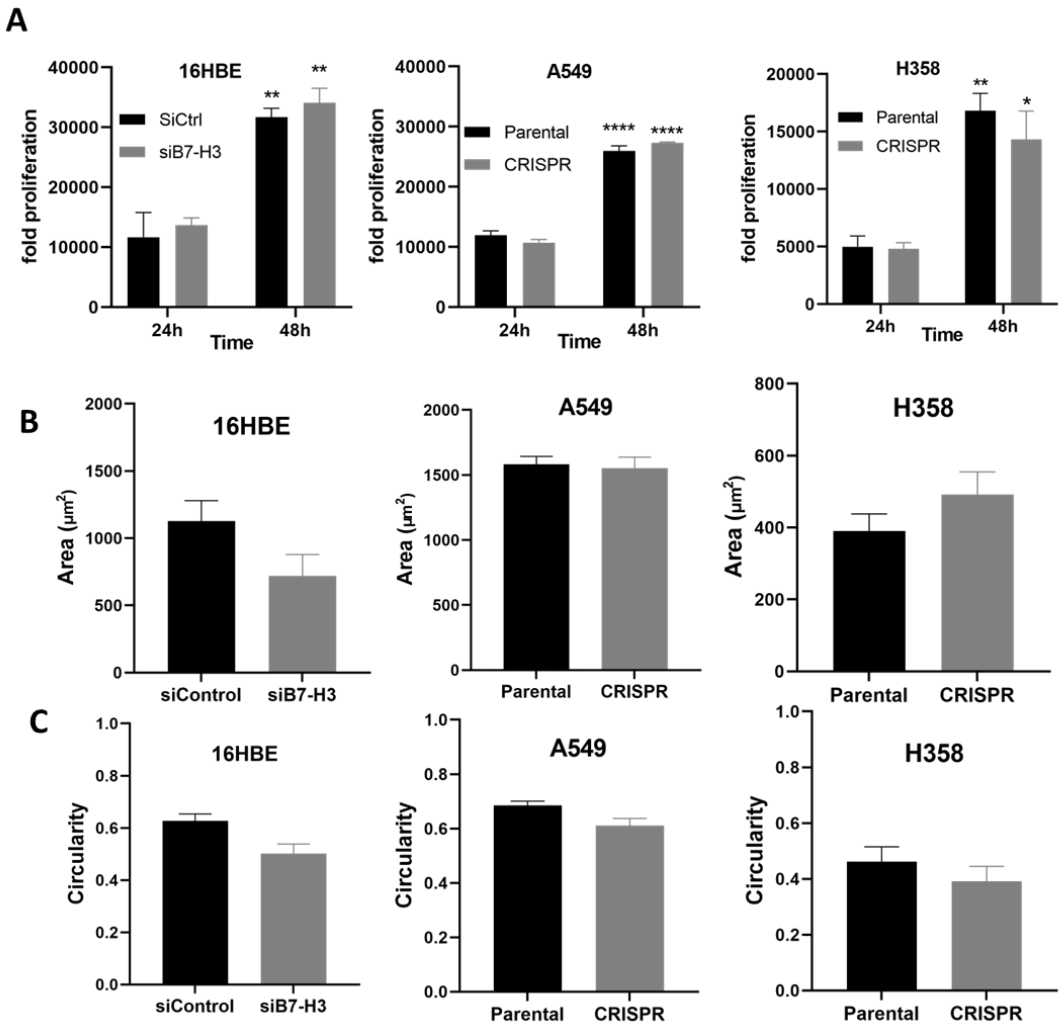

Figure 46: B7-H3 knockdown does not affect proliferation, area or circularity in 2D.
(A) Equal numbers of parental/siControl and B7-H3 siRNA/CRISPR cells were plated and fixed at 24- and 48-hours post-plating. Nuclei were stained with DAPI and fold proliferation was determined. **(B)** Quantification of cell area and **(C)** circularity represents 20 cells/cell line per experiment pooled from 3 independent experiments. Values are plotted as mean +/- SEM. One-way ANOVA or t-test was used to determine statistical significance. *=p<0.05. **=p<0.01 ****=p<0.0001.

4.2.13 B7-H3 knockdown does not alter migration speed in 2D

Previous data in this chapter showed that depleting B7-H3 led to increased F-actin ruffles and reduced focal adhesion size, indicating a potential impact on cell migration. Indeed, B7-H3 has been previously reported to promote cancer cell migration (Yu *et al*., 2018). To investigate the association between B7-H3 expression and cell migration, 16HBE, A549 and H358 parental/siControl and B7-H3KDs were plated and left to adhere for 24 hours. Time-lapse movies were acquired for 16 hours and then used to compare migration speed and distance moved (Figure 47A). As all cells are epithelial-like in nature, most of the movement in single cells was to forming clusters (Figure 47A). Cells were tracked using the manual track and ADAPT plugins in ImageJ, velocity was calculated as μm/h. A549 parental cells seemed to be the fastest compared to normal cell line 16HBE. However, H358 cells were the slowest out of the three parental lines. Which agrees with previous *in vitro* reports of H358 NSCLC cells moving and growing slowly (Scherzer et al., 2015; Wright Muelas et al., 2018). Nonetheless, resulting data demonstrated no change in migration velocity or distance travelled in B7-H3KD cells compared to respective controls (Figure 47B-C), suggesting that B7-H3 does not play a role in migration of these cells on 2D surfaces.

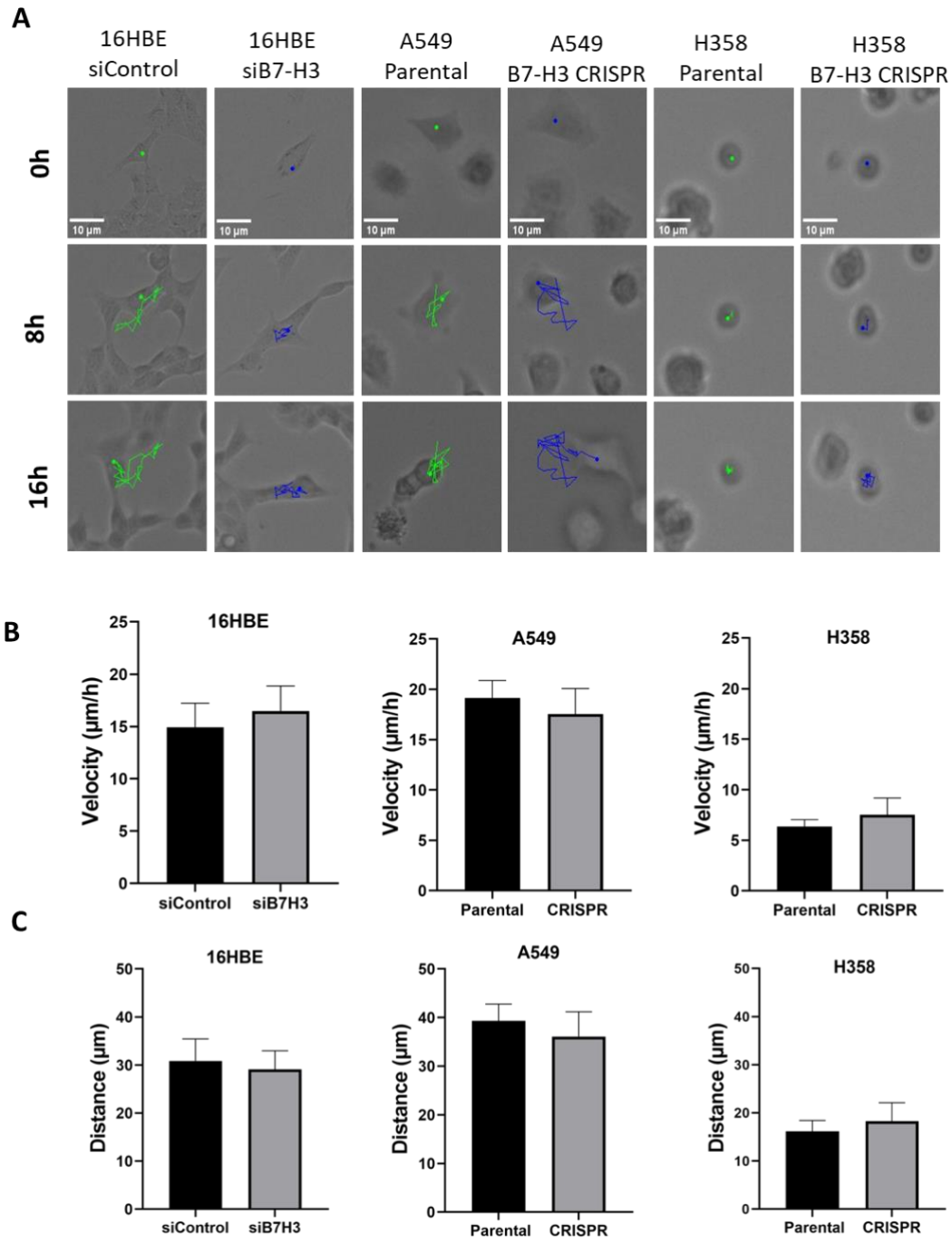

Figure 47: B7-H3 knockdown does not alter migration speed in 2D.
(A) 16HBE, A549 and H358 parental/siRNA control and B7-H3 siRNA/CRISPR cells were plated in a 24 well plate and time-lapse videos were taken for 16 hours to show the migration of cells towards each other to form clusters. Representative frames taken from time-lapse videos are shown for each cell line. **(B)** Quantification of the velocity and **(C)** distance of cells from movies as in (A), using ADAPT plugin in ImageJ. Graphs shown as mean +/- SEM. Significance assessed by t-test. Scale bars 10 µm.

4.2.14 B7-H3 knockdown alters cell colony size/formation in 2D

Images from time lapse movies in Figure 47A indicated a trend towards a decrease in colony sizes formed by B7-H3KD cells. To investigate this in more detail, cells were plated in equal numbers of 24 well plates, fixed and stained with phalloidin after 24 hours and imaged on a confocal microscope (Figure 48A). Subsequent analysis revealed a significant reduction in the size of colonies formed in B7-H3 depleted cells in all lines compared to respective controls (Figure 48B).

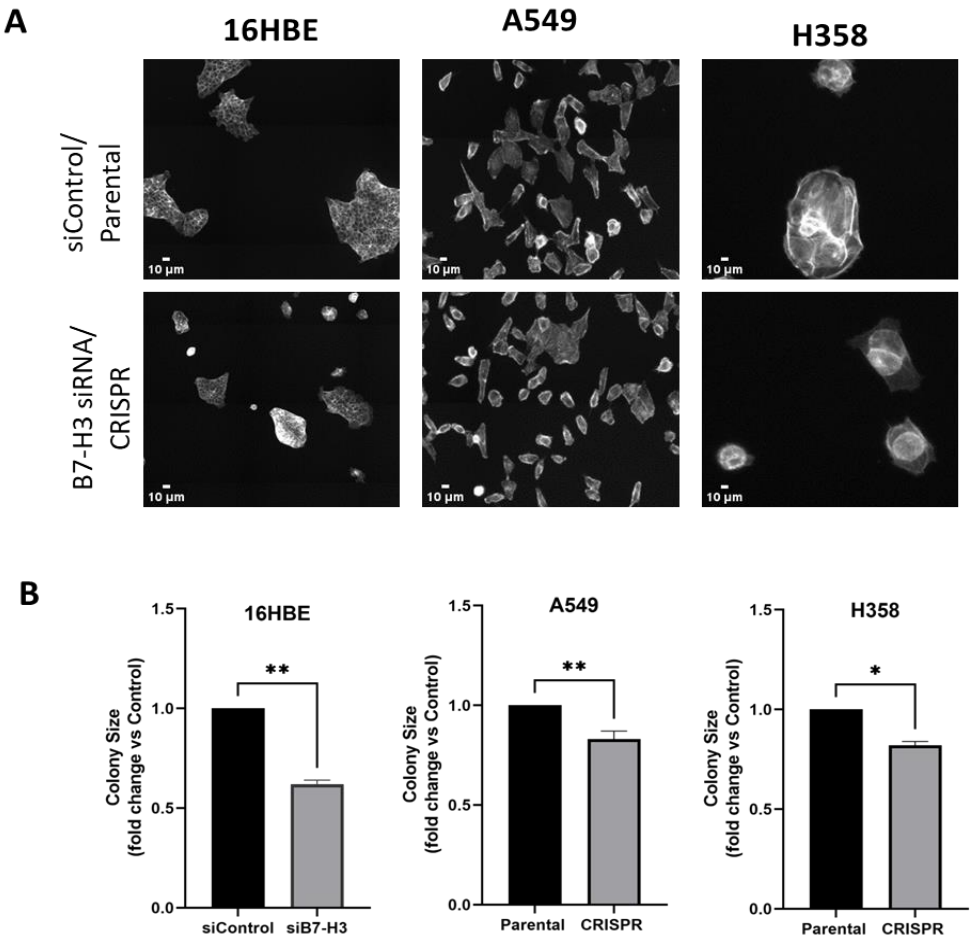

Figure 48: B7-H3 knockdown alters cell colony size/formation but not migration speed in 2D.

(A) 16HBE, A549 and H358 parental/siRNA control and B7-H3 siRNA/CRISPR cells were plated in same numbers in a 24 well plate, fixed 24 hours post-plating and stained for phalloidin. **(B)** Quantification of cell colonies size from cells as in (A). Data were pooled from three independent experiments analysing no less than 60 colonies per cell line and the mean number of each was plotted. Graphs shown as mean +/- SEM. Significance assessed by t-test; *=p<0. 05, **=p<0.01. Scale bars 10 µm.

4.2.15 B7-H3 mAb/ectodomain treatment does not affect cell proliferation, Circularity or spread area

Previous data in this chapter showed that treatment of cells with the B7-H3 mAb or ectodomain results in changes to F-actin reorganisation. To further investigate the potential role of B7-H3 manipulation on modulating proliferation and cell shape, 16HBE, A549 and H358 cell lines were treated for 24 hours with either Control IgG, B7-H3-mAb or B7-H3 Ecto. IgG treatment was included to control for any potential off-target effects induced by addition of the antibody. Cells were then fixed and stained for DAPI and phalloidin to allow measurements of nuclei and cell area/circularity, respectively. Analysis revealed that manipulating B7-H3 ectodomain did not lead to any significant changes to cell proliferation (Figure 49A), cell area (Figure 49B) or circularity (Figure 49C) across all cell lines compared to controls. This data suggests that the altered F-actin seen with the different B7-H3 treatments did not result in measurable changes to cell growth or shape.

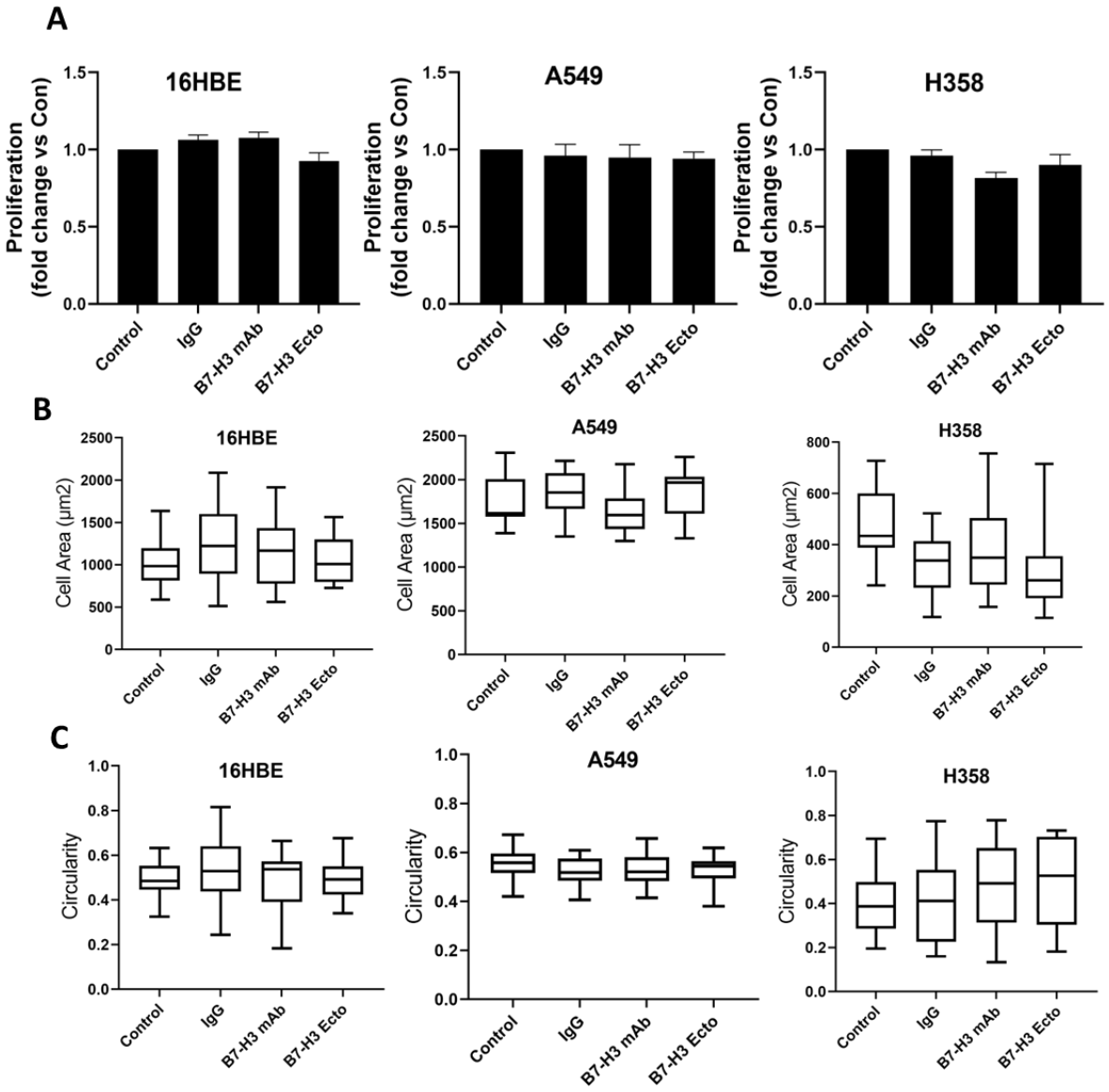

Figure 49: B7-H3 mAb/ectodomain treatment does not affect proliferation, cell circularity or area.

(A) Equal numbers of 16HBE, A549 and H358 parental cells treated with either; IgG control, B7-H3 mAb or B7-H3 ectodomain (Ecto) were plated and fixed at 24 hours. Nuclei were stained with DAPI and fold proliferation was determined. **(B)** Quantification of cell area and **(C)** circularity represented 20 cells/cell line per experiment pooled from 3 independent experiments. Values plotted as mean +/-SEM. One-way ANOVA was used to determine statistical significance.

4.2.16 B7-H3 mAb/ectodomain treatment does not alter 2D cell colony size

To investigate whether the effect of B7-H3 reduction on 2D colony formation could be modulated by external manipulation of B7-H3, cells were plated in equal numbers, fixed and stained for actin 24 hours post-treatment with either control IgG, B7-H3 mAb or B7-H3 ectodomain (Figure 50A). The size of colonies forming was measured and demonstrated that treatment with B7-H3 mAb or ectodomain did not lead to a significant change in colony size (Figure 50B). This data suggests that B7-H3 mAb and recombinant human ectodomain treatments result in changes to cytoskeletal organisation, but this does not change colony size.

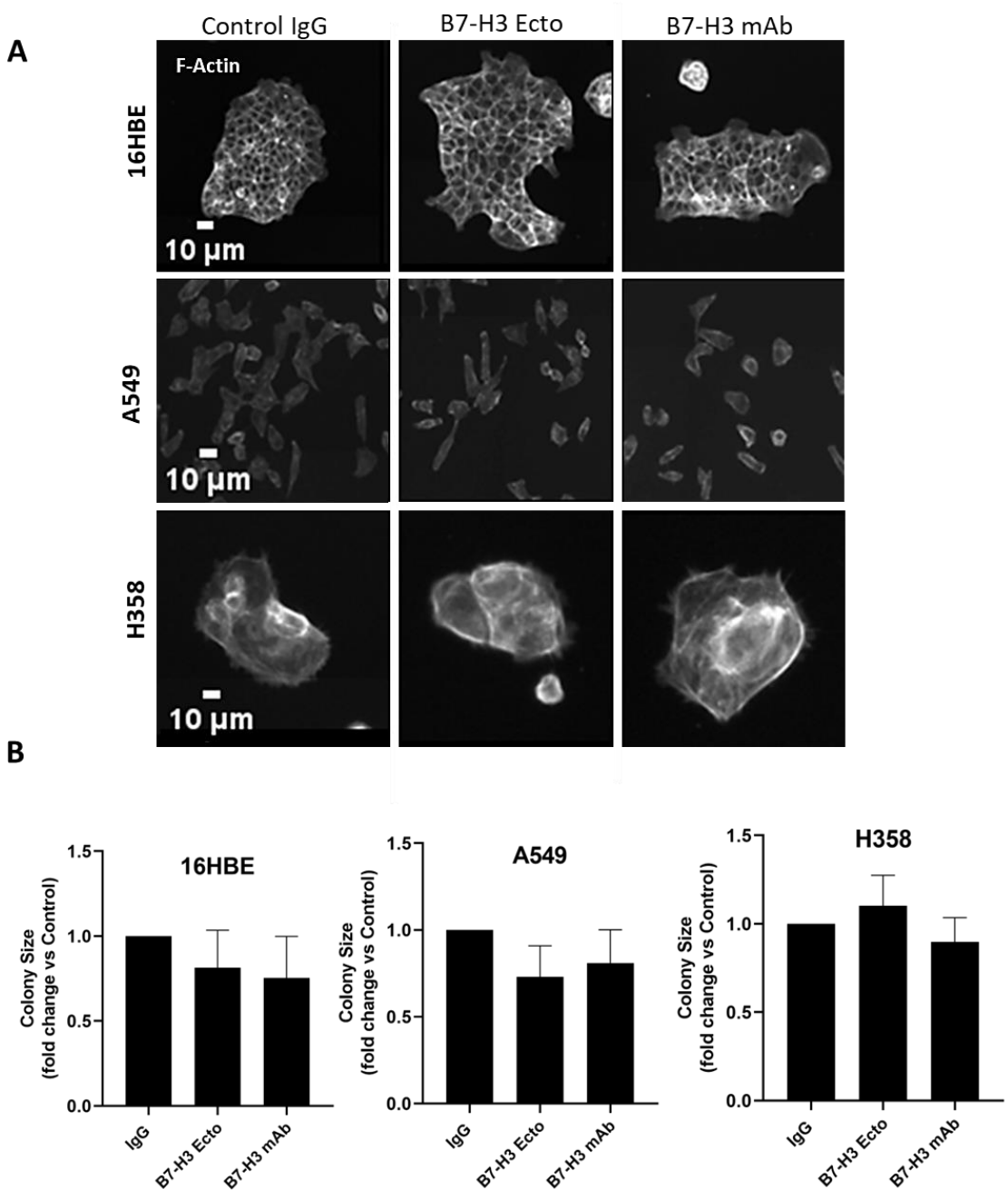

Figure 50: B7-H3 mAb/ectodomain treatment does not affect colony size.
A) Representative confocal images of 16HBE, A549 and H358 cells treated with either; IgG control, B7-H3 ectodomain or B7-H3 mAb fixed 24 hours post-treatment and stained with phalloidin. **(B)** Quantification of cell colonies from cells as in (A). Data were pooled from three independent experiments analysing 60 colonies per cell line per experiment. Graphs shown as mean +/- SEM. Significance assessed by one-way ANOVA. Scale bars 10 µm.

4.2.17 B7-H3 knockdown increases cell invasion and proliferation in 3D

Previous data in this chapter focused on characterising functional roles for B7-H3 in cells plated on 2D surfaces, which is the standard approach used by the vast majority of research groups to study these phenotypes. However, 2D surfaces do not recapitulate the more complex environment experienced by tumour cells *in vivo*. Tumour growth and invasion occurs within a 3D ECM network, where cells within the solid tumour mass experience both cell-cell and cell-matrix interactions. To investigate the effect of B7-H3 expression on cancer cell growth and invasion within 3D ECM, A549 and H358 parental and B7-H3 CRISPR spheroids were formed via the hanging drop method, embedded in 3D collagen and left to invade for 24 hours. Spheroids were then fixed 24 hours post embedding and stained with DAPI and Phalloidin. Confocal images indicated larger spheroids in B7-H3 CRISPRs compared to parentals in both cell lines (Figure 51A). 16HBE normal cell line did not form a proper 3D spheroid in culture and were not included in the 3D study as the main focus of this experiment was to examine the effect of B7-H3 levels on cell growth/ invasion in tumours. Future optimisation of 16HBE 3D spheroids, and using readily available human pulmonary alveolar epithelial cell spheroids to test the results of this experiment as well as cross validate and confirm the outcomes of this thesis would be valuable.

The invasion of cells in the collagen matrix was quantified as fold change in spheroid area at 0- and 24-hours post-embedding. Further analysis of the confocal images confirmed that knockdown of B7-H3 resulted in a significant increase in spheroid cell area and therefore cell invasion (Figure 51B). To determine whether this was due to increased cell number, DAPI stained cells were quantified and showed a significant increase in proliferation in B7-H3 CRISPR lines compared to parental (Figure 51B). Delaunay mean distance between each pair of neighbouring nuclei at 24 hours was also measured to examine the impact of cell proliferation and whether invasion was due to cells not being tightly compacted in spheroids. This analysis showed no significant changes in cell packing, but a trend towards a decrease in cell packing was observed in H358 CRISPR spheroids (Figure 51C). Taken together, this data suggests that B7-H3 can restrict lung cancer spheroid growth and invasion in 3D matrices.

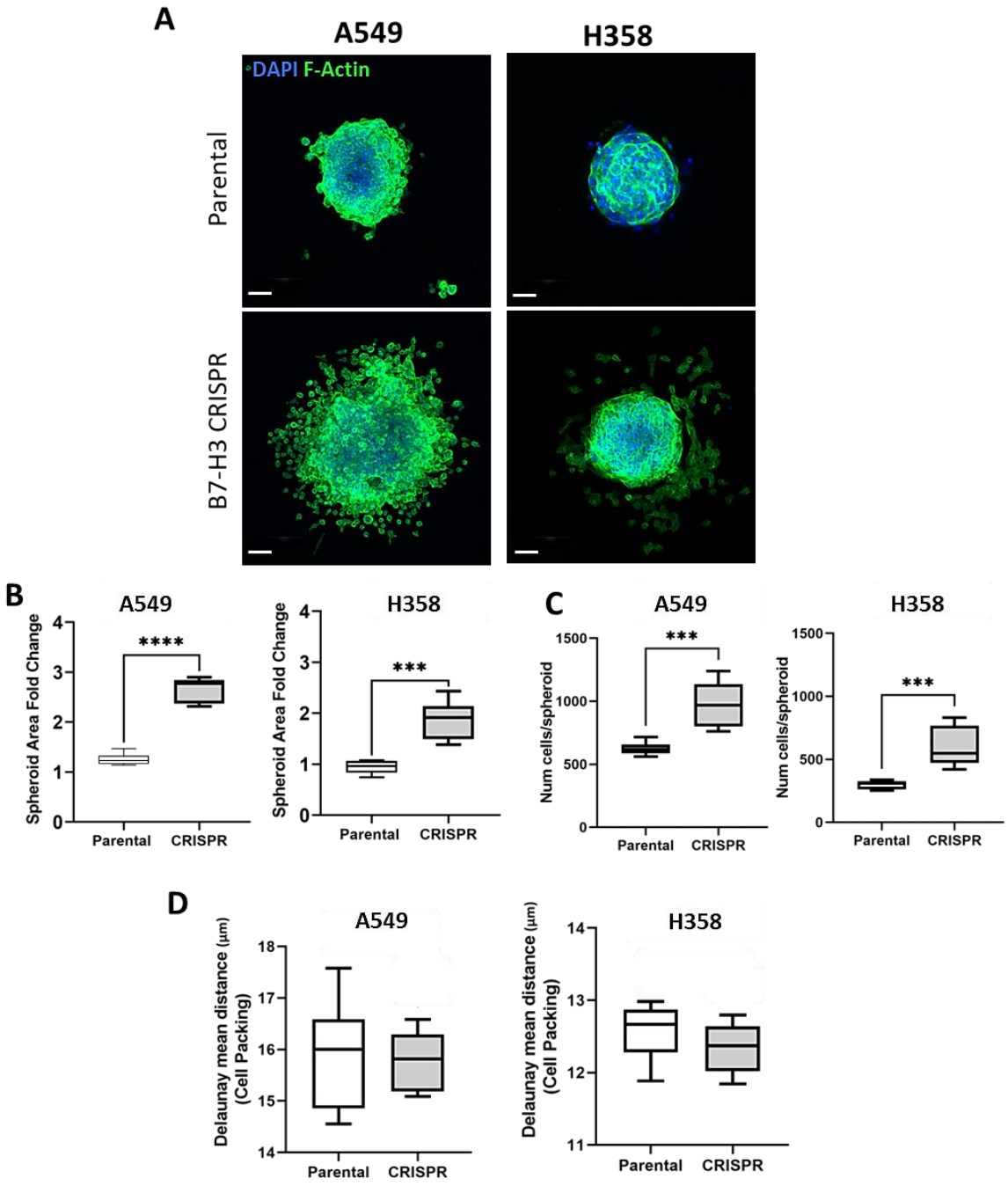

Figure 51: B7-H3 knockdown increases cell invasion and proliferation in 3D.
(A) Representative confocal images of spheroids from control and B7-H3 CRISPR A549 and H358 cells embedded in collagen, fixed and stained for DAPI (blue) and F-actin (green) 24 hours post embedding. **(B)** Quantification of spheroid area over 24 hours post-embedding. **(C)** Quantification of the number of cells per spheroid and **(D)** cell packing using QuPath software. Data shown is a representative of three independent experiments where a total of 6 spheroids were analysed per experiment**.** Graphs shown as mean +/- SEM. Significance assessed by t-test; *** $p<0.001$. Scale bars 50 µm.

4.3 Discussion

4.3.1 B7-H3 ectodomain plays a role in actin signalling

Data presented in this chapter shows different cellular phenotypes occur in response to manipulating B7-H3 ectodomain via mAb or B7-H3 recombinant ectodomain treatments. Both of these reagents are expected to recognise the same region of the 4IgB7-H3, yet interestingly resulted in different changes to actin organisation. The ectodomain-treated cells seemed to be more motile and assembled larger ruffles and actin protrusions in all cell lines which agrees with previous findings where incubation of B7-H3 recombinant human ectodomain with pancreatic cancer cells increased motility and invasion, suggesting a role for B7-H3 in signalling to actin (Xie *et al*., 2016). This does not prove the hypothesis that B7-H3 acts as homodimer for itself but suggests the B7-H3 ectodomain could either bind to B7-H3 or other receptor on the cells that would promote actin re-organisation. It would be interesting to analyse this further by adding exogenous small epitope-tagged purified B7-H3 ectodomain to cell membrane preparations or intact cells followed by analysis of potential associated proteins by proteomics.

Interestingly, the same ruffling phenotypes were formed by B7-H3 depletion, which is counterintuitive to the activation hypothesis of ectodomain treatment yet supports the notion of another binding partner for B7-H3 that the ectodomain might be binding to. This unidentified B7-H3 membrane receptor/binding protein could be suppressed by B7-H3, so by knocking B7-H3 down the same actin phenotypes are seen as treating with ectodomain. This might suggest B7-H3 acts 'transdominantly' on other membrane receptors that removing it leads to changes in surface receptors profiles which makes cells assemble F-actin ruffles. This coreceptor concept has been reported for other B7 family members, where the co-stimulatory molecules B7-1 (CD80) and B7-2 (CD86) have dual specificity for CD28 and CTLA-4 (CD152) receptors. CD28 is expressed on T cells and its activation increases T cell receptor (TCR) signalling. CTLA-4 is a higher affinity receptor and rapidly induced in T cells upon TCR stimulation and its engagement reduces TCR signalling (Sansom, 2000). B7-1 and B7-2 molecules are expressed on APCs as well as on T cells. B7 on T cells have been reported to play a role in regulating responses and delivering signals into T cells (Butte *et al*., 2007). Another member of the B7 family; the Programmed Death-1 (PD-1) receptor (CD279) has two

ligands, PD- L1 (B7-H1; CD274) (Freeman *et al*., 2000) and PD-L2 (B7-DC; CD273) (Latchman *et al*., 2001). The expression patterns of the two PD-1 ligands differ: PD-L1 is constitutively expressed and upregulated to higher levels on murine hematopoietic cells (such as T cells, B cells, macrophages and DCs) and non-hematopoietic cells (e.g., endothelial and epithelial cells), while PD-L2 expression is only inducible on DCs, macrophages, and bone marrow-derived mast cells. Studies have shown inhibitory functions for PD-L1 and PD-L2, others demonstrated that PD-L1 and PD-L2 can stimulate T cell proliferation and cytokine production (Dong *et al*., 2002). PD-L1 and B7-1 have also been reported to be binding partners and their interaction are inhibitory, resulting in reduced expression of cell-surface activation markers, T cell proliferation, and cytokine production. The B7-1:PD-L1 interaction and those of B7-1:CTLA-4 or PD-L1:PD-1 overlap, resulting in distinct functional outcomes of blockade of PD-L1, PD-L2, and PD-1 by mAbs in mouse models of colitis (Kanai *et al*., 2003), allogeneic heart transplantation (Ito *et al*., 2005), contact hypersensitivity (Tsushima *et al*., 2003) and asthma (Matsumoto *et al*., 2004). This adds to the complexity of B7:CD28 family pathways and their functions and supports the hypothesis of B7-H3 acting as a transdominant receptor on the cell surface.

Despite the blocking mAb of B7-H3 driving stress fibre formation, both mAb and ectodomain treatments did not influence adherens junction formation in agreement with B7-H3KD not altering β-catenin localisation. Thus, confirming that B7-H3 does not play a role in adherens junction formation. This might explain the lack of change in cells shape and size, however single cells were not analysed as the epithelial cells used in this project grow in contact with each other. It would be valuable to analyse single cells from time-lapse movies that are infected with GFP-lifeact to further confirm whether B7-H3 manipulation plays a role in altering F-actin dynamics without the impact of cell-cell junctions. Moreover, B7-H3KD reduced tight junctions and focal adhesions formation indicating that presence of B7-H3, and availability of ectodomain to bind to 'ligand X' is required to maintain cell-cell adhesion. Blocking B7-H3 could induce a destabilisation of TJ and cells adapt by assembling more stress fibres to stabilise their architecture. Analysis of the effect of B7-H3 ectodomain manipulation on FA and TJ assembly would be valuable to further understand the role of B7-H3 on regulating these cellular structures. The B7-H3-dependent effects on F-actin reorganisation

led us to analyse Rho GTPase activation. G-LISA analysis on RhoA and Rac displayed no statistically significant change on their activity upon B7-H3KD in adenocarcinoma lines, but acute knockdown of B7-H3 by siRNA in 16HBE reduced both Rac and RhoA GTPase activity. Stable removal of B7-H3 by CRISPR may have allowed cancer cells to adapt to B7-H3 depletion and regulate GTPase activity via other pathways. It would be interesting to examine GTPase activity in 16HBE CRISPR cells and A549/H358 siRNA-treated cells in the future to test this hypothesis. Alternatively, the lack of change of activation in CRISPR lines might instead indicate changes to spatial GTPase activity rather than total levels, which could mediate the observed F-actin reorganisation. The spatiotemporal activity of RhoA in migrating cells and growth factor stimulated cells were examined by Kurokawa & Matsuda using fluorescence resonance energy transfer (FRET) probes. The study found RhoA was activated in migrating HeLa cells at the leading edge and the contractile tail (Kurokawa & Matsuda, 2005). However, in Madin-Darby Canine Kidney cells (MDCK) migrating as a monolayer sheet, RhoA was only activated at the leading edge. In growth factor-stimulated NIH3T3 cells, the activity of RhoA was significantly reduced at the plasma membrane, but remained high at the membrane ruffles in early lamellipodia (Kurokawa & Matsuda, 2005). Furthermore, high levels of RhoA activity at the leading edge of migrating cells and at the membrane ruffles of growth factor-stimulated cells demonstrated that RhoA plays positive roles in cell migration and in the induction of membrane ruffles (Kurokawa *et al*., 2004). This confirms that GTPases are tightly co-ordinated in time and space to mediate downstream actin phenotypes. It would be interesting to visualize the activity and complex spatiotemporal regulation of Rho-family GTPases in living cells by using FRET-based probes for Rho-GTPases in B7-H3KD cells or upon the addition of B7-H3 mAb or ectodomain.

4.3.2 B7-H3 suppresses RR and cilia assembly

Data in this chapter has shown B7-H3 is located at cell-cell junctions at low levels as well as in both RR and primary cilia in 16HBE cells. The expression of B7-H3 is upregulated in tumours which also show few to no cilia and RR (Carcamo *et al*., 2011; Higgins *et al*., 2019). Overexpressing B7-H3 in 16HBE cells to mimic upregulation in cancer resulted in loss of both structures, suggesting that increase in B7-H3 levels could divert it away from both structures and move it to the junctions. However, depleting B7-H3 increased the assembly of primary

cilia and RR, suggesting a correlative relationship between RR and cilia. Previous studies have reported a possible link between ARL13B and IMPDH2. A mass spectrometry analysis of ARL13B has previously identified IMPDH2 as a binding partner for this cilia protein (Shireman *et al*., 2018). Another study demonstrated ARL13B as a negative regulator of the purine recycling salvage pathway and the ARL13B-IMPDH2 binding allows cells to adapt to chemotherapeutic stress and switch to *de novo* purine biosynthesis for survival (Shireman *et al*., 2021). Previous data from chapter 3 supports the negative correlation between ARL13B and IMPDH2, as the number of primary cilia increased when IMPDH2 was knocked down. It would be interesting to further investigate the relationship between B7-H3, primary cilia and RRs and how B7-H3 translocates from these compartments to the junction upon overexpression. This could be assessed by using fluorescently-tagged ciliary and RR proteins (or downstream signals) and analysing the dynamics of both upon B7-H3 overexpression. The potential B7-H3 signalling partners that mediate this will be examined in the next chapter.

RRs can be induced by inhibiting IMPDH2 via treating cells with MPA (Keppeke *et al*., 2015), and several studies have reported cells form aggregates of RRs upon MPA treatment (Carcamo *et al*., 2011; Gunter *et al*., 2008; Noree *et al*., 2010; Ramer *et al*., 2010). RR form as a response to disturbances in the CTP or GTP synthetic pathways (Ji *et al*., 2006). Furthermore, MPA binding to IMPDH causes conformational change and subsequently formation of inactive aggregates (Carcamo *et al*., 2011). Treating 16HBE B7-H3KD cells with MPA led to fewer MPA-driven RRs compared to controls. This could be because B7-H3 plays a role in promoting IMPDH2 activation and depleting it mimics MPA treatment, thereby RRs are induced to form as seen in B7-H3KD cells. Consequently, treating B7-H3KD cells with MPA did not increase RR induction as we postulated B7-H3KD have less active IMPDH2 as RR and subsequently less of MPA effect on RR. This could explain the tight junction deregulation in B7-H3KD cells, as previous studies have shown MPA disrupts tight junction formation to modulate cellular permeability via increasing activation of p38MAPK (Khan *et al*., 2015). This pathway has also been reported to disrupt cilia formation, and depleting B7-H3 decreases p38 MAPK phosphorylation (Flem-Karlsen *et al*., 2019; Wagner & Nebreda, 2009). Moreover, activation of the p38 pathway is involved in actin-mediated mechano-responses (Hoffman *et al*., 2017).

It would be interesting to analyse activation of p38 MAPK in future studies to determine potential involvement in the reported phenotypes in this thesis.

The close associations between the actin cytoskeleton and cilia have been demonstrated with the requirement of actin for centrosome/basal body migration and anchoring of cilia to the actin cytoskeleton (Antoniades *et al*., 2014). Reports have shown F-actin facilitating the transport of ciliary proteins, bundles of actin were identified close to the ciliary membrane and a structure similar to F-actin was found within the ciliary axoneme intertwined with microtubules (Kiesel *et al*., 2020; Kim *et al*., 2015). This could suggest a role for F-actin or actin associated proteins in facilitating cargo transport to RR and primary cilia when B7-H3 is depleted as the actin cytoskeleton is reorganised. Apical actin enrichment is required for ciliogenesis and has been shown to be mediated through Rho GTPases activation (Pan *et al*., 2007). Signalling events initiated at the primary cilia lead to Rac1/RhoA activation (Park *et al*., 2008; Valente *et al*., 2010). As previously demonstrated in this thesis, both cilia and RR co-localise with B7-H3 in 16HBE cells and B7-H3 depletion leads to changes in both structures as well as F-actin organisation. This indicates a role for GTPases to modulate these downstream effects of B7-H3. ARL2 is one of the regulatory GTPases localised at the centrosome (Wright *et al*., 2018), which is important for tubulin dynamics, cilia assembly and has been demonstrated to co-localise with RRs (Taniuchi, 2011; Tian *et al*., 2010; Zhou *et al*., 2006; Schiavon *et al*., 2018). It would be interesting to further investigate the role and activation cascade of ARL2 in B7-H3 depleted/overexpressed cells, and whether it plays a role in regulating trafficking of B7-H3 between different compartments (Fansa & Wittinghofer, 2016).

4.3.3 B7-H3 suppresses cancer cell growth and invasion in 3D

Data from 2D methods used in this thesis demonstrated that B7-H3KD did not play a role in proliferation, yet it reduced colony size formation. However, 3D data showed an increase in proliferation and invasion in B7-H3KD cells. Previous studies have shown conflicting data indicating positive and negative roles for B7-H3 in mediating tumour progression. Furthermore, the mechanisms by which B7-H3 could contribute to a malignant phenotype

remain controversial. *In vivo* studies have shown shRNA of B7-H3 inhibited the expression of metastasis-related proteins in melanoma cells (Tekle *et al*., 2012). In a murine model of colon cancer, injection of Ad-B7-H3-GFP intratumorally led to significant induction CD8 + T-cells producing IFN-γ- and higher IL-12 levels (Lupu *et al*., 2007). Similar findings have also been shown in an orthotopic colon cancer model (Lupu *et al*., 2006). Conversely, loss of B7-H3 in murine mice model had a significant increase on tumour size (Kreymborg *et al*., 2015). Lack of B7-H3 in mice resulted in decreased CD4 and CD8 T-cells proliferation and reduced IFN-γ-induced chemokines (Wang *et al*., 2005). Yu *et al* found B7-H3 promoted proliferation, invasion and migration of lung adenocarcinoma cells *in vitro* where transwell inserts chambers were used to measure invasion (Yu *et al*., 2018). All these studies had different models where different factors could explain the disparity between the results obtained in 2D and 3D.

Epithelial-like cells *in vitro* assemble cell-cell and cell-ECM adhesions which are interdependent and compensate for each other (Goodwin *et al*., 2017). Indeed, cells rely on their extracellular matrix to survive where spatial changes in the environment lead to adaptation in adhesion and F-actin organisation (Katsumi *et al*., 2004). Accordingly, vast majority of cells grown in 3D spheroids to mimic a 'solid tumour'-like structure are in contact only with each other rather than with the ECM which is more physiologically representative of an *in vivo* setting. Conversely in 2D, all cells grow as a monolayer and subsequently have cell-matrix and cell-cell adhesions. Therefore, the proliferation rate of cells in 3D culture better represents the growth of tumours *in vivo* and have different signals and organisation compared to 2D cultures (Gurski *et al*., 2010). The increased proliferation of B7-H3KD in 3D may indicate that B7-H3 suppresses growth in the core of the tumour where cells are only in contact with each other, which would be in agreement with B7-H3 localising at cell-cell adhesions only in tumour cells and potentially supporting tight junction formation as seen in 2D data. Therefore, increased invasion in B7-H3KD in 3D might be due to weakening of TJ in cells within the inner spheroid core, triggering invasion of the peripheral cells in contact with the ECM. Recent studies have shown TJ proteins contribute to the control of cell proliferation (Bhat *et al*., 2019). Thus, weakening TJ in inner cells of the spheroids may also promote proliferation. Analysis of tight junction assembly in B7-H3KD cells in 3D would be important

in further confirming this. Increased invasion of B7-H3KD cells seen in 3D could also be due to increased proliferation, this could be tested by treating B7-H3KD cells with mitomycin C to block cell division and evaluating the invasive potential.

Increased 3D proliferation and invasion of B7-H3KD seen here conflicts with some previous *in vivo* published work (Hashiguchi *et al*., 2008; Kanayama *et al*., 2021; Liu *et al*., 2021; Lupu *et al*., 2007; Tekle *et al*., 2012). Studies of B7-H3 in 3D have been limited to tumoursphere models to study the interplay between tumour and T-cells (Digregorio *et al*., 2021; Huang *et al*., 2020). B7-H3 increased expression and correlation to poor outcomes have been reported in different types of tumours such as renal cell carcinoma (Qin *et al*., 2013; Zhao *et al*., 2013), lung cancer (Wu *et al*., 2016), prostate cancer (Benzon *et al*., 2017), gall-bladder cancer (Liu *et al*., 2016), colorectal cancer (Fan *et al*., 2016; Jiang, Zhang, *et al*., 2016), oesophageal squamous cancer (Song *et al*., 2016), cervical cancer (Zhuang & Xu, 2016), breast cancer (Bachawal *et al*., 2015) and osteosarcoma (Wang *et al*., 2016). However, little is known about the spatial expression level and localisation of B7-H3 in human tumours. To the best of our knowledge, no available studies have reported the correlation between B7-H3 expression within a solid tumour and its localisation. However, a study on PD-L1, one of the B7 family of immune checkpoints, evaluated the expression of the protein on tumour-infiltrating immune cell (TIIC) within the clear cell renal cell carcinoma and found the mean PD-L1-positive TIIC score at the tumour periphery was significantly higher than that at the tumour nest (Mikami *et al*., 2019). It would be interesting to know if this is also the case for B7-H3 with different levels of expressions in different parts of the tumour. Nonetheless, 3D spheroids model still lack the complexity of *in vivo* vascular systems for oxygenation, nutrients, waste removal and immune components. Future studies on the localisation of B7-H3 within the solid tumour would be beneficial to unravel the association between B7-H3 expression, localisation and tumour progression.

Cells within the outer layer of a spheroid interact with the ECM (Khaitan *et al*., 2006). This could suggest that adenocarcinoma B7-H3KD cells at the outer layer assemble primary cilia as seen in 2D which may also contribute to invasion. As primary cilia are known to be signalling

hubs to transduce extracellular signals to regulate proliferation and migration, and RR are involved in purine biosynthesis pathway, B7-H3 might suppress metabolic balance or alter susceptibility to chemotherapy by playing a role in stress response to mediate proliferation and cellular reorganisation. These effects will be further explored in the next chapter.

Taken together, data so far suggests B7-H3 promotes epithelial-like behaviour and is a tumour suppressor in respects to proliferation and invasion. Nonetheless, this may be due to B7-H3 playing a protective role to promote tumourigenesis under stress conditions which will be investigated in the next chapter.

4.3.4 B7-H3 plays a similar role in normal and cancer cells

As mentioned above, B7-H3 is highly expressed in different types of cancers and has been linked to poor prognosis which makes it a promising target for anti-cancer therapeutics. Despite the interest in B7-H3 as a target, the biological function of B7-H3 in cancer cells remain unknown, as most of the previous studies have mainly focused on its interaction with immune cells. Consequently, we aimed to identify B7-H3's role in tumourigenesis in absence of immune/checkpoint components.

Data so far suggests B7-H3 is functionally similar in normal lung epithelial cells vs. adenocarcinoma cells. However, changes of B7-H3 expression in tumour cells alters its localisation and role. In cancer/overexpressing cells, the protein increases at the cell-cell junctions and reduces cilia/RR assembly thereby potentially modulating responses to signals from external cues. B7-H3 may therefore promote some hallmarks of tumourigenesis by supressing formation of the cilia and RRs and maintenance of TJ formation. This is potentially due to the influence of B7-H3 on RRs and cilia as data from previous chapter showed no alteration in B7-H3 localisation/levels upon IMPDH2 and KIF3A knockdown. The role of B7-H3 in tumourigenesis will be elucidated in the next chapter using MPA and a chemotherapeutic reagent.

5. Defining B7-H3-dependent mechanisms contributing to tumourigenesis

5.1 Introduction

Previous data have demonstrated B7-H3 as a tumour suppressor with respect to proliferation and invasion. Data also showed B7-H3 co-localised with IMPDH2 in rods and rings and ARL13B in primary cilia in normal lung epithelial cells, yet these structures were absent in cancer cells. Since IMPDH2 is involved in purine biosynthesis pathway, and cilia regulate proliferation and migration through extracellular cues, we postulated that B7-H3 might supress metabolic balance or alter chemoresistance by playing a role in stress response to mediate tumourigenesis.

Metabolism in cancer cells is reprogrammed to support the demands of uncontrolled proliferation (Pavlova & Thompson, 2016). Accordingly, metabolic patterns are different within normal cells from those in cancer cells and this is consequently regarded as a hallmark of cancer (Pavlova & Thompson, 2016). Cancer-associated modifications in metabolism are now recognised to play a vital and direct role in facilitating tumourigenesis rather than as an indirect response to the development of tumours as previously suggested (Dang, 2012). One of the well-known metabolic alterations in cancer cells is elevated glucose consumption by tumours (Koppenol *et al*., 2011). Glutathione (GSH) metabolism plays both pathogenic and beneficial roles in different types of cancers. It is important for the detoxification of carcinogens, and changes in this pathway can have a colossal effect on cell survival. Elevated GSH levels promotes tumour development and correlates with increased metastasis (Bansal & Simon, 2018). GSH deficiency or a change in GSH/GSSG ratio increases the sensitivity of cells to oxidative stress and tumour progression. However, increased GSH levels elevates antioxidative capacity and resistance to oxidative stress as demonstrated in many tumours (Reczek & Chandel, 2015). Recently, creatine has been found to be both suppressor and activator of cancer growth depending on cancer type studied (Zhang & Bu, 2022). It has been shown to promote colorectal and breast cancer metastasis and shortens survival in mouse models (L. Zhang *et al*., 2021). While another study has demonstrated creatine conserves bioenergy to power anti-tumour reactivity of CD8+ T cell in a tumour microenvironment (Li & Yang, 2021).

Recent research has explored the role of B7-H3 in metabolic reprogramming of cancer cells. B7-H3 has been proposed to mediate glucose metabolism by increasing aerobic glycolytic capacity, also known as the Warburg effect, determined by enhancing glucose uptake as well as extracellular lactate levels in metastatic breast cancer cells and melanoma cells (Flem-Karlsen *et al*., 2017). Additionally, B7-H3 has been shown to play a role in lipid metabolism reprogramming by increasing fatty acid synthesis, which is a common characteristic of cancer (Cairns *et al*., 2011; D. Luo *et al*., 2017). These studies indicate that B7-H3 may play a role in the metabolic reprogramming of cells during tumourigenesis and consequently possible new developments of cancer therapy. However, the potential mechanism by which B7-H3 contributes to cancer cell metabolism is poorly understood. To understand the effects of B7-H3 expression levels on primary cilia, RRs, actin reorganisation and RhoGTPase activity, we investigated in this chapter the potential binding partners of B7-H3 that could contribute to and link these phenotypes. B7-H3 co-localisation with IMPDH2 led us to explore the possible role of B7-H3 on modulating purine biosynthesis metabolites, chemoresistance and survival in lung adenocarcinoma cells.

5.2 Results

5.2.1 B7-H3 knockdown increases amino acid metabolites in 16HBE cells

Data from previous chapter has shown that B7-H3 depletion led to decreased RhoA and Rac1 activity in 16HBE cells. We therefore hypothesised that B7-H3 might contribute to maintenance of steady state GTP levels in cells, potentially through IMPDH2, to regulate GTPase activity and F-actin organisation. To investigate whether B7-H3 contributes to the balance of GTP levels, 16HBE cells were transfected with control siRNA or siB7-H3 followed by preparation of lysates for metabolomics as described in the methods section. Nuclear Magnetic Resonance (NMR) allows the detection of a wide range of metabolites simultaneously by providing a metabolic 'snapshot' profile (Beckonert *et al*., 2007). However, the NMR technique we used here was not sensitive enough to detect GTP/GDP/GMP levels. Nonetheless, some other glutathione and amino acid synthesis metabolites displayed interesting alterations upon B7-H3 reduction. It is worth noting that in some cases there was a significant difference between parental line and siControl transfected cells, thereby the statistical differences with siB7-H3 for these data sets were not plotted despite both controls being higher/lower than siB7-H3 (Figure 52, black vs. blue bars). However, several key amino acid metabolites were increased upon B7-H3 depletion as compared to controls, including, isoleucine, asparagine, creatine phosphate, CDP and NAD (Figure 52, green boxes). Each of these amino acids are involved in different pathways, yet all are largely involved in providing energy to normal cells. Isoleucine is involved in protein metabolism and important in immunity (Gu *et al*., 2019). Asparagine is also involved in protein biosynthesis and cell development (Zhang et al., 2014). Creatine phosphate provides energy for cell viability and activity (Gaddi *et al*., 2017). The nucleolipid cytidine diphosphate (CDP) acts as a high energy donor in the synthesis of different phospholipids (Lilley *et al*., 2014). Nicotinamide adenine dinucleotide (NAD) is a coenzyme for redox reactions and contributes to metabolic homeostasis (Covarrubias *et al*., 2021). Taken together, these data suggest an important role for B7-H3 in regulating energy levels in normal lung epithelial cells. Reducing B7-H3 levels could result in increased metabolites that regulate proteins and phospholipids biosynthesis.

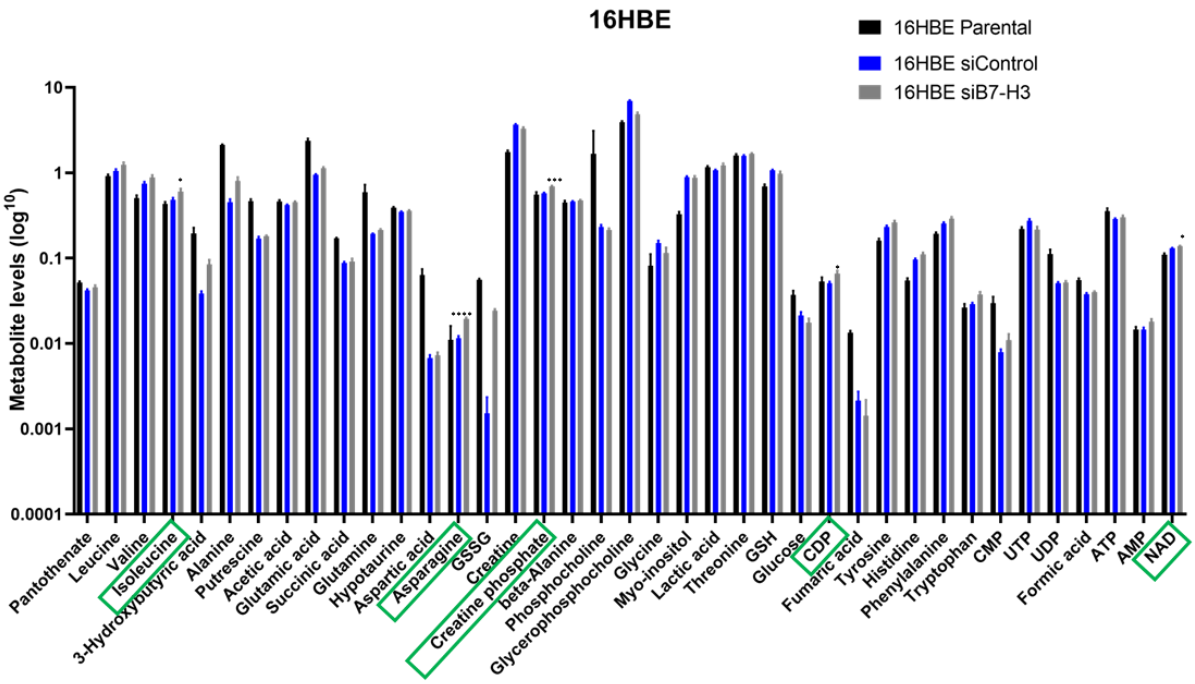

Figure 52: B7-H3 knockout increased amino acids metabolites in 16HBE cells.
An overview of 39 selected metabolites levels in 16HBE parental, siRNA control and siB7-H3 cells from NMR spectroscopy. Data pooled from 5 independent experiments. Data show means +/- SEM statistical analysis assessed by multiple unpaired t-test between siControl and siB7-H3; *p<0.05, ** p<0.01, ***p<0.005. Green boxes indicate increased key data points by siB7-H3.

5.2.2 Analysis of B7-H3 contributions to metabolites in lung adenocarcinoma cells

To analyse the effects of B7-H3 expression on metabolite balance levels in lung cancer cells, parental and B7-H3 CRISPR A549 and H358 cells were processed for NMR analysis as per the previous figure. In A549, two metabolites, fumaric acid and pantothenic acid, involved in the Krebs cycle to release energy were reduced in CRISPR cells (Moharregh-Khiabani *et al*., 2009; Penet *et al*., 2016) (Figure 53A-red boxes). Conversely, GSSG levels were significantly increased in B7-H3KD cells (Figure 53A, green box). GSSG is a peptide involved in glutathione-dependent metabolism and its ratio with GSH is considered an indicator of oxidative stress (Hellou *et al*., 2012).

Interestingly, H358 CRISPR cells displayed more metabolic changes in response to B7-H3 depletion. Putrescine, glutamic acid, hypotaurine, GSSG, GSH, creatine, creatine phosphate, myo-inositol, and NAD were significantly increased (Figure 53B-green boxes). These products are involved in polyamine protein biosynthesis, glutamine metabolism, cysteine catabolism, glutathione metabolism, arginine and methionine metabolism, glucose metabolism, energy metabolism, respectively (Bansal & Simon, 2018; Fried *et al*., 2021; Gonzalez-Uarquin *et al*., 2020; Qin *et al*., 2020; Shen *et al*., 2021; Taegtmeyer & Ingwall, 2013). On the other hand, Glutamine, Formic acid, Aspartic acid, Phenylalanine, Cytidine 3',5'-Monophosphate (CMP) and glucose were significantly reduced (Figure 53B-red boxes).

In this thesis, we focused on GSSG levels as they were significantly increased in all B7-H3 knockdowns compared to controls (and siControl in 16HBE). This suggest a role for B7-H3 in regulating energy as well as in glutathione metabolism, which will be further analysed later in this chapter.

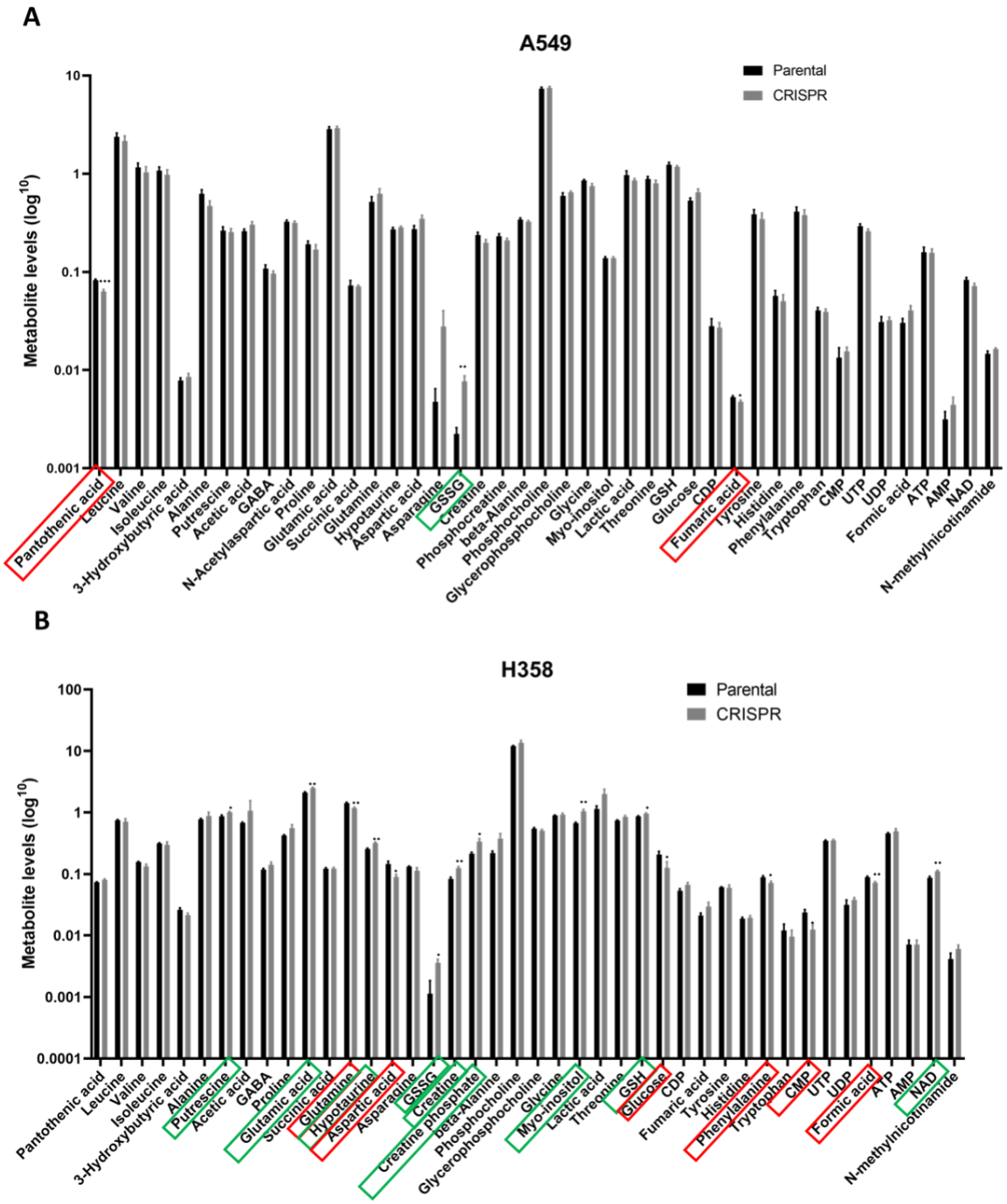

Figure 53: Analysis of B7-H3 contributions to amino acid metabolism in adenocarcinoma cells.

A-B) An overview of selected metabolites levels in A549 **(A)** and H358 **(B)** parental and respective B7-H3 CRISPR knockdown cells from nuclear magnetic resonance spectroscopy. Data pooled from 5 independent experiments. Data show means +/- SEM statistical analysis assessed by multiple unpaired t-test between siControl and siB7-H3; *p<0.05, ** p<0.01, ***p<0.005. Green boxes indicate significantly increased while red boxes indicate significantly reduced data points in B7-H3 CRISPR cells.

5.2.3 B7-H3 regulates GSH:GSSG ratio

Data from previous NMR analysis suggests B7-H3 may have an effect on GSSG and GSH levels which could result in an altered ratio between the two enzymes and subsequently increased oxidative stress. To further analyse this, ratios of GSH and GSSG levels in all cell lines from NMR data were analysed. Data revealed that the ratio between GSH/GSSG was significantly decreased in B7-H3KD cells for all cell lines (Figure 54), indicating a role for B7-H3 in suppression of oxidative stress and increased stress tolerance.

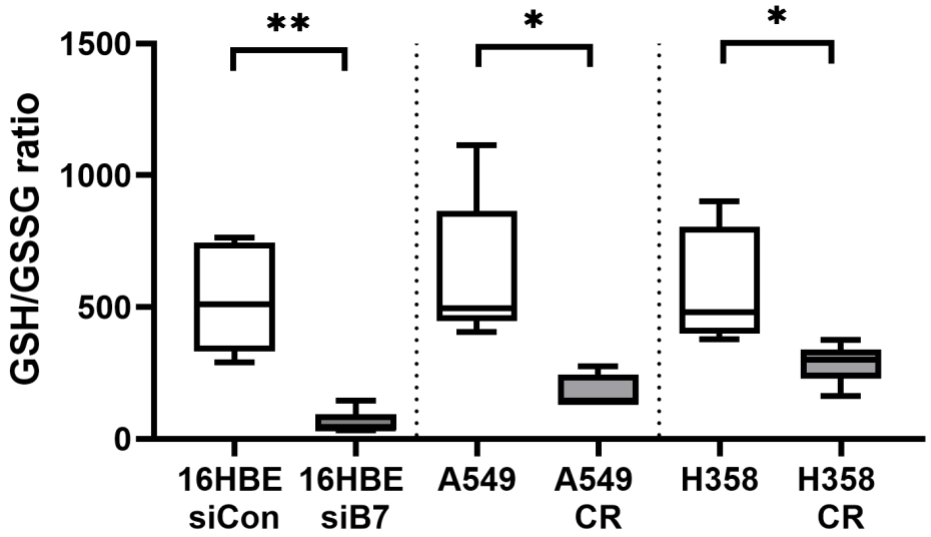

Figure 54: B7-H3 knockdown reduced GSH: GSSG ratio.
Graph of GSH:GSSG ratio measured from NMR metabolomics analysis in 16HBE, A549 and H358 parental cells compared to B7-H3 knockdowns. Data pooled from 5 independent experiments. Values are plotted as mean ± SEM. One-way ANOVA was used to determine statistical significance. *=$p<0.05$. **=$p<0.01$.

5.2.4 Reducing B7-H3 leads to reduced IMPDH2 pathway metabolites

Data in chapter 4 demonstrated a role for B7-H3 in regulating RR formation in all cells, and Rho GTPase activation in 16HBE cells. RRs are IMPDH2 polymers which play a critical role in regulation of *de novo* guanine nucleotide synthesis and subsequently intercellular GTP pool (Papakonstanti & Stournaras, 2008; Sassi *et al*., 2021). To test the hypothesis of whether B7-H3 was involved in purine biosynthesis and ultimately regulating GTP/GDP/GMP levels, parental, B7-H3KDs and MPA-treated cells metabolites were extracted and processed via LC-MS as described in the methods section. Although NMR-based metabolomics has been widely employed in metabolomic studies, it was not very sensitive with respect to detecting GTP levels in cells. Therefore, LC-MS/MS-based metabolomics was used instead. LC-MS/MS analysis allows profiling of small metabolomics molecules downstream of cellular machinery (i.e., enzymes). Compared to NMR, LC-MS/MS is more sensitive with 10 to 100 times better lower limits of detection (Emwas *et al*., 2019; Lee *et al*., 2010). Data revealed that 16HBE cells showed a significant reduction in NAPDH levels following MPA treatment (Figure 55A). This metabolite is involved in the purine biosynthesis and was reported to be upregulated in cancer (Rather *et al*., 2021). Guanosine was upregulated in siB7-H3 and MPA-treated cells. Guanosine is a nucleoside that plays a role in *de novo* biosynthesis of GMP and cell invasion (Bianchi-Smiraglia *et al*., 2015). Other metabolites such as IMP, AMP, ADP, ATP, GMP, GTP and GDP were significantly reduced in MPA and siB7-H3KD cells, however there were also significant differences in these metabolites between siControl and parental cells, so the relevance of this data remains unclear.

A549 and H358 cells showed similar profiles to 16HBE cells: a significant decrease in ADP, AMP, GMP, GTP and GDP levels were seen in both MPA and B7-H3 CRISPR cells compared to controls. All of these metabolites are involved in the purine biosynthesis pathway (de Vitto *et al*., 2021). Like 16HBE siB7-H3, Guanosine levels were also increased in A549 B7-H3KD cells (Figure 55A), and Xanthine levels were decreased in H358 MPA-treated cells (Figure 55B). Xanthine expression has been linked to malignancy and poor prognosis (Battelli *et al*., 2016). GSH/GSSG ratios were also all significantly reduced in all B7-H3KD and MPA-treated cells in all cell lines, confirming that seen in NMR data (Figure 55B).

Finally, a significant decrease in GTP levels was seen upon both MPA treatment and B7-H3KD in all cell lines, indicating a role for B7-H3 in regulating the guanine *de novo* purine synthesis pathway (Figure 55C).

Taken together, these data suggest B7-H3 plays a protective role to reduce oxidative stress and promotes *de novo* guanine synthesis in both normal lung epithelial and lung cancer cells.

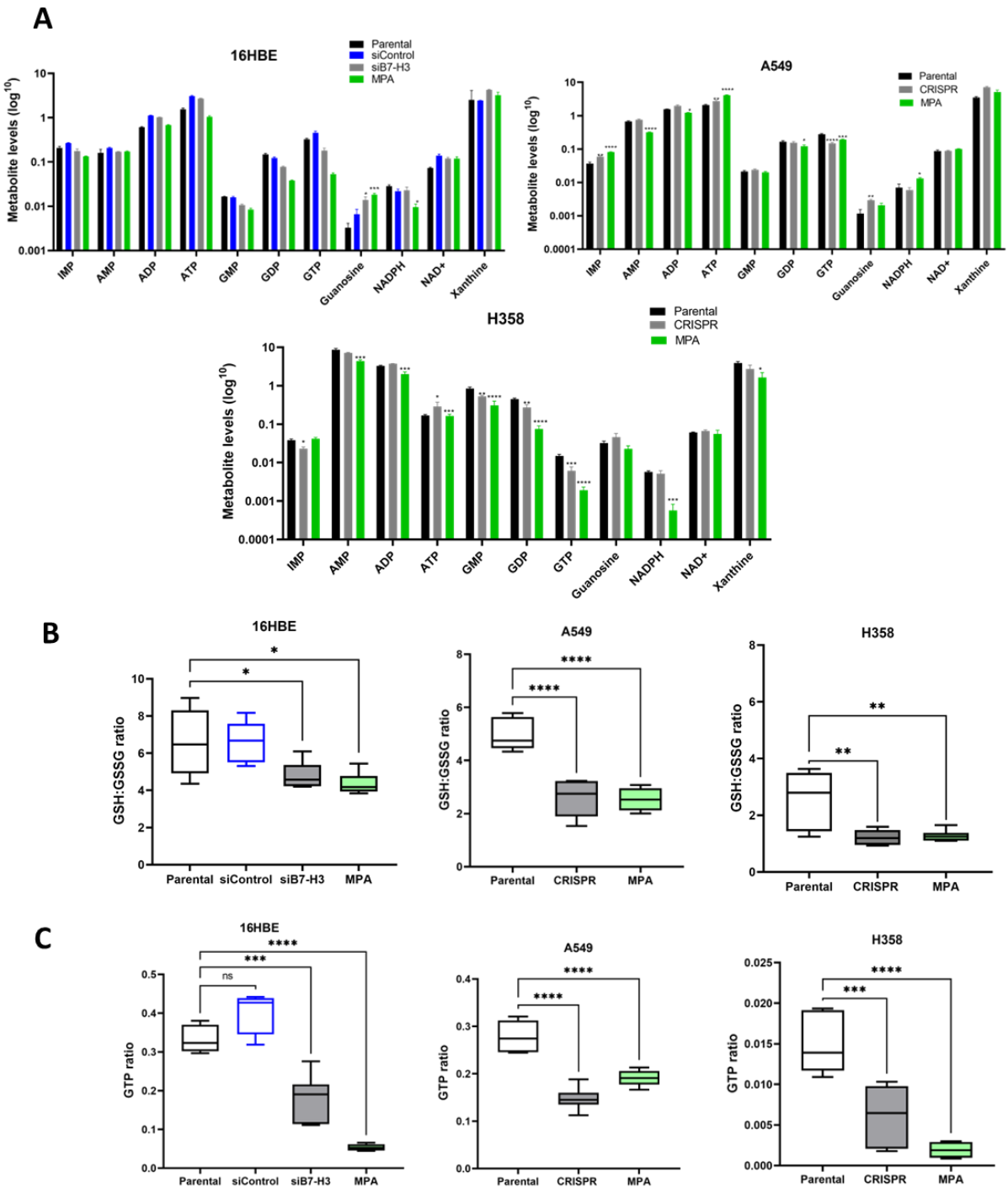

Figure 55: Reducing B7-H3 leads to reduced IMPDH2 pathway metabolites.
A) Graph of key changes in metabolites levels of the purine pathway analysed by mass spectrometry in parental/siControl, B7-H3 siRNA/CRISPR knockdowns and MPA-treated in 16HBE, A549 and H358 cells. **(B)** Graphs of GSH:GSSG ratio quantified from cells as in (A). **(C)** Quantification of GTP ratio in cells as in (A)**.** Data pooled from 2 samples per experiment and 2 independent experiments. Values are plotted as mean +/- SEM. One-way ANOVA was used to determine statistical significance. *=p<0.05. **=p<0.01, ***=p<0.001, ****=p<0.0001.

5.2.5 B7-H3 suppresses oxidative stress

Previous NMR and MS data both demonstrated reduced GSH/GSSG ratios following depletion of B7-H3, suggesting a role in regulating oxidative stress. To further validate increased oxidative stress in B7-H3KD cells, the CellRox probe was used to detect and quantify reactive oxygen species (ROS) in live cells.

16HBE, A549 and H358 siControl/Parental or siB7-H3/CRISPRs were either grown under normal conditions or serum-starved for 48 hours prior to incubating cells with the CellRox probe for 30 minutes. Subsequently, live cells were imaged where bright cells indicated oxidative stress (Figure 56A). The fluorescence intensity of the CellRox probe was analysed from siControl/parental and B7-H3KD cells (Figure 56B). Analysis revealed a significant increase in fluorescence levels in starved siControl cells compared to control conditions, as would be expected under stress conditions (Figure 56B, top graph). However, this was not seen in either cancer cell lines (Figure 56B, middle and bottom graphs). However, all B7-H3KD cells showed a significant increase in fluorescence compared to siControl/parental in control and starved conditions indicating an increase in ROS upon B7-H3KD (Figure 56B). This data suggests that B7-H3 suppresses oxidative stress in normal and lung cancer cells.

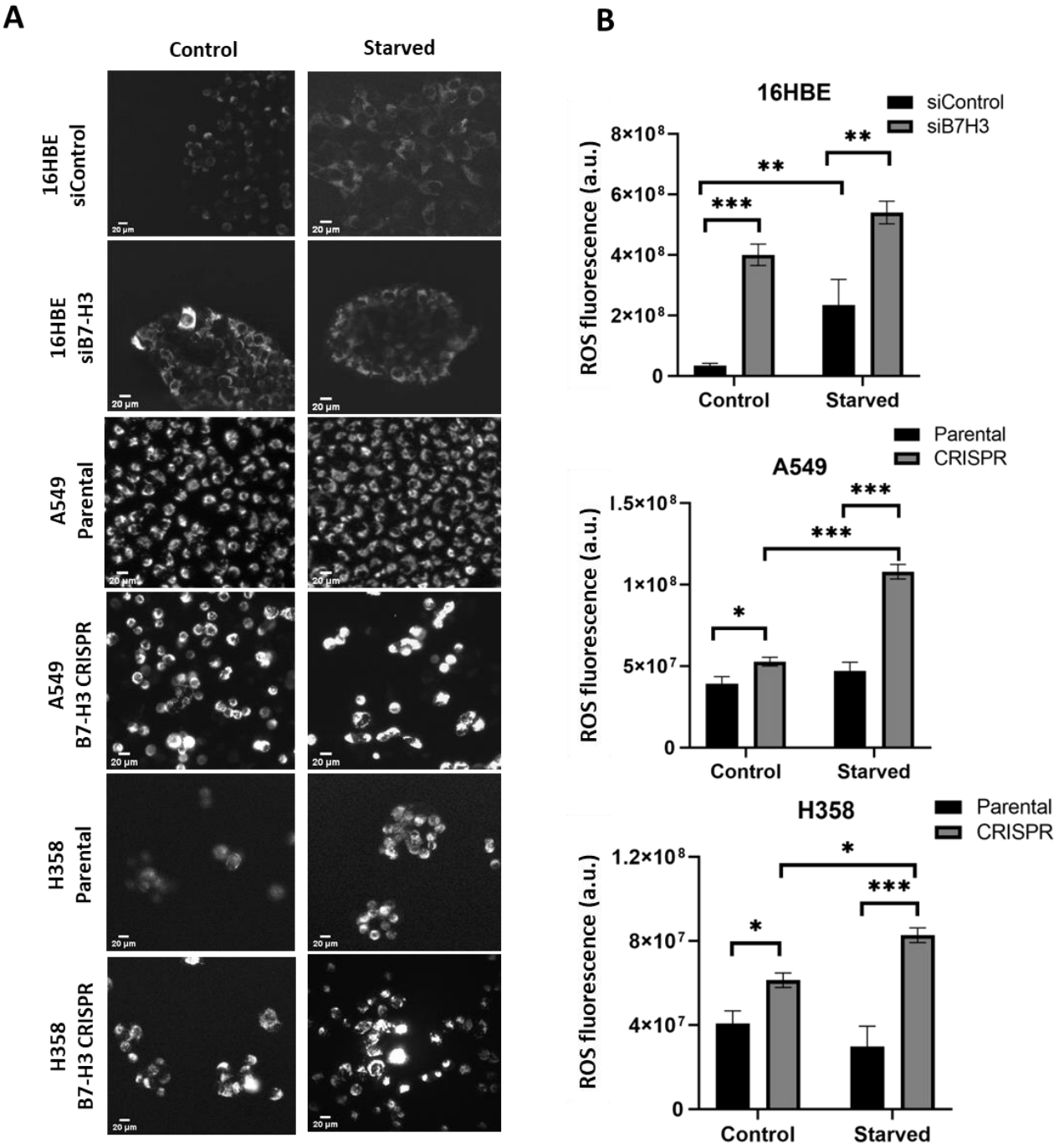

Figure 56: B7-H3 suppresses oxidative stress.

A) Representative confocal images of siControl/Parental or B7-H3 siRNA/CRISPR cells plated in a 96-well plate, cells were left under basal conditions (control), or serum staved for 48 hours prior to incubation with CellROX reagent. **(B)** Quantification of the oxidative stress levels of cells in (A) by measuring the CellROX fluorescence signal. Data pooled from 3 independent experiments, 3 replicates per experiment. Values are plotted as mean +/- SEM. One-way ANOVA was used to determine statistical significance. *=p<0.05. **=p<0.01, ***=p<0.001. Scale bars 20 µm.

5.2.6 B7-H3 promotes chemoresistance and cell survival

Some chemotherapeutic agents induce oxidative stress as a means for killing cancer cells (Chen *et al*., 2007). Targeting cancer cells by increasing ROS production or inhibition of the cellular antioxidant network has been reported to be successful in murine xenograft model and *in vitro* (Noh *et al*., 2015; Ogiwara *et al*., 2019; Trachootham *et al*., 2009). Excess levels of ROS cause damage to vital cellular pathways which can lead to activation of cell death processes such as apoptosis (Redza-Dutordoir & Averill-Bates, 2016). Apoptosis is induced through caspase activation (Azad & Iyer, 2014). To investigate whether B7-H3KD cancer cells are susceptible to chemo-stress, A549 and H358 parental and B7-H3KD cells were subjected to either normal growth conditions or serum starvation for 48 hours (Figure 57A, B). In parallel, cells were either treated with DMSO (vehicle control) or cisplatin for 48 hours (Figure 57C, D). Cisplatin is a chemotherapeutic drug that activates pathways leading to apoptosis (Cregan *et al*., 2013). DAPI was added to live cells to allow measurements of cell number and CellEvent™ caspase detection reagent was added as a measure of apoptosis, which fluoresces green only upon induction of active caspases. Live cells were imaged, and the levels of caspase reporter measured in all conditions at 48 hours post-treatment. Data demonstrated a significant increase in apoptosis in B7-H3KD-starved cells compared to both starved parental cells and B7-H3KD control cells (Figures 57A, B, left panels). Moreover, upon cisplatin treatment, A549 and H358 parental cells showed increased apoptosis compared to control DMSO cells, and B7-H3 CRISPR cells showed a significant increase in apoptosis compared to both CRISPR control and parental cisplatin-treated cells (Figure 57C, D left panels). No statistical significance was found between parental and CRISPR cells under DMSO treatments.

To further confirm the viability of cells, DAPI positive cells were counted and normalised to parental control cells. Serum starvation led to a significant reduction in cell number in B7-H3KD cells compared to controls, B7-H3KD and parental-starved cells, in both A549 and H358 (Figures 57A, B – right panels). Cisplatin-treated CRISPR and parental cells showed a significant reduction in cell number in both A549 and H358 compared to their control counterparts (Figures 57C, D - right panels).

Taken together, these data suggest a role for B7-H3 in promoting chemoresistance and survival by suppression of oxidative stress and subsequently apoptosis.

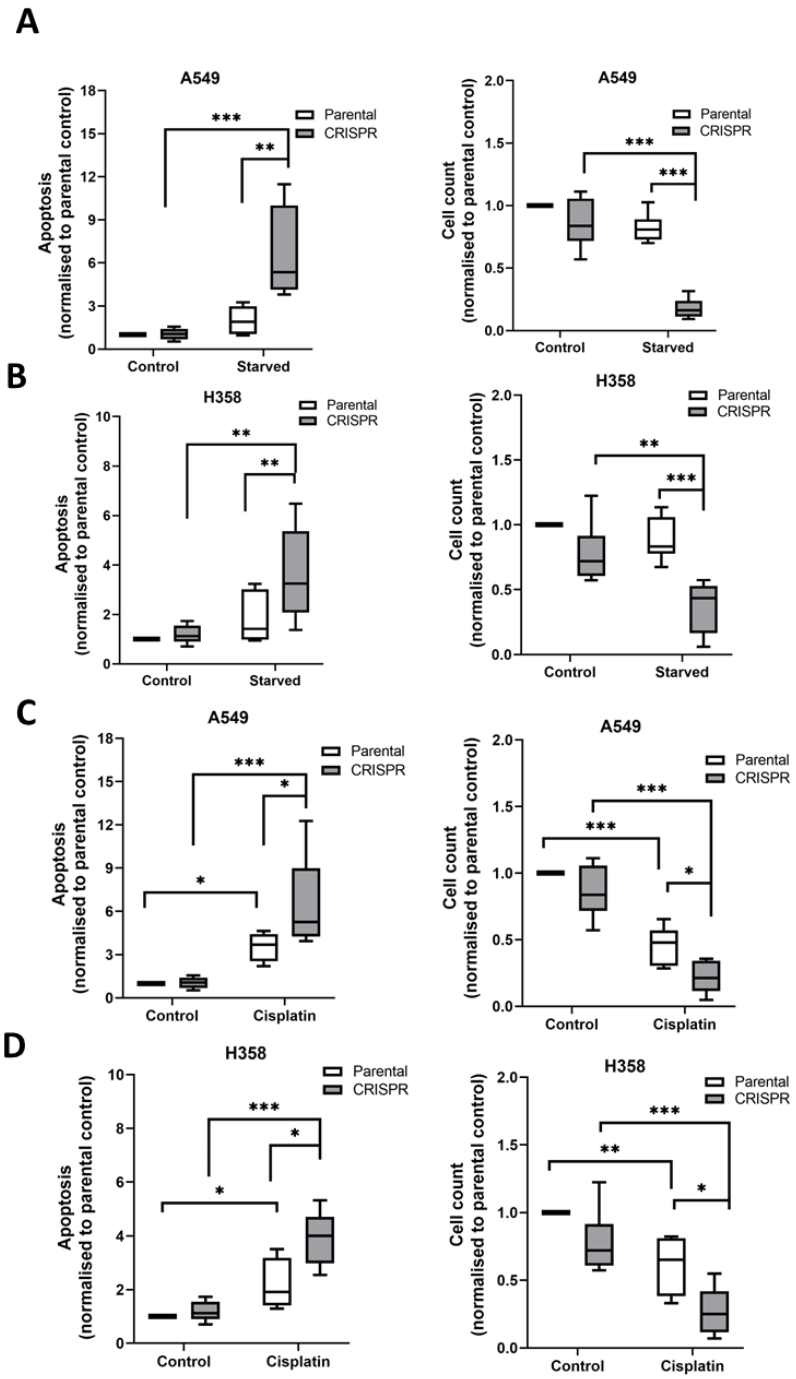

Figure 57: B7-H3 Promotes chemoresistance and survival.
Quantification of apoptosis (left panel) and cell count (right panel) in parental or B7-H3 CRISPR A549 and H358 cells (**A**, **C** and **B, D**, respectively). Cells were either left under basal conditions or serum-starved **(A, B)**, or were treated with DMSO as vehicle control or cisplatin **(C, D)** for 48 hours prior to staining the live cells with DAPI and CellEvent™ Caspase-3/7 Green detection reagent for apoptosis. Data pooled from 3 independent experiments; each experiment performed in triplicate. Values are plotted as mean +/- SEM. One-way ANOVA was used to determine statistical significance. *=p<0.05. **=p<0.01, ***=p<0.001.

5.2.7 B7-H3 forms a complex with IMPDH2

To investigate possible binding partners that may complex with B7-H3 to contribute to purine synthesis pathway, actin rearrangement and aid in suppressing stress response, mass spectrometry analysis was carried out on GFP-Traps. 16HBE, A549 and H358 cells were transfected with GFP control or B7-H3-GFP and treated with either vehicle control or MPA for 48 hours. Resulting complexes were subjected to SDS PAGE and bands were excised and sent for LC-MS/MS analysis as described in the methods section. This analysis revealed several proteins hits, six (IMPDH2, actin, annexin, myosin A, myosin B and tubulin) were chosen to be further validated as they have been previously associated with cytoskeleton rearrangements (Figure 58A). IMPDH2 was seen to co-localise with B7-H3 at RR in normal cells and cancer cells at the junction (data not shown) and is also involved in purine biosynthesis pathway as well as support cytoskeletal assembly (Keppeke *et al*., 2015; Wolfe *et al*., 2019). The actin cytoskeleton was rearranged when B7-H3 was manipulated, and actin is known to mediate essential biological functions and is modulated by Rho GTPases to allow cell motility (Parri & Chiarugi, 2010). Annexin plays a role in the cell life cycle, apoptosis, and exocytosis (Mirsaeidi *et al*., 2016). Myosins are actin-based motor proteins, myosin II motors are key effectors in primary cilium biogenesis and cilium function (Rao *et al*., 2014). Tubulin polymerises into microtubules that are vital for the cytoskeleton, mitosis, primary cilia assembly and it regulates intercellular transport (Gadadhar *et al*., 2017; Yang *et al*., 2021).

Interactions with the selected potential B7-H3 partners were validated by immunoprecipitation (IP) of endogenous B7-H3 from cells treated with MPA. Protein complexes were then probed by Western blot with antibodies against IMPDH2, actin, annexin, myosin A, myosin B and tubulin. B7-H3 was used as a control to confirm the validity of the IP (Figure 58B). Data revealed that actin, annexin and myosin A showed very high non-specific binding in IgG alone controls which could not be reduced upon increased detergent washing, making it difficult to conclude specificity of binding to B7-H3. Myosin B and tubulin were not identified in IPs indicating these targets are likely artefacts of the IP/mass spectrometry process. However, IMPDH2 was present in B7-H3 immunoprecipitates in all cells and not in IgG controls and appeared to potentially be increased in B7-H3 complexes in lysates from cells treated with MPA (Figure 58B).

GFP pull downs were carried out in GFP control or B7-H3-GFP expressing cells treated with MPA to further confirm this association by other means. Western blot analysis confirmed the presence of IMPDH2 in B7-H3 immunoprecipitates in both MPA-treated and untreated cells (Figure 58C). Quantification of Western blot bands from endogenous IP and B7-H3-GFP IP showed a significant increase in IMPDH2 binding to B7-H3 in 16HBE MPA-treated cells, with a trend to increased binding also seen in A549 and H358 cells (Figure 58D).

Data from previous chapters have shown B7-H3 localising at ARL13B-positive primary cilia and RR with formation of these structures being negatively regulated by B7-H3 expression. ARL13B and IMPDH2 has been previously reported to interact with each other to modulate purine synthesis (Shireman *et al*., 2019). To determine whether ARL13B, IMPDH2 and B7-H3 form a complex, 16HBE, A549 and H358 cells were treated with MPA, cell lysates were incubated with control IgG or IMPDH2 antibody followed by IP and Western blot probed for IMPDH2, B7-H3 and ARL13B (Figure 58E). Data revealed specific association between ARL13B and IMPDH2 and further confirmed the B7-H3:IMPDH2 complex seen in B7-H3 IPs.

Collectively these data demonstrate that B7-H3 can form a complex with both IMPDH2 and ARL13B in all cell lines, potentially explaining the co-localisation of these proteins, particularly in 16HBE cells shown in previous chapters. Blocking IMPDH2 activity increases association between B7-H3 and IMPDH2, further confirming increased B7-H3 and IMPDH2 co-localisation shown in chapter 3.

A

Protein ID	Function
IMPDH2	Plays an important role in the regulation of cell growth
Actin	Promotes cell spreading and cell contraction
Annexin A2	Cross-links plasma membrane phospholipids with actin and the cytoskeleton
Myosin-9 (A)	Promotes cell motility and cytoskeleton reorganization
Myosin-10 (B)	Promotes cell motility and cytoskeleton reorganization
Tubulin alpha-1C chain	Major constituent of microtubules

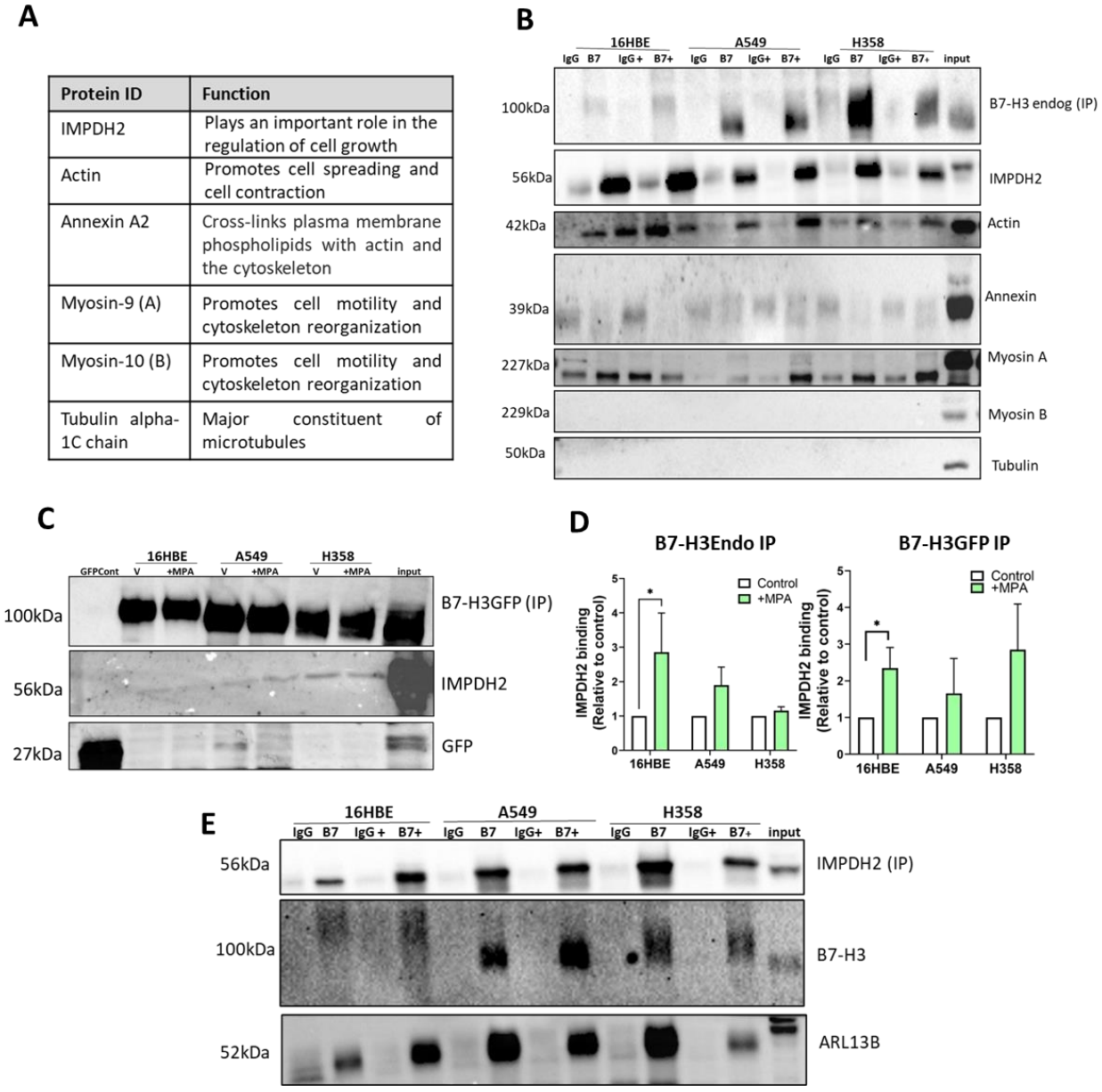

Figure 58: B7-H3 forms a complex with IMPDH2.

A) Table of protein IDs from LC-MS/MS analysis chosen for follow-up. **(B)** Western blot of endogenous B7-H3 immunoprecipitation from 16HBE, A549 and H358 cells treated with vehicle or MPA (+) for 48 hours, probed for IMPDH2, Actin, Annexin, Myosin A, Myosin B and Tubulin. **(C)** Cells expressing GFP or B7-H3-GFP treated with vehicle control (V) or MPA (+) for 48 hours, subjected to GFP-Trap immunoprecipitation followed by probing for IMPDH2, B7-H3 and GFP. **(D)** Quantitative analysis of IMPDH2 levels in B7-H3 Endogenous and B7-H3 GFP pulldowns as in (B) and (C). Data pooled from 5 independent experiments. Values are plotted as mean ± SEM. **(E)** Cells as in (B) were incubated with either IMPDH2 or IgG control antibody followed by blotting for B7-H3 and ARL13B. One-way ANOVA was used to determine statistical significance. *=p<0. 05.

5.2.8 B7-H3 sensitises cells to IMPDH2-dependent oxidative stress

Previous data showed oxidative stress was increased following depletion of B7-H3. Moreover, IMPDH2 was identified as a possible binding partner and this enzyme regulates several metabolites identified as being differentially regulated by B7-H3 expression. To further explore whether there is synergy between B7-H3 and IMPDH2 in controlling oxidative stress, 16HBE, A549 and H358 parental and B7-H3KD cells were subjected to vehicle control or MPA treatment for 48 hours followed by the addition of the CellRox reagent to measure oxidative stress as previously described.

As previously observed, all B7-H3KD cells displayed a significant increase in levels of oxidative stress compared to siControl/parental cells under control vehicle conditions (Figure 59A-C, left bars). MPA treatment also increased oxidative stress in both 16HBE and A549 siControl/parental cells compared to vehicle control-treated cells (Figure 59A, B). Moreover, B7-H3 knockdown in all cells led to an increase in oxidative stress levels following MPA treatment, compared to MPA-treated siControl/parental cells (Figures 59A-C, right bars). These data suggest that removing B7-H3, which would also disrupt the identified B7-H3/IMPDH2 complex results in increased oxidative stress levels, and that further inhibition of IMPDH2 activity enhances this phenotype. This suggests a role for B7-H3 in modulating oxidative stress in an IMPDH2-dependent manner.

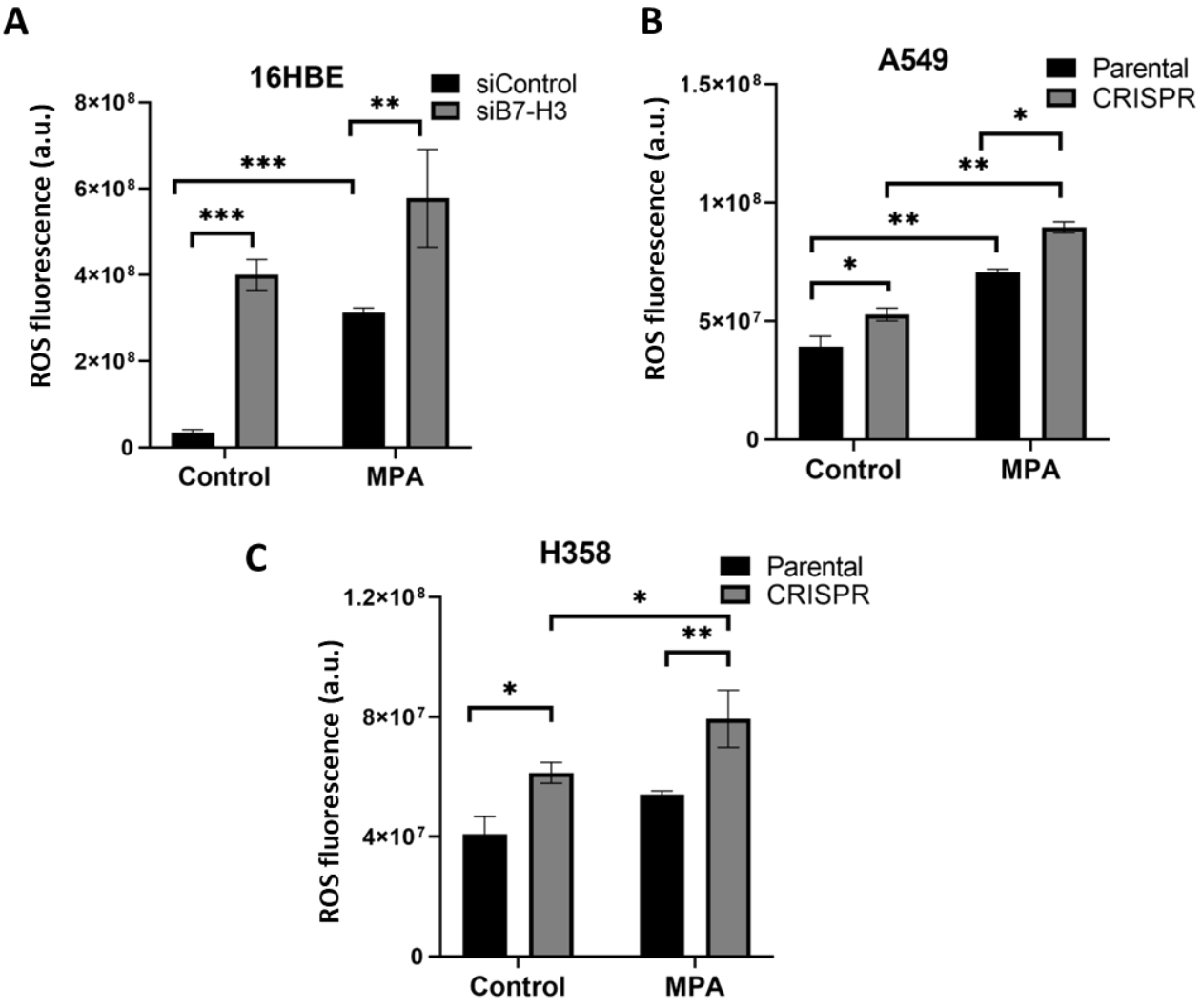

Figure 59: B7-H3 sensitises cells to IMPDH2-dependent oxidative stress
Quantification of oxidative stress levels of siRNA control/parental or B7-H3 siRNA/CRISPR in 16HBE **(A)**, A549 **(B)** and H358 **(C)** cells treated with MPA or vehicle control for 48 hours prior to incubation with CellROX reagent. Fluorescence signal was measured by imageJ. Data pooled from 3 independent experiments; each experiment performed in triplicate. Values are plotted as mean ± SEM. One-way ANOVA was used to determine statistical significance. *=p<0.05. **=p<0.01, ***=p<0.001.

5.2.9 B7-H3 sensitises cells to IMPDH2-dependent chemoresistance and cell survival

Previous data in this thesis has shown that depleting B7-H3 increases oxidative stress and apoptosis in tumour cells in response to chemotherapy. To determine whether IMPDH2 may play a role in these phenotypes, A549 and H358 parental and CRISPR cells were vehicle or MPA-treated for 48 hours prior to adding DAPI and CellEvent™ detection reagent, as described previously in this chapter.

Apoptosis was quantified by measuring the fluorescence levels emitted by the cells and normalising the values to parental controls. MPA treatment led to a significant increase in apoptosis in parental A549 cells (Figure 60A – left graph) and this was mirrored by a significant reduction in cell number (Figure 60A – right graph). Moreover, MPA treatment in both B7-H3 depleted cell lines led to a significant increase in apoptosis which was higher than that seen in untreated cells and parentals in the presence of MPA (Figures 60A, B – left graphs), this was also coupled with reduced cell number in both cases (Figures 60A, B – right graphs). These data suggest that B7-H3 promotes chemoresistance and thereby promotes cancer cell survival following MPA treatment.

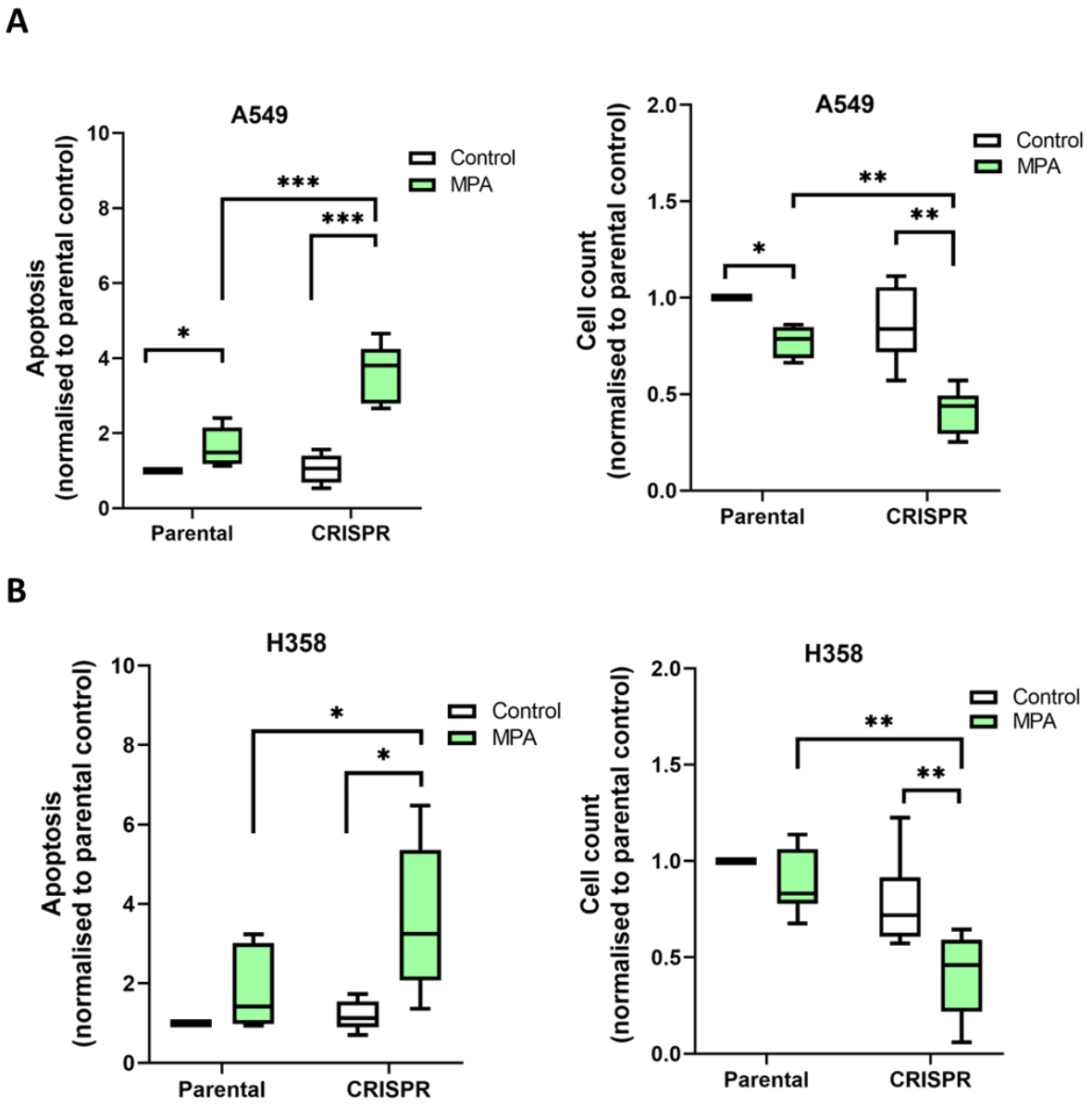

Figure 60: B7-H3 sensitises cells to IMPDH2-dependent chemoresistance and survival.
(A, B) Graphs of quantified apoptosis (left panel) and cell count (right panel) in Parental or B7-H3 CRISPR A549 **(A)** and H358 **(B)**. Cells were treated with methanol as vehicle control or MPA for 48 hours prior to staining the live cells with DAPI and CellEvent™ Caspase-3/7 Green detection reagent to measure apoptosis. Data pooled from 3 independent experiments; each experiment performed in triplicate. Values are plotted as mean +/- SEM. One-way ANOVA was used to determine statistical significance. *=p<0.05. **=p<0.01, ***=p<0.001

5.2.10 Inhibition of IMPDH2 leads to reduced 3D invasion and proliferation in B7-H3 depleted cells

Data in chapter 4 demonstrated that B7-H3 depletion leads to increased proliferation and invasion in 3D spheroid models. To determine whether IMPDH2 may play a role in these pro-tumourigenic phenotypes, A549 and H358 parental and B7-H3KD spheroids were formed via hanging drop method, and then embedded into 3D collagen gels. MPA was added to the media and left to incubate for 24 hours. Spheroids were imaged within one hour of embedding and at 24 hours post-embedding to enable quantification of invasion.

Confocal images of stained spheroids confirmed enhanced invasion in A549 and H358 CRISPR spheroids compared to parental spheroids as shown in Chapter 4 Figure 51. However, treating CRISPR spheroids with MPA appeared to reduce this enhanced invasive phenotype (Figure 61A). This was confirmed by measuring the invasion as fold change in spheroid area at 0 and 24- hours post-embedding which demonstrated significantly reduced invasion in MPA-treated B7-H3 CRISPR cells compared to control CRISPR cells (Figure 61B). No change in invasion was seen in parental cells treated with MPA compared to vehicle controls. To further explore the effect of MPA on proliferation and cell organisation, the number of nuclei and cell packing was quantified in all spheroids. Analysis of spheroid cell number also showed a significant increase in cell proliferation in both CRISPR lines compared to controls as previously shown in Figure 51, but notably a significant reduction in cell number was seen upon MPA treatment in B7-H3 CRISPR cells, but not in parentals (Figure 61C). Moreover, this reduced proliferation in B7-H3 CRISPR cells was coupled with a significant increase in cell packing following treatment with MPA compared to untreated cells (Figure 61D). Altogether, this data suggests that depletion of B7-H3 increases proliferation in an IMPDH2-dependent manner.

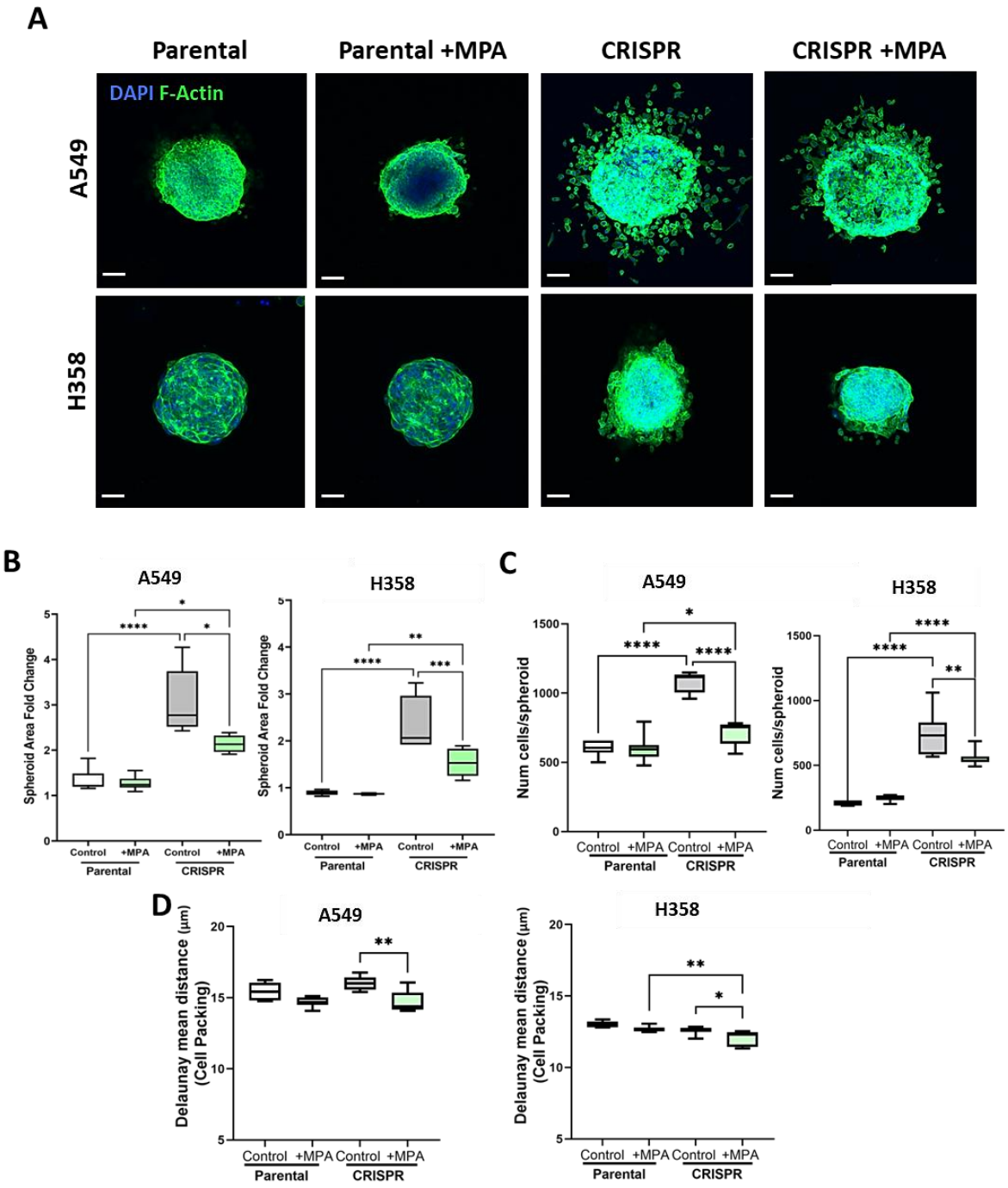

Figure 61: Inhibition of IMPDH2 leads to reduced 3D invasion and proliferation in B7-H3 knockdown cells.

(A) Representative confocal images of parental and B7-H3 CRISPR A549 and H358 spheroids embedded in collagen, either vehicle or MPA-treated, fixed and stained for DAPI (blue) and F-actin (green) at 24 hours post embedding **(B)** Quantification of spheroid area over 24 hours post-embedding. **(C)** Quantification of the number of cells per spheroid and **(D)** cell packing using QuPath software. Data shown is pooled from three independent experiments with a total of 6 spheroids were analysed per experiment**.** One-way ANOVA was used to determine statistical significance. *=p<0.05. **=p<0.01, ***=p<0.001 p<0.001. Scale bars 50 µm.

5.3 Discussion

5.3.1 B7-H3KD promotes anti-tumour phenotypes in 2D

Previous data in chapter 4 suggested that B7-H3 depletion led to reduced tumourigenic phenotypes such as actin reorganisation, reduced colony size, increased RRs and primary cilia formation. These results were further complimented by increased oxidative stress, decreased cellular GTP levels and cancer associated metabolites such as fumaric acid and glucose which both have been reported to be oncometabolites with increased expression in cancer cells (Khatami *et al*., 2019; Xiang *et al*., 2020). These findings indicate that knocking down B7-H3 would lead to reduced IMPDH2 activity due to enhanced RR formation and decreased purine biosynthesis pathway as evidenced by reduced GTP levels. Moreover, MPA treatment that is known to block IMPDH2 activity also resulted in same oxidative stress and GTP levels seen in B7-H3KD. These datasets (all generated in 2D culture conditions) suggest that B7-H3 can support tumourigenesis through suppressing oxidative stress response and promoting *de novo* purine synthesis pathway.

Purines provide essential components for DNA and RNA synthesis as well as cofactors and energy to promote proliferation and cell survival. Therefore, purines widely contribute to various biological processes as well as immune response (Virgilio & Adinolfi, 2017). As B7-H3 co-localises and forms a complex with IMPDH2, we hypothesised that B7-H3KD phenotypes may be IMPDH2-dependent. Reports have shown that IMPDH2 polymerises in cells in response to alterations in metabolic demand (Johnson & Kollman, 2020). These polymers contain active and inactive forms of IMPDH2 depending on the binding partners that can dictate its activity. For instance, ATP promotes IMPDH2 octamer polymerization, whereas GTP promotes compact inactive conformation. IMPDH2 polymerisation may allow co-operative transitions between conformationally active and inactive states that are finely tuned by purine balance and availability of substrates (Anthony *et al*., 2017)**.** This may explain the difference in activity of IMPDH2 in cancer cells. In parental A549 and H358 cells, IMPDH2 is not assembled into RR but instead partially co-localises with B7-H3 at cell-cell junctions (data not shown). However, when B7-H3 is depleted, IMPDH2 becomes more cytoplasmic but does not form RRs unless MPA is added (data not shown). We therefore postulate that B7-H3 forms a complex with IMPDH2 in cancer cell lines at the cell periphery and sequesters the enzyme

there as a polymer, but upon B7-H3 reduction IMPDH2 becomes more cytoplasmic. Therefore, the IMPDH2 activity balance may be dependent in part on coupling with B7-H3 through altered subcellular localisation in cancer cells compared to normal lung epithelial cells. This notion is supported by a study in melanoma cells which demonstrated that the enhancer of zeste homolog 2 (EZH2) oncoprotein promoted tumourigenesis and metastasis in cells by associating with IMPDH2 at the plasma membrane to promote GTP generation and subsequently upregulated metabolism that supports cancer progression (Kuser Abali *et al*., 2021).

The activity of Rho GTPases and subsequent regulation of the actomyosin cytoskeleton which promotes cell migration, is modulated by intracellular GTP, which is critical for purine synthesis (Bianchi-Smiraglia *et al*., 2021). Recent studies have reported IMPDH2 to be localised at the membrane where it can support cytoskeletal assembly in an actin-dependent manner (Wolfe *et al*., 2019, 2020). Therefore, B7-H3 coupling with IMPDH2 at the membrane in cancer cells may support a local pool of GTP synthesis to permit cytoskeletal remodelling and adaptation to extracellular cues. As a result, B7-H3 is acting in an IMPDH2-dependent manner to promote tumourigenesis in cancer cells and modulate activity of this enzyme depending on its localisation, which differs to that seen in normal cells. Further experiments should be carried out to confirm IMPDH2 polymerisation in B7-H3KD cells and how would this affect its activity as total intracellular GTP levels determined via mass spectroscopy do not inform on the localisation of GTP levels inside the cell, nor reflect subcellular variation in local GTP levels, which would have major effects on local G-protein activation (Bianchi-Smiraglia *et al*., 2021).

5.3.2 Pro-tumourigenic effects of B7-H3 depletion in 3D spheroids

The anti-tumourigenic phenotypes exhibited by B7-H3KD cells in 2D were not recapitulated in 3D model systems. B7-H3 CRISPR cell spheroids showed increased proliferation and invasion, which in turn was reduced by the addition of MPA indicating an opposite effect of B7-H3KD on metabolite levels and the purine biosynthesis pathway compared to 2D. Further research on metabolite levels of B7-H3KD in 3D spheroid models would be valuable in

confirming whether this differential regulation exists depending on the environment the cells are in.

In the previous chapter we postulated that cells at the periphery of the tumour which are more invasive may exhibit increased B7-H3 expression and that this may support cytoskeletal remodelling and migration by increasing activity of IMPDH2. However, data from this chapter indicates that knocking down B7-H3 in 3D could instead act to increase IMPDH2 activity as the enhanced invasion and proliferation in these cells was blocked by treatment with MPA. In 2D, B7-H3KD did not induce RRs formation in cancer cells, but IMPDH2 instead re-localised to the cytoplasm which may indicate increased activity. It would be important to analyse IMPDH2 localisation in 3D models and assess RR formation in MPA-treated spheroids to determine whether a 3D environment could lead to alterations in IMPDH2 localisation and function in B7-H3-dependent manner.

Data in this chapter has shown that metabolites were altered in 2D upon B7-H3KD but how this might also translate to more physiological 3D settings remains unclear. Interestingly, previous reports have shown that cells grown in 2D compared to 3D environments can indeed display differences in metabolic activity. One study identified a unique form of metabolism that was employed to facilitate cell survival under 2D conditions that was not seen *in vivo*. Furthermore, cells in 3D exhibited higher levels of amino acid biosynthesis compared to those in 2D (Murakami *et al*., 2021). Elevated levels of glutamic acid and glutamine were detected in 3D compared to those in 2D, and mitochondrial function in 3D cancer cells was not impaired which produced energy simultaneous with aerobic glycolysis (Wolfe *et al*., 2020). Furthermore, metabolic profiling of cells in 3D have shown significant changes to those in 2D due to a decreased sensitivity to ATP synthase (Ferrick *et al*., 2008). This difference was suggested to support altered responses to various chemotherapeutics in 2D and 3D, as anticancer drug sensitivity tests showed cytotoxicity can be drastically different in 3D spheroids compared to 2D monolayer cultures (Tung *et al*., 2011). This could explain how the 2D monolayer affected B7-H3KD cell response to stress caused by ROS or cisplatin and on GTP levels, as cells on 2D would be more receptive than compacted 3D spheroid. Furthermore,

some chemotherapeutic drugs are active in 3D cultures as they are triggered by hypoxia, where diffusive oxygen transport is limited and oxygen consumption by cells is activated thus, creating a hypoxic core similar to solid tumours (Kucinska *et al*., 2021).

Cells adapt rapidly to variations in nutrient availability, cellular differentiation status as well as growth conditions in cell culture environment leading to changes in metabolite production (Riedl *et al*., 2016). In a 3D setting, nutrient availability would be expected to vary across the spheroid, with outer cells receiving high nutrients from the medium, while cells at the core are more nutrient deprived. A recent study has shown that cells in 2D have high levels of glycolysis intermediates, lipids and amino acids, and these were significantly reduced in cells in spheroids and freshly isolated primary tissues (Lagies *et al*., 2020). Additionally, 3D spheroids started to differentiate and produce metabolites similar to their tissue of origin and retained many metabolic similarities to the original tissue, whereas cells in 2D show artificially upregulated growth signatures compared to a 3D setting (Lagies *et al*., 2020). This discrepancy in metabolic profiles could explain the differences seen in terms of colony size and growth in B7-H3KD cells in 2D vs. 3D in this thesis. Furthermore, a study on breast cancer cells showed that growing cells in 3D led to elevated ROS levels and higher resistance to cisplatin compared to those grown in 2D environments (Liu *et al*., 2018). This may explain the high levels of oxidative stress upon B7-H3KD in 2D which was accompanied by increased sensitivity to chemotherapy treatment and apoptosis compared to 3D with increased proliferation and invasion. It would be interesting to investigate metabolic profiles and IMPDH2 localisation upon cisplatin treatment in B7-H3KD in 3D culture models in the future to help in further understanding how B7-H3 affects 3D tumourigenesis phenotypes.

5.3.3 B7-H3 between 2D and 3D systems

A further explanation for the discrepancies seen in 2D vs. 3D settings in this thesis could be down to the different ECM topography and organisation in 3D that can alter signalling and metabolic programming (Nazemi & Rainero, 2020). We have shown in this thesis that B7-H3 forms a complex with IMPDH2, and both proteins have been reported to show increased expression in different types of tumours (Amori *et al*., 2021; He *et al*., 2018). IMPDH2 elevated

expression has been reported to be pro-tumourigenic and induces proliferation and invasion in colorectal cancer in both *in vivo* and *in vitro* models (Duan *et al*., 2018). Additionally, inhibition of IMPDH2 activity induces growth arrest in human multiple myeloma cells (Ishitsuka *et al*., 2005). Furthermore, overexpression of IMPDH2 induces invasion, migration and EMT in an mTOR-dependent manner (Duan *et al*., 2018). Moreover, MPA inhibits cell proliferation through the mTOR pathway and induces caspase-dependant apoptosis (Dun *et al*., 2013). It would be interesting to test whether mTOR signalling is also altered in B7-H3KD cells in 2D vs. 3D and analyse the effect of blocking mTOR on invasion in the presence and absence of MPA to determine whether this pathway may contribute to the observed B7-H3 dependent phenotypes. Targeting B7-H3 with blocking antibodies is currently in clinical trials for different types of cancers (Zhou & Jin, 2021). MPA also induces S-phase arrest and apoptosis in osteosarcoma cell lines (Klangjorhor *et al*., 2020). Additionally, MPA inhibits cancer cell proliferation and induces apoptosis *in vitro* and *in vivo* in prostate cancer cells, multiple myeloma cells, lymphoma, pancreatic, colon and lung cancer (Floryk & Huberman, 2006; Takebe *et al*., 2006; Tressler *et al*., 1994; Végső *et al*., 2007). Therefore, MPA may serve as an antimetastatic drug as seen to reduce cell proliferation in B7-H3KD spheroids.

B7-H3 overexpression in various types of cancers have driven interest in this molecule for targeted therapy (Mao *et al*., 2017). Indeed, reports have shown B7-H3KD inhibits tumour proliferation *in vitro and in vivo*. Data in this thesis showed that B7-H3KD promotes increased cell proliferation and invasion in 3D. However, it is worth noting that these previous studies used different models with immune components included, which are not present in the 2D and 3D spheroids models used in this thesis. The experiments in this thesis aimed to analyse roles for B7-H3 in cancer cells in the absence of any influence from B7-H3-immune cell associations. We postulate that data shown here supports a role for B7-H3 in control of IMPDH2 activity and that cells in solid tumours can use B7-H3 to modulate activity of this enzyme in response to different extracellular settings or chemotoxic stress. It would be interesting in future studies to assess the contribution of this B7-H3 driven IMPDH2 activity in the presence of immune cells in a 3D setting to determine potential contributions of B7-H3 to so-called immune ‘hot’ vs. immune ‘cold’ tumours. Such experiments might inform on whether B7-H3 is only a promising target in certain tumour immune environments.

In summary, data presented in this chapter has revealed that B7-H3 forms a complex with IMPDH2 and can promote tumour growth and invasion in a 3D spheroid model, and that this may be regulated by IMPDH2-dependent activation that triggers metabolic programming to promote tumourigenesis.

6. Discussion and future Directions

6.1 General Discussion

The goal of this thesis was to investigate the role of B7-H3 in normal lung epithelial cells and lung cancer cells, to determine whether increased expression of B7-H3 in lung cancer was coupled with changes to function of this protein in different contexts. A summary of all the key findings from this thesis is presented in Figure 62. Data presented here demonstrates lower expression of B7-H3 in normal lung epithelial cells compared to cancer cells, which agrees with previous findings (Flem-Karlsen *et al*., 2018). B7-H3 was localised at the cell-cell junctions in all cell types studied but was higher at the plasma membrane in cancer cells compared to normal epithelia (Figure 62A). Moreover, B7-H3 in normal epithelia was found to co-localise with ARL13B at the primary cilia and formed a complex with IMPDH2 at the RR (Figure 62A left cell). In normal epithelia, data suggests that B7-H3 protects cells against oxidative stress to promote viability and lung epithelial homeostasis potentially through maintenance of tight junctions and optimal IMPDH2 activity, thereby maintaining GTPase activity and primary cilia assembly for optimal sensing of environmental cues (Figure 62B top left).

In cancer cells, B7-H3 expression was increased. We propose that this would drive constitutive IMPDH2 activity and GTPase activation to promote growth and invasion, suppresses cilia and thereby reduce sensing from external cues in addition to enhancing protection against oxidative stress and apoptosis (Figure 62B bottom left). IMPDH2 did not localise to RR in cancer cells indicating an active role of the enzyme to drive cell proliferation, actin reorganisation and invasion. B7-H3KD led to similar phenotypes in normal and cancer cells (Figure 62B, C). A key difference was in RR formation, which was only increased in normal lung epithelial cells following B7-H3 knockdown, indicating an increase in the inactive form of the enzyme. B7-H3KD in 2D altered cancer associated phenotypes, indicated in green and red arrows for induced and reduced phenotypes respectively (Figure 62C). However, B7-H3KD in 3D appeared to lead to opposite phenotypes with increased proliferation, invasion and IMPDH2 activity. This was evidenced by the reduction in these phenotypes following MPA treatment in both cancer cell lines used in this study compared to controls (Figure 62D, E).

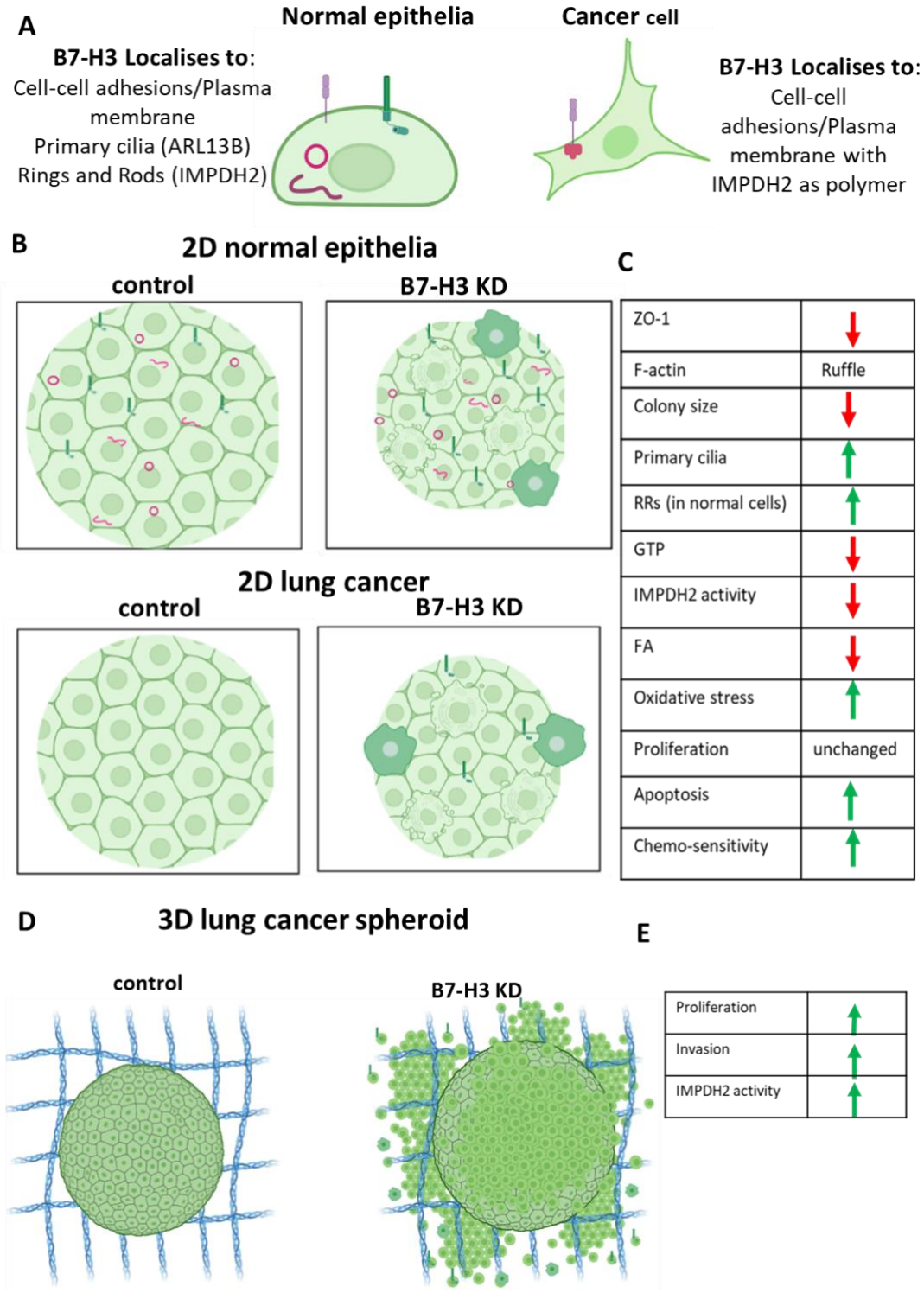

Figure 62: Summary of findings and proposed model.
A) illustration of B7-H3 different localisation between normal vs cancer cell. **(B)** Model of 2D epithelial cells in normal (top) and cancer (bottom), control (left) and B7-H3KD (right) cells. **(C)** Table of key changes in 2D culture upon B7-H3KD. **(D)** 3D spheroid model in control (right) and B7-H3KD cells (left). **(E)** Table of key changes upon B7-H3KD in 3D models. Arrows indicate increased (green) or reduced (red) in B7-H3KD cells. Figure created with Biorender.com.

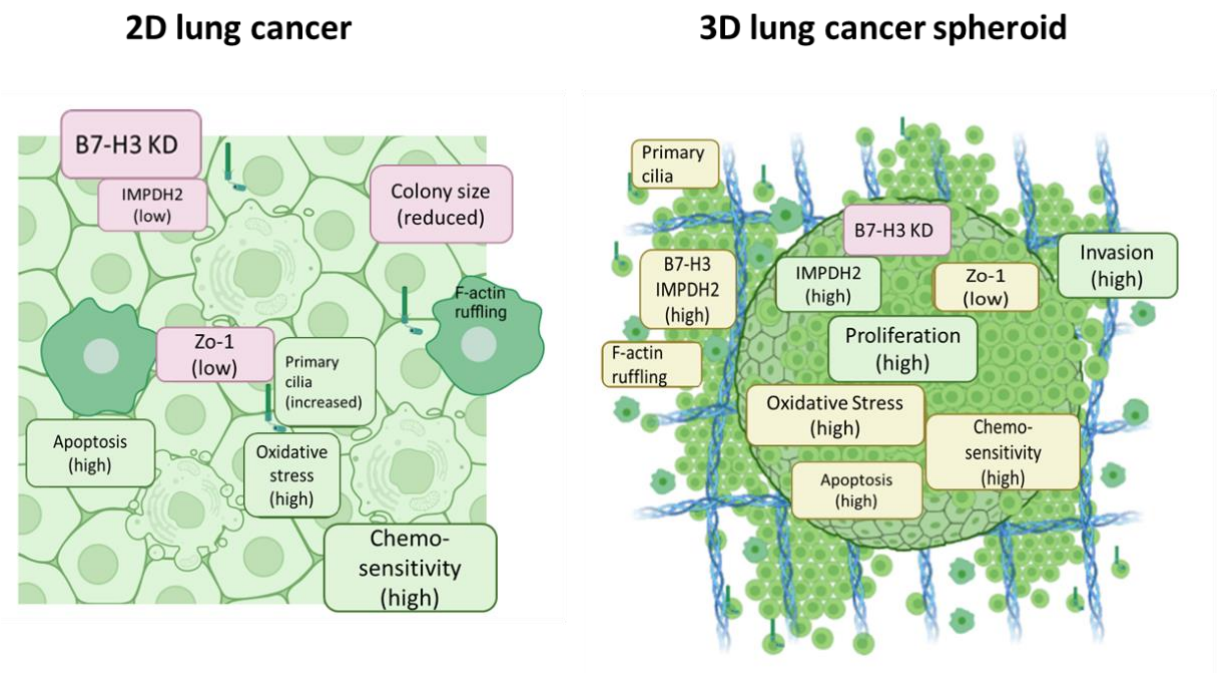

Figure 63: Model of B7-H3 effects in cancer cells in 2D vs. 3D culture.
Model of 2D (left) and 3D (right) B7-H3KD cancer cells showing phenotypical changes, green box (increased) and red box (reduced). Yellow in 3D indicates not measured in 3D in this study. Figure created with Biorender.com.

Various factors could be contributing to the observed differences in B7-H3 function in cancer cells in 3D vs. 2D culture (Figure 63). Cells in 3D can exhibit altered signalling and metabolic reprogramming due to different topography and organisation of the ECM, as well as the fact that most cells in 3D spheroids are in contact with each other but not the ECM. B7-H3KD in 3D resulted in phenotypes that differ to some of the *in vivo* published literature which showed pro-tumourigenic roles for B7-H3 (Castellanos *et al*., 2017; Tekle *et al*., 2012). However, previous work very often uses immunocompetent mice and thereby B7-H3KD would be expected to be influencing T cells and altering the immune response. Alternatively, in xenograft or immunodeficient mouse models using human cancer cells, the presence of a vascular system and mechanical shear/forces may also contribute to different outcomes. In our 3D model, cells were in contact with each other with no T-cell infiltrations, more reflective of the environment seen in 'immune cold' tumours. We propose that B7-H3KD in these types of tumours might drive pro-tumourgenic activity through downstream IMPDH2 activation.

6.1.1 Autonomous roles for B7-H3 in control of tumour cell behaviour and as a therapeutic target

One of the main aims of this thesis was to evaluate B7-H3 function in the absence of, or influence from immune cells. As B7-H3 is overexpressed in NSCLC and other tumour types compared to normal cells, this makes it a promising target for cancer therapy (Altan *et al*., 2017). Efficacy of response to monoclonal antibodies targeting immune checkpoints remains relatively low, one major factor in resistance to these inhibitors is the lack of tumour infiltrating lymphocytes (TILs), rendering tumours 'immune cold' (Bonaventura *et al*., 2019). Checkpoint inhibitors may contribute to treating diverse types of tumours by unleashing the brakes on the immune system. However, in 'immune cold' tumours, checkpoint inhibitors are usually unsuccessful, resulting in poor response and survival rates. Conversely, 'immune hot' tumours containing TILs offer a potentially more favourable environment to target immune checkpoints brought about by either the tumour or by the tumour immunosuppressive microenvironment (Draganov *et al*., 2021). Thus, the nature of the tumour microenvironment can correlate with the effectiveness of chemotherapy and immunotherapy (Binnewies *et al*., 2018). Immunotherapy treatment of some solid lung cancers has been a challenge up until recently due to multiple factors including the lack of responding T cells within the tumour (Steven *et al*., 2016). Studies of B7-H3 in immune cold vs. hot tumours are relatively limited to date, with one recent study showing B7-H3 expression was significantly associated with overall survival in the immune hot group and the prognostic power of the protein may be lost in immune cold oral tongue tumours (Sieviläinen *et al*., 2021). However, most studies indicate that elevated expression of B7-H3 in SCLC and NSCLC is associated with poor survival and could mediate immune evasion contributing to the resistance of anti-cancer drugs via various mechanisms (Carvajal-Hausdorf *et al*., 2019; Yang *et al*., 2020).

Studies on other B7 family members have shown different correlations between the molecules and TILs. PD-L1 and B7-H4 were positively and negatively correlated with TILs, respectively. High expression of both was seen in immune-cold tumours, which might not be appropriate for immunotherapy. Moreover, B7-H3 expression correlated with poorly differentiated grades in pancreatic cancer but did not correlate with TILs (Yang *et al*., 2022). However, another study on the same three B7 family receptors showed limited co-expression

in SCLC with B7-H3 being the highest (Carvajal-Hausdorf *et al*., 2019). Moreover, PD-L1, B7-H3 and B7-H4 expression were not associated with TILs levels in this study, and high levels of CD3+ TIL was associated with survival in SCLC (Carvajal-Hausdorf *et al*., 2019). Furthermore, in pancreatic cancer high expression of B7-H3 was significantly associated with higher tumour stage and negatively correlated with CD8+ TILs (Zhou *et al*., 2021). Similar results were presented in studies on SCLC and NSCLC, where high expression of B7-H3 negatively correlates with the number of TILs and the density of the latter was critical for responsiveness to immunotherapy and patient survival (Jin *et al*., 2015; Y. Sun *et al*., 2006; Qiu *et al*., 2021). As a result, B7-H3 expression does not clearly correlate with TILs. This adds to the complexity of targeting B7-H3 using immune checkpoint inhibitors, as response to immune-related therapy would be difficult to predict. Understanding B7-H3 function in cold tumours would help in better therapeutic assessment and clinical diagnosis.

Despite promising anti-tumour phenotypes seen upon B7-H3 depletion in our 2D model of study, as well as previous published reports on different types of cancers in 2D and 3D models (Zhang *et al*., 2015; Zhao, LI, *et al*., 2013), knocking down B7-H3 in 3D models here in the absence of immune cells promoted pro-metastatic phenotypes possibly through increased IMPDH2 activity. Our data shows that MPA treatment alone had no significant effect on 3D growth or invasion in parental cells, indicating a role for IMPDH2 in tumourigenesis only in the context of drug resistance or increased oxidative stress. Chemoresistance to 5-FU in colorectal cancer has been shown to be induced by B7-H3 through enhanced PI3K/AKT signalling (Jiang *et al*., 2016) but the role of IMPDH2 in this system was not explored. B7-H3 expression has also been correlated with paclitaxel resistance in breast cancer, and B7-H3 knockdown increased drug sensitivity (Zhao et al., 2013). It would be interesting to explore the mechanisms by which B7-H3 contributes to drug resistance and whether IMPDH2 plays a role in these pro-tumourigenic phenotypes. Moreover, as B7-H3 depletion did not mimic the effects seen with the B7-H3 blocking mAb in terms of F-actin reorganisation, knocking down the protein might elicit downstream signals that are different than blocking the extracellular domain alone. This might indicate that intracellular B7-H3 (not accessible to the blocking antibody) can signal to control IMPDH2 activity and downstream actin organisation. Analysing

IMPDH2 activity in cells treated with mAb compared to B7-H3 depleted cells would help to determine if this is the case.

As a protein that is thought to be specifically upregulated in tumours, B7-H3 has been the focus of targeted therapies for antibody-drug conjugates (ADCs). ADCs use antibodies for 'tumour specific' surface markers to guide binding of target antibodies linked to 'payload' chemo-toxins to solid tumours, reducing off-target toxicity. Studies in mice have shown that treatment with B7-H3 ADCs lead to increased overall survival and reduced metastases, suggesting that this might be an exciting reagent for anti-cancer therapy (Yang *et al*., 2020). DS-7300, an ADC that targets B7-H3, is well tolerated with signs of clinical activity and an acceptable safety profile (Patel *et al*., 2022). Even though the ADC activity on tumour burden is not clear, DS-7300a is currently in phase 2 clinical trial for late-stage SCLC (clinical trial NCT05280470). Targeting B7-H3 using ADCs to a pyrrolobenzodiazepine cytotoxic agent, m276-PBD, reduced paediatric solid tumours in both patient-derived-xenograft mouse and cell line derived xenograft models (Kendsersky *et al*., 2021). Similar conclusions were also reported in metastatic prostate cancer mouse models with elevated B7-H3 expression (Agarwal *et al*., 2022). Similarly, another B7-H3 ADC, Enoblituzumab (MGA271) activates killer T cells, and elicits strong antibody-dependant cellular cytotoxicity against many xenograft cancers and is now in clinical trials in refractory tumours (Loo *et al*., 2012). Enoblituzumab has completed phase 1 trial examining safety and anti-neoplastic efficacy in B7-H3-expressing solid tumours (Desantes *et al*., 2017). ADCs target tumour cells by being rapidly internalised to release the antibody-linked toxins inducing cell death (Criscitiello *et al*., 2021). However, the internalisation mechanism and the intracellular trafficking of B7-H3 remains elusive. Therefore, the action of these ADCs on apoptosis and whether they would be cleaved from the surface remains a concern for treating patients. Recently, a clinical trial was discontinued after a combination of Enoblituzumab and Retifanlimab, anti-B7-H3 ADC and anti-PD-L1 mAb, respectively, caused death to 7 patients (clinical trial CP-MGA271-06). Therefore, further investigation of B7-H3 internalisation and function could help in developing better targeted drugs.

Data presented in this thesis suggests that in the absence of immune cells, B7-H3 could maintain cell growth by regulating IMPDH2 activity and subsequently the *de novo* purine pathway resulting in increased GTP levels. This would be expected to activate GTPases, increasing both proliferation and invasion at the periphery of the tumour and protecting cells against oxidative stress in 3D. Knocking down B7-H3 further activates IMPDH2 indicated by increased IMPDH2 in the cytoplasm, increased proliferation, and invasion in 3D spheroids. It would be interesting to identify the exact sites within the B7-H3 cytoplasmic domain that can induce IMPDH2-dependent intracellular signalling, which would lead to increased tumour cell proliferation. Moreover, PD-L1 has been reported to mediate cell intrinsic functions in cold tumours through mTOR activation (Han *et al*., 2020). IMPDH2 has been shown to promote cell proliferation and migration through activating mTOR pathway, and this pathway has also been speculated to be one of B7-H3's downstream effectors (Guo, *et al*., 2017; Li *et al*., 2019; Nunes-Xavier *et al*., 2016). It would be valuable to further investigate the involvement of this pathway in B7-H3 signalling in tumours independently of immunomodulation.

6.1.2 Non-autonomous roles for B7-H3 in broader TME

B7-H3 is a promising target for immunotherapy but mixed results in clinics have led to renewed efforts focused on understanding the rationale behind tumour response to B7-H3 immunotherapy. B7-H3 can directly regulate immunity and tumourigenic behaviour in cancer cells and has been reported to play conflicting roles on the immune system.

B7-H3 was initially identified as a co-stimulatory molecule that increases the proliferation of CD4+ and CD8+ T-cells and cytotoxic activity of T-cells (Chapoval *et al*., 2001). However, several recent studies have shown co-inhibitory roles of B7-H3 on the anti-tumour immune response as it facilitates immune evasion. The tumour microenvironment is constantly supporting the progression of cancer cells through the interaction of its diverse components. B7-H3 expression on APCs, tumour cells, and tumour-infiltrating lymphocytes highly supports its regulatory immune role in the TME (Lee *et al*., 2017). Studies have demonstrated that B7-H3 in tumour cells reduces the proliferation of CD4+ and CD8+ T cells and decreases the production of cytokines, possibly through activator protein-1-mediated signalling and the

nuclear factor of activated T cells (NF-$_k$B) pathways (Li *et al*., 2018). Moreover, B7-H3 can inhibit T cell proliferation and IFN-γ, IL-13, IL-10, and IL-2 production during T cell activation (Prasad *et al*., 2004; Suh *et al*., 2003). In addition, B7-H3 inhibits NK cell activity (Steinberger *et al*., 2004). Therefore, targeting B7-H3 using monoclonal antibodies to block and neutralize the B7-H3 checkpoint has been reported to be a promising approach to targeting different types of tumours. B7-H3 MJ18 mAb is reported to inhibit the growth of pancreatic cancer in mouse models and increased CD8+ T cells (Huang *et al*., 2016). In murine models, B7-H3 mAbs activated cytotoxic T cells and NK cells within tumours, reducing tumour burden and improving survival (Kanchan *et al*., 2022). 8H9 is a mouse IgG1 mAb targeting B7-H3, shown to be highly active against primary tumours. As a result, a humanised 8H9 form is now being investigated in phase 1 clinical trials (Liu *et al*., 2021; Modak *et al*., 2001). However, even though the effects of these B7-H3 mAbs have been focused on blocking the immune checkpoint, the autonomous effects on tumours remain possible as it is difficult to unpick their specific effectors *in vivo* where immune cells are present. Moreover, the role of B7-H3 mAbs in targeting late-stage metastatic disease or recurrent cancers has yet to be explored (Kanchan *et al*., 2022). Given this data, together with published anti-tumour effects of mAb, it would be valuable to study the effect of B7-H3 mAb in 3D with and without infiltrating immune cells to determine how this might influence the phenotypes we have observed in our studies, as well as the tumour-immune interactions.

Our data indicates that *de novo* purine biosynthesis and metabolic reprogramming can both be regulated by B7-H3, as blocking IMPDH2 reduced the pro-tumourigenic phenotypes seen in 3D in B7-H3KD cells. This indicates that activating IMPDH2 (upon B7-H3 depletion) increases proliferation and blocking this metabolic pathway slows tumour growth, in agreement with other studies (Huang *et al*., 2018). Moreover, the activity of metabolic pathways can influence the DNA damage response (DDR) by regulating the substrate availability required for the repair process. Increased oxidative stress during cellular metabolism can increase DNA damage and influence the activity of DDR (Cucchi *et al*., 2021). If we assume that the data showing increased oxidative stress in B7-H3KD cells in 2D holds true in a 3D environment, then increased oxidative stress might cause DNA damage and genomic instability, thereby promoting tumour mutation burden and pro-tumourigenic

phenotypes (Alhmoud *et al*., 2020; Cucchi *et al*., 2021). *In vivo* studies have reported that ROS are involved in the induction of tumour-promoting immune cells such as regulatory T cells (Tregs) as well as suppression of other immunocytes. Elevated numbers of Tregs are often present in TME, therefore, contributing to resistance to oxidative stress (Aboelella *et al*., 2021). It would be interesting to investigate roles for B7-H3 in the DNA damage response pathway and the different levels of oxidative stress in 2D vs. 3D models to understand this further, as oxidative stress can promote both tumour-suppressive and tumour-promotive activities depending on ROS levels (Azmanova & Pitto-Barry, 2022).

In conclusion, based on the data presented in this thesis as well as previous publications, B7-H3 remains an interesting therapeutic target; however, the impact of blocking B7-H3 function on metabolism and oxidative stress in lung cancer should be further investigated in both immune competent and incompetent environments to determine whether only specific clinical settings might be appropriate for B7-H3 therapy.

6.2 Future Directions

This thesis provides novel insight into roles for B7-H3 in tumour cell proliferation, invasion, actin reorganisation and altered metabolism. However, many of the mechanisms controlling these phenotypes remain poorly understood. We postulate, based on our data, that B7-H3 association with IMPDH2 regulates purine metabolism and tumour growth. Data shown here demonstrated that B7-H3 forms a complex with IMPDH2 and ARL13B, and their activity as well as the localisation is altered when B7-H3 is overexpressed in normal lung epithelial or cancer cells. IMPDH2 activity seems to be downstream of B7-H3, but the pathways and B7-H3 ligand(s) mediating this remains unknown.

6.2.1 B7-H3 in normal lung epithelial cells and association with primary cilia/RR

We have shown that B7-H3 localises to RR in normal cells, but not in cancer cells where these structures are largely absent. The correlation between higher B7-H3 expression, more B7-H3 at the plasma membrane and reduced RR indicates a role for B7-H3 in increasing IMPDH2 activity.

Given the above, it would be interesting to define the domain controlling B7-H3 functions and phenotypes. This could be achieved by generating mutants of B7-H3 lacking intracellular components. To allow visualisation, B7-H3-GFP with truncated or without cytoplasmic tail could be expressed at low levels in 16HBE cells, followed by analysis of B7-H3 localisation via confocal imaging to explore whether loss of cytoplasmic tail affects its intercellular activity/location at the primary cilia or RRs compared to parental and B7-H3-overexpressed cell lines. Additionally, treating this cell line with MPA and analysing co-localisation of B7-H3 and IMPDH2 could help to determine if the cytoplasmic tail is required for B7-H3 to assemble into RR. This could be further tested for A549 or H358 B7-H3KD cells by transfecting B7-H3 CRISPR lines with B7-H3 GFP lacking the cytoplasmic tail to “rescue” cells then score primary cilia formation, by staining for ARL13B and other primary cilia markers and compare the results with B7-H3KD cells. Moreover, effects on actin reorganisation in these cells could be observed by co-infecting cells with lifeact-RFP, as a reporter for F-actin dynamics, and

analysing actin reorganisation upon B7-H3 mAb or ectodomain treatments, as both B7-H3 reagents target the extracellular domain.

Data in this thesis indicated a role for IMPDH2 in regulating primary cilia numbers in cells, whereas reducing cilia by KIF3A siRNA did not affect RR formation. However, complete knockdown for both was not achieved in this study. Therefore, repeating primary cilia depletion, by either KIF3A or ARL13B siRNA/CRISPR, and further optimisation of IMPDH2KD, followed by analysis of B7-H3, primary cilia and RR via Western blotting to detect expression levels, and IF for localisation would help to further confirm the results from this thesis and whether further reduction of both proteins influence B7-H3 stability. Additionally, knockdown of IMPDH2 or B7-H3 showed increased primary cilia numbers, confirming the interplay between IMPDH2 and ARL13B in this thesis and in a previous published study (Shireman *et al*., 2019). It would be interesting to score primary cilia formation in 16HBE cells upon overexpressing IMPDH2 tagged with GFP and measure B7-H3 localisation with ARL13B. Published work have shown overexpressing IMPDH2 induced RR disassembly, and cells failed to form these structures despite the addition of inducers (Carcamo *et al*., 2011; Keppeke *et al*., 2015). This is similar to observations seen in 16HBE-overexpressing B7-H3 GFP as well as A549 and H358 cells, indicating that high expression of both proteins could lead to decreased RR formation. This could be confirmed by overexpressing IMPDH2 in 16HBE cells and stain for RRs and B7-H3 to observe any changes in localisation of either proteins and whether B7-H3 would be sequestered at the junction with IMPDH2. FRET experiments using B7-H3 and IMPDH2 fluorescently-tagged proteins could be used to further determine whether B7-H3 and IMPDH2 interact directly on the membrane at cell junctions or elsewhere in cancer cells.

The order of B7-H3 recruitment to RRs remains unclear. ARL2 GTPases, similar to B7-H3, localise at the RR, centrosome and are required for primary cilia formation. Calnexin is an endoplasmic reticulum protein localised at RR, yet it is not clear what functional role it may play in those structures. This protein is the last one recruited to RR after ARL2 and IMPDH2 (Schiavon *et al*., 2018; Zhou *et al*., 2006). This order of recruitment could be explored for B7-H3 by treating 16HBE cells with MPA and fixing coverslips every 5 minutes for an hour,

followed by staining cells for IMPDH2, ARL2, calnexin and B7-H3 to observe when each protein was shown and recruited to RR. Also, this experiment could help to understand whether B7-H3 co-localises with ARL2 or calnexin. This is important because ARL2 could regulate centrosome assembly or work as a cargo (Quidwai *et al*., 2021), thereby might provide a link between B7-H3, RR and primary cilia.

Investigating the pathway in which B7-H3 exerts its activity in normal cells independently of immune cells interactions would be valuable in developing new therapeutics. Given B7-H3 association with RR and primary cilia, and that primary cilia, IMPDH2 and B7-H3 have been reported to be involved in Wnt signalling pathway (Kontos *et al*., 2021; Wheway *et al*., 2018; Xu *et al*., 2020), inhibiting this pathway in cell culture and analysing B7-H3:IMPDH2 stability and localisation in 16HBE compared to cancer cells by Western blot and IF, would give valuable insight on this pathway's involvement in B7-H3 signalling. Furthermore, analysis of B7-H3's role in activating key transduction pathways involved in signalling within primary cilia would help to determine if B7-H3 assists in cilia-dependent signalling rather than initial assembly. This could be explored by treating cells with Shh or Wnt ligands that bind to Ptc1 or Frizzled 3 receptors in primary cilia activating Hedgehog or Wnt signalling, respectively (Wheway *et al*., 2018). Cells could then be lysed for Western blot to measure stability and stained for B7-H3 to assess localisation. This could be further confirmed by using lysates from B7-H3 parental, KD or overexpressing cells to measure activity of potential target proteins using ELISA-based assays.

Another important aspect that remains unclear is the extracellular ligand for B7-H3 that could regulate its function. This could be explored by cloning myc-tag into B7-H3 ectodomain and performing pulldowns, followed by proteomics analysis of possible hits. Additionally, B7-H3 is glycosylated in all cells and is significantly increased in terminal galactose in cancer cells, making it a possible target for galectin binding (Chen *et al*., 2015). Galectins are expressed on both T cells and tumour cells and have been reported to modulate T cell activation and crosstalk with PD-1 to promote apoptosis (Yang *et al*., 2021). Galectin-3 and 7 have been reported to associate with primary cilia (Chiu *et al*., 2006; Rondanino *et al*., 2011). It would

be interesting to test whether galectins are a possible binding partner for B7-H3 by co-staining 16HBE cells with Galectin-3 and measuring B7-H3 co-localisation.

6.2.2 B7-H3 manipulation and actin reorganisation

B7-H3KD or manipulation using blocking mAb or ectodomain treatment resulted in actin reorganisation. However, knocking down B7-H3 did not alter migration behaviour in 2D, although it is notable that these experiments were conducted using cells seeded in pre-formed colonies and this may influence interpretation. It is plausible that the actin changes could contribute to other functional endpoints such as cell division, shape adaptation during growth or extrusion. Therefore, it would be interesting to study single epithelial cell behaviour vs. those in colonies in more detail under these treatment conditions using live imaging of cells expressing GFP-lifeact. This would help to determine whether dynamic reorganisation occurs and if so, what the functional consequences of this might be. Moreover, coupling this with cells expressing FRET-based probes for Rho GTPases would offer additional insight into the way in which B7-H3 manipulation contributes to spatial activation of GTPases that might explain the F-actin reorganisation observed.

Data in this thesis demonstrated similar phenotypic effects upon treating cells with the B7-H3 ectodomain or knocking down B7-H3, suggesting that B7-H3 might bind to another receptor presented on the surface of adjacent epithelial cells. This could be explored further by adding exogenous small epitope/fluorescently-tagged purified B7-H3 ectodomain to cells followed by analysis of potential associated proteins from cell lysates by proteomics. This might also reveal soluble factors that could bind to the ectodomain, noting that soluble B7-H3 has also been reported to be found in cancer cell culture media as well as the sera of cancer patients (Xie *et al*., 2016).

Treating B7-H3KD cells with MPA resulted in a reduction in the enhanced proliferation and invasion seen in 3D cultures, which agrees with recent reports of MPA reducing tumour growth (Klangjorhor *et al*., 2020). Given the published work and the ongoing B7-H3 mAb

clinical trials, combining both MPA and a B7-H3 blocking mAb could represent a new avenue to explore in cancer therapy. This could be tested in 3D models, with and without immune cells, by analysing cell proliferation and invasion to test how B7-H3 and IMPDH2 co-operate in the presence and absence of an immune component.

6.2.3 Purine metabolite profiles in 3D

IMPDH2 is a novel B7-H3 associated protein and a rate limiting enzyme in *de novo* purine biosynthesis. Our data suggests that IMPDH2 activity is increased in B7-H3KD cells in 3D as evidenced through increased proliferation in these cells, which was reduced upon IMPDH2 inhibition. Investigating the metabolic profiles of B7-H3KD cells in 3D, coupled with IMPDH2 localisation with and without cisplatin treatment could be carried out to understand how B7-H3 affects 3D tumourigenesis phenotypes. Moreover, further analysis on whether RR and primary cilia form upon MPA treatment in 3D cancer cells or in clinical cancer tissue samples would help to determine whether cell packing and /or hypoxia influences the assembly of these structures within distinct regions of solid tumours. Furthermore, analysing IMPDH2 localisation and purine metabolic activity via LC-MS/MS in normal and cancer cells treated with B7-H3 mAb/ectodomain could be carried out to determine the role of blocking B7-H3 on its complex protein and tumourigenesis, compared to depleting B7-H3 which had elicit different phenotypes in 2D cells. If further experiments showed that blocking B7-H3 via mAb was not sufficient to downregulate IMPDH2 activity in 3D settings, this would present a potentially interesting avenue for follow-up using pre-clinical models to assess the effects on tumour growth and invasion.

6.2.4 Analysing mechanisms linking B7-H3, oxidative stress and cell survival

We postulate that increased oxidative stress seen in 3D cultures may be influencing cancer cells' ability to undertake efficient DNA damage response. ATR is a DDR effector that senses single-stranded DNA breaks and is required for cells to survive nucleotide imbalance (Diehl *et al*., 2022). It would be interesting to analyse DDR in more detail in B7-H3 depleted cells in 2D and 3D by staining for makers of DDR such as gH2AX or p53BP1 to ascertain a relationship between this, and the enhanced oxidative stress observed in these cells. Moreover, inhibiting

ATR in B7-H3KD cells could help in understanding whether oxidative stress-regulated DDR and ATR-dependent nucleotide sensing, contributes to B7-H3-dependent proliferation or survival. It would additionally be interesting to take this further using co-cultures with tumour and immune cells in 2D or 3D to determine contributions of tumour-immune interactions in mediating this process.

Given the importance of mTOR signalling in regulating proliferation downstream of IMPDH2 and potential role downstream of B7-H3, it would be interesting to also block mTOR activity and analyse growth and invasion in the presence and absence of MPA, to determine whether this pathway contributes to the observed B7-H3-dependent phenotypes. Finally, it would be important to conduct 3D invasion assays in the presence of drugs such as mitomycin C that block proliferation, to confirm whether enhanced invasion in B7-H3 depleted cells is dependent upon increased growth or can operate via an independent pathway.

Further experiments could also be carried out using B7-H3KD cells that have been transfected with B7-H3 GFP lacking cytoplasmic tail, to measure 3D growth in spheroids and ZO-1 levels by immunofluorescent staining in comparison to parental and B7-H3KD cells and whether the cytoplasmic domain is required for B7-H3 proliferation.

6.2.5 B7-H3 trafficking

Data presented in this thesis showed B7-H3 localises to different subcellular compartments and its localisation in cancer cells changes upon increased expression levels. B7-H3 is shown to be degraded through lysosomes. However, co-staining B7-H3 with lysotracker did not show clear co-localisation. One study has found that B7-H3 localised at the lysosomes by staining breast cancer cells with lysotracker, followed by treatment with a B7-H3 affibody (ABY) conjugated to Alexa Fluor 633 (Bam *et al.*, 2019). The main difference between this study and our data is the size of the antibody. Using B7-H3 ABY in the future to test this would be valuable in further confirming B7-H3 lysosomal degradation and internalisation.

The specific mechanism of how B7-H3 is internalised remains unknown. Previous work in the Parsons lab have shown B7-H3 does not localise with clathrin, an endocytosis mediator of cell membrane receptors, after 4 hours of mAb treatment. This could be confirmed by co-staining cells with clathrin in tandem with mAb treatment for time periods used in this thesis (24 hours and 48 hours). Another process of uptake is the macropinocytosis that traffics and organises membrane receptors to modulate their adhesion, cancer cell invasion and metastasis (Le *et al*., 2021). Interestingly, this process has been reported to mediate internalisation of E-cadherin as well as IFN-γ induced TJ internalisation (Bruewer *et al*., 2005; Delva & Kowalczyk, 2009). To investigate whether B7-H3 is internalising via macropinocytosis, cells could be treated with B7-H3 mAb followed by incubation with rhodamine-labelled dextran as a marker for macropinocytosis, finally cells could be fixed and stained for B7-H3 to allow co-localisation quantifications. Moreover, to explore how B7-H3 is regulated at the surface, B7-H3 could be labelled with biotin to help in quantifying the internalisation. This could be done by incubating cells at $4^{O}C$ with membrane impermeable sulfo-NHS-SS-biotin reagent to allow biotin labels to covalently attach to B7-H3, then allow endocytosis to occur by incubating cells at $37\ ^{O}C$. To release the biotin groups from labelled, un-endocytosed protein, L-glutathione should be added. Cells could be lysed and added to streptavidin-coated beads allowing biotinylated proteins to bind. Then, measurements of endocytosis could be caried out by Western blotting.

Understanding how B7-H3 is internalised, the domain/s responsible for exerting its tumourigenic effects and whether blocking B7-H3 via mAb, as in previous clinical trials, is sufficient to downregulate IMPDH2 activity is valuable and would present a potentially interesting avenue for follow-up using pre-clinical models to assess the effects on tumour growth, invasion and cancer recurrence and help in future therapeutic drug development.

References

1. Aberle, H., Butz, S., Stappert, J., Weissig, H., Kemler, R., & Hoschuetzky, H. (1994). Assembly of the cadherin-catenin complex in vitro with recombinant proteins. *Journal of Cell Science*, *107*(12), 3655–3663. https://doi.org/10.1242/jcs.107.12.3655
2. Aboelella, N. S., Brandle, C., Kim, T., Ding, Z.-C., & Zhou, G. (2021a). Oxidative Stress in the Tumor Microenvironment and Its Relevance to Cancer Immunotherapy. *Cancers*, *13*(5), 986. https://doi.org/10.3390/cancers13050986
3. Aboelella, N. S., Brandle, C., Kim, T., Ding, Z.-C., & Zhou, G. (2021b). Oxidative Stress in the Tumor Microenvironment and Its Relevance to Cancer Immunotherapy. *Cancers*, *13*(5), 986. https://doi.org/10.3390/cancers13050986
4. Agarwal, S., Fang, L., Mcgowen, K., Yin, J., Bowman, J., Ku, A. T., Alilin, A. N., Corey, E., Roudier, M., True, L., Dumpit, R., Coleman, I., Lee, J., Nelson, P. S., Capaldo, B. J., Senatorov, I. S., Sowalsky, A. G., Hurt, E. M., & Kelly, K. (2022). Title: A CD276/B7H3 targeted antibody drug conjugate is efficacious across multiple biomarker defined classes of metastatic prostate cancer. *BioRxiv*. https://doi.org/10.1101/2022.04.19.488784
5. ALBERG, A., YUNG, R., STRICKLAND, P., & NELSON, J. (2002). Respiratory cancer and exposure to arsenic, chromium, nickel, and polycyclic aromatic hydrocarbons. *Clinics in Occupational and Environmental Medicine*, *2*(4), 779–801. https://doi.org/10.1016/S1526-0046(02)00056-0
6. Alexandrov, L. B., & Stratton, M. R. (2014). Mutational signatures: the patterns of somatic mutations hidden in cancer genomes. *Current Opinion in Genetics & Development*, *24*, 52–60. https://doi.org/10.1016/j.gde.2013.11.014
7. Alhmoud, J. F., Woolley, J. F., al Moustafa, A.-E., & Malki, M. I. (2020). DNA Damage/Repair Management in Cancers. *Cancers*, *12*(4), 1050. https://doi.org/10.3390/cancers12041050
8. Altan, M., Pelekanou, V., Schalper, K. A., Toki, M., Gaule, P., Syrigos, K., Herbst, R. S., & Rimm, D. L. (2017). B7-H3 Expression in NSCLC and Its Association with B7-H4, PD-L1 and Tumor-Infiltrating Lymphocytes. *Clinical Cancer Research*, *23*(17), 5202–5209. https://doi.org/10.1158/1078-0432.CCR-16-3107
9. Alvarado, A. G., Thiagarajan, P. S., Mulkearns-Hubert, E. E., Silver, D. J., Hale, J. S., Alban, T. J., Turaga, S. M., Jarrar, A., Reizes, O., Longworth, M. S., Vogelbaum, M. A., & Lathia, J. D. (2017). Glioblastoma Cancer Stem Cells Evade Innate Immune Suppression of Self-Renewal through Reduced TLR4 Expression. *Cell Stem Cell*, *20*(4), 450-461.e4. https://doi.org/10.1016/j.stem.2016.12.001
10. Amori, G., Sugawara, E., Shigematsu, Y., Akiya, M., Kunieda, J., Yuasa, T., Yamamoto, S., Yonese, J., Takeuchi, K., & Inamura, K. (2021). Tumor B7-H3 expression in diagnostic biopsy specimens and survival in patients with metastatic prostate cancer. *Prostate Cancer and Prostatic Diseases*, *24*(3), 767–774. https://doi.org/10.1038/s41391-021-00331-6
11. An, S., Kumar, R., Sheets, E. D., & Benkovic, S. J. (2008). Reversible Compartmentalization of de Novo Purine Biosynthetic Complexes in Living Cells. *Science*, *320*(5872), 103–106. https://doi.org/10.1126/science.1152241
12. Anderson, J. M., & van Itallie, C. M. (2009). Physiology and Function of the Tight Junction. *Cold Spring Harbor Perspectives in Biology*, *1*(2), a002584–a002584. https://doi.org/10.1101/cshperspect.a002584
13. Anthony, S. A., Burrell, A. L., Johnson, M. C., Duong-Ly, K. C., Kuo, Y.-M., Simonet, J. C., Michener, P., Andrews, A., Kollman, J. M., & Peterson, J. R. (2017a). Reconstituted IMPDH

polymers accommodate both catalytically active and inactive conformations. *Molecular Biology of the Cell*, *28*(20), 2600–2608. https://doi.org/10.1091/mbc.e17-04-0263
14. Anthony, S. A., Burrell, A. L., Johnson, M. C., Duong-Ly, K. C., Kuo, Y.-M., Simonet, J. C., Michener, P., Andrews, A., Kollman, J. M., & Peterson, J. R. (2017b). Reconstituted IMPDH polymers accommodate both catalytically active and inactive conformations. *Molecular Biology of the Cell*, *28*(20), 2600–2608. https://doi.org/10.1091/mbc.e17-04-0263
15. Antoniades, I., Stylianou, P., & Skourides, P. A. (2014). Making the Connection: Ciliary Adhesion Complexes Anchor Basal Bodies to the Actin Cytoskeleton. *Developmental Cell*, *28*(1), 70–80. https://doi.org/10.1016/j.devcel.2013.12.003
16. Arfin, S., Jha, N. K., Jha, S. K., Kesari, K. K., Ruokolainen, J., Roychoudhury, S., Rathi, B., & Kumar, D. (2021). Oxidative Stress in Cancer Cell Metabolism. *Antioxidants*, *10*(5), 642. https://doi.org/10.3390/antiox10050642
17. Arjumand, W., & Sultana, S. (2012). Role of VHL gene mutation in human renal cell carcinoma. *Tumor Biology*, *33*(1), 9–16. https://doi.org/10.1007/s13277-011-0257-3
18. Ayukawa, S., Kamoshita, N., Nakayama, J., Teramoto, R., Pishesha, N., Ohba, K., Sato, N., Kozawa, K., Abe, H., Semba, K., Goda, N., Fujita, Y., & Maruyama, T. (2021). Epithelial cells remove precancerous cells by cell competition via MHC class I–LILRB3 interaction. *Nature Immunology*, *22*(11), 1391–1402. https://doi.org/10.1038/s41590-021-01045-6
19. Azad, N., & Iyer, A. K. v. (2014). Reactive Oxygen Species and Apoptosis. In *Systems Biology of Free Radicals and Antioxidants* (pp. 113–135). Springer Berlin Heidelberg. https://doi.org/10.1007/978-3-642-30018-9_15
20. Azmanova, M., & Pitto-Barry, A. (2022). Oxidative Stress in Cancer Therapy: Friend or Enemy? *ChemBioChem*, *23*(10). https://doi.org/10.1002/cbic.202100641
21. Bachawal, S., Bean, G. R., Krings, G., & Wilson, K. E. (2020). Evaluation of ductal carcinoma in situ grade via triple-modal molecular imaging of B7-H3 expression. *Npj Breast Cancer*, *6*(1), 14. https://doi.org/10.1038/s41523-020-0158-y
22. Bachawal, S. v., Jensen, K. C., Wilson, K. E., Tian, L., Lutz, A. M., & Willmann, J. K. (2015). Breast Cancer Detection by B7-H3–Targeted Ultrasound Molecular Imaging. *Cancer Research*, *75*(12), 2501–2509. https://doi.org/10.1158/0008-5472.CAN-14-3361
23. Balda, M. S., & Matter, K. (2009). Tight junctions and the regulation of gene expression. *Biochimica et Biophysica Acta (BBA) - Biomembranes*, *1788*(4), 761–767. https://doi.org/10.1016/j.bbamem.2008.11.024
24. Bam, R., Laffey, M., Nottberg, K., Lown, P. S., Hackel, B. J., & Wilson, K. E. (2019). Affibody-Indocyanine Green Based Contrast Agent for Photoacoustic and Fluorescence Molecular Imaging of B7–H3 Expression in Breast Cancer. *Bioconjugate Chemistry*, *30*(6), 1677–1689. https://doi.org/10.1021/acs.bioconjchem.9b00239
25. Bansal, A., & Simon, M. C. (2018). Glutathione metabolism in cancer progression and treatment resistance. *Journal of Cell Biology*, *217*(7), 2291–2298. https://doi.org/10.1083/jcb.201804161
26. Barfeld, S. J., Fazli, L., Persson, M., Marjavaara, L., Urbanucci, A., Kaukoniemi, K. M., Rennie, P. S., Ceder, Y., Chabes, A., Visakorpi, T., & Mills, I. G. (2015). Myc-dependent purine biosynthesis affects nucleolar stress and therapy response in prostate cancer. *Oncotarget*, *6*(14), 12587–12602. https://doi.org/10.18632/oncotarget.3494
27. Basten, S. G., Willekers, S., Vermaat, J. S., Slaats, G. G., Voest, E. E., van Diest, P. J., & Giles, R. H. (2013). Reduced cilia frequencies in human renal cell carcinomas versus neighboring parenchymal tissue. *Cilia*, *2*(1), 2. https://doi.org/10.1186/2046-2530-2-2
28. Basu, I., Locker, J., Cassera, M. B., Belbin, T. J., Merino, E. F., Dong, X., Hemeon, I., Evans, G. B., Guha, C., & Schramm, V. L. (2011). Growth and Metastases of Human Lung Cancer Are

Inhibited in Mouse Xenografts by a Transition State Analogue of 5'-Methylthioadenosine Phosphorylase. *Journal of Biological Chemistry*, *286*(6), 4902–4911. https://doi.org/10.1074/jbc.M110.198374

29. Battelli, M. G., Polito, L., Bortolotti, M., & Bolognesi, A. (2016). Xanthine oxidoreductase in cancer: more than a differentiation marker. *Cancer Medicine*, *5*(3), 546–557. https://doi.org/10.1002/cam4.601
30. Beckonert, O., Keun, H. C., Ebbels, T. M. D., Bundy, J., Holmes, E., Lindon, J. C., & Nicholson, J. K. (2007). Metabolic profiling, metabolomic and metabonomic procedures for NMR spectroscopy of urine, plasma, serum and tissue extracts. *Nature Protocols*, *2*(11), 2692–2703. https://doi.org/10.1038/nprot.2007.376
31. Bedi, S., Vidyasagar, A., & Djamali, A. (2008). Epithelial-to-mesenchymal transition and chronic allograft tubulointerstitial fibrosis. *Transplantation Reviews*, *22*(1), 1–5. https://doi.org/10.1016/j.trre.2007.09.004
32. Benzon, B., Zhao, S. G., Haffner, M. C., Takhar, M., Erho, N., Yousefi, K., Hurley, P., Bishop, J. L., Tosoian, J., Ghabili, K., Alshalalfa, M., Glavaris, S., Simons, B. W., Tran, P., Davicioni, E., Karnes, R. J., Boudadi, K., Antonarakis, E. S., Schaeffer, E. M., … Ross, A. E. (2017). Correlation of B7-H3 with androgen receptor, immune pathways and poor outcome in prostate cancer: an expression-based analysis. *Prostate Cancer and Prostatic Diseases*, *20*(1), 28–35. https://doi.org/10.1038/pcan.2016.49
33. Bhat, A. A., Uppada, S., Achkar, I. W., Hashem, S., Yadav, S. K., Shanmugakonar, M., Al-Naemi, H. A., Haris, M., & Uddin, S. (2019). Tight Junction Proteins and Signaling Pathways in Cancer and Inflammation: A Functional Crosstalk. *Frontiers in Physiology*, *9*. https://doi.org/10.3389/fphys.2018.01942
34. Bian, J., Dannappel, M., Wan, C., & Firestein, R. (2020). Transcriptional Regulation of Wnt/β-Catenin Pathway in Colorectal Cancer. *Cells*, *9*(9), 2125. https://doi.org/10.3390/cells9092125
35. Bianchi-Smiraglia, A., Wawrzyniak, J. A., Bagati, A., Marvin, E. K., Ackroyd, J., Moparthy, S., Bshara, W., Fink, E. E., Foley, C. E., Morozevich, G. E., Berman, A. E., Shewach, D. S., & Nikiforov, M. A. (2015). Pharmacological targeting of guanosine monophosphate synthase suppresses melanoma cell invasion and tumorigenicity. *Cell Death & Differentiation*, *22*(11), 1858–1864. https://doi.org/10.1038/cdd.2015.47
36. Bianchi-Smiraglia, A., Wolff, D. W., Marston, D. J., Deng, Z., Han, Z., Moparthy, S., Wombacher, R. M., Mussell, A. L., Shen, S., Chen, J., Yun, D.-H., O'Brien Cox, A., Furdui, C. M., Hurley, E., Feltri, M. L., Qu, J., Hollis, T., Kengne, J. B. N., Fongang, B., … Nikiforov, M. A. (2021). Regulation of local GTP availability controls RAC1 activity and cell invasion. *Nature Communications*, *12*(1), 6091. https://doi.org/10.1038/s41467-021-26324-6
37. Binker, M. G., Binker-Cosen, A. A., Richards, D., Oliver, B., & Cosen-Binker, L. I. (2009). EGF promotes invasion by PANC-1 cells through Rac1/ROS-dependent secretion and activation of MMP-2. *Biochemical and Biophysical Research Communications*, *379*(2), 445–450. https://doi.org/10.1016/j.bbrc.2008.12.080
38. Binnewies, M., Roberts, E. W., Kersten, K., Chan, V., Fearon, D. F., Merad, M., Coussens, L. M., Gabrilovich, D. I., Ostrand-Rosenberg, S., Hedrick, C. C., Vonderheide, R. H., Pittet, M. J., Jain, R. K., Zou, W., Howcroft, T. K., Woodhouse, E. C., Weinberg, R. A., & Krummel, M. F. (2018). Understanding the tumor immune microenvironment (TIME) for effective therapy. *Nature Medicine*, *24*(5), 541–550. https://doi.org/10.1038/s41591-018-0014-x
39. Bisgrove, B. W., & Yost, H. J. (2006). The roles of cilia in developmental disorders and disease. *Development*, *133*(21), 4131–4143. https://doi.org/10.1242/dev.02595

40. Bonaventura, P., Shekarian, T., Alcazer, V., Valladeau-Guilemond, J., Valsesia-Wittmann, S., Amigorena, S., Caux, C., & Depil, S. (2019). Cold Tumors: A Therapeutic Challenge for Immunotherapy. *Frontiers in Immunology*, *10*. https://doi.org/10.3389/fimmu.2019.00168
41. Borghaei, H., Paz-Ares, L., Horn, L., Spigel, D. R., Steins, M., Ready, N. E., Chow, L. Q., Vokes, E. E., Felip, E., Holgado, E., Barlesi, F., Kohlhäufl, M., Arrieta, O., Burgio, M. A., Fayette, J., Lena, H., Poddubskaya, E., Gerber, D. E., Gettinger, S. N., … Brahmer, J. R. (2015). Nivolumab versus Docetaxel in Advanced Nonsquamous Non–Small-Cell Lung Cancer. *New England Journal of Medicine*, *373*(17), 1627–1639. https://doi.org/10.1056/NEJMoa1507643
42. Borghi, N., Lowndes, M., Maruthamuthu, V., Gardel, M. L., & Nelson, W. J. (2010). Regulation of cell motile behavior by crosstalk between cadherin- and integrin-mediated adhesions. *Proceedings of the National Academy of Sciences*, *107*(30), 13324–13329. https://doi.org/10.1073/pnas.1002662107
43. Bower, J. J., Vance, L. D., Psioda, M., Smith-Roe, S. L., Simpson, D. A., Ibrahim, J. G., Hoadley, K. A., Perou, C. M., & Kaufmann, W. K. (2017). Patterns of cell cycle checkpoint deregulation associated with intrinsic molecular subtypes of human breast cancer cells. *Npj Breast Cancer*, *3*(1), 9. https://doi.org/10.1038/s41523-017-0009-7
44. Braga, V. M. M., del Maschio, A., Machesky, L., & Dejana, E. (1999). Regulation of Cadherin Function by Rho and Rac: Modulation by Junction Maturation and Cellular Context. *Molecular Biology of the Cell*, *10*(1), 9–22. https://doi.org/10.1091/mbc.10.1.9
45. Brahmer, J. R. (2014). Immune Checkpoint Blockade: The Hope for Immunotherapy as a Treatment of Lung Cancer? *Seminars in Oncology*, *41*(1), 126–132. https://doi.org/10.1053/j.seminoncol.2013.12.014
46. Brose, M. S., Volpe, P., Feldman, M., Kumar, M., Rishi, I., Gerrero, R., Einhorn, E., Herlyn, M., Minna, J., Nicholson, A., Roth, J. A., Albelda, S. M., Davies, H., Cox, C., Brignell, G., Stephens, P., Futreal, P. A., Wooster, R., Stratton, M. R., & Weber, B. L. (2002). BRAF and RAS mutations in human lung cancer and melanoma. *Cancer Research*, *62*(23), 6997–7000.
47. Bruewer, M., Utech, M., Ivanov, A. I., Hopkins, A. M., Parkos, C. A., & Nusrat, A. (2005). Interferon-γ induces internalization of epithelial tight junction proteins via a macropinocytosis-like process. *The FASEB Journal*, *19*(8), 923–933. https://doi.org/10.1096/fj.04-3260com
48. Brunner, A., Hinterholzer, S., Riss, P., Heinze, G., & Brustmann, H. (2012). Immunoexpression of B7-H3 in endometrial cancer: Relation to tumor T-cell infiltration and prognosis. *Gynecologic Oncology*, *124*(1), 105–111. https://doi.org/10.1016/j.ygyno.2011.09.012
49. Butte, M. J., Keir, M. E., Phamduy, T. B., Sharpe, A. H., & Freeman, G. J. (2007). Programmed Death-1 Ligand 1 Interacts Specifically with the B7-1 Costimulatory Molecule to Inhibit T Cell Responses. *Immunity*, *27*(1), 111–122. https://doi.org/10.1016/j.immuni.2007.05.016
50. Byrne, E. F. X., Sircar, R., Miller, P. S., Hedger, G., Luchetti, G., Nachtergaele, S., Tully, M. D., Mydock-McGrane, L., Covey, D. F., Rambo, R. P., Sansom, M. S. P., Newstead, S., Rohatgi, R., & Siebold, C. (2016). Structural basis of Smoothened regulation by its extracellular domains. *Nature*, *535*(7613), 517–522. https://doi.org/10.1038/nature18934
51. Cai, Y., Fedeles, S. v., Dong, K., Anyatonwu, G., Onoe, T., Mitobe, M., Gao, J.-D., Okuhara, D., Tian, X., Gallagher, A.-R., Tang, Z., Xie, X., Lalioti, M. D., Lee, A.-H., Ehrlich, B. E., & Somlo, S. (2014). Altered trafficking and stability of polycystins underlie polycystic kidney disease. *Journal of Clinical Investigation*, *124*(12), 5129–5144. https://doi.org/10.1172/JCI67273
52. Cairns, R. A., Harris, I. S., & Mak, T. W. (2011). Regulation of cancer cell metabolism. *Nature Reviews Cancer*, *11*(2), 85–95. https://doi.org/10.1038/nrc2981

53. Capaldo, C. T., & Macara, I. G. (2007). Depletion of E-Cadherin Disrupts Establishment but Not Maintenance of Cell Junctions in Madin-Darby Canine Kidney Epithelial Cells. *Molecular Biology of the Cell*, *18*(1), 189–200. https://doi.org/10.1091/mbc.e06-05-0471
54. Carcamo, W. C., Calise, S. J., von Mühlen, C. A., Satoh, M., & Chan, E. K. L. (2014). *Molecular Cell Biology and Immunobiology of Mammalian Rod/Ring Structures* (pp. 35–74). https://doi.org/10.1016/B978-0-12-800097-7.00002-6
55. Carcamo, W. C., Satoh, M., Kasahara, H., Terada, N., Hamazaki, T., Chan, J. Y. F., Yao, B., Tamayo, S., Covini, G., von Mühlen, C. A., & Chan, E. K. L. (2011). Induction of Cytoplasmic Rods and Rings Structures by Inhibition of the CTP and GTP Synthetic Pathway in Mammalian Cells. *PLoS ONE*, *6*(12), e29690. https://doi.org/10.1371/journal.pone.0029690
56. Cardarella, S., Ogino, A., Nishino, M., Butaney, M., Shen, J., Lydon, C., Yeap, B. Y., Sholl, L. M., Johnson, B. E., & Jänne, P. A. (2013). Clinical, Pathologic, and Biologic Features Associated with *BRAF* Mutations in Non–Small Cell Lung Cancer. *Clinical Cancer Research*, *19*(16), 4532–4540. https://doi.org/10.1158/1078-0432.CCR-13-0657
57. Carvajal-Hausdorf, D., Altan, M., Velcheti, V., Gettinger, S. N., Herbst, R. S., Rimm, D. L., & Schalper, K. A. (2019). Expression and clinical significance of PD-L1, B7-H3, B7-H4 and TILs in human small cell lung Cancer (SCLC). *Journal for ImmunoTherapy of Cancer*, *7*(1), 65. https://doi.org/10.1186/s40425-019-0540-1
58. Castellanos, J. R., Purvis, I. J., Labak, C. M., Guda, M. R., Tsung, A. J., Velpula, K. K., & Asuthkar, S. (2017). B7-H3 role in the immune landscape of cancer. *American Journal of Clinical and Experimental Immunology*, *6*(4), 66–75.
59. Chang, C.-C., Lin, W.-C., Pai, L.-M., Lee, H.-S., Wu, S.-C., Ding, S.-T., Liu, J.-L., & Sung, L.-Y. (2015). Cytoophidium assembly reflects upregulation of IMPDH activity. *Journal of Cell Science*. https://doi.org/10.1242/jcs.175265
60. Chang, C.-F., & Serra, R. (2013). Ift88 regulates Hedgehog signaling, *Sfrp5* expression, and β-catenin activity in post-natal growth plate. *Journal of Orthopaedic Research*, *31*(3), 350–356. https://doi.org/10.1002/jor.22237
61. Chang, J., & Chaudhuri, O. (2019). Beyond proteases: Basement membrane mechanics and cancer invasion. *Journal of Cell Biology*, *218*(8), 2456–2469. https://doi.org/10.1083/jcb.201903066
62. Chao, H. X., Poovey, C. E., Privette, A. A., Grant, G. D., Chao, H. Y., Cook, J. G., & Purvis, J. E. (2017). DNA damage checkpoint dynamics drive cell cycle phase transitions. *BioRxiv*. https://doi.org/10.1101/137307
63. Chapoval, A. I., Ni, J., Lau, J. S., Wilcox, R. A., Flies, D. B., Liu, D., Dong, H., Sica, G. L., Zhu, G., Tamada, K., & Chen, L. (2001). B7-H3: A costimulatory molecule for T cell activation and IFN-γ production. *Nature Immunology*, *2*(3), 269–274. https://doi.org/10.1038/85339
64. Chefetz, I., Holmberg, J. C., Alvero, A. B., Visintin, I., & Mor, G. (2011). Inhibition of Aurora-A kinase induces cell cycle arrest in epithelial ovarian cancer stem cells by affecting NFκB pathway. *Cell Cycle*, *10*(13), 2206–2214. https://doi.org/10.4161/cc.10.13.16348
65. Chen, G., Tu, Y., Aladelusi, T. O., Zhao, S., Chen, J., Jin, L., & Zhu, D. (2020). Knocking down B7H3 expression enhances cell proliferation of SHEDs via the SHP1/AKT signal axis. *Biochemical and Biophysical Research Communications*, *531*(3), 282–289. https://doi.org/10.1016/j.bbrc.2020.06.154
66. Chen, J.-T., Chen, C.-H., Ku, K.-L., Hsiao, M., Chiang, C.-P., Hsu, T.-L., Chen, M.-H., & Wong, C.-H. (2015). Glycoprotein B7-H3 overexpression and aberrant glycosylation in oral cancer and immune response. *Proceedings of the National Academy of Sciences*, *112*(42), 13057–13062. https://doi.org/10.1073/pnas.1516991112

67. Chen, W., Liu, P., Wang, Y., Nie, W., Li, Z., Xu, W., Li, F., Zhou, Z., Zhao, M., & Liu, H. (2013). Characterization of a Soluble B7-H3 (sB7-H3) Spliced from the Intron and Analysis of sB7-H3 in the Sera of Patients with Hepatocellular Carcinoma. *PLoS ONE*, *8*(10), e76965. https://doi.org/10.1371/journal.pone.0076965
68. Chen, X., Song, M., Zhang, B., & Zhang, Y. (2016). Reactive Oxygen Species Regulate T Cell Immune Response in the Tumor Microenvironment. *Oxidative Medicine and Cellular Longevity*, *2016*, 1–10. https://doi.org/10.1155/2016/1580967
69. Chen, Y., Jungsuwadee, P., Vore, M., Butterfield, D. A., & st. Clair, D. K. (2007). Collateral Damage in Cancer Chemotherapy: Oxidative Stress in Nontargeted Tissues. *Molecular Interventions*, *7*(3), 147–156. https://doi.org/10.1124/mi.7.3.6
70. Chen, Y.-W., Tekle, C., & Fodstad, O. (2008). The Immunoregulatory Protein Human B7H3 is a Tumor-Associated Antigen that Regulates Tumor Cell Migration and Invasion. *Current Cancer Drug Targets*, *8*(5), 404–413. https://doi.org/10.2174/156800908785133141
71. Chio, I. I. C., & Tuveson, D. A. (2017). ROS in Cancer: The Burning Question. *Trends in Molecular Medicine*, *23*(5), 411–429. https://doi.org/10.1016/j.molmed.2017.03.004
72. Chiu, M. G., Johnson, T. M., Woolf, A. S., Dahm-Vicker, E. M., Long, D. A., Guay-Woodford, L., Hillman, K. A., Bawumia, S., Venner, K., Hughes, R. C., Poirier, F., & Winyard, P. J. D. (2006). Galectin-3 Associates with the Primary Cilium and Modulates Cyst Growth in Congenital Polycystic Kidney Disease. *The American Journal of Pathology*, *169*(6), 1925–1938. https://doi.org/10.2353/ajpath.2006.060245
73. Collins, M., Ling, V., & Carreno, B. M. (2005). The B7 family of immune-regulatory ligands. *Genome Biology*, *6*(6), 223. https://doi.org/10.1186/gb-2005-6-6-223
74. Corbit, K. C., Aanstad, P., Singla, V., Norman, A. R., Stainier, D. Y. R., & Reiter, J. F. (2005). Vertebrate Smoothened functions at the primary cilium. *Nature*, *437*(7061), 1018–1021. https://doi.org/10.1038/nature04117
75. Corbit, K. C., Shyer, A. E., Dowdle, W. E., Gaulden, J., Singla, V., & Reiter, J. F. (2008). Kif3a constrains β-catenin-dependent Wnt signalling through dual ciliary and non-ciliary mechanisms. *Nature Cell Biology*, *10*(1), 70–76. https://doi.org/10.1038/ncb1670
76. Covarrubias, A. J., Perrone, R., Grozio, A., & Verdin, E. (2021). NAD+ metabolism and its roles in cellular processes during ageing. *Nature Reviews Molecular Cell Biology*, *22*(2), 119–141. https://doi.org/10.1038/s41580-020-00313-x
77. Covini, G., Carcamo, W. C., Bredi, E., von Mühlen, C. A., Colombo, M., & Chan, E. K. (2012). Cytoplasmic Rods and Rings Autoantibodies Developed during Pegylated Interferon and Ribavirin Therapy in Patients with Chronic Hepatitis C. *Antiviral Therapy*, *17*(5), 805–811. https://doi.org/10.3851/IMP1993
78. Cregan, Inezl., DHARMARAJAN, A. M., & FOX, S. A. (2013). Mechanisms of cisplatin-induced cell death in malignant mesothelioma cells: Role of inhibitor of apoptosis proteins (IAPs) and caspases. *International Journal of Oncology*, *42*(2), 444–452. https://doi.org/10.3892/ijo.2012.1715
79. Criscitiello, C., Morganti, S., & Curigliano, G. (2021). Antibody–drug conjugates in solid tumors: a look into novel targets. *Journal of Hematology & Oncology*, *14*(1), 20. https://doi.org/10.1186/s13045-021-01035-z
80. Cucchi, D., Gibson, A., & Martin, S. a. (2021). The emerging relationship between metabolism and DNA repair. *Cell Cycle*, *20*(10), 943–959. https://doi.org/10.1080/15384101.2021.1912889
81. Dang, C. v. (2012). Links between metabolism and cancer. *Genes & Development*, *26*(9), 877–890. https://doi.org/10.1101/gad.189365.112

82. De Groot, P. M., Wu, C. C., Carter, B. W., & Munden, R. F. (2018). The epidemiology of lung cancer. *Translational Lung Cancer Research*, *7*(3), 220–233. https://doi.org/10.21037/tlcr.2018.05.06
83. de Vitto, H., Arachchige, D. B., Richardson, B. C., & French, J. B. (2021). The Intersection of Purine and Mitochondrial Metabolism in Cancer. *Cells*, *10*(10), 2603. https://doi.org/10.3390/cells10102603
84. Delva, E., & Kowalczyk, A. P. (2009). Regulation of Cadherin Trafficking. *Traffic*, *10*(3), 259–267. https://doi.org/10.1111/j.1600-0854.2008.00862.x
85. DeNicola, G. M., Karreth, F. A., Humpton, T. J., Gopinathan, A., Wei, C., Frese, K., Mangal, D., Yu, K. H., Yeo, C. J., Calhoun, E. S., Scrimieri, F., Winter, J. M., Hruban, R. H., Iacobuzio-Donahue, C., Kern, S. E., Blair, I. A., & Tuveson, D. A. (2011). Oncogene-induced Nrf2 transcription promotes ROS detoxification and tumorigenesis. *Nature*, *475*(7354), 106–109. https://doi.org/10.1038/nature10189
86. Deng, M., Wu, D., Zhang, Y., Jin, Z., & Miao, J. (2021). MiR-29c downregulates tumor-expressed B7-H3 to mediate the antitumor NK-cell functions in ovarian cancer. *Gynecologic Oncology*, *162*(1), 190–199. https://doi.org/10.1016/j.ygyno.2021.04.013
87.
88. Desantes, K., Maris, J. M., McDowell, K., Mackall, C., Shankar, S., Vasselli, J., Chen, F., Loo, D., Moore, P. A., Wigginton, J. M., & Sondel, P. M. (2017). A phase 1, open-label, dose escalation study of enoblituzumab (MGA271) in pediatric patients with B7-H3-expressing relapsed or refractory solid tumors. *Journal of Clinical Oncology*, *35*(15_suppl), TPS2596–TPS2596. https://doi.org/10.1200/JCO.2017.35.15_suppl.TPS2596
89. di Virgilio, F., & Adinolfi, E. (2017). Extracellular purines, purinergic receptors and tumor growth. *Oncogene*, *36*(3), 293–303. https://doi.org/10.1038/onc.2016.206
90. Diehl, F. F., Miettinen, T. P., Elbashir, R., Nabel, C. S., Darnell, A. M., Do, B. T., Manalis, S. R., Lewis, C. A., & vander Heiden, M. G. (2022). Nucleotide imbalance decouples cell growth from cell proliferation. *Nature Cell Biology*, *24*(8), 1252–1264. https://doi.org/10.1038/s41556-022-00965-1
91. Digregorio, M., Coppieters, N., Lombard, A., Lumapat, P. N., Scholtes, F., & Rogister, B. (2021). The expression of B7-H3 isoforms in newly diagnosed glioblastoma and recurrence and their functional role. *Acta Neuropathologica Communications*, *9*(1), 59. https://doi.org/10.1186/s40478-021-01167-w
92. Ding, L., Cao, J., Lin, W., Chen, H., Xiong, X., Ao, H., Yu, M., Lin, J., & Cui, Q. (2020). The Roles of Cyclin-Dependent Kinases in Cell-Cycle Progression and Therapeutic Strategies in Human Breast Cancer. *International Journal of Molecular Sciences*, *21*(6), 1960. https://doi.org/10.3390/ijms21061960
93. Doi, Y., Yashiro, M., Yamada, N., Amano, R., Noda, S., & Hirakawa, K. (2012). VEGF-A/VEGFR-2 Signaling Plays an Important Role for the Motility of Pancreas Cancer Cells. *Annals of Surgical Oncology*, *19*(8), 2733–2743. https://doi.org/10.1245/s10434-011-2181-6
94. Domazet-Lošo, T., & Tautz, D. (2010). Phylostratigraphic tracking of cancer genes suggests a link to the emergence of multicellularity in metazoa. *BMC Biology*, *8*(1), 66. https://doi.org/10.1186/1741-7007-8-66
95. Dominguez, R., & Holmes, K. C. (2011). Actin Structure and Function. *Annual Review of Biophysics*, *40*(1), 169–186. https://doi.org/10.1146/annurev-biophys-042910-155359
96. Dong, H., Strome, S. E., Salomao, D. R., Tamura, H., Hirano, F., Flies, D. B., Roche, P. C., Lu, J., Zhu, G., Tamada, K., Lennon, V. A., Celis, E., & Chen, L. (2002). Tumor-associated B7-H1 promotes T-cell apoptosis: A potential mechanism of immune evasion. *Nature Medicine*, *8*(8), 793–800. https://doi.org/10.1038/nm730

97. Dong, P., Xiong, Y., Yue, J., Hanley, S. J. B., & Watari, H. (2018). B7H3 As a Promoter of Metastasis and Promising Therapeutic Target. *Frontiers in Oncology*, *8*. https://doi.org/10.3389/fonc.2018.00264
98. Donnelly, E., Ascenzi, M.-G., & Farnum, C. (2009). Primary cilia are highly oriented with respect to collagen direction and long axis of extensor tendon. *Journal of Orthopaedic Research*, n/a-n/a. https://doi.org/10.1002/jor.20946
99. Dostalek, M., Gohh, R. Y., & Akhlaghi, F. (2013). Inosine Monophosphate Dehydrogenase Expression and Activity Are Significantly Lower in Kidney Transplant Recipients With Diabetes Mellitus. *Therapeutic Drug Monitoring*, *35*(3), 374–383. https://doi.org/10.1097/FTD.0b013e3182852697
100. Draganov, D., Han, Z., Rana, A., Bennett, N., Irvine, D. J., & Lee, P. P. (2021). Ivermectin converts cold tumors hot and synergizes with immune checkpoint blockade for treatment of breast cancer. *Npj Breast Cancer*, *7*(1), 22. https://doi.org/10.1038/s41523-021-00229-5
101. Drees, F., Pokutta, S., Yamada, S., Nelson, W. J., & Weis, W. I. (2005). α-Catenin Is a Molecular Switch that Binds E-Cadherin-β-Catenin and Regulates Actin-Filament Assembly. *Cell*, *123*(5), 903–915. https://doi.org/10.1016/j.cell.2005.09.021
102.
103. Du, H., Hirabayashi, K., Ahn, S., Kren, N. P., Montgomery, S. A., Wang, X., Tiruthani, K., Mirlekar, B., Michaud, D., Greene, K., Herrera, S. G., Xu, Y., Sun, C., Chen, Y., Ma, X., Ferrone, C. R., Pylayeva-Gupta, Y., Yeh, J. J., Liu, R., … Dotti, G. (2019). Antitumor Responses in the Absence of Toxicity in Solid Tumors by Targeting B7-H3 via Chimeric Antigen Receptor T Cells. *Cancer Cell*, *35*(2), 221-237.e8. https://doi.org/10.1016/j.ccell.2019.01.002
104. Duan, S., Huang, W., Liu, X., Liu, X., Chen, N., Xu, Q., Hu, Y., Song, W., & Zhou, J. (2018). IMPDH2 promotes colorectal cancer progression through activation of the PI3K/AKT/mTOR and PI3K/AKT/FOXO1 signaling pathways. *Journal of Experimental & Clinical Cancer Research*, *37*(1), 304. https://doi.org/10.1186/s13046-018-0980-3
105. Dun, B., Xu, H., Sharma, A., Liu, H., Yu, H., Yi, B., Liu, X., He, M., Zeng, L., & She, J.-X. (2013). Delineation of biological and molecular mechanisms underlying the diverse anticancer activities of mycophenolic acid. *International Journal of Clinical and Experimental Pathology*, *6*(12), 2880–2886.
106. Egeberg, D. L., Lethan, M., Manguso, R., Schneider, L., Awan, A., Jørgensen, T. S., Byskov, A. G., Pedersen, L. B., & Christensen, S. T. (2012). Primary cilia and aberrant cell signaling in epithelial ovarian cancer. *Cilia*, *1*(1), 15. https://doi.org/10.1186/2046-2530-1-15
107. Eisenhoffer, G. T., Loftus, P. D., Yoshigi, M., Otsuna, H., Chien, C.-B., Morcos, P. A., & Rosenblatt, J. (2012). Crowding induces live cell extrusion to maintain homeostatic cell numbers in epithelia. *Nature*, *484*(7395), 546–549. https://doi.org/10.1038/nature10999
108. Emoto, K., Masugi, Y., Yamazaki, K., Effendi, K., Tsujikawa, H., Tanabe, M., Kitagawa, Y., & Sakamoto, M. (2014). Presence of primary cilia in cancer cells correlates with prognosis of pancreatic ductal adenocarcinoma. *Human Pathology*, *45*(4), 817–825. https://doi.org/10.1016/j.humpath.2013.11.017
109. Emwas, A.-H., Roy, R., McKay, R. T., Tenori, L., Saccenti, E., Gowda, G. A. N., Raftery, D., Alahmari, F., Jaremko, L., Jaremko, M., & Wishart, D. S. (2019). NMR Spectroscopy for Metabolomics Research. *Metabolites*, *9*(7), 123. https://doi.org/10.3390/metabo9070123
110. Esteban, M. A., Harten, S. K., Tran, M. G., & Maxwell, P. H. (2006). Formation of Primary Cilia in the Renal Epithelium Is Regulated by the von Hippel-Lindau Tumor Suppressor Protein. *Journal of the American Society of Nephrology*, *17*(7), 1801–1806. https://doi.org/10.1681/ASN.2006020181

111. Etienne-Manneville, S. (2004). Actin and Microtubules in Cell Motility: Which One is in Control? *Traffic*, *5*(7), 470–477. https://doi.org/10.1111/j.1600-0854.2004.00196.x
112. Etienne-Manneville, S., & Hall, A. (2002). Rho GTPases in cell biology. *Nature*, *420*(6916), 629–635. https://doi.org/10.1038/nature01148
113. Ezratty, E. J., Stokes, N., Chai, S., Shah, A. S., Williams, S. E., & Fuchs, E. (2011). A Role for the Primary Cilium in Notch Signaling and Epidermal Differentiation during Skin Development. *Cell*, *145*(7), 1129–1141. https://doi.org/10.1016/j.cell.2011.05.030
114. Fabbri, L., Bost, F., & Mazure, N. (2019). Primary Cilium in Cancer Hallmarks. *International Journal of Molecular Sciences*, *20*(6), 1336. https://doi.org/10.3390/ijms20061336
115. Fan, H., Zhu, J., & Yao, X. (2016). Prognostic significance of B7-H3 expression in patients with colorectal cancer: A meta-analysis. *Pakistan Journal of Medical Sciences*, *32*(6). https://doi.org/10.12669/pjms.326.11511
116. Fan, Y., & Bergmann, A. (2008). Apoptosis-induced compensatory proliferation. The Cell is dead. Long live the Cell! *Trends in Cell Biology*, *18*(10), 467–473. https://doi.org/10.1016/j.tcb.2008.08.001
117. Fansa, E. K., & Wittinghofer, A. (2016). Sorting of lipidated cargo by the Arl2/Arl3 system. *Small GTPases*, *7*(4), 222–230. https://doi.org/10.1080/21541248.2016.1224454
118. Fauci, J. M., Straughn, J. M., Ferrone, S., & Buchsbaum, D. J. (2012). A review of B7-H3 and B7-H4 immune molecules and their role in ovarian cancer. *Gynecologic Oncology*, *127*(2), 420–425. https://doi.org/10.1016/j.ygyno.2012.08.017
119. Ferrick, D. A., Neilson, A., & Beeson, C. (2008). Advances in measuring cellular bioenergetics using extracellular flux. *Drug Discovery Today*, *13*(5–6), 268–274. https://doi.org/10.1016/j.drudis.2007.12.008
120. Fischer, R. S., Lam, P.-Y., Huttenlocher, A., & Waterman, C. M. (2019). Filopodia and focal adhesions: An integrated system driving branching morphogenesis in neuronal pathfinding and angiogenesis. *Developmental Biology*, *451*(1), 86–95. https://doi.org/10.1016/j.ydbio.2018.08.015
121. Flem-Karlsen, K., Fodstad, Ø., Tan, M., & Nunes-Xavier, C. E. (2018). B7-H3 in Cancer – Beyond Immune Regulation. *Trends in Cancer*, *4*(6), 401–404. https://doi.org/10.1016/j.trecan.2018.03.010
122. Flem-Karlsen, K., Tekle, C., Andersson, Y., Flatmark, K., Fodstad, Ø., & Nunes-Xavier, C. E. (2017). Immunoregulatory protein B7-H3 promotes growth and decreases sensitivity to therapy in metastatic melanoma cells. *Pigment Cell & Melanoma Research*, *30*(5), 467–476. https://doi.org/10.1111/pcmr.12599
123. Flem-Karlsen, K., Tekle, C., Øyjord, T., Flørenes, V. A., Mælandsmo, G. M., Fodstad, Ø., & Nunes-Xavier, C. E. (2019). p38 MAPK activation through B7-H3-mediated DUSP10 repression promotes chemoresistance. *Scientific Reports*, *9*(1), 5839. https://doi.org/10.1038/s41598-019-42303-w
124. Flies, D. B., Han, X., Higuchi, T., Zheng, L., Sun, J., Ye, J. J., & Chen, L. (2014). Coinhibitory receptor PD-1H preferentially suppresses CD4+ T cell–mediated immunity. *Journal of Clinical Investigation*, *124*(5), 1966–1975. https://doi.org/10.1172/JCI74589
125. Floryk, D., & Huberman, E. (2006). Mycophenolic acid-induced replication arrest, differentiation markers and cell death of androgen-independent prostate cancer cells DU145. *Cancer Letters*, *231*(1), 20–29. https://doi.org/10.1016/j.canlet.2005.01.006
126. Floryk, D., Tollaksen, S. L., Giometti, C. S., & Huberman, E. (2004). Differentiation of Human Prostate Cancer PC-3 Cells Induced by Inhibitors of Inosine 5'-Monophosphate

Dehydrogenase. *Cancer Research*, *64*(24), 9049–9056. https://doi.org/10.1158/0008-5472.CAN-04-1553

127. Foster, D. A., Yellen, P., Xu, L., & Saqcena, M. (2010). Regulation of G1 Cell Cycle Progression: Distinguishing the Restriction Point from a Nutrient-Sensing Cell Growth Checkpoint(s). *Genes & Cancer*, *1*(11), 1124–1131. https://doi.org/10.1177/1947601910392989

128. Franchina, D. G., Dostert, C., & Brenner, D. (2018). Reactive Oxygen Species: Involvement in T Cell Signaling and Metabolism. *Trends in Immunology*, *39*(6), 489–502. https://doi.org/10.1016/j.it.2018.01.005

129. Francis, J. W., Turn, R. E., Newman, L. E., Schiavon, C., & Kahn, R. A. (2016). Higher order signaling: ARL2 as regulator of both mitochondrial fusion and microtubule dynamics allows integration of 2 essential cell functions. *Small GTPases*, *7*(4), 188–196. https://doi.org/10.1080/21541248.2016.1211069

130. Franssen, L. C., Lorenzi, T., Burgess, A. E. F., & Chaplain, M. A. J. (2019). A Mathematical Framework for Modelling the Metastatic Spread of Cancer. *Bulletin of Mathematical Biology*, *81*(6), 1965–2010. https://doi.org/10.1007/s11538-019-00597-x

131. Freeman, G. J., Long, A. J., Iwai, Y., Bourque, K., Chernova, T., Nishimura, H., Fitz, L. J., Malenkovich, N., Okazaki, T., Byrne, M. C., Horton, H. F., Fouser, L., Carter, L., Ling, V., Bowman, M. R., Carreno, B. M., Collins, M., Wood, C. R., & Honjo, T. (2000). Engagement of the Pd-1 Immunoinhibitory Receptor by a Novel B7 Family Member Leads to Negative Regulation of Lymphocyte Activation. *Journal of Experimental Medicine*, *192*(7), 1027–1034. https://doi.org/10.1084/jem.192.7.1027

132. Fried, R., Carlton, R. M., & Fried, D. A. (2021). Tumor starvation by L-arginine deprivation. In *Starving Cancer Cells: Evidence-Based Strategies to Slow Cancer Progression* (pp. 25–111). Elsevier. https://doi.org/10.1016/B978-0-12-824013-7.00005-5

133. Gadadhar, S., Dadi, H., Bodakuntla, S., Schnitzler, A., Bièche, I., Rusconi, F., & Janke, C. (2017). Tubulin glycylation controls primary cilia length. *Journal of Cell Biology*, *216*(9), 2701–2713. https://doi.org/10.1083/jcb.201612050

134. Gaddi, A. V., Galuppo, P., & Yang, J. (2017). Creatine Phosphate Administration in Cell Energy Impairment Conditions: A Summary of Past and Present Research. *Heart, Lung and Circulation*, *26*(10), 1026–1035. https://doi.org/10.1016/j.hlc.2016.12.020

135. Gadiyar, V., Lahey, K. C., Calianese, D., Devoe, C., Mehta, D., Bono, K., Desind, S., Davra, V., & Birge, R. B. (2020). Cell Death in the Tumor Microenvironment: Implications for Cancer Immunotherapy. *Cells*, *9*(10), 2207. https://doi.org/10.3390/cells9102207

136. Garcia, M. A., Nelson, W. J., & Chavez, N. (2018). Cell–Cell Junctions Organize Structural and Signaling Networks. *Cold Spring Harbor Perspectives in Biology*, *10*(4), a029181. https://doi.org/10.1101/cshperspect.a029181

137. Gardel, M. L., Schneider, I. C., Aratyn-Schaus, , Yvonne, & Waterman, C. M. (2010). Mechanical Integration of Actin and Adhesion Dynamics in Cell Migration. *Annual Review of Cell and Developmental Biology*, *26*(1), 315–333. https://doi.org/10.1146/annurev.cellbio.011209.122036

138. Garon, E. B., Rizvi, N. A., Hui, R., Leighl, N., Balmanoukian, A. S., Eder, J. P., Patnaik, A., Aggarwal, C., Gubens, M., Horn, L., Carcereny, E., Ahn, M.-J., Felip, E., Lee, J.-S., Hellmann, M. D., Hamid, O., Goldman, J. W., Soria, J.-C., Dolled-Filhart, M., … Gandhi, L. (2015). Pembrolizumab for the Treatment of Non–Small-Cell Lung Cancer. *New England Journal of Medicine*, *372*(21), 2018–2028. https://doi.org/10.1056/NEJMoa1501824

139. Geiger, B., & Yamada, K. M. (2011). Molecular Architecture and Function of Matrix Adhesions. *Cold Spring Harbor Perspectives in Biology*, *3*(5), a005033–a005033. https://doi.org/10.1101/cshperspect.a005033

140. Geppert, E. F., Williams, M. C., & Mason, R. J. (1980). Primary culture of rat alveolar type II cells on floating collagen membranes. *Experimental Cell Research*, *128*(2), 363–374. https://doi.org/10.1016/0014-4827(80)90072-5

141. Giard, D. J., Aaronson, S. A., Todaro, G. J., Arnstein, P., Kersey, J. H., Dosik, H., & Parks, W. P. (1973). In Vitro Cultivation of Human Tumors: Establishment of Cell Lines Derived From a Series of Solid Tumors2. *JNCI: Journal of the National Cancer Institute*, *51*(5), 1417–1423. https://doi.org/10.1093/jnci/51.5.1417

142. Gigante, E. D., Taylor, M. R., Ivanova, A. A., Kahn, R. A., & Caspary, T. (2020). ARL13B regulates Sonic hedgehog signaling from outside primary cilia. *ELife*, *9*. https://doi.org/10.7554/eLife.50434

143. Gluenz, E., Höög, J. L., Smith, A. E., Dawe, H. R., Shaw, M. K., & Gull, K. (2010a). Beyond 9+0: noncanonical axoneme structures characterize sensory cilia from protists to humans. *The FASEB Journal*, *24*(9), 3117–3121. https://doi.org/10.1096/fj.09-151381

144. Gluenz, E., Höög, J. L., Smith, A. E., Dawe, H. R., Shaw, M. K., & Gull, K. (2010b). Beyond 9+0: noncanonical axoneme structures characterize sensory cilia from protists to humans. *The FASEB Journal*, *24*(9), 3117–3121. https://doi.org/10.1096/fj.09-151381

145. González-Mariscal, L., Betanzos, A., Nava, P., & Jaramillo, B. E. (2003). Tight junction proteins. *Progress in Biophysics and Molecular Biology*, *81*(1), 1–44. https://doi.org/10.1016/S0079-6107(02)00037-8

146. Gonzalez-Uarquin, F., Rodehutscord, M., & Huber, K. (2020). Myo-inositol: its metabolism and potential implications for poultry nutrition—a review. *Poultry Science*, *99*(2), 893–905. https://doi.org/10.1016/j.psj.2019.10.014

147. Gooding, J. M., Yap, K. L., & Ikura, M. (2004). The cadherin-catenin complex as a focal point of cell adhesion and signalling: new insights from three-dimensional structures. *BioEssays*, *26*(5), 497–511. https://doi.org/10.1002/bies.20033

148. Goodman, A., Patel, S. P., & Kurzrock, R. (2017). PD-1–PD-L1 immune-checkpoint blockade in B-cell lymphomas. *Nature Reviews Clinical Oncology*, *14*(4), 203–220. https://doi.org/10.1038/nrclinonc.2016.168

149. Goodwin, K., Lostchuck, E. E., Cramb, K. M. L., Zulueta-Coarasa, T., Fernandez-Gonzalez, R., & Tanentzapf, G. (2017). Cell–cell and cell–extracellular matrix adhesions cooperate to organize actomyosin networks and maintain force transmission during dorsal closure. *Molecular Biology of the Cell*, *28*(10), 1301–1310. https://doi.org/10.1091/mbc.e17-01-0033

150. Goto, H., Inoko, A., & Inagaki, M. (2013). Cell cycle progression by the repression of primary cilia formation in proliferating cells. *Cellular and Molecular Life Sciences*, *70*(20), 3893–3905. https://doi.org/10.1007/s00018-013-1302-8

151. Gotthardt, K., Lokaj, M., Koerner, C., Falk, N., Gießl, A., & Wittinghofer, A. (2015). A G-protein activation cascade from Arl13B to Arl3 and implications for ciliary targeting of lipidated proteins. *ELife*, *4*. https://doi.org/10.7554/eLife.11859

152. Grisanti, L., Revenkova, E., Gordon, R. E., & Iomini, C. (2016). Primary cilia maintain corneal epithelial homeostasis by regulation of the Notch signaling pathway. *Development*. https://doi.org/10.1242/dev.132704

153. Gu, C., Mao, X., Chen, D., Yu, B., & Yang, Q. (2019). Isoleucine Plays an Important Role for Maintaining Immune Function. *Current Protein & Peptide Science*, *20*(7), 644–651. https://doi.org/10.2174/1389203720666190305163135
154. Guillemot, L., Paschoud, S., Pulimeno, P., Foglia, A., & Citi, S. (2008). The cytoplasmic plaque of tight junctions: A scaffolding and signalling center. *Biochimica et Biophysica Acta (BBA) - Biomembranes*, *1778*(3), 601–613. https://doi.org/10.1016/j.bbamem.2007.09.032
155. Gunter, J. H., Thomas, E. C., Lengefeld, N., Kruger, S. J., Worton, L., Gardiner, E. M., Jones, A., Barnett, N. L., & Whitehead, J. P. (2008). Characterisation of inosine monophosphate dehydrogenase expression during retinal development: Differences between variants and isoforms. *The International Journal of Biochemistry & Cell Biology*, *40*(9), 1716–1728. https://doi.org/10.1016/j.biocel.2007.12.018
156. Gurski, L. A., Petrelli, N. J., Jia, X., & Farach-Carson, M. C. (2010). 3D Matrices for Anti-Cancer Drug Testing and Development. *Oncology Issues*, *25*(1), 20–25. https://doi.org/10.1080/10463356.2010.11883480
157. Ha, K., Nobuhara, M., Wang, Q., Walker, R. v, Qian, F., Schartner, C., Cao, E., & Delling, M. (2020). The heteromeric PC-1/PC-2 polycystin complex is activated by the PC-1 N-terminus. *ELife*, *9*. https://doi.org/10.7554/eLife.60684
158. Haga, R. B., & Ridley, A. J. (2016). Rho GTPases: Regulation and roles in cancer cell biology. *Small GTPases*, *7*(4), 207–221. https://doi.org/10.1080/21541248.2016.1232583
159. Halbleib, J. M., & Nelson, W. J. (2006). Cadherins in development: cell adhesion, sorting, and tissue morphogenesis. *Genes & Development*, *20*(23), 3199–3214. https://doi.org/10.1101/gad.1486806
160. Hall, A. (1998). Rho GTPases and the Actin Cytoskeleton. *Science*, *279*(5350), 509–514. https://doi.org/10.1126/science.279.5350.509
161. Han, Y., Liu, D., & Li, L. (2020). PD-1/PD-L1 pathway: current researches in cancer. *American Journal of Cancer Research*, *10*(3), 727–742.
162. Hanahan, D., & Weinberg, R. A. (2011). Hallmarks of Cancer: The Next Generation. *Cell*, *144*(5), 646–674. https://doi.org/10.1016/j.cell.2011.02.013
163. Hanna, S. J., McCoy-Simandle, K., Miskolci, V., Guo, P., Cammer, M., Hodgson, L., & Cox, D. (2017). The Role of Rho-GTPases and actin polymerization during Macrophage Tunneling Nanotube Biogenesis. *Scientific Reports*, *7*(1), 8547. https://doi.org/10.1038/s41598-017-08950-7
164. Hapach, L. A., Mosier, J. A., Wang, W., & Reinhart-King, C. A. (2019). Engineered models to parse apart the metastatic cascade. *Npj Precision Oncology*, *3*(1), 20. https://doi.org/10.1038/s41698-019-0092-3
165. Harris, T. J. C. (2012). Adherens junction assembly and function in the Drosophila embryo. *International Review of Cell and Molecular Biology*, *293*, 45–83. https://doi.org/10.1016/B978-0-12-394304-0.00007-5
166. Hartsock, A., & Nelson, W. J. (2008). Adherens and tight junctions: Structure, function and connections to the actin cytoskeleton. *Biochimica et Biophysica Acta (BBA) - Biomembranes*, *1778*(3), 660–669. https://doi.org/10.1016/j.bbamem.2007.07.012
167. Hashiguchi, M., Kobori, H., Ritprajak, P., Kamimura, Y., Kozono, H., & Azuma, M. (2008). Triggering receptor expressed on myeloid cell-like transcript 2 (TLT-2) is a counter-receptor for B7-H3 and enhances T cell responses. *Proceedings of the National Academy of Sciences*, *105*(30), 10495–10500. https://doi.org/10.1073/pnas.0802423105
168. He, Y., Zheng, Z., Xu, Y., Weng, H., Gao, Y., Qin, K., Rong, J., Chen, C., Yun, M., Zhang, J., & Ye, S. (2018). Over-expression of IMPDH2 is associated with tumor progression and poor

prognosis in hepatocellular carcinoma. *American Journal of Cancer Research*, *8*(8), 1604–1614.

169. Hedstrom, L. (2009). IMP Dehydrogenase: Structure, Mechanism, and Inhibition. *Chemical Reviews*, *109*(7), 2903–2928. https://doi.org/10.1021/cr900021w

170. Hellou, J., Ross, N. W., & Moon, T. W. (2012). Glutathione, glutathione S-transferase, and glutathione conjugates, complementary markers of oxidative stress in aquatic biota. *Environmental Science and Pollution Research*, *19*(6), 2007–2023. https://doi.org/10.1007/s11356-012-0909-x

171. Herbst, R. S., Morgensztern, D., & Boshoff, C. (2018). The biology and management of non-small cell lung cancer. *Nature*, *553*(7689), 446–454. https://doi.org/10.1038/nature25183

172. Heuberger, J., & Birchmeier, W. (2010). Interplay of Cadherin-Mediated Cell Adhesion and Canonical Wnt Signaling. *Cold Spring Harbor Perspectives in Biology*, *2*(2), a002915–a002915. https://doi.org/10.1101/cshperspect.a002915

173. Hiddinga, B. I., Raskin, J., Janssens, A., Pauwels, P., & van Meerbeeck, J. P. (2021). Recent developments in the treatment of small cell lung cancer. *European Respiratory Review*, *30*(161), 210079. https://doi.org/10.1183/16000617.0079-2021

174. Higgins, M., Obaidi, I., & McMorrow, T. (2019). Primary cilia and their role in cancer (Review). *Oncology Letters*. https://doi.org/10.3892/ol.2019.9942

175. Hoffman, L., Jensen, C. C., Yoshigi, M., & Beckerle, M. (2017). Mechanical signals activate p38 MAPK pathway-dependent reinforcement of actin via mechanosensitive HspB1. *Molecular Biology of the Cell*, *28*(20), 2661–2675. https://doi.org/10.1091/mbc.e17-02-0087

176. Hohmann, & Dehghani. (2019). The Cytoskeleton—A Complex Interacting Meshwork. *Cells*, *8*(4), 362. https://doi.org/10.3390/cells8040362

177. Huang, C., Li, H., Feng, Y., Li, X., Zhang, Z., Jiang, C., Wang, J., Yang, C., Fu, Y., Mu, M., Zhao, S., Wang, Z., Kuang, Y., Hou, H., Wang, Y., Guo, W., Xu, J., Yang, H., Zhou, L., … Guo, G. (2020). Combination therapy with B7H3-redirected bispecific antibody and Sorafenib elicits enhanced synergistic antitumor efficacy. *Theranostics*, *10*(23), 10498–10512. https://doi.org/10.7150/thno.49480

178. Huang, C., ZHOU, L., CHANG, X., PANG, X., ZHANG, H., & ZHANG, S. (2016). B7-H3, B7-H4, Foxp3 and IL-2 expression in cervical cancer: Associations with patient outcome and clinical significance. *Oncology Reports*, *35*(4), 2183–2190. https://doi.org/10.3892/or.2016.4607

179. Huang, F., Ni, M., Chalishazar, M. D., Huffman, K. E., Kim, J., Cai, L., Shi, X., Cai, F., Zacharias, L. G., Ireland, A. S., Li, K., Gu, W., Kaushik, A. K., Liu, X., Gazdar, A. F., Oliver, T. G., Minna, J. D., Hu, Z., & DeBerardinis, R. J. (2018). Inosine Monophosphate Dehydrogenase Dependence in a Subset of Small Cell Lung Cancers. *Cell Metabolism*, *28*(3), 369-382.e5. https://doi.org/10.1016/j.cmet.2018.06.005

180. Huang, M., Ji, Y., Itahana, K., Zhang, Y., & Mitchell, B. (2008). Guanine nucleotide depletion inhibits pre-ribosomal RNA synthesis and causes nucleolar disruption. *Leukemia Research*, *32*(1), 131–141. https://doi.org/10.1016/j.leukres.2007.03.025

181. Huang, P., Nedelcu, D., Watanabe, M., Jao, C., Kim, Y., Liu, J., & Salic, A. (2016). Cellular Cholesterol Directly Activates Smoothened in Hedgehog Signaling. *Cell*, *166*(5), 1176-1187.e14. https://doi.org/10.1016/j.cell.2016.08.003

182. Hudson, L. E., Anderson, S. E., Corbett, A. H., & Lamb, T. J. (2017). Gleaning Insights from Fecal Microbiota Transplantation and Probiotic Studies for the Rational Design of Combination Microbial Therapies. *Clinical Microbiology Reviews*, *30*(1), 191–231. https://doi.org/10.1128/CMR.00049-16

183. Hurst, I. R., Zuo, J., Jiang, J., & Holliday, L. S. (2003). Actin-Related Protein 2/3 Complex Is Required for Actin Ring Formation. *Journal of Bone and Mineral Research*, *19*(3), 499–506. https://doi.org/10.1359/JBMR.0301238

184. Hurwitz, S. N., Cheerathodi, M. R., Nkosi, D., York, S. B., & Meckes, D. G. (2018). Tetraspanin CD63 Bridges Autophagic and Endosomal Processes To Regulate Exosomal Secretion and Intracellular Signaling of Epstein-Barr Virus LMP1. *Journal of Virology*, *92*(5). https://doi.org/10.1128/JVI.01969-17

185. Inamura, K., Amori, G., Yuasa, T., Yamamoto, S., Yonese, J., & Ishikawa, Y. (2019). Relationship of B7-H3 expression in tumor cells and tumor vasculature with FOXP3+ regulatory T cells in renal cell carcinoma . *Cancer Management and Research*, *Volume 11*, 7021–7030. https://doi.org/10.2147/CMAR.S209205

186. Ingebrigtsen, V. A., Boye, K., Tekle, C., Nesland, J. M., Flatmark, K., & Fodstad, Ø. (2012). B7-H3 expression in colorectal cancer: Nuclear localization strongly predicts poor outcome in colon cancer. *International Journal of Cancer*, *131*(11), 2528–2536. https://doi.org/10.1002/ijc.27566

187. Ishimoto, T., Nagano, O., Yae, T., Tamada, M., Motohara, T., Oshima, H., Oshima, M., Ikeda, T., Asaba, R., Yagi, H., Masuko, T., Shimizu, T., Ishikawa, T., Kai, K., Takahashi, E., Imamura, Y., Baba, Y., Ohmura, M., Suematsu, M., … Saya, H. (2011). CD44 Variant Regulates Redox Status in Cancer Cells by Stabilizing the xCT Subunit of System xc− and Thereby Promotes Tumor Growth. *Cancer Cell*, *19*(3), 387–400. https://doi.org/10.1016/j.ccr.2011.01.038

188. Ishitsuka, K., Hideshima, T., Hamasaki, M., Raje, N., Kumar, S., Podar, K., le Gouill, S., Shiraishi, N., Yasui, H., Roccaro, A. M., Tai, Y.-Z., Chauhan, D., Fram, R., Tamura, K., Jain, J., & Anderson, K. C. (2005). Novel inosine monophosphate dehydrogenase inhibitor VX-944 induces apoptosis in multiple myeloma cells primarily via caspase-independent AIF/Endo G pathway. *Oncogene*, *24*(38), 5888–5896. https://doi.org/10.1038/sj.onc.1208739

189. Ito, T., Ueno, T., Clarkson, M. R., Yuan, X., Jurewicz, M. M., Yagita, H., Azuma, M., Sharpe, A. H., Auchincloss, H., Sayegh, M. H., & Najafian, N. (2005). Analysis of the Role of Negative T Cell Costimulatory Pathways in CD4 and CD8 T Cell-Mediated Alloimmune Responses In Vivo. *The Journal of Immunology*, *174*(11), 6648–6656. https://doi.org/10.4049/jimmunol.174.11.6648

190. Izawa, I., Goto, H., Kasahara, K., & Inagaki, M. (2015). Current topics of functional links between primary cilia and cell cycle. *Cilia*, *4*(1), 12. https://doi.org/10.1186/s13630-015-0021-1

191. Jain, J., Almquist, S. J., Ford, P. J., Shlyakhter, D., Wang, Y., Nimmesgern, E., & Germann, U. A. (2004). Regulation of inosine monophosphate dehydrogenase type I and type II isoforms in human lymphocytes. *Biochemical Pharmacology*, *67*(4), 767–776. https://doi.org/10.1016/j.bcp.2003.09.043

192. Jaiswal, M., Fansa, E. K., Kösling, S. K., Mejuch, T., Waldmann, H., & Wittinghofer, A. (2016). Novel Biochemical and Structural Insights into the Interaction of Myristoylated Cargo with Unc119 Protein and Their Release by Arl2/3. *Journal of Biological Chemistry*, *291*(39), 20766–20778. https://doi.org/10.1074/jbc.M116.741827

193. Jamora, C., & Fuchs, E. (2002). Intercellular adhesion, signalling and the cytoskeleton. *Nature Cell Biology*, *4*(4), E101–E108. https://doi.org/10.1038/ncb0402-e101

194. Janiszewska, M., Primi, M. C., & Izard, T. (2020). Cell adhesion in cancer: Beyond the migration of single cells. *Journal of Biological Chemistry*, *295*(8), 2495–2505. https://doi.org/10.1074/jbc.REV119.007759

195. Ji, Y., Gu, J., Makhov, A. M., Griffith, J. D., & Mitchell, B. S. (2006). Regulation of the Interaction of Inosine Monophosphate Dehydrogenase with Mycophenolic Acid by GTP. *Journal of Biological Chemistry*, *281*(1), 206–212. https://doi.org/10.1074/jbc.M507056200
196. Jiang, B., Liu, F., Liu, Z., Zhang, T., & Hua, D. (2016). B7-H3 increases thymidylate synthase expression via the PI3k-Akt pathway. *Tumor Biology*, *37*(7), 9465–9472. https://doi.org/10.1007/s13277-015-4740-0
197. Jiang, B., Zhang, T., Liu, F., Sun, Z., Shi, H., Hua, D., & Yang, C. (2016). The co-stimulatory molecule B7-H3 promotes the epithelial-mesenchymal transition in colorectal cancer. *Oncotarget*, *7*(22), 31755–31771. https://doi.org/10.18632/oncotarget.9035
198. Jin, Y., Zhang, P., Li, J., Zhao, J., Liu, C., Yang, F., Yang, D., Gao, A., Lin, W., Ma, X., & Sun, Y. (2015). B7-H3 in combination with regulatory T cell is associated with tumor progression in primary human non-small cell lung cancer. *International Journal of Clinical and Experimental Pathology*, *8*(11), 13987–13995.
199. Johnson, M. C., & Kollman, J. M. (2020). Cryo-EM structures demonstrate human IMPDH2 filament assembly tunes allosteric regulation. *ELife*, *9*. https://doi.org/10.7554/eLife.53243
200. Juda, P., Šmigová, J., Kováčik, L., Bártová, E., & Raška, I. (2014). Ultrastructure of Cytoplasmic and Nuclear Inosine-5'-Monophosphate Dehydrogenase 2 "Rods and Rings" Inclusions. *Journal of Histochemistry & Cytochemistry*, *62*(10), 739–750. https://doi.org/10.1369/0022155414543853
201. Jurczyk, A., Gromley, A., Redick, S., Agustin, J. S., Witman, G., Pazour, G. J., Peters, D. J. M., & Doxsey, S. (2004). Pericentrin forms a complex with intraflagellar transport proteins and polycystin-2 and is required for primary cilia assembly. *Journal of Cell Biology*, *166*(5), 637–643. https://doi.org/10.1083/jcb.200405023
202. Kaihara, T., Kusaka, T., Nishi, M., Kawamata, H., Imura, J., Kitajima, K., Itoh-Minami, R., Aoyama, N., Kasuga, M., Oda, Y., Hattori, M., & Fujimori, T. (2003). Dedifferentiation and decreased expression of adhesion molecules, E-cadherin and ZO-1, in colorectal cancer are closely related to liver metastasis. *Journal of Experimental & Clinical Cancer Research : CR*, *22*(1), 117–123.
203. Kanai, T., Totsuka, T., Uraushihara, K., Makita, S., Nakamura, T., Koganei, K., Fukushima, T., Akiba, H., Yagita, H., Okumura, K., Machida, U., Iwai, H., Azuma, M., Chen, L., & Watanabe, M. (2003). Blockade of B7-H1 Suppresses the Development of Chronic Intestinal Inflammation. *The Journal of Immunology*, *171*(8), 4156–4163. https://doi.org/10.4049/jimmunol.171.8.4156
204. Kanayama, T., Miyachi, M., Sugimoto, Y., Yagyu, S., Kikuchi, K., Tsuchiya, K., Iehara, T., & Hosoi, H. (2021). Reduced B7-H3 expression by PAX3-FOXO1 knockdown inhibits cellular motility and promotes myogenic differentiation in alveolar rhabdomyosarcoma. *Scientific Reports*, *11*(1), 18802. https://doi.org/10.1038/s41598-021-98322-z
205. Kanchan, R. K., Doss, D., Khan, P., Nasser, Mohd. W., & Mahapatra, S. (2022). To kill a cancer: Targeting the immune inhibitory checkpoint molecule, B7-H3. *Biochimica et Biophysica Acta (BBA) - Reviews on Cancer*, 188783. https://doi.org/10.1016/j.bbcan.2022.188783
206. Kang, F., Wang, L., Jia, H., Li, D., Li, H., Zhang, Y., & Sun, D. (2015). B7-H3 promotes aggression and invasion of hepatocellular carcinoma by targeting epithelial-to-mesenchymal transition via JAK2/STAT3/Slug signaling pathway. *Cancer Cell International*, *15*(1), 45. https://doi.org/10.1186/s12935-015-0195-z

207. Katayama. (2011). Expression of B7-H3 in hypopharyngeal squamous cell carcinoma as a predictive indicator for tumor metastasis and prognosis. *International Journal of Oncology*, *38*(5). https://doi.org/10.3892/ijo.2011.949
208. Katsumi, A., Orr, A. W., Tzima, E., & Schwartz, M. A. (2004). Integrins in Mechanotransduction. *Journal of Biological Chemistry*, *279*(13), 12001–12004. https://doi.org/10.1074/jbc.R300038200
209. Kendsersky, N. M., Lindsay, J., Kolb, E. A., Smith, M. A., Teicher, B. A., Erickson, S. W., Earley, E. J., Mosse, Y. P., Martinez, D., Pogoriler, J., Krytska, K., Patel, K., Groff, D., Tsang, M., Ghilu, S., Wang, Y., Seaman, S., Feng, Y., Croix, B. st., … Maris, J. M. (2021). The B7-H3–Targeting Antibody–Drug Conjugate m276-SL-PBD Is Potently Effective Against Pediatric Cancer Preclinical Solid Tumor Models. *Clinical Cancer Research*, *27*(10), 2938–2946. https://doi.org/10.1158/1078-0432.CCR-20-4221
210. Kenfield, S. A., Wei, E. K., Stampfer, M. J., Rosner, B. A., & Colditz, G. A. (2008). Comparison of aspects of smoking among the four histological types of lung cancer. *Tobacco Control*, *17*(3), 198–204. https://doi.org/10.1136/tc.2007.022582
211. Kengaku, M. (2018). Cytoskeletal control of nuclear migration in neurons and non-neuronal cells. *Proceedings of the Japan Academy, Series B*, *94*(9), 337–349. https://doi.org/10.2183/pjab.94.022
212. Kennel, K. B., & Greten, F. R. (2021). Immune cell - produced ROS and their impact on tumor growth and metastasis. *Redox Biology*, *42*, 101891. https://doi.org/10.1016/j.redox.2021.101891
213. Keppeke, G. D., Andrade, L. E. C., Grieshaber, S. S., & Chan, E. K. L. (2015). Microinjection of specific anti-IMPDH2 antibodies induces disassembly of cytoplasmic rods/rings that are primarily stationary and stable structures. *Cell & Bioscience*, *5*(1), 1. https://doi.org/10.1186/2045-3701-5-1
214. Keppeke, G. D., Calise, S. J., Chan, E. K. L., & Andrade, L. E. C. (2015). Assembly of IMPDH2-Based, CTPS-Based, and Mixed Rod/Ring Structures Is Dependent on Cell Type and Conditions of Induction. *Journal of Genetics and Genomics*, *42*(6), 287–299. https://doi.org/10.1016/j.jgg.2015.04.002
215. Keppeke, G. D., Chang, C. C., Peng, M., Chen, L.-Y., Lin, W.-C., Pai, L.-M., Andrade, L. E. C., Sung, L.-Y., & Liu, J.-L. (2018). IMP/GTP balance modulates cytoophidium assembly and IMPDH activity. *Cell Division*, *13*(1), 5. https://doi.org/10.1186/s13008-018-0038-0
216. Keppeke, G. D., Prado, M. S., Nunes, E., Perazzio, S. F., Rodrigues, S. H., Ferraz, M. L. G., Chan, E. K. L., & Andrade, L. E. C. (2016). Differential capacity of therapeutic drugs to induce Rods/Rings structures in vitro and in vivo and generation of anti-Rods/Rings autoantibodies. *Clinical Immunology*, *173*, 149–156. https://doi.org/10.1016/j.clim.2016.10.004
217. Khaitan, D., Chandna, S., Arya, M., & Dwarakanath, B. (2006). Establishment and characterization of multicellular spheroids from a human glioma cell line; Implications for tumor therapy. *Journal of Translational Medicine*, *4*(1), 12. https://doi.org/10.1186/1479-5876-4-12
218. Khalifa, A. A. Z., Ichikawa, M., Dai, D., Kubo, S., Black, C. S., Peri, K., McAlear, T. S., Veyron, S., Yang, S. K., Vargas, J., Bechstedt, S., Trempe, J.-F., & Bui, K. H. (2020). The inner junction complex of the cilia is an interaction hub that involves tubulin post-translational modifications. *ELife*, *9*. https://doi.org/10.7554/eLife.52760
219. Khan, N., Pantakani, D. V. K., Binder, L., Qasim, M., & Asif, A. R. (2015). Immunosuppressant MPA Modulates Tight Junction through Epigenetic Activation of

MLCK/MLC-2 Pathway via p38MAPK. *Frontiers in Physiology*, *6*. https://doi.org/10.3389/fphys.2015.00381

220. Khatami, F., Aghamir, S. M. K., & Tavangar, S. M. (2019). Oncometabolites: A new insight for oncology. *Molecular Genetics & Genomic Medicine*, *7*(9). https://doi.org/10.1002/mgg3.873

221. Khramtsov, A. I., Khramtsova, G. F., Tretiakova, M., Huo, D., Olopade, O. I., & Goss, K. H. (2010). Wnt/β-Catenin Pathway Activation Is Enriched in Basal-Like Breast Cancers and Predicts Poor Outcome. *The American Journal of Pathology*, *176*(6), 2911–2920. https://doi.org/10.2353/ajpath.2010.091125

222. Kiesel, P., Alvarez Viar, G., Tsoy, N., Maraspini, R., Gorilak, P., Varga, V., Honigmann, A., & Pigino, G. (2020). The molecular structure of mammalian primary cilia revealed by cryo-electron tomography. *Nature Structural & Molecular Biology*, *27*(12), 1115–1124. https://doi.org/10.1038/s41594-020-0507-4

223. Kim, J., Jo, H., Hong, H., Kim, M. H., Kim, J. M., Lee, J.-K., Heo, W. do, & Kim, J. (2015). Actin remodelling factors control ciliogenesis by regulating YAP/TAZ activity and vesicle trafficking. *Nature Communications*, *6*(1), 6781. https://doi.org/10.1038/ncomms7781

224. Kim, S., & Dynlacht, B. D. (2013). Assembling a primary cilium. *Current Opinion in Cell Biology*, *25*(4), 506–511. https://doi.org/10.1016/j.ceb.2013.04.011

225. Kim, S., & Tsiokas, L. (2011). Cilia and cell cycle re-entry. *Cell Cycle*, *10*(16), 2683–2690. https://doi.org/10.4161/cc.10.16.17009

226. Kim, W. K., Kwon, Y., Jang, M., Park, M., Kim, J., Cho, S., Jang, D. G., Lee, W.-B., Jung, S. H., Choi, H. J., Min, B. S., il Kim, T., Hong, S. P., Paik, Y.-K., & Kim, H. (2019). β-catenin activation down-regulates cell-cell junction-related genes and induces epithelial-to-mesenchymal transition in colorectal cancers. *Scientific Reports*, *9*(1), 18440. https://doi.org/10.1038/s41598-019-54890-9

227. Klangjorhor, J., Chaiyawat, P., Teeyakasem, P., Sirikaew, N., Phanphaisarn, A., Settakorn, J., Lirdprapamongkol, K., Yama, S., Svasti, J., & Pruksakorn, D. (2020). Mycophenolic acid is a drug with the potential to be repurposed for suppressing tumor growth and metastasis in osteosarcoma treatment. *International Journal of Cancer*, *146*(12), 3397–3409. https://doi.org/10.1002/ijc.32735

228. Kleeff, J., Shi, X., Bode, H. P., Hoover, K., Shrikhande, S., Bryant, P. J., Korc, M., Büchler, M. W., & Friess, H. (2001). Altered Expression and Localization of the Tight Junction Protein ZO-1 in Primary and Metastatic Pancreatic Cancer. *Pancreas*, *23*(3), 259–265. https://doi.org/10.1097/00006676-200110000-00006

229. Knights, A. J., Funnell, A. P. W., Crossley, M., & Pearson, R. C. M. (2012). Holding Tight: Cell Junctions and Cancer Spread. *Trends in Cancer Research*, *8*, 61–69.

230. Kofuji, S., & Sasaki, A. T. (2020). GTP metabolic reprogramming by IMPDH2: unlocking cancer cells' fuelling mechanism. *The Journal of Biochemistry*, *168*(4), 319–328. https://doi.org/10.1093/jb/mvaa085

231. Koivunen, J. P., Mermel, C., Zejnullahu, K., Murphy, C., Lifshits, E., Holmes, A. J., Choi, H. G., Kim, J., Chiang, D., Thomas, R., Lee, J., Richards, W. G., Sugarbaker, D. J., Ducko, C., Lindeman, N., Marcoux, J. P., Engelman, J. A., Gray, N. S., Lee, C., … Jänne, P. A. (2008). *EML4-ALK* Fusion Gene and Efficacy of an ALK Kinase Inhibitor in Lung Cancer. *Clinical Cancer Research*, *14*(13), 4275–4283. https://doi.org/10.1158/1078-0432.CCR-08-0168

232. Kontos, F., Michelakos, T., Kurokawa, T., Sadagopan, A., Schwab, J. H., Ferrone, C. R., & Ferrone, S. (2021). B7-H3: An Attractive Target for Antibody-based Immunotherapy. *Clinical Cancer Research*, *27*(5), 1227–1235. https://doi.org/10.1158/1078-0432.CCR-20-2584

233. Koppenol, W. H., Bounds, P. L., & Dang, C. v. (2011). Otto Warburg's contributions to current concepts of cancer metabolism. *Nature Reviews Cancer*, *11*(5), 325–337. https://doi.org/10.1038/nrc3038
234. Kreymborg, K., Haak, S., Murali, R., Wei, J., Waitz, R., Gasteiger, G., Savage, P. A., van den Brink, M. R. M., & Allison, J. P. (2015). Ablation of B7-H3 but Not B7-H4 Results in Highly Increased Tumor Burden in a Murine Model of Spontaneous Prostate Cancer. *Cancer Immunology Research*, *3*(8), 849–854. https://doi.org/10.1158/2326-6066.CIR-15-0100
235. Kucinska, M., Plewinski, A., Szczolko, W., Kaczmarek, M., Goslinski, T., & Murias, M. (2021). Modeling the photodynamic effect in 2D versus 3D cell culture under normoxic and hypoxic conditions. *Free Radical Biology and Medicine*, *162*, 309–326. https://doi.org/10.1016/j.freeradbiomed.2020.10.304
236. Kurokawa, K., & Matsuda, M. (2005). Localized RhoA activation as a requirement for the induction of membrane ruffling. *Molecular Biology of the Cell*, *16*(9), 4294–4303. https://doi.org/10.1091/mbc.e04-12-1076
237. Kurokawa, K., Takaya, A., Terai, K., Fujioka, A., & Matsuda, M. (2004). Visualizing the Signal Transduction Pathways in Living Cells with GFP-Based FRET Probes. *ACTA HISTOCHEMICA ET CYTOCHEMICA*, *37*(6), 347–355. https://doi.org/10.1267/ahc.37.347
238. Kuser Abali, Gamze Noguchi, Fumihito Szeto, & Pacman Zhang, Y. H. C. B. C. K. P. G. C. C. M. M. S. Z. P. A. M. L. I. C. J. G. A. M. W. N. C. S. R. B. W. A. S. M. (2021). Cytosolic EZH2-IMPDH2 complex regulates melanoma progression and metastasis via GTP regulation. *BioRxiv*. https://doi.org/10.1101/2021.11.02.467024
239. Kyun, M.-L., Kim, S.-O., Lee, H. G., Hwang, J.-A., Hwang, J., Soung, N.-K., Cha-Molstad, H., Lee, S., Kwon, Y. T., Kim, B. Y., & Lee, K. H. (2020). Wnt3a Stimulation Promotes Primary Ciliogenesis through β-Catenin Phosphorylation-Induced Reorganization of Centriolar Satellites. *Cell Reports*, *30*(5), 1447-1462.e5. https://doi.org/10.1016/j.celrep.2020.01.019
240. Lagies, S., Schlimpert, M., Neumann, S., Wäldin, A., Kammerer, B., Borner, C., & Peintner, L. (2020). Cells grown in three-dimensional spheroids mirror in vivo metabolic response of epithelial cells. *Communications Biology*, *3*(1), 246. https://doi.org/10.1038/s42003-020-0973-6
241. Lai, X., Li, Q., Wu, F., Lin, J., Chen, J., Zheng, H., & Guo, L. (2020). Epithelial-Mesenchymal Transition and Metabolic Switching in Cancer: Lessons From Somatic Cell Reprogramming. *Frontiers in Cell and Developmental Biology*, *8*. https://doi.org/10.3389/fcell.2020.00760
242. Lamouille, S., Xu, J., & Derynck, R. (2014). Molecular mechanisms of epithelial–mesenchymal transition. *Nature Reviews Molecular Cell Biology*, *15*(3), 178–196. https://doi.org/10.1038/nrm3758
243. Lancaster, M. A., & Gleeson, J. G. (2009). The primary cilium as a cellular signaling center: lessons from disease. *Current Opinion in Genetics & Development*, *19*(3), 220–229. https://doi.org/10.1016/j.gde.2009.04.008
244. Larsen, J. E., & Minna, J. D. (2011). Molecular Biology of Lung Cancer: Clinical Implications. *Clinics in Chest Medicine*, *32*(4), 703–740. https://doi.org/10.1016/j.ccm.2011.08.003
245. Läsche, M., Emons, G., & Gründker, C. (2020). Shedding New Light on Cancer Metabolism: A Metabolic Tightrope Between Life and Death. *Frontiers in Oncology*, *10*. https://doi.org/10.3389/fonc.2020.00409
246. Latchman, Y., Wood, C. R., Chernova, T., Chaudhary, D., Borde, M., Chernova, I., Iwai, Y., Long, A. J., Brown, J. A., Nunes, R., Greenfield, E. A., Bourque, K., Boussiotis, V. A., Carter, L. L., Carreno, B. M., Malenkovich, N., Nishimura, H., Okazaki, T., Honjo, T., … Freeman, G. J.

(2001). PD-L2 is a second ligand for PD-1 and inhibits T cell activation. *Nature Immunology*, *2*(3), 261–268. https://doi.org/10.1038/85330

247. Lattao, R., Kovács, L., & Glover, D. M. (2017). The Centrioles,Centrosomes, Basal Bodies, and Cilia of *Drosophila melanogaster*. *Genetics*, *206*(1), 33–53. https://doi.org/10.1534/genetics.116.198168

248. Le, A. H., Yelland, T., Paul, N. R., Fort, L., Nikolaou, S., Ismail, S., & Machesky, L. M. (2021). CYRI-A limits invasive migration through macropinosome formation and integrin uptake regulation. *Journal of Cell Biology*, *220*(9). https://doi.org/10.1083/jcb.202012114

249. le Bras, S., & le Borgne, R. (2014). Epithelial cell division – multiplying without losing touch. *Journal of Cell Science*. https://doi.org/10.1242/jcs.151472

250. Lee, D. Y., Bowen, B. P., & Northen, T. R. (2010). Mass spectrometry—based metabolomics, analysis of metabolite-protein interactions, and imaging. *BioTechniques*, *49*(2), 557–565. https://doi.org/10.2144/000113451

251. Lee, H. S., Qi, Y., & Im, W. (2015). *Effects of N-glycosylation on protein conformation and dynamics: Protein Data Bank analysis and molecular dynamics simulation study*. https://doi.org/10.1038/srep08926

252. Lee, J. L., & Streuli, C. H. (2014). Integrins and epithelial cell polarity. *Journal of Cell Science*. https://doi.org/10.1242/jcs.146142

253. Lee, Y., Martin-Orozco, N., Zheng, P., Li, J., Zhang, P., Tan, H., Park, H. J., Jeong, M., Chang, S. H., Kim, B.-S., Xiong, W., Zang, W., Guo, L., Liu, Y., Dong, Z., Overwijk, W. W., Hwu, P., Yi, Q., Kwak, L., … Dong, C. (2017). Inhibition of the B7-H3 immune checkpoint limits tumor growth by enhancing cytotoxic lymphocyte function. *Cell Research*, *27*(8), 1034–1045. https://doi.org/10.1038/cr.2017.90

254. Lemjabbar-Alaoui, H., Hassan, O. U., Yang, Y.-W., & Buchanan, P. (2015). Lung cancer: Biology and treatment options. *Biochimica et Biophysica Acta (BBA) - Reviews on Cancer*, *1856*(2), 189–210. https://doi.org/10.1016/j.bbcan.2015.08.002

255. Lemke, D., Pfenning, P.-N., Sahm, F., Klein, A.-C., Kempf, T., Warnken, U., Schnölzer, M., Tudoran, R., Weller, M., Platten, M., & Wick, W. (2012). Costimulatory Protein 4IgB7H3 Drives the Malignant Phenotype of Glioblastoma by Mediating Immune Escape and Invasiveness. *Clinical Cancer Research*, *18*(1), 105–117. https://doi.org/10.1158/1078-0432.CCR-11-0880

256. Lemmens, B., & Lindqvist, A. (2019). DNA replication and mitotic entry: A brake model for cell cycle progression. *Journal of Cell Biology*, *218*(12), 3892–3902. https://doi.org/10.1083/jcb.201909032

257. Li, B., & Yang, L. (2021). Creatine in T Cell Antitumor Immunity and Cancer Immunotherapy. *Nutrients*, *13*(5), 1633. https://doi.org/10.3390/nu13051633

258. Li, D., Xiang, S., Shen, J., Xiao, M., Zhao, Y., Wu, X., Du, F., Ji, H., Li, M., Zhao, Q., Kaboli, P. J., Yang, X., Xiao, Z., Qin, B., & Wen, Q. (2020). Comprehensive understanding of B7 family in gastric cancer: expression profile, association with clinicopathological parameters and downstream targets. *International Journal of Biological Sciences*, *16*(4), 568–582. https://doi.org/10.7150/ijbs.39769

259. Li, G., Quan, Y., Che, F., & Wang, L. (2018). B7-H3 in tumors: friend or foe for tumor immunity? *Cancer Chemotherapy and Pharmacology*, *81*(2), 245–253. https://doi.org/10.1007/s00280-017-3508-1

260. Li, H.-X., Meng, Q.-P., Liu, W., Li, Y.-G., Zhang, H.-M., Bao, F.-C., Song, L.-L., & Li, H.-J. (2014). IMPDH2 mediate radioresistance and chemoresistance in osteosarcoma cells. *European Review for Medical and Pharmacological Sciences*, *18*(20), 3038–3044.

261. Li, J., Zhang, X., Hou, Z., Cai, S., Guo, Y., Sun, L., Li, A., Li, Q., Wang, E., & Miao, Y. (2022). P130cas-FAK interaction is essential for YAP-mediated radioresistance of non-small cell lung cancer. *Cell Death & Disease*, *13*(9), 783. https://doi.org/10.1038/s41419-022-05224-7
262. Li, Q., Leija, C., Rijo-Ferreira, F., Chen, J., Cestari, I., Stuart, K., Tu, B. P., & Phillips, M. A. (2015). GMP synthase is essential for viability and infectivity of *T rypanosoma brucei* despite a redundant purine salvage pathway. *Molecular Microbiology*, *97*(5), 1006–1020. https://doi.org/10.1111/mmi.13083
263. Li, Y., Guo, G., Song, J., Cai, Z., Yang, J., Chen, Z., Wang, Y., Huang, Y., & Gao, Q. (2017). B7-H3 Promotes the Migration and Invasion of Human Bladder Cancer Cells via the PI3K/Akt/STAT3 Signaling Pathway. *Journal of Cancer*, *8*(5), 816–824. https://doi.org/10.7150/jca.17759
264. Li, Y., Zhang, J., Han, S., Qian, Q., Chen, Q., Liu, L., & Zhang, Y. (2017). B7-H3 promotes the proliferation, migration and invasiveness of cervical cancer cells and is an indicator of poor prognosis. *Oncology Reports*, *38*(2), 1043–1050. https://doi.org/10.3892/or.2017.5730
265. Li, Z., Liu, J., Que, L., & Tang, X. (2019). The immunoregulatory protein B7-H3 promotes aerobic glycolysis in oral squamous carcinoma via PI3K/Akt/mTOR pathway. *Journal of Cancer*, *10*(23), 5770–5784. https://doi.org/10.7150/jca.29838
266. Liao, D., Wang, M., Liao, Y., Li, J., & Niu, T. (2019). A Review of Efficacy and Safety of Checkpoint Inhibitor for the Treatment of Acute Myeloid Leukemia. *Frontiers in Pharmacology*, *10*. https://doi.org/10.3389/fphar.2019.00609
267. Liberti, M. v., & Locasale, J. W. (2016). The Warburg Effect: How Does it Benefit Cancer Cells? *Trends in Biochemical Sciences*, *41*(3), 211–218. https://doi.org/10.1016/j.tibs.2015.12.001
268. Lilley, A. C., Major, L., Young, S., Stark, M. J. R., & Smith, T. K. (2014). The essential roles of cytidine diphosphate-diacylglycerol synthase in bloodstream form *<scp>T</scp> rypanosoma brucei. Molecular Microbiology*, *92*(3), 453–470. https://doi.org/10.1111/mmi.12553
269. Lim, J. P., & Gleeson, P. A. (2011). Macropinocytosis: an endocytic pathway for internalising large gulps. *Immunology & Cell Biology*, *89*(8), 836–843. https://doi.org/10.1038/icb.2011.20
270. Lin, Y.-C., Chen, B.-M., Lu, W.-C., Su, C.-I., Prijovich, Z. M., Chung, W.-C., Wu, P.-Y., Chen, K.-C., Lee, I.-C., Juan, T.-Y., & Roffler, S. R. (2013). The B7-1 Cytoplasmic Tail Enhances Intracellular Transport and Mammalian Cell Surface Display of Chimeric Proteins in the Absence of a Linear ER Export Motif. *PLoS ONE*, *8*(9), e75084. https://doi.org/10.1371/journal.pone.0075084
271. Liou, G.-Y., & Storz, P. (2010). Reactive oxygen species in cancer. *Free Radical Research*, *44*(5), 479–496. https://doi.org/10.3109/10715761003667554
272. Lipinski, B. (2011). Hydroxyl Radical and Its Scavengers in Health and Disease. *Oxidative Medicine and Cellular Longevity*, *2011*, 1–9. https://doi.org/10.1155/2011/809696
273. Liu, C., LIU, J., WANG, J., LIU, Y., ZHANG, F., LIN, W., GAO, A., SUN, M., WANG, Y., & SUN, Y. (2013). B7-H3 expression in ductal and lobular breast cancer and its association with IL-10. *Molecular Medicine Reports*, *7*(1), 134–138. https://doi.org/10.3892/mmr.2012.1158
274. Liu, C.-L., Zang, X.-X., Huang, H., Zhang, H., Wang, C., Kong, Y.-L., & Zhang, H.-Y. (2016). The expression of B7-H3 and B7-H4 in human gallbladder carcinoma and their clinical implications. *European Review for Medical and Pharmacological Sciences*, *20*(21), 4466–4473.
275. Liu, C.-Y., Lin, H.-H., Tang, M.-J., & Wang, Y.-K. (2015). Vimentin contributes to epithelial-mesenchymal transition cancer cell mechanics by mediating cytoskeletal

organization and focal adhesion maturation. *Oncotarget*, *6*(18), 15966–15983. https://doi.org/10.18632/oncotarget.3862

276. Liu, F., Zhang, T., Zou, S., JIANG, B., & HUA, D. (2015). B7-H3 promotes cell migration and invasion through the Jak2/Stat3/MMP9 signaling pathway in colorectal cancer. *Molecular Medicine Reports*, *12*(4), 5455–5460. https://doi.org/10.3892/mmr.2015.4050

277. Liu, H., Tekle, C., Chen, Y.-W., Kristian, A., Zhao, Y., Zhou, M., Liu, Z., Ding, Y., Wang, B., Mælandsmo, G. M., Nesland, J. M., Fodstad, O., & Tan, M. (2011). B7-H3 Silencing Increases Paclitaxel Sensitivity by Abrogating Jak2/Stat3 Phosphorylation. *Molecular Cancer Therapeutics*, *10*(6), 960–971. https://doi.org/10.1158/1535-7163.MCT-11-0072

278. Liu, J., Yang, S., Cao, B., Zhou, G., Zhang, F., Wang, Y., Wang, R., Zhu, L., Meng, Y., Hu, C., Liang, H., Lin, X., Zhu, K., Chen, G., Luo, K. Q., Di, L., & Zhao, Q. (2021). Targeting B7-H3 via chimeric antigen receptor T cells and bispecific killer cell engagers augments antitumor response of cytotoxic lymphocytes. *Journal of Hematology & Oncology*, *14*(1), 21. https://doi.org/10.1186/s13045-020-01024-8

279. Liu, Q., Zhang, Z., Liu, Y., Cui, Z., Zhang, T., Li, Z., & Ma, W. (2018). Cancer cells growing on perfused 3D collagen model produced higher reactive oxygen species level and were more resistant to cisplatin compared to the 2D model. *Journal of Applied Biomaterials & Functional Materials*, *16*(3), 144–150. https://doi.org/10.1177/2280800018764763

280. Liu, Y., Li, Q., Zhou, L., Xie, N., Nice, E. C., Zhang, H., Huang, C., & Lei, Y. (2106). Cancer drug resistance: redox resetting renders a way. *Oncotarget*, *7*(27), 42740–42761. https://doi.org/10.18632/oncotarget.8600

281. Loh, C.-Y., Chai, J., Tang, T., Wong, W., Sethi, G., Shanmugam, M., Chong, P., & Looi, C. (2019). The E-Cadherin and N-Cadherin Switch in Epithelial-to-Mesenchymal Transition: Signaling, Therapeutic Implications, and Challenges. *Cells*, *8*(10), 1118. https://doi.org/10.3390/cells8101118

282. Lolo, F.-N., Casas-Tintó, S., & Moreno, E. (2012). Cell Competition Time Line: Winners Kill Losers, which Are Extruded and Engulfed by Hemocytes. *Cell Reports*, *2*(3), 526–539. https://doi.org/10.1016/j.celrep.2012.08.012

283. Loo, D., Alderson, R. F., Chen, F. Z., Huang, L., Zhang, W., Gorlatov, S., Burke, S., Ciccarone, V., Li, H., Yang, Y., Son, T., Chen, Y., Easton, A. N., Li, J. C., Rillema, J. R., Licea, M., Fieger, C., Liang, T. W., Mather, J. P., … Moore, P. A. (2012). Development of an Fc-Enhanced Anti–B7-H3 Monoclonal Antibody with Potent Antitumor Activity. *Clinical Cancer Research*, *18*(14), 3834–3845. https://doi.org/10.1158/1078-0432.CCR-12-0715

284. Lucken-Ardjomande Häsler, S., Vallis, Y., Pasche, M., & McMahon, H. T. (2020). GRAF2, WDR44, and MICAL1 mediate Rab8/10/11–dependent export of E-cadherin, MMP14, and CFTR ΔF508. *Journal of Cell Biology*, *219*(5). https://doi.org/10.1083/jcb.201811014

285. Ludwig, B. S., Kessler, H., Kossatz, S., & Reuning, U. (2021). RGD-Binding Integrins Revisited: How Recently Discovered Functions and Novel Synthetic Ligands (Re-)Shape an Ever-Evolving Field. *Cancers*, *13*(7), 1711. https://doi.org/10.3390/cancers13071711

286. Luo, D., Xiao, H., Dong, J., Li, Y., Feng, G., Cui, M., & Fan, S. (2017). B7-H3 regulates lipid metabolism of lung cancer through SREBP1-mediated expression of FASN. *Biochemical and Biophysical Research Communications*, *482*(4), 1246–1251. https://doi.org/10.1016/j.bbrc.2016.12.021

287. Luo, L., Chapoval, A. I., Flies, D. B., Zhu, G., Hirano, F., Wang, S., Lau, J. S., Dong, H., Tamada, K., Flies, A. S., Liu, Y., & Chen, L. (2004). B7-H3 Enhances Tumor Immunity In Vivo by Costimulating Rapid Clonal Expansion of Antigen-Specific CD8 $^{+}$ Cytolytic T Cells. *The Journal of Immunology*, *173*(9), 5445–5450. https://doi.org/10.4049/jimmunol.173.9.5445

288. Lupu, C. M., Eisenbach, C., Kuefner, M. A., Schmidt, J., Lupu, A. D., Stremmel, W., & Encke, J. (2006). An orthotopic colon cancer model for studying the B7-H3 antitumor effect in vivo. *Journal of Gastrointestinal Surgery*, *10*(5), 635–645. https://doi.org/10.1007/BF03239969
289. Lupu, C. M., Eisenbach, C., Lupu, A. D., Kuefner, M. A., Hoyler, B., Stremmel, W., & Encke, J. (2007). Adenoviral B7-H3 therapy induces tumor specific immune responses and reduces secondary metastasis in a murine model of colon cancer. *Oncology Reports*, *18*(3), 745–748.
290. Luyten, A., Su, X., Gondela, S., Chen, Y., Rompani, S., Takakura, A., & Zhou, J. (2010). Aberrant Regulation of Planar Cell Polarity in Polycystic Kidney Disease. *Journal of the American Society of Nephrology*, *21*(9), 1521–1532. https://doi.org/10.1681/ASN.2010010127
291. Lynch, T. J., Bell, D. W., Sordella, R., Gurubhagavatula, S., Okimoto, R. A., Brannigan, B. W., Harris, P. L., Haserlat, S. M., Supko, J. G., Haluska, F. G., Louis, D. N., Christiani, D. C., Settleman, J., & Haber, D. A. (2004). Activating Mutations in the Epidermal Growth Factor Receptor Underlying Responsiveness of Non–Small-Cell Lung Cancer to Gefitinib. *New England Journal of Medicine*, *350*(21), 2129–2139. https://doi.org/10.1056/NEJMoa040938
292. Ma, Z., Qin, M., Liang, H., Chen, R., Cai, S., Huang, Z., & Tai, G. (2020). Primary cilia-dependent signaling is involved in regulating mesenchymal stem cell proliferation and pluripotency maintenance. *Journal of Molecular Histology*, *51*(3), 241–250. https://doi.org/10.1007/s10735-020-09876-7
293. Majzner, R. G., Theruvath, J. L., Nellan, A., Heitzeneder, S., Cui, Y., Mount, C. W., Rietberg, S. P., Linde, M. H., Xu, P., Rota, C., Sotillo, E., Labanieh, L., Lee, D. W., Orentas, R. J., Dimitrov, D. S., Zhu, Z., Croix, B. S., Delaidelli, A., Sekunova, A., … Mackall, C. L. (2019). CAR T Cells Targeting B7-H3, a Pan-Cancer Antigen, Demonstrate Potent Preclinical Activity Against Pediatric Solid Tumors and Brain Tumors. *Clinical Cancer Research*, *25*(8), 2560–2574. https://doi.org/10.1158/1078-0432.CCR-18-0432
294. Mao, Y., Chen, L., Wang, F., Zhu, D., Ge, X., Hua, D., & Sun, J. (2017). Cancer cell-expressed B7-H3 regulates the differentiation of tumor-associated macrophages in human colorectal carcinoma. *Oncology Letters*. https://doi.org/10.3892/ol.2017.6935
295. Marcucci, F., Stassi, G., & de Maria, R. (2016). Epithelial–mesenchymal transition: a new target in anticancer drug discovery. *Nature Reviews Drug Discovery*, *15*(5), 311–325. https://doi.org/10.1038/nrd.2015.13
296. Martin, T. A., & Jiang, W. G. (2009). Loss of tight junction barrier function and its role in cancer metastasis. *Biochimica et Biophysica Acta (BBA) - Biomembranes*, *1788*(4), 872–891. https://doi.org/10.1016/j.bbamem.2008.11.005
297. Masella, R., di Benedetto, R., Varì, R., Filesi, C., & Giovannini, C. (2005). Novel mechanisms of natural antioxidant compounds in biological systems: involvement of glutathione and glutathione-related enzymes. *The Journal of Nutritional Biochemistry*, *16*(10), 577–586. https://doi.org/10.1016/j.jnutbio.2005.05.013
298. Matson, J. P., & Cook, J. G. (2017). Cell cycle proliferation decisions: the impact of single cell analyses. *The FEBS Journal*, *284*(3), 362–375. https://doi.org/10.1111/febs.13898
299. Matsumoto, K., Inoue, H., Nakano, T., Tsuda, M., Yoshiura, Y., Fukuyama, S., Tsushima, F., Hoshino, T., Aizawa, H., Akiba, H., Pardoll, D., Hara, N., Yagita, H., Azuma, M., & Nakanishi, Y. (2004). B7-DC Regulates Asthmatic Response by an IFN-γ-Dependent Mechanism. *The Journal of Immunology*, *172*(4), 2530–2541. https://doi.org/10.4049/jimmunol.172.4.2530
300. May-Simera, H. L., & Kelley, M. W. (2012). Cilia, Wnt signaling, and the cytoskeleton. *Cilia*, *1*(1), 7. https://doi.org/10.1186/2046-2530-1-7

301. Maziveyi, M., & Alahari, S. K. (2017). *Cell matrix adhesions in cancer: The proteins that form the glue*. www.impactjournals.com/oncotarget

302. Mendonsa, A. M., Na, T.-Y., & Gumbiner, B. M. (2018). E-cadherin in contact inhibition and cancer. *Oncogene*, *37*(35), 4769–4780. https://doi.org/10.1038/s41388-018-0304-2

303. Mikami, S., Mizuno, R., Kondo, T., Shinohara, N., Nonomura, N., Ozono, S., Eto, M., Tatsugami, K., Takayama, T., Matsuyama, H., Kishida, T., & Oya, M. (2019). Clinical significance of programmed death-1 and programmed death-ligand 1 expression in the tumor microenvironment of clear cell renal cell carcinoma. *Cancer Science*, cas.14019. https://doi.org/10.1111/cas.14019

304. Milenkovic, L., Scott, M. P., & Rohatgi, R. (2009). Lateral transport of Smoothened from the plasma membrane to the membrane of the cilium. *Journal of Cell Biology*, *187*(3), 365–374. https://doi.org/10.1083/jcb.200907126

305. Miller, P. W., Clarke, D. N., Weis, W. I., Lowe, C. J., & Nelson, W. J. (2013). *The Evolutionary Origin of Epithelial Cell–Cell Adhesion Mechanisms* (pp. 267–311). https://doi.org/10.1016/B978-0-12-417027-8.00008-8

306. Mirabelli, Coppola, & Salvatore. (2019). Cancer Cell Lines Are Useful Model Systems for Medical Research. *Cancers*, *11*(8), 1098. https://doi.org/10.3390/cancers11081098

307. Mirsaeidi, M., Gidfar, S., Vu, A., & Schraufnagel, D. (2016). Annexins family: insights into their functions and potential role in pathogenesis of sarcoidosis. *Journal of Translational Medicine*, *14*(1), 89. https://doi.org/10.1186/s12967-016-0843-7

308. Modak, S., Kramer, K., Gultekin, S. H., Guo, H. F., & Cheung, N. K. (2001). Monoclonal antibody 8H9 targets a novel cell surface antigen expressed by a wide spectrum of human solid tumors. *Cancer Research*, *61*(10), 4048–4054.

309. Moharregh-Khiabani, D., Linker, R., Gold, R., & Stangel, M. (2009). Fumaric Acid and its Esters: An Emerging Treatment for Multiple Sclerosis. *Current Neuropharmacology*, *7*(1), 60–64. https://doi.org/10.2174/157015909787602788

310. Moody, P. R., Sayers, E. J., Magnusson, J. P., Alexander, C., Borri, P., Watson, P., & Jones, A. T. (2015). Receptor Crosslinking: A General Method to Trigger Internalization and Lysosomal Targeting of Therapeutic Receptor:Ligand Complexes. *Molecular Therapy*, *23*(12), 1888–1898. https://doi.org/10.1038/mt.2015.178

311. Morris, M. A., Young, L. S., & Dawson, C. W. (2008). DNA tumour viruses promote tumour cell invasion and metastasis by deregulating the normal processes of cell adhesion and motility. *European Journal of Cell Biology*, *87*(8–9), 677–697. https://doi.org/10.1016/j.ejcb.2008.03.005

312. Motzer, R. J., Escudier, B., McDermott, D. F., George, S., Hammers, H. J., Srinivas, S., Tykodi, S. S., Sosman, J. A., Procopio, G., Plimack, E. R., Castellano, D., Choueiri, T. K., Gurney, H., Donskov, F., Bono, P., Wagstaff, J., Gauler, T. C., Ueda, T., Tomita, Y., … Sharma, P. (2015). Nivolumab versus Everolimus in Advanced Renal-Cell Carcinoma. *New England Journal of Medicine*, *373*(19), 1803–1813. https://doi.org/10.1056/NEJMoa1510665

313. Murakami, S., Tanaka, H., Nakayama, T., Taniura, N., Miyake, T., Tani, M., Kushima, R., Yamamoto, G., Sugihara, H., & Mukaisho, K. (2021). Similarities and differences in metabolites of tongue cancer cells among two- and three-dimensional cultures and xenografts. *Cancer Science*, *112*(2), 918–931. https://doi.org/10.1111/cas.14749

314. Muthuswamy, S. K., & Xue, B. (2012). Cell Polarity as a Regulator of Cancer Cell Behavior Plasticity. *Annual Review of Cell and Developmental Biology*, *28*(1), 599–625. https://doi.org/10.1146/annurev-cellbio-092910-154244

315. Muz, B., de la Puente, P., Azab, F., & Azab, A. K. (2015). The role of hypoxia in cancer progression, angiogenesis, metastasis, and resistance to therapy. *Hypoxia*, 83. https://doi.org/10.2147/HP.S93413

316. Mylavarapu, S., Kumar, H., Kumari, S., Sravanthi, L. S., Jain, M., Basu, A., Biswas, M., Mylavarapu, S. V. S., Das, A., & Roy, M. (2019). Activation of Epithelial-Mesenchymal Transition and Altered β-Catenin Signaling in a Novel Indian Colorectal Carcinoma Cell Line. *Frontiers in Oncology*, *9*. https://doi.org/10.3389/fonc.2019.00054

317. Naffouje, Grover, Yu, Sendilnathan, Wolfe, Majd, Smith, Takeuchi, Senda, Kofuji, & Sasaki. (2019). Anti-Tumor Potential of IMP Dehydrogenase Inhibitors: A Century-Long Story. *Cancers*, *11*(9), 1346. https://doi.org/10.3390/cancers11091346

318. Nakamura, H., & Takada, K. (2021). Reactive oxygen species in cancer: Current findings and future directions. *Cancer Science*, *112*(10), 3945–3952. https://doi.org/10.1111/cas.15068

319. Nathan, C., & Cunningham-Bussel, A. (2013). Beyond oxidative stress: an immunologist's guide to reactive oxygen species. *Nature Reviews Immunology*, *13*(5), 349–361. https://doi.org/10.1038/nri3423

320. Nazemi, M., & Rainero, E. (2020). Cross-Talk Between the Tumor Microenvironment, Extracellular Matrix, and Cell Metabolism in Cancer. *Frontiers in Oncology*, *10*. https://doi.org/10.3389/fonc.2020.00239

321. Neyrinck-Leglantier, D., Lesage, J., Blacher, S., Bonnomet, A., Hunziker, W., Noël, A., Dormoy, V., Nawrocki-Raby, B., Gilles, C., & Polette, M. (2021). ZO-1 Intracellular Localization Organizes Immune Response in Non-Small Cell Lung Cancer. *Frontiers in Cell and Developmental Biology*, *9*. https://doi.org/10.3389/fcell.2021.749364

322. Nikolaou, S., & Machesky, L. M. (2020). The stressful tumour environment drives plasticity of cell migration programmes, contributing to metastasis. *The Journal of Pathology*, *250*(5), 612–623. https://doi.org/10.1002/path.5395

323. Nobes, C. D., & Hall, A. (1995). Rho, Rac, and Cdc42 GTPases regulate the assembly of multimolecular focal complexes associated with actin stress fibers, lamellipodia, and filopodia. *Cell*, *81*(1), 53–62. https://doi.org/10.1016/0092-8674(95)90370-4

324. Noh, J., Kwon, B., Han, E., Park, M., Yang, W., Cho, W., Yoo, W., Khang, G., & Lee, D. (2015). Amplification of oxidative stress by a dual stimuli-responsive hybrid drug enhances cancer cell death. *Nature Communications*, *6*(1), 6907. https://doi.org/10.1038/ncomms7907

325. Noree, C., Sato, B. K., Broyer, R. M., & Wilhelm, J. E. (2010). Identification of novel filament-forming proteins in Saccharomyces cerevisiae and Drosophila melanogaster. *Journal of Cell Biology*, *190*(4), 541–551. https://doi.org/10.1083/jcb.201003001

326. Noronha, C., Ribeiro, A. S., Taipa, R., Castro, D. S., Reis, J., Faria, C., & Paredes, J. (2021). Cadherin Expression and EMT: A Focus on Gliomas. *Biomedicines*, *9*(10), 1328. https://doi.org/10.3390/biomedicines9101328

327. Nunes-Xavier, C. E., Karlsen, K. F., Tekle, C., Pedersen, C., Øyjord, T., Hongisto, V., Nesland, J. M., Tan, M., Sahlberg, K. K., & Fodstad, Ø. (2016). Decreased expression of B7-H3 reduces the glycolytic capacity and sensitizes breast cancer cells to AKT/mTOR inhibitors. *Oncotarget*, *7*(6), 6891–6901. https://doi.org/10.18632/oncotarget.6902

328. Ogiwara, H., Takahashi, K., Sasaki, M., Kuroda, T., Yoshida, H., Watanabe, R., Maruyama, A., Makinoshima, H., Chiwaki, F., Sasaki, H., Kato, T., Okamoto, A., & Kohno, T. (2019). Targeting the Vulnerability of Glutathione Metabolism in ARID1A-Deficient Cancers. *Cancer Cell*, *35*(2), 177-190.e8. https://doi.org/10.1016/j.ccell.2018.12.009

329. Oh, E. C., & Katsanis, N. (2013). Context-Dependent Regulation of Wnt Signaling through the Primary Cilium. *Journal of the American Society of Nephrology*, *24*(1), 10–18. https://doi.org/10.1681/ASN.2012050526
330.
331. Okegawa, T., Pong, R.-C., Li, Y., & Hsieh, J.-T. (2004). The role of cell adhesion molecule in cancer progression and its application in cancer therapy. *Acta Biochimica Polonica*, *51*(2), 445–457. https://doi.org/035001445
332. Padmanaban, V., Krol, I., Suhail, Y., Szczerba, B. M., Aceto, N., Bader, J. S., & Ewald, A. J. (2019). E-cadherin is required for metastasis in multiple models of breast cancer. *Nature*, *573*(7774), 439–444. https://doi.org/10.1038/s41586-019-1526-3
333. Pan, J., You, Y., Huang, T., & Brody, S. L. (2007). RhoA-mediated apical actin enrichment is required for ciliogenesis and promoted by Foxj1. *Journal of Cell Science*, *120*(11), 1868–1876. https://doi.org/10.1242/jcs.005306
334. Pao, W., Miller, V., Zakowski, M., Doherty, J., Politi, K., Sarkaria, I., Singh, B., Heelan, R., Rusch, V., Fulton, L., Mardis, E., Kupfer, D., Wilson, R., Kris, M., & Varmus, H. (2004). EGF receptor gene mutations are common in lung cancers from "never smokers" and are associated with sensitivity of tumors to gefitinib and erlotinib. *Proceedings of the National Academy of Sciences*, *101*(36), 13306–13311. https://doi.org/10.1073/pnas.0405220101
335. Papakonstanti, E. A., & Stournaras, C. (2008). Cell responses regulated by early reorganization of actin cytoskeleton. *FEBS Letters*, *582*(14), 2120–2127. https://doi.org/10.1016/j.febslet.2008.02.064
336. Parekh', R. B., Dwek', R. A., Rademacher', T. W., Opdenakker', G., & van Damme', J. (1992). Glycosylation of interleukin-6 purified from normal human blood mononuclear cells. In *Eur. J. Biochem* (Vol. 203).
337. Park, T. J., Mitchell, B. J., Abitua, P. B., Kintner, C., & Wallingford, J. B. (2008). Dishevelled controls apical docking and planar polarization of basal bodies in ciliated epithelial cells. *Nature Genetics*, *40*(7), 871–879. https://doi.org/10.1038/ng.104
338. Parker, W. B. (2009). Enzymology of Purine and Pyrimidine Antimetabolites Used in the Treatment of Cancer. *Chemical Reviews*, *109*(7), 2880–2893. https://doi.org/10.1021/cr900028p
339. Parri, M., & Chiarugi, P. (2010). Rac and Rho GTPases in cancer cell motility control. *Cell Communication and Signaling*, *8*(1), 23. https://doi.org/10.1186/1478-811X-8-23
340. Pastar, I., Stojadinovic, O., Yin, N. C., Ramirez, H., Nusbaum, A. G., Sawaya, A., Patel, S. B., Khalid, L., Isseroff, R. R., & Tomic-Canic, M. (2014). Epithelialization in Wound Healing: A Comprehensive Review. *Advances in Wound Care*, *3*(7), 445–464. https://doi.org/10.1089/wound.2013.0473
341. Patel, M. R., Johnson, M. L., Falchook, G. S., Doi, T., Friedman, C. F., Piha-Paul, S. A., Gutierrez, M., Shimizu, T., Cheng, B., Qian, M., Qian, X., Myobatake, Y., Laadem, A., Yoshizuka, N., Hammett, T., Kirui, J., & Arkenau, H.-T. (2022). DS-7300 (B7-H3 DXd-ADC) in patients (pts) with metastatic castration-resistant prostate cancer (mCRPC): A subgroup analysis of a phase 1/2 multicenter study. *Journal of Clinical Oncology*, *40*(6_suppl), 87–87. https://doi.org/10.1200/JCO.2022.40.6_suppl.087
342. Patel, S. D., Ciatto, C., Chen, C. P., Bahna, F., Rajebhosale, M., Arkus, N., Schieren, I., Jessell, T. M., Honig, B., Price, S. R., & Shapiro, L. (2006). Type II Cadherin Ectodomain Structures: Implications for Classical Cadherin Specificity. *Cell*, *124*(6), 1255–1268. https://doi.org/10.1016/j.cell.2005.12.046
343. Pavlova, N. N., & Thompson, C. B. (2016). The Emerging Hallmarks of Cancer Metabolism. *Cell Metabolism*, *23*(1), 27–47. https://doi.org/10.1016/j.cmet.2015.12.006

344. Pazour, G. J., San Agustin, J. T., Follit, J. A., Rosenbaum, J. L., & Witman, G. B. (2002). Polycystin-2 localizes to kidney cilia and the ciliary level is elevated in orpk mice with polycystic kidney disease. *Current Biology*, *12*(11), R378–R380. https://doi.org/10.1016/S0960-9822(02)00877-1
345. Pedersen, L. B., & Rosenbaum, J. L. (2008). *Chapter Two Intraflagellar Transport (IFT)* (pp. 23–61). https://doi.org/10.1016/S0070-2153(08)00802-8
346. Penet, M.-F., Krishnamachary, B., Wildes, F., Mironchik, Y., Mezzanzanica, D., Podo, F., de Reggi, M., Gharib, B., & Bhujwalla, Z. M. (2016). Effect of Pantethine on Ovarian Tumor Progression and Choline Metabolism. *Frontiers in Oncology*, *6*. https://doi.org/10.3389/fonc.2016.00244
347. Peotter, J., Kasberg, W., Pustova, I., & Audhya, A. (2019). COPII-mediated trafficking at the ER/ERGIC interface. *Traffic*, *20*(7), 491–503. https://doi.org/10.1111/tra.12654
348. Perez-Moreno, P., Brambilla, E., Thomas, R., & Soria, J.-C. (2012). Squamous Cell Carcinoma of the Lung: Molecular Subtypes and Therapeutic Opportunities. *Clinical Cancer Research*, *18*(9), 2443–2451. https://doi.org/10.1158/1078-0432.CCR-11-2370
349. Picarda, E., Ohaegbulam, K. C., & Zang, X. (2016). Molecular Pathways: Targeting B7-H3 (CD276) for Human Cancer Immunotherapy. *Clinical Cancer Research*, *22*(14), 3425–3431. https://doi.org/10.1158/1078-0432.CCR-15-2428
350. Pietro, F., Echard, A., & Morin, X. (2016). Regulation of mitotic spindle orientation: an integrated view. *EMBO Reports*, *17*(8), 1106–1130. https://doi.org/10.15252/embr.201642292
351. Piñeiro Fernández, J., Luddy, K. A., Harmon, C., & O'Farrelly, C. (2019). Hepatic Tumor Microenvironments and Effects on NK Cell Phenotype and Function. *International Journal of Molecular Sciences*, *20*(17), 4131. https://doi.org/10.3390/ijms20174131
352. Pokutta, S., HERRENKNECHT, K., KEMLER, R., & ENGEL, J. (1994). Conformational changes of the recombinant extracellular domain of E-cadherin upon calcium binding. *European Journal of Biochemistry*, *223*(3), 1019–1026. https://doi.org/10.1111/j.1432-1033.1994.tb19080.x
353. Pollard, T. D. (2016). Actin and Actin-Binding Proteins. *Cold Spring Harbor Perspectives in Biology*, *8*(8), a018226. https://doi.org/10.1101/cshperspect.a018226
354. Powell, L., Samarakoon, Y. H., Ismail, S., & Sayer, J. A. (2021). ARL3, a small GTPase with a functionally conserved role in primary cilia and immune synapses. *Small GTPases*, *12*(3), 167–176. https://doi.org/10.1080/21541248.2019.1703466
355. Prasad, D. V. R., Nguyen, T., Li, Z., Yang, Y., Duong, J., Wang, Y., & Dong, C. (2004a). Murine B7-H3 Is a Negative Regulator of T Cells. *The Journal of Immunology*, *173*(4), 2500–2506. https://doi.org/10.4049/jimmunol.173.4.2500
356. Pratilas, C. A., Hanrahan, A. J., Halilovic, E., Persaud, Y., Soh, J., Chitale, D., Shigematsu, H., Yamamoto, H., Sawai, A., Janakiraman, M., Taylor, B. S., Pao, W., Toyooka, S., Ladanyi, M., Gazdar, A., Rosen, N., & Solit, D. B. (2008). Genetic Predictors of MEK Dependence in Non–Small Cell Lung Cancer. *Cancer Research*, *68*(22), 9375–9383. https://doi.org/10.1158/0008-5472.CAN-08-2223
357. Proteinatlas.org. (2022). *Rods and rings - The Human Protein Atlas*.
358. Pugacheva, E. N., Jablonski, S. A., Hartman, T. R., Henske, E. P., & Golemis, E. A. (2007). HEF1-Dependent Aurora A Activation Induces Disassembly of the Primary Cilium. *Cell*, *129*(7), 1351–1363. https://doi.org/10.1016/j.cell.2007.04.035
359. Qin, C., Yang, G., Yang, J., Ren, B., Wang, H., Chen, G., Zhao, F., You, L., Wang, W., & Zhao, Y. (2020). Metabolism of pancreatic cancer: paving the way to better anticancer strategies. *Molecular Cancer*, *19*(1), 50. https://doi.org/10.1186/s12943-020-01169-7

360. Qin, X., Zhang, H., Ye, D., Dai, B., Zhu, Y., & Shi, G. (2013). B7-H3 is a new cancer-specific endothelial marker in clear cell renal cell carcinoma. *OncoTargets and Therapy*, 1667. https://doi.org/10.2147/OTT.S53565
361. Qiu, M., Xia, Q., Chen, Y., Fang, X., Li, Q., Zhu, L., Jiang, X., Xiong, Z., & Yang, S. (2021). The Expression of Three Negative Co-Stimulatory B7 Family Molecules in Small Cell Lung Cancer and Their Effect on Prognosis. *Frontiers in Oncology*, *11*. https://doi.org/10.3389/fonc.2021.600238
362. Quidwai, T., Wang, J., Hall, E. A., Petriman, N. A., Leng, W., Kiesel, P., Wells, J. N., Murphy, L. C., Keighren, M. A., Marsh, J. A., Lorentzen, E., Pigino, G., & Mill, P. (2021). A WDR35-dependent coat protein complex transports ciliary membrane cargo vesicles to cilia. *ELife*, *10*. https://doi.org/10.7554/eLife.69786
363. Ragkousi, K., & Gibson, M. C. (2014). Cell division and the maintenance of epithelial order. *Journal of Cell Biology*, *207*(2), 181–188. https://doi.org/10.1083/jcb.201408044
364. Ramer, M. S., Cruz Cabrera, M. A., Alan, N., Scott, A. L. M., & Inskip, J. A. (2010). A New Organellar Complex in Rat Sympathetic Neurons. *PLoS ONE*, *5*(5), e10872. https://doi.org/10.1371/journal.pone.0010872
365. Rao, Y., Hao, R., Wang, B., & Yao, T.-P. (2014). A Mec17-Myosin II Effector Axis Coordinates Microtubule Acetylation and Actin Dynamics to Control Primary Cilium Biogenesis. *PLoS ONE*, *9*(12), e114087. https://doi.org/10.1371/journal.pone.0114087
366. Rather, G. M., Pramono, A. A., Szekely, Z., Bertino, J. R., & Tedeschi, P. M. (2021). In cancer, all roads lead to NADPH. *Pharmacology & Therapeutics*, *226*, 107864. https://doi.org/10.1016/j.pharmthera.2021.107864
367. Recouvreux, M. V., & Commisso, C. (2017). Macropinocytosis: A Metabolic Adaptation to Nutrient Stress in Cancer. *Frontiers in Endocrinology*, *8*. https://doi.org/10.3389/fendo.2017.00261
368. Reczek, C. R., & Chandel, N. S. (2015). ROS-dependent signal transduction. *Current Opinion in Cell Biology*, *33*, 8–13. https://doi.org/10.1016/j.ceb.2014.09.010
369. Reczek, C. R., & Chandel, N. S. (2017). The Two Faces of Reactive Oxygen Species in Cancer. *Annual Review of Cancer Biology*, *1*(1), 79–98. https://doi.org/10.1146/annurev-cancerbio-041916-065808
370. Redza-Dutordoir, M., & Averill-Bates, D. A. (2016). Activation of apoptosis signalling pathways by reactive oxygen species. *Biochimica et Biophysica Acta (BBA) - Molecular Cell Research*, *1863*(12), 2977–2992. https://doi.org/10.1016/j.bbamcr.2016.09.012
371. Reita, D., Pabst, L., Pencreach, E., Guérin, E., Dano, L., Rimelen, V., Voegeli, A.-C., Vallat, L., Mascaux, C., & Beau-Faller, M. (2022). Direct Targeting KRAS Mutation in Non-Small Cell Lung Cancer: Focus on Resistance. *Cancers*, *14*(5), 1321. https://doi.org/10.3390/cancers14051321
372. Resnick, M. B., Gavilanez, M., Newton, E., Konkin, T., Bhattacharya, B., Britt, D. E., Sabo, E., & Moss, S. F. (2005). Claudin expression in gastric adenocarcinomas: a tissue microarray study with prognostic correlation. *Human Pathology*, *36*(8), 886–892. https://doi.org/10.1016/j.humpath.2005.05.019
373. Resnick, M. B., Konkin, T., Routhier, J., Sabo, E., & Pricolo, V. E. (2005). Claudin-1 is a strong prognostic indicator in stage II colonic cancer: a tissue microarray study. *Modern Pathology*, *18*(4), 511–518. https://doi.org/10.1038/modpathol.3800301
374. Ridley, A. J. (2015). Rho GTPase signalling in cell migration. *Current Opinion in Cell Biology*, *36*, 103–112. https://doi.org/10.1016/j.ceb.2015.08.005
375. Riedl, A., Schlederer, M., Pudelko, K., Stadler, M., Walter, S., Unterleuthner, D., Unger, C., Kramer, N., Hengstschläger, M., Kenner, L., Pfeiffer, D., Krupitza, G., & Dolznig, H. (2016).

Comparison of cancer cells cultured in 2D vs 3D reveals differences in AKT/mTOR/S6-kinase signaling and drug response. *Journal of Cell Science*. https://doi.org/10.1242/jcs.188102

376. Riely, G. J., Marks, J., & Pao, W. (2009). KRAS Mutations in Non-Small Cell Lung Cancer. *Proceedings of the American Thoracic Society*, *6*(2), 201–205. https://doi.org/10.1513/pats.200809-107LC

377. Roche, J. (2018). The Epithelial-to-Mesenchymal Transition in Cancer. *Cancers*, *10*(2), 52. https://doi.org/10.3390/cancers10020052

378. Rohatgi, R., Milenkovic, L., & Scott, M. P. (2007). Patched1 Regulates Hedgehog Signaling at the Primary Cilium. *Science*, *317*(5836), 372–376. https://doi.org/10.1126/science.1139740

379. Rondanino, C., Poland, P. A., Kinlough, C. L., Li, H., Rbaibi, Y., Myerburg, M. M., Al-bataineh, M. M., Kashlan, O. B., Pastor-Soler, N. M., Hallows, K. R., Weisz, O. A., Apodaca, G., & Hughey, R. P. (2011). Galectin-7 modulates the length of the primary cilia and wound repair in polarized kidney epithelial cells. *American Journal of Physiology-Renal Physiology*, *301*(3), F622–F633. https://doi.org/10.1152/ajprenal.00134.2011

380. Rosenblatt, J., Raff, M. C., & Cramer, L. P. (2001). An epithelial cell destined for apoptosis signals its neighbors to extrude it by an actin- and myosin-dependent mechanism. *Current Biology*, *11*(23), 1847–1857. https://doi.org/10.1016/S0960-9822(01)00587-5

381. Rotty, J. D., & Bear, J. E. (2015). Competition and collaboration between different actin assembly pathways allows for homeostatic control of the actin cytoskeleton. *BioArchitecture*, *5*(1–2), 27–34. https://doi.org/10.1080/19490992.2015.1090670

382. Roy, K., Jerman, S., Jozsef, L., McNamara, T., Onyekaba, G., Sun, Z., & Marin, E. P. (2017). Palmitoylation of the ciliary GTPase ARL13b is necessary for its stability and its role in cilia formation. *Journal of Biological Chemistry*, *292*(43), 17703–17717. https://doi.org/10.1074/jbc.M117.792937

383. Rudin, C. M., Brambilla, E., Faivre-Finn, C., & Sage, J. (2021). Small-cell lung cancer. *Nature Reviews Disease Primers*, *7*(1), 3. https://doi.org/10.1038/s41572-020-00235-0

384. Saab, S., Zalzale, H., Rahal, Z., Khalifeh, Y., Sinjab, A., & Kadara, H. (2020). Insights Into Lung Cancer Immune-Based Biology, Prevention, and Treatment. *Frontiers in Immunology*, *11*. https://doi.org/10.3389/fimmu.2020.00159

385. Saburi, S., Hester, I., Fischer, E., Pontoglio, M., Eremina, V., Gessler, M., Quaggin, S. E., Harrison, R., Mount, R., & McNeill, H. (2008). Loss of Fat4 disrupts PCP signaling and oriented cell division and leads to cystic kidney disease. *Nature Genetics*, *40*(8), 1010–1015. https://doi.org/10.1038/ng.179

386. Sadeghi, F., Asgari, M., Matloubi, M., Ranjbar, M., Karkhaneh Yousefi, N., Azari, T., & Zaki-Dizaji, M. (2020). Molecular contribution of BRCA1 and BRCA2 to genome instability in breast cancer patients: review of radiosensitivity assays. *Biological Procedures Online*, *22*(1), 23. https://doi.org/10.1186/s12575-020-00133-5

387. Sah, V. P., Seasholtz, T. M., Sagi, S. A., & Brown, J. H. (2000). The Role of Rho in G Protein-Coupled Receptor Signal Transduction. *Annual Review of Pharmacology and Toxicology*, *40*(1), 459–489. https://doi.org/10.1146/annurev.pharmtox.40.1.459

388. Saito, S., Tampe, B., Müller, G. A., & Zeisberg, M. (2015). Primary cilia modulate balance of canonical and non-canonical Wnt signaling responses in the injured kidney. *Fibrogenesis & Tissue Repair*, *8*(1), 6. https://doi.org/10.1186/s13069-015-0024-y

389. Saitoh, M. (2018). Involvement of partial EMT in cancer progression. *The Journal of Biochemistry*, *164*(4), 257–264. https://doi.org/10.1093/jb/mvy047

390. Sampath, D., Rao, V. A., & Plunkett, W. (2003). Mechanisms of apoptosis induction by nucleoside analogs. *Oncogene*, *22*(56), 9063–9074. https://doi.org/10.1038/sj.onc.1207229
391. Sandalio, L. M., Rodríguez-Serrano, M., Romero-Puertas, M. C., & del Río, L. A. (2013). *Role of Peroxisomes as a Source of Reactive Oxygen Species (ROS) Signaling Molecules* (pp. 231–255). https://doi.org/10.1007/978-94-007-6889-5_13
392. Sansom, D. M. (2000). CD28, CTLA-4 and their ligands: who does what and to whom? *Immunology*, *101*(2), 169–177. https://doi.org/10.1046/j.1365-2567.2000.00121.x
393. Sassi, K., Nury, T., Samadi, M., Fennira, F. B.-A., Vejux, A., & Lizard, G. (2021). Cholesterol Derivatives as Promising Anticancer Agents in Glioblastoma Metabolic Therapy. In *Gliomas* (pp. 97–120). Exon Publications. https://doi.org/10.36255/exonpublications.gliomas.2021.chapter6
394. Saxena, K., Jolly, M. K., & Balamurugan, K. (2020). Hypoxia, partial EMT and collective migration: Emerging culprits in metastasis. *Translational Oncology*, *13*(11), 100845. https://doi.org/10.1016/j.tranon.2020.100845
395. Schiavon, C. R., Griffin, M. E., Pirozzi, M., Parashuraman, R., Zhou, W., Jinnah, H. A., Reines, D., & Kahn, R. A. (2018). Compositional complexity of rods and rings. *Molecular Biology of the Cell*, *29*(19), 2303–2316. https://doi.org/10.1091/mbc.E18-05-0274
396. Scherzer, M. T., Waigel, S., Donninger, H., Arumugam, V., Zacharias, W., Clark, G., Siskind, L. J., Soucy, P., & Beverly, L. (2015). Fibroblast-Derived Extracellular Matrices: An Alternative Cell Culture System That Increases Metastatic Cellular Properties. *PLOS ONE*, *10*(9), e0138065. https://doi.org/10.1371/journal.pone.0138065
397. Schiavon, C. R., Turn, R. E., Newman, L. E., & Kahn, R. A. (2019). ELMOD2 regulates mitochondrial fusion in a mitofusin-dependent manner, downstream of ARL2. *Molecular Biology of the Cell*, *30*(10), 1198–1213. https://doi.org/10.1091/mbc.E18-12-0804
398. Schwartz, M. A. (2010). Integrins and Extracellular Matrix in Mechanotransduction. *Cold Spring Harbor Perspectives in Biology*, *2*(12), a005066–a005066. https://doi.org/10.1101/cshperspect.a005066
399. Seeger-Nukpezah, T., & Golemis, E. A. (2012). The extracellular matrix and ciliary signaling. *Current Opinion in Cell Biology*, *24*(5), 652–661. https://doi.org/10.1016/j.ceb.2012.06.002
400. Seeley, E. S., Carrière, C., Goetze, T., Longnecker, D. S., & Korc, M. (2009). Pancreatic Cancer and Precursor Pancreatic Intraepithelial Neoplasia Lesions Are Devoid of Primary Cilia. *Cancer Research*, *69*(2), 422–430. https://doi.org/10.1158/0008-5472.CAN-08-1290
401. Seelig, H. P., Appelhans, H., Bauer, O., Blüthner, M., Hartung, K., Schranz, P., Schultze, D., Seelig, C. A., & Volkmann, M. (2011). Autoantibodies against inosine-5'-monophosphate dehydrogenase 2--characteristics and prevalence in patients with HCV-infection. *Clinical Laboratory*, *57*(9–10), 753–765.
402. Seetharamu, N., Budman, D. R., & Sullivan, K. M. (2016). Immune checkpoint inhibitors in lung cancer: past, present and future. *Future Oncology*, *12*(9), 1151–1163. https://doi.org/10.2217/fon.16.20
403. Shah, M. A., & Rogoff, H. A. (2021). Implications of reactive oxygen species on cancer formation and its treatment. *Seminars in Oncology*, *48*(3), 238–245. https://doi.org/10.1053/j.seminoncol.2021.05.002
404. Shahid, K., Khalife, M., Dabney, R., & Phan, A. T. (2019). Immunotherapy and targeted therapy—the new roadmap in cancer treatment. *Annals of Translational Medicine*, *7*(20), 595–595. https://doi.org/10.21037/atm.2019.05.58

405. Shen, D., Tian, L., Yang, F., Li, J., Li, X., Yao, Y., Lam, E. W.-F., Gao, P., Jin, B., & Wang, R. (2021). ADO/hypotaurine: a novel metabolic pathway contributing to glioblastoma development. *Cell Death Discovery*, *7*(1), 21. https://doi.org/10.1038/s41420-020-00398-5
406. Shireman, J., Ali, E., Saathoff, M., Park, C., Ben-Sahra, I., & Ahmed, A. U. (2019). Abstract 81: ARL13B interacts with IMPDH2 to modulate purine synthesis and temozolomide resistance in glioblastoma. *Cancer Research*, *79*(13_Supplement), 81–81. https://doi.org/10.1158/1538-7445.AM2019-81
407. Shireman, J., Atashi, F., Park, C., Warnke, L., Miska, J., & Ahmed, A. (2018). DRES-02. CILIARY PROTEIN ARL13B PROMOTES CHEMORESISTANCE BY MODULATE GLIOBLASTOMA PURINE BIOSYNTHESIS. *Neuro-Oncology*, *20*(suppl_6), vi75–vi75. https://doi.org/10.1093/neuonc/noy148.309
408. Shireman, J. M., Atashi, F., Lee, G., Ali, E. S., Saathoff, M. R., Park, C. H., Savchuk, S., Baisiwala, S., Miska, J., Lesniak, M. S., James, C. D., Stupp, R., Kumthekar, P., Horbinski, C. M., Ben-Sahra, I., & Ahmed, A. U. (2021). *De novo* purine biosynthesis is a major driver of chemoresistance in glioblastoma. *Brain*, *144*(4), 1230–1246. https://doi.org/10.1093/brain/awab020
409. Shoshan, E., Mobley, A. K., Braeuer, R. R., Kamiya, T., Huang, L., Vasquez, M. E., Salameh, A., Lee, H. J., Kim, S. J., Ivan, C., Velazquez-Torres, G., Nip, K. M., Zhu, K., Brooks, D., Jones, S. J. M., Birol, I., Mosqueda, M., Wen, Y., Eterovic, A. K., … Bar-Eli, M. (2015). Reduced adenosine-to-inosine miR-455-5p editing promotes melanoma growth and metastasis. *Nature Cell Biology*, *17*(3), 311–321. https://doi.org/10.1038/ncb3110
410. Siddiqui, I. A., Sanna, V., Ahmad, N., Sechi, M., & Mukhtar, H. (2015). Resveratrol nanoformulation for cancer prevention and therapy. *Annals of the New York Academy of Sciences*, *1348*(1), 20–31. https://doi.org/10.1111/nyas.12811
411. Sieviläinen, M., Wirsing, A. M., Hyytiäinen, A., Almahmoudi, R., Rodrigues, P., Bjerkli, I.-H., Åström, P., Toppila-Salmi, S., Paavonen, T., Coletta, R. D., Hadler-Olsen, E., Salo, T., & Al-Samadi, A. (2021). Evaluation Challenges in the Validation of B7-H3 as Oral Tongue Cancer Prognosticator. *Head and Neck Pathology*, *15*(2), 469–478. https://doi.org/10.1007/s12105-020-01222-3
412. Slattum, G. M., & Rosenblatt, J. (2014). Tumour cell invasion: an emerging role for basal epithelial cell extrusion. *Nature Reviews Cancer*, *14*(7), 495–501. https://doi.org/10.1038/nrc3767
413. Smalley, K. S. M., Brafford, P., Haass, N. K., Brandner, J. M., Brown, E., & Herlyn, M. (2005a). Up-Regulated Expression of Zonula Occludens Protein-1 in Human Melanoma Associates with N-Cadherin and Contributes to Invasion and Adhesion. *The American Journal of Pathology*, *166*(5), 1541–1554. https://doi.org/10.1016/S0002-9440(10)62370-X
414. Smalley, K. S. M., Brafford, P., Haass, N. K., Brandner, J. M., Brown, E., & Herlyn, M. (2005b). Up-Regulated Expression of Zonula Occludens Protein-1 in Human Melanoma Associates with N-Cadherin and Contributes to Invasion and Adhesion. *The American Journal of Pathology*, *166*(5), 1541–1554. https://doi.org/10.1016/S0002-9440(10)62370-X
415. Smith, Y., ESri HariKrishna Vellanki, & Ann M Hopkins. (2016). Dynamic interplay between adhesion surfaces in carcinomas: Cell-cell and cell-matrix crosstalk. *World Journal of Biological Chemistry*, *7*(1), 64. https://doi.org/10.4331/wjbc.v7.i1.64
416. Snedecor, E. R., Sung, C. C., Moncayo, A., Rothstein, B. E., Mockler, D. C., Tonnesen, M. G., Jones, E. C., Fujita, M., Clark, R. A., Shroyer, K. R., & Chen, J. (2015). Loss of Primary Cilia in Melanoma Cells is Likely Independent of Proliferation and Cell Cycle Progression. *Journal of Investigative Dermatology*, *135*(5), 1456–1458. https://doi.org/10.1038/jid.2015.22

417. Sobiak, J., Jóźwiak, A., Wziętek, H., Zachwieja, J., & Ostalska-Nowicka, D. (2020). The Application of Inosine 5'-Monophosphate Dehydrogenase Activity Determination in Peripheral Blood Mononuclear Cells for Monitoring Mycophenolate Mofetil Therapy in Children with Nephrotic Syndrome. *Pharmaceuticals*, *13*(8), 200. https://doi.org/10.3390/ph13080200

418. Soda, M., Choi, Y. L., Enomoto, M., Takada, S., Yamashita, Y., Ishikawa, S., Fujiwara, S., Watanabe, H., Kurashina, K., Hatanaka, H., Bando, M., Ohno, S., Ishikawa, Y., Aburatani, H., Niki, T., Sohara, Y., Sugiyama, Y., & Mano, H. (2007). Identification of the transforming EML4–ALK fusion gene in non-small-cell lung cancer. *Nature*, *448*(7153), 561–566. https://doi.org/10.1038/nature05945

419. Song, J., Shi, W., Zhang, Y., Sun, M., Liang, X., & Zheng, S. (2016). Epidermal growth factor receptor and B7-H3 expression in esophageal squamous tissues correlate to patient prognosis. *OncoTargets and Therapy*, *Volume 9*, 6257–6263. https://doi.org/10.2147/OTT.S111691

420. Steinberger, P., Majdic, O., Derdak, S. v., Pfistershammer, K., Kirchberger, S., Klauser, C., Zlabinger, G., Pickl, W. F., Stöckl, J., & Knapp, W. (2004). Molecular Characterization of Human 4Ig-B7-H3, a Member of the B7 Family with Four Ig-Like Domains. *The Journal of Immunology*, *172*(4), 2352–2359. https://doi.org/10.4049/jimmunol.172.4.2352

421. Steven, A., Fisher, S. A., & Robinson, B. W. (2016). Immunotherapy for lung cancer. *Respirology*, *21*(5), 821–833. https://doi.org/10.1111/resp.12789

422. Strom, S. P., Clark, M. J., Martinez, A., Garcia, S., Abelazeem, A. A., Matynia, A., Parikh, S., Sullivan, L. S., Bowne, S. J., Daiger, S. P., & Gorin, M. B. (2016). De Novo Occurrence of a Variant in ARL3 and Apparent Autosomal Dominant Transmission of Retinitis Pigmentosa. *PLOS ONE*, *11*(3), e0150944. https://doi.org/10.1371/journal.pone.0150944

423. Stutchbury, B., Atherton, P., Tsang, R., Wang, D.-Y., & Ballestrem, C. (2017). Distinct focal adhesion protein modules control different aspects of mechanotransduction. *Journal of Cell Science*. https://doi.org/10.1242/jcs.195362

424. Suh, W.-K., Gajewska, B. U., Okada, H., Gronski, M. A., Bertram, E. M., Dawicki, W., Duncan, G. S., Bukczynski, J., Plyte, S., Elia, A., Wakeham, A., Itie, A., Chung, S., da Costa, J., Arya, S., Horan, T., Campbell, P., Gaida, K., Ohashi, P. S., … Mak, T. W. (2003). The B7 family member B7-H3 preferentially down-regulates T helper type 1–mediated immune responses. *Nature Immunology*, *4*(9), 899–906. https://doi.org/10.1038/ni967

425. Sun, J., Fu, F., Gu, W., Yan, R., Zhang, G., Shen, Z., Zhou, Y., Wang, H., Shen, B., & Zhang, X. (2011). Origination of New Immunological Functions in the Costimulatory Molecule B7-H3: The Role of Exon Duplication in Evolution of the Immune System. *PLoS ONE*, *6*(9), e24751. https://doi.org/10.1371/journal.pone.0024751

426. Sun, M., Richards, S., Prasad, D. V. R., Mai, X. M., Rudensky, A., & Dong, C. (2002). Characterization of Mouse and Human B7-H3 Genes. *The Journal of Immunology*, *168*(12), 6294–6297. https://doi.org/10.4049/jimmunol.168.12.6294

427. Sun, X., Vale, M., Leung, E., Kanwar, J. R., Gupta, R., & Krissansen, G. W. (2003). Mouse B7-H3 induces antitumor immunity. *Gene Therapy*, *10*(20), 1728–1734. https://doi.org/10.1038/sj.gt.3302070

428. Sun, Y., Wang, Y., Zhao, J., Gu, M., Giscombe, R., Lefvert, A. K., & Wang, X. (2006). B7-H3 and B7-H4 expression in non-small-cell lung cancer. *Lung Cancer*, *53*(2), 143–151. https://doi.org/10.1016/j.lungcan.2006.05.012

429. Taegtmeyer, H., & Ingwall, J. S. (2013). Creatine—A Dispensable Metabolite? *Circulation Research*, *112*(6), 878–880. https://doi.org/10.1161/CIRCRESAHA.113.300974

430. Takebe, N., Cheng, X., Fandy, T. E., Srivastava, R. K., Wu, S., Shankar, S., Bauer, K., Shaughnessy, J., & Tricot, G. (2006). IMP dehydrogenase inhibitor mycophenolate mofetil induces caspase-dependent apoptosis and cell cycle inhibition in multiple myeloma cells. *Molecular Cancer Therapeutics*, *5*(2), 457–466. https://doi.org/10.1158/1535-7163.MCT-05-0340

431. Taniuchi, K. (2011). BART inhibits pancreatic cancer cell invasion by inhibiting ARL2-mediated RhoA inactivation. *International Journal of Oncology*. https://doi.org/10.3892/ijo.2011.1156

432. Tcherkezian, J., & Lamarche-Vane, N. (2007). Current knowledge of the large RhoGAP family of proteins. *Biology of the Cell*, *99*(2), 67–86. https://doi.org/10.1042/BC20060086

433. Tekle, C., Nygren, M. K., Chen, Y.-W., Dybsjord, I., Nesland, J. M., Maelandsmo, G. M., & Fodstad, Ø. (2012). B7-H3 contributes to the metastatic capacity of melanoma cells by modulation of known metastasis-associated genes. *International Journal of Cancer*, *130*(10), 2282–2290. https://doi.org/10.1002/ijc.26238

434. Thomas, D., Rathinavel, A. K., & Radhakrishnan, P. (2021). Altered glycosylation in cancer: A promising target for biomarkers and therapeutics. *Biochimica et Biophysica Acta (BBA) - Reviews on Cancer*, *1875*(1), 188464. https://doi.org/10.1016/j.bbcan.2020.188464

435. Thomas, E. C., Gunter, J. H., Webster, J. A., Schieber, N. L., Oorschot, V., Parton, R. G., & Whitehead, J. P. (2012). Different Characteristics and Nucleotide Binding Properties of Inosine Monophosphate Dehydrogenase (IMPDH) Isoforms. *PLoS ONE*, *7*(12), e51096. https://doi.org/10.1371/journal.pone.0051096

436. Thowfeequ, S., Stower, M. J., & Srinivas, S. (2022). Epithelial dynamics during early mouse development. *Current Opinion in Genetics & Development*, *72*, 110–117. https://doi.org/10.1016/j.gde.2021.11.006

437. Tian, G., Thomas, S., & Cowan, N. J. (2010). Effect of TBCD and its regulatory interactor Arl2 on tubulin and microtubule integrity. *Cytoskeleton*, *67*(11), 706–714. https://doi.org/10.1002/cm.20480

438. Trachootham, D., Alexandre, J., & Huang, P. (2009). Targeting cancer cells by ROS-mediated mechanisms: a radical therapeutic approach? *Nature Reviews Drug Discovery*, *8*(7), 579–591. https://doi.org/10.1038/nrd2803

439. Trepat, X., Chen, Z., & Jacobson, K. (2012). Cell Migration. In *Comprehensive Physiology* (pp. 2369–2392). Wiley. https://doi.org/10.1002/cphy.c110012

440. Tressler, R. J., Garvin, L. J., & Slate, D. L. (1994). Anti-tumor activity of mycophenolate mofetil against human and mouse tumorsin vivo. *International Journal of Cancer*, *57*(4), 568–573. https://doi.org/10.1002/ijc.2910570421

441. Troyanovsky, R. B., Laur, O., & Troyanovsky, S. M. (2007). Stable and Unstable Cadherin Dimers: Mechanisms of Formation and Roles in Cell Adhesion. *Molecular Biology of the Cell*, *18*(11), 4343–4352. https://doi.org/10.1091/mbc.e07-01-0084

442. Tsushima, F., Iwai, H., Otsuki, N., Abe, M., Hirose, S., Yamazaki, T., Akiba, H., Yagita, H., Takahashi, Y., Omura, K., Okumura, K., & Azuma, M. (2003). Preferential contribution of B7-H1 to programmed death-1-mediated regulation of hapten-specific allergic inflammatory responses. *European Journal of Immunology*, *33*(10), 2773–2782. https://doi.org/10.1002/eji.200324084

443. Tucker, R. P., & Adams, J. C. (2014). *Adhesion Networks of Cnidarians* (pp. 323–377). https://doi.org/10.1016/B978-0-12-800097-7.00008-7

444. Tung, Y.-C., Hsiao, A. Y., Allen, S. G., Torisawa, Y., Ho, M., & Takayama, S. (2011). High-throughput 3D spheroid culture and drug testing using a 384 hanging drop array. *The Analyst*, *136*(3), 473–478. https://doi.org/10.1039/C0AN00609B

445. Uchida, C. (2012). The Retinoblastoma Protein: Functions Beyond the G1-S Regulator. *Current Drug Targets*, *13*(13), 1622–1632. https://doi.org/10.2174/138945012803529938
446. Ushio-Fukai, M., & Nakamura, Y. (2008). Reactive oxygen species and angiogenesis: NADPH oxidase as target for cancer therapy. *Cancer Letters*, *266*(1), 37–52. https://doi.org/10.1016/j.canlet.2008.02.044
447. Valacchi, G., Virgili, F., Cervellati, C., & Pecorelli, A. (2018). OxInflammation: From Subclinical Condition to Pathological Biomarker. *Frontiers in Physiology*, *9*. https://doi.org/10.3389/fphys.2018.00858
448. Valenta, T., Hausmann, G., & Basler, K. (2012). The many faces and functions of β-catenin. *The EMBO Journal*, *31*(12), 2714–2736. https://doi.org/10.1038/emboj.2012.150
449. Valente, E. M., Logan, C. v, Mougou-Zerelli, S., Lee, J. H., Silhavy, J. L., Brancati, F., Iannicelli, M., Travaglini, L., Romani, S., Illi, B., Adams, M., Szymanska, K., Mazzotta, A., Lee, J. E., Tolentino, J. C., Swistun, D., Salpietro, C. D., Fede, C., Gabriel, S., … Gleeson, J. G. (2010). Mutations in TMEM216 perturb ciliogenesis and cause Joubert, Meckel and related syndromes. *Nature Genetics*, *42*(7), 619–625. https://doi.org/10.1038/ng.594
450. vander Heiden, M. G., & DeBerardinis, R. J. (2017). Understanding the Intersections between Metabolism and Cancer Biology. *Cell*, *168*(4), 657–669. https://doi.org/10.1016/j.cell.2016.12.039
451. Végső, G., Sebestyén, A., Paku, S., Barna, G., Hajdu, M., Tóth, M., Járay, J., & Kopper, L. (2007). Antiproliferative and apoptotic effects of mycophenolic acid in human B-cell non-Hodgkin lymphomas. *Leukemia Research*, *31*(7), 1003–1008. https://doi.org/10.1016/j.leukres.2006.12.019
452. Vigdorovich, V., Ramagopal, U. A., Lázár-Molnár, E., Sylvestre, E., Lee, J. S., Hofmeyer, K. A., Zang, X., Nathenson, S. G., & Almo, S. C. (2013). Structure and T Cell Inhibition Properties of B7 Family Member, B7-H3. *Structure*, *21*(5), 707–717. https://doi.org/10.1016/j.str.2013.03.003
453. Villalobos, P., & Wistuba, I. I. (2017). Lung Cancer Biomarkers. *Hematology/Oncology Clinics of North America*, *31*(1), 13–29. https://doi.org/10.1016/j.hoc.2016.08.006
454. Vincent, J.-P., Fletcher, A. G., & Baena-Lopez, L. Al. (2013). Mechanisms and mechanics of cell competition in epithelia. *Nature Reviews Molecular Cell Biology*, *14*(9), 581–591. https://doi.org/10.1038/nrm3639
455. Wagner, E. F., & Nebreda, Á. R. (2009). Signal integration by JNK and p38 MAPK pathways in cancer development. *Nature Reviews Cancer*, *9*(8), 537–549. https://doi.org/10.1038/nrc2694
456. Walser, T., Cui, X., Yanagawa, J., Lee, J. M., Heinrich, E., Lee, G., Sharma, S., & Dubinett, S. M. (2008). Smoking and Lung Cancer: The Role of Inflammation. *Proceedings of the American Thoracic Society*, *5*(8), 811–815. https://doi.org/10.1513/pats.200809-100TH
457. Wang, C., Feng, H., Cheng, X., Liu, K., Cai, D., & Zhao, R. (2020). Potential Therapeutic Targets of B7 Family in Colorectal Cancer. *Frontiers in Immunology*, *11*. https://doi.org/10.3389/fimmu.2020.00681
458. Wang, C., Li, Y., Jia, L., Kim, J. koo, Li, J., Deng, P., Zhang, W., Krebsbach, P. H., & Wang, C.-Y. (2021). CD276 expression enables squamous cell carcinoma stem cells to evade immune surveillance. *Cell Stem Cell*, *28*(9), 1597-1613.e7. https://doi.org/10.1016/j.stem.2021.04.011
459. Wang, G., Wu, Z., Wang, Y., Li, X., Zhang, G., & Hou, J. (2016). Therapy to target renal cell carcinoma using 131I-labeled B7-H3 monoclonal antibody. *Oncotarget*, *7*(17), 24888–24898. https://doi.org/10.18632/oncotarget.8550

460. Wang, J., Chong, K. K., Nakamura, Y., Nguyen, L., Huang, S. K., Kuo, C., Zhang, W., Yu, H., Morton, D. L., & Hoon, D. S. B. (2013). B7-H3 Associated with Tumor Progression and Epigenetic Regulatory Activity in Cutaneous Melanoma. *Journal of Investigative Dermatology*, *133*(8), 2050–2058. https://doi.org/10.1038/jid.2013.114

461. Wang, L., Fraser, C. C., Kikly, K., Wells, A., Han, R., Coyle, A., Chen, L., & Hancock, W. (2005). B7-H3 promotes acute and chronic allograft rejection. *European Journal of Immunology*, *35*(2), 428–438. https://doi.org/10.1002/eji.200425518

462. Wang, L., Kang, F., Sun, N., Wang, J., Chen, W., Li, D., & Shan, B. (2016). The tumor suppressor miR-124 inhibits cell proliferation and invasion by targeting B7-H3 in osteosarcoma. *Tumor Biology*, *37*(11), 14939–14947. https://doi.org/10.1007/s13277-016-5386-2

463. Wang, L., Kang, F., Zhang, G., Wang, J., Xie, M., & Zhang, Y. (2018). Clinical significance of serum soluble B7-H3 in patients with osteosarcoma. *Cancer Cell International*, *18*(1), 115. https://doi.org/10.1186/s12935-018-0614-z

464. Wang, L., Zhang, Q., Chen, W., Shan, B., Ding, Y., Zhang, G., Cao, N., Liu, L., & Zhang, Y. (2013). B7-H3 is Overexpressed in Patients Suffering Osteosarcoma and Associated with Tumor Aggressiveness and Metastasis. *PLoS ONE*, *8*(8), e70689. https://doi.org/10.1371/journal.pone.0070689

465. Wheaton, A. K., Velikoff, M., Agarwal, M., Loo, T. T., Horowitz, J. C., Sisson, T. H., & Kim, K. K. (2016). The vitronectin RGD motif regulates TGF-β-induced alveolar epithelial cell apoptosis. *American Journal of Physiology-Lung Cellular and Molecular Physiology*, *310*(11), L1206–L1217. https://doi.org/10.1152/ajplung.00424.2015

466. Wheway, G., Nazlamova, L., & Hancock, J. T. (2018). Signaling through the Primary Cilium. *Frontiers in Cell and Developmental Biology*, *6*. https://doi.org/10.3389/fcell.2018.00008

467. Willingham, M. C., Richert, N. D., & Rutherford, A. v. (1987). A novel fibrillar structure in cultured cells detected by a monoclonal antibody. *Experimental Cell Research*, *171*(2), 284–295. https://doi.org/10.1016/0014-4827(87)90162-5

468. Wilson, J. M., de Hoop, M., Zorzi, N., Toh, B.-H., Dotti, C. G., & Parton, R. G. (2000). EEA1, a Tethering Protein of the Early Sorting Endosome, Shows a Polarized Distribution in Hippocampal Neurons, Epithelial Cells, and Fibroblasts. In *Molecular Biology of the Cell* (Vol. 11).

469. Wilson, K. E., Bachawal, S. v., Abou-Elkacem, L., Jensen, K., Machtaler, S., Tian, L., & Willmann, J. K. (2017). Spectroscopic Photoacoustic Molecular Imaging of Breast Cancer using a B7-H3-targeted ICG Contrast Agent. *Theranostics*, *7*(6), 1463–1476. https://doi.org/10.7150/thno.18217

470. Wolfe, K., Kamata, R., Coutinho, K., Inoue, T., & Sasaki, A. T. (2020). Metabolic Compartmentalization at the Leading Edge of Metastatic Cancer Cells. *Frontiers in Oncology*, *10*. https://doi.org/10.3389/fonc.2020.554272

471. Wolfe, K., Kofuji, S., Yoshino, H., Sasaki, M., Okumura, K., & Sasaki, A. T. (2019). Dynamic compartmentalization of purine nucleotide metabolic enzymes at leading edge in highly motile renal cell carcinoma. *Biochemical and Biophysical Research Communications*, *516*(1), 50–56. https://doi.org/10.1016/j.bbrc.2019.05.190

472. Wozniak, M. A., Modzelewska, K., Kwong, L., & Keely, P. J. (2004). Focal adhesion regulation of cell behavior. *Biochimica et Biophysica Acta (BBA) - Molecular Cell Research*, *1692*(2–3), 103–119. https://doi.org/10.1016/j.bbamcr.2004.04.007

473. Wright Muelas, M., Ortega, F., Breitling, R., Bendtsen, C., & Westerhoff, H. v. (2018). Rational cell culture optimization enhances experimental reproducibility in cancer cells. *Scientific Reports*, *8*(1), 3029. https://doi.org/10.1038/s41598-018-21050-4

474. Wright, Z. C., Loskutov, Y., Murphy, D., Stoilov, P., Pugacheva, E., Goldberg, A. F. X., & Ramamurthy, V. (2018). ADP-Ribosylation Factor-Like 2 (ARL2) regulates cilia stability and development of outer segments in rod photoreceptor neurons. *Scientific Reports*, *8*(1), 16967. https://doi.org/10.1038/s41598-018-35395-3

475. Wu, S., Zhao, X., Wu, S., Du, R., Zhu, Q., Fang, H., Zhang, X., Zhang, C., Zheng, W., Yang, J., & Feng, H. (2016). Overexpression of B7-H3 correlates with aggressive clinicopathological characteristics in non-small cell lung cancer. *Oncotarget*, *7*(49), 81750–81756. https://doi.org/10.18632/oncotarget.13177

476. Wu, W.-S. (2007). The signaling mechanism of ROS in tumor progression. *Cancer and Metastasis Reviews*, *25*(4), 695–705. https://doi.org/10.1007/s10555-006-9037-8

477. Wu, Y.-L., Liang, J., Zhang, W., Tanaka, Y., & Sugiyama, H. (2012). Immunotherapies: The Blockade of Inhibitory Signals. *International Journal of Biological Sciences*, *8*(10), 1420–1430. https://doi.org/10.7150/ijbs.5273

478. Xiang, K., Jendrossek, V., & Matschke, J. (2020). Oncometabolites and the response to radiotherapy. *Radiation Oncology*, *15*(1), 197. https://doi.org/10.1186/s13014-020-01638-9

479. Xie, C., Liu, D., Chen, Q., Yang, C., Wang, B., & Wu, H. (2016). Soluble B7-H3 promotes the invasion and metastasis of pancreatic carcinoma cells through the TLR4/NF-κB pathway. *Scientific Reports*, *6*(1), 27528. https://doi.org/10.1038/srep27528

480. Xu, H., Ma, H., Zha, L., Li, Q., Yang, G., Pan, H., Fei, X., Xu, X., Xing, C., & Zhang, L. (2020). IMPDH2 promotes cell proliferation and epithelial-mesenchymal transition of non-small cell lung cancer by activating the Wnt/β-catenin signaling pathway. *Oncology Letters*, *20*(5), 1–1. https://doi.org/10.3892/ol.2020.12082

481. Yam, J. W. P., Tse, E. Y. T., & Ng, I. O.-L. (2009). Role and significance of focal adhesion proteins in hepatocellular carcinoma. *Journal of Gastroenterology and Hepatology*, *24*(4), 520–530. https://doi.org/10.1111/j.1440-1746.2009.05813.x

482. Yamato, I., Sho, M., Nomi, T., Akahori, T., Shimada, K., Hotta, K., Kanehiro, H., Konishi, N., Yagita, H., & Nakajima, Y. (2009). Clinical importance of B7-H3 expression in human pancreatic cancer. *British Journal of Cancer*, *101*(10), 1709–1716. https://doi.org/10.1038/sj.bjc.6605375

483. Yamben, I. F., Rachel, R. A., Shatadal, S., Copeland, N. G., Jenkins, N. A., Warming, S., & Griep, A. E. (2013). Scrib is required for epithelial cell identity and prevents epithelial to mesenchymal transition in the mouse. *Developmental Biology*, *384*(1), 41–52. https://doi.org/10.1016/j.ydbio.2013.09.027

484. Yang, J., Tian, Z., Gao, H., Xiong, F., Cao, C., Yu, J., Shi, W., Zhan, Q., & Yang, C. (2022). Clinical significance and correlation of PD-L1, B7-H3, B7-H4, and TILs in pancreatic cancer. *BMC Cancer*, *22*(1), 584. https://doi.org/10.1186/s12885-022-09639-5

485. Yang, R., Sun, L., Li, C.-F., Wang, Y.-H., Yao, J., Li, H., Yan, M., Chang, W.-C., Hsu, J.-M., Cha, J.-H., Hsu, J. L., Chou, C.-W., Sun, X., Deng, Y., Chou, C.-K., Yu, D., & Hung, M.-C. (2021). Galectin-9 interacts with PD-1 and TIM-3 to regulate T cell death and is a target for cancer immunotherapy. *Nature Communications*, *12*(1), 832. https://doi.org/10.1038/s41467-021-21099-2

486. Yang, S., Wei, W., & Zhao, Q. (2020). B7-H3, a checkpoint molecule, as a target for cancer immunotherapy. *International Journal of Biological Sciences*, *16*(11), 1767–1773. https://doi.org/10.7150/ijbs.41105

487. Yang, W.-T., Hong, S.-R., He, K., Ling, K., Shaiv, K., Hu, J., & Lin, Y.-C. (2021). The Emerging Roles of Axonemal Glutamylation in Regulation of Cilia Architecture and Functions. *Frontiers in Cell and Developmental Biology*, *9*. https://doi.org/10.3389/fcell.2021.622302
488. Yap, A. S., Niessen, C. M., & Gumbiner, B. M. (1998). The Juxtamembrane Region of the Cadherin Cytoplasmic Tail Supports Lateral Clustering, Adhesive Strengthening, and Interaction with p120ctn. *Journal of Cell Biology*, *141*(3), 779–789. https://doi.org/10.1083/jcb.141.3.779
489. Yin, J., Ren, W., Huang, X., Deng, J., Li, T., & Yin, Y. (2018). Potential Mechanisms Connecting Purine Metabolism and Cancer Therapy. *Frontiers in Immunology*, *9*. https://doi.org/10.3389/fimmu.2018.01697
490. Yu, T.-T., Zhang, T., Lu, X., & Wang, R.-Z. (2018). B7-H3 promotes metastasis, proliferation, and epithelial-mesenchymal transition in lung adenocarcinoma. *OncoTargets and Therapy*, *Volume 11*, 4693–4700. https://doi.org/10.2147/OTT.S169811
491. Yuan, H., Wei, X., Zhang, G., Li, C., Zhang, X., & Hou, J. (2011). B7-H3 Over Expression in Prostate Cancer Promotes Tumor Cell Progression. *Journal of Urology*, *186*(3), 1093–1099. https://doi.org/10.1016/j.juro.2011.04.103
492. Yuan, K., Frolova, N., Xie, Y., Wang, D., Cook, L., Kwon, Y.-J., Steg, A. D., Serra, R., & Frost, A. R. (2010). Primary Cilia Are Decreased in Breast Cancer: Analysis of a Collection of Human Breast Cancer Cell Lines and Tissues. *Journal of Histochemistry & Cytochemistry*, *58*(10), 857–870. https://doi.org/10.1369/jhc.2010.955856
493. Zang, X., Thompson, R. H., Al-Ahmadie, H. A., Serio, A. M., Reuter, V. E., Eastham, J. A., Scardino, P. T., Sharma, P., & Allison, J. P. (2007). B7-H3 and B7x are highly expressed in human prostate cancer and associated with disease spread and poor outcome. *Proceedings of the National Academy of Sciences*, *104*(49), 19458–19463. https://doi.org/10.1073/pnas.0709802104
494. Zappa, C., & Mousa, S. A. (2016). Non-small cell lung cancer: current treatment and future advances. *Translational Lung Cancer Research*, *5*(3), 288–300. https://doi.org/10.21037/tlcr.2016.06.07
495. Zhang, B., Zhang, T., Wang, G., Wang, G., Chi, W., Jiang, Q., & Zhang, C. (2015). GSK3β-Dzip1-Rab8 Cascade Regulates Ciliogenesis after Mitosis. *PLOS Biology*, *13*(4), e1002129. https://doi.org/10.1371/journal.pbio.1002129
496. Zhang, G., Hou, J., Shi, J., Yu, G., Lu, B., & Zhang, X. (2008). Soluble CD276 (B7-H3) is released from monocytes, dendritic cells and activated T cells and is detectable in normal human serum. *Immunology*, *123*(4), 538–546. https://doi.org/10.1111/j.1365-2567.2007.02723.x
497. Zhang, J., Fan, J., Venneti, S., Cross, J. R., Takagi, T., Bhinder, B., Djaballah, H., Kanai, M., Cheng, E. H., Judkins, A. R., Pawel, B., Baggs, J., Cherry, S., Rabinowitz, J. D., & Thompson, C. B. (2014). Asparagine Plays a Critical Role in Regulating Cellular Adaptation to Glutamine Depletion. *Molecular Cell*, *56*(2), 205–218. https://doi.org/10.1016/j.molcel.2014.08.018
498. Zhang, J., Visser, F., King, K. M., Baldwin, S. A., Young, J. D., & Cass, C. E. (2007). The role of nucleoside transporters in cancer chemotherapy with nucleoside drugs. *Cancer and Metastasis Reviews*, *26*(1), 85–110. https://doi.org/10.1007/s10555-007-9044-4
499. Zhang, L., & Bu, P. (2022). The two sides of creatine in cancer. *Trends in Cell Biology*, *32*(5), 380–390. https://doi.org/10.1016/j.tcb.2021.11.004
500. Zhang, L., Zhu, Z., Yan, H., Wang, W., Wu, Z., Zhang, F., Zhang, Q., Shi, G., Du, J., Cai, H., Zhang, X., Hsu, D., Gao, P., Piao, H., Chen, G., & Bu, P. (2021). Creatine promotes cancer metastasis through activation of Smad2/3. *Cell Metabolism*, *33*(6), 1111-1123.e4. https://doi.org/10.1016/j.cmet.2021.03.009

501. Zhang, M., Zhang, H., Fu, M., Zhang, J., Zhang, C., Lv, Y., Fan, F., Zhang, J., Xu, H., Ye, D., Yang, H., Hua, W., & Mao, Y. (2021). The Inhibition of B7H3 by 2-HG Accumulation Is Associated With Downregulation of VEGFA in IDH Mutated Gliomas. *Frontiers in Cell and Developmental Biology*, *9*. https://doi.org/10.3389/fcell.2021.670145
502. Zhang, P., Yu, S., Li, H., Liu, C., Li, J., Lin, W., Gao, A., Wang, L., Gao, W., & Sun, Y. (2015). ILT4 drives B7-H3 expression via PI3K/AKT/mTOR signalling and ILT4/B7-H3 co-expression correlates with poor prognosis in non-small cell lung cancer. *FEBS Letters*, *589*(17), 2248–2256. https://doi.org/10.1016/j.febslet.2015.06.037
503. Zhang, W., Wang, Y., WANG, J., DONG, F., ZHU, M., WAN, W., LI, H., WU, F., YAN, X., & KE, X. (2015). B7-H3 silencing inhibits tumor progression of mantle cell lymphoma and enhances chemosensitivity. *International Journal of Oncology*, *46*(6), 2562–2572. https://doi.org/10.3892/ijo.2015.2962
504. Zhang, Y., & Wong, H. S. (2021). Are mitochondria the main contributor of reactive oxygen species in cells? *Journal of Experimental Biology*, *224*(5). https://doi.org/10.1242/jeb.221606
505. Zhao, J., Lei, T., Xu, C., Li, H., Ma, W., Yang, Y., Fan, S., & Liu, Y. (2013). MicroRNA-187, down-regulated in clear cell renal cell carcinoma and associated with lower survival, inhibits cell growth and migration though targeting B7-H3. *Biochemical and Biophysical Research Communications*, *438*(2), 439–444. https://doi.org/10.1016/j.bbrc.2013.07.095
506. Zhao, X., LI, D.-C., ZHU, X.-G., GAN, W.-J., LI, Z., XIONG, F., ZHANG, Z.-X., ZHANG, G.-B., ZHANG, X.-G., & ZHAO, H. (2013). B7-H3 overexpression in pancreatic cancer promotes tumor progression. *International Journal of Molecular Medicine*, *31*(2), 283–291. https://doi.org/10.3892/ijmm.2012.1212
507. Zhao, X., ZHANG, G.-B., GAN, W.-J., XIONG, F., LI, Z., ZHAO, H., ZHU, D.-M., ZHANG, B., ZHANG, X.-G., & LI, D.-C. (2013). Silencing of B7-H3 increases gemcitabine sensitivity by promoting apoptosis in pancreatic carcinoma. *Oncology Letters*, *5*(3), 805–812. https://doi.org/10.3892/ol.2013.1118
508. Zhong, X., Zhang, H., Zhu, Y., Liang, Y., Yuan, Z., Li, J., Li, J., Li, X., Jia, Y., He, T., Zhu, J., Sun, Y., Jiang, W., Zhang, H., Wang, C., & Ke, Z. (2020). Circulating tumor cells in cancer patients: developments and clinical applications for immunotherapy. *Molecular Cancer*, *19*(1), 15. https://doi.org/10.1186/s12943-020-1141-9
509. Zhou, C., Cunningham, L., Marcus, A. I., Li, Y., & Kahn, R. A. (2006). Arl2 and Arl3 Regulate Different Microtubule-dependent Processes. *Molecular Biology of the Cell*, *17*(5), 2476–2487. https://doi.org/10.1091/mbc.e05-10-0929
510. Zhou, Q., Li, K., Lai, Y., Yao, K., Wang, Q., Zhan, X., Peng, S., Cai, W., Yao, W., Zang, X., Xu, K., Huang, J., & Huang, H. (2021). B7 score and T cell infiltration stratify immune status in prostate cancer. *Journal for ImmunoTherapy of Cancer*, *9*(8), e002455. https://doi.org/10.1136/jitc-2021-002455
511. Zhou, W.-T., & Jin, W.-L. (2021). B7-H3/CD276: An Emerging Cancer Immunotherapy. *Frontiers in Immunology*, *12*. https://doi.org/10.3389/fimmu.2021.701006
512. Zhou, Z., Luther, N., Ibrahim, G. M., Hawkins, C., Vibhakar, R., Handler, M. H., & Souweidane, M. M. (2013). B7-H3, a potential therapeutic target, is expressed in diffuse intrinsic pontine glioma. *Journal of Neuro-Oncology*, *111*(3), 257–264. https://doi.org/10.1007/s11060-012-1021-2
513. Zhuang, X., & Xu, C. (2016). [B7-H3 monoclonal antibody attenuates the inflammation and tissue injury in mice with cerulein-induced acute pancreatitis]. *Xi Bao Yu Fen Zi Mian Yi Xue Za Zhi = Chinese Journal of Cellular and Molecular Immunology*, *32*(3), 323–327.

514. Zou, W., & Chen, L. (2008). Inhibitory B7-family molecules in the tumour microenvironment. *Nature Reviews Immunology*, *8*(6), 467–477. https://doi.org/10.1038/nri2326

515. Zuo, J., Wang, B., Long, M., Gao, Z., Zhang, Z., Wang, H., Wang, X., Li, R., Dong, K., & Zhang, H. (2018). The type 1 transmembrane glycoprotein B7-H3 interacts with the glycolytic enzyme <scp>ENO</scp> 1 to promote malignancy and glycolysis in HeLa cells. *FEBS Letters*, *592*(14), 2476–2488. https://doi.org/10.1002/1873-3468.13164